

Mathematical modelling of SERK mediated BR signalling

G. Wilma van Esse

Thesis committee

Promotor

Prof. Dr S.C. de Vries
Professor of Biochemistry
Wageningen University

Co-promotors

Dr *ing.* J.W. Borst
Assistant professor, Laboratory of Biochemistry
Wageningen University

Dr *ir.* S. van Mourik
Researcher, Mathematical and Statistical Methods Group, Biometris
Wageningen University

Other members

Prof. Dr B.M. Mulder, Wageningen University
Prof. Dr *ir.* C.M.J. Pieterse, Utrecht University
Dr G.A. Vert, Centre National de la Recherche Scientifique, Gif-sur-Yvette, France
Prof. Dr C.J. Kuhlemeier, University of Bern, Switzerland

This research was conducted under the auspices of the Graduate School of
Experimental Plant Sciences

Mathematical modelling of SERK mediated BR signalling

G. Wilma van Esse

Thesis

submitted in fulfilment of the requirements for the degree of doctor

at Wageningen University

by the authority of the Rector Magnificus

Prof. Dr M.J. Kropff,

in the presence of the

Thesis Committee appointed by the Academic Board

to be defended in public

on Wednesday 18 September 2013

at 4 p.m. in the Aula.

G. Wilma van Esse

Mathematical modelling of SERK mediated BR signalling

252 pages.

PhD thesis, Wageningen University, Wageningen, NL (2013)

With references, with summaries in Dutch and English

ISBN 978-94-6173-555-3

The research described in this thesis was financially supported by the Instellingsplan en Ondernemingsplan (IP/OP) 2007-2011 Systems Biology Research Program of Wageningen University and Research Centre.

TABLE OF CONTENTS

Chapter 1	Introduction	9
Chapter 2	Quantification of the BRASSINOSTEROID INSENSITIVE1 receptor <i>in planta</i>	25
Chapter 3	A mathematical model for BRASSINOSTEROID INSENSITIVE1-mediated signalling in root growth and hypocotyl elongation	65
Chapter 4	A mathematical model for the co-receptors SERK1 and SERK3 in BRI1 mediated signalling	111
Chapter 5	Monitoring BRI1 and SERK3 mobility in Arabidopsis roots by Fluorescence Recovery after Photobleaching	149
Chapter 6	Transcriptional analysis of <i>serk1</i> and <i>serk3</i> mutants	161
Chapter 7	General discussion	213
	References	228
	Summary	246
	Samenvatting	250
	Dankwoord	255
	<i>Curriculum Vitae</i>	259

Chapter 1

Introduction



G. Wilma van Esse

At macroscopic level, the behaviour of a single cell seems relatively straightforward; the cell can elongate or divide into two, forming a mother and daughter cell with identical DNA and features and eventually the cell can die. Multicellular organisms consist of individual cells, which can differentiate into specialised cells. Groups of cells can form an individual functional unit, an organ that has its own task and shape. At this point the behaviour of a cell already becomes more complicated; when and how does a cell in a tissue decide to grow, divide or differentiate. To enable this, single cells have to communicate via external and internal signals to orchestrate regulation of specific genes that eventually affect cellular behaviour. In principle, each cell in an organism has the same set of genes, which are transferred to the daughter cell following each division. For every cellular response different genes have to be switched on. Transcriptional regulation of target genes is the result of signal transduction cascades. In any biological system, a typical signal transduction cascade is initiated by binding of a ligand to a receptor molecule after which the receptor can interact with other downstream components. A receptor often binds only to specific ligands thereby translating the signal into a cellular response (Fig. 1A). The ligand can be secreted by the same cell as where it is perceived (autocrine signalling) by a neighbouring cell (paracrine signalling) or be transferred over larger distances (endocrine singling). Activation of the signal transduction cascade does not only result in transcriptional regulation of target genes, but also induces regulatory mechanisms which can positively or negatively enhance the signal transduction cascade (Fig. 1B). Negative feedback of the signal can be used to stabilise a basal signal, limit the maximal signalling output, generate transient pulses or enable adaptive responses whereas positive feedback can be used to accelerate and amplify signals (Brandman and Meyer, 2008). Feedback mechanisms can create hysteresis which results in two stable steady states (Ferrell, 2002). Eventually, coupling of positive and negative feedback mechanisms can result in oscillations, thereby giving spatial and temporal dynamics to the system. Signal transduction cascades are built up from biochemical interactions between proteins, which are coupled to one another by for example sharing proteins or target genes. This results in a bow-tie-architected signalling network (Citri and Yarden, 2006). In other words, multiple inputs from the extracellular environment go through one core process consisting of biochemical networks to regulate transcription of specific target genes. The robustness of the system is ensured by the presence of functional redundant proteins, which can fulfil the same role within a signal transduction cascade (Citri and Yarden, 2006).

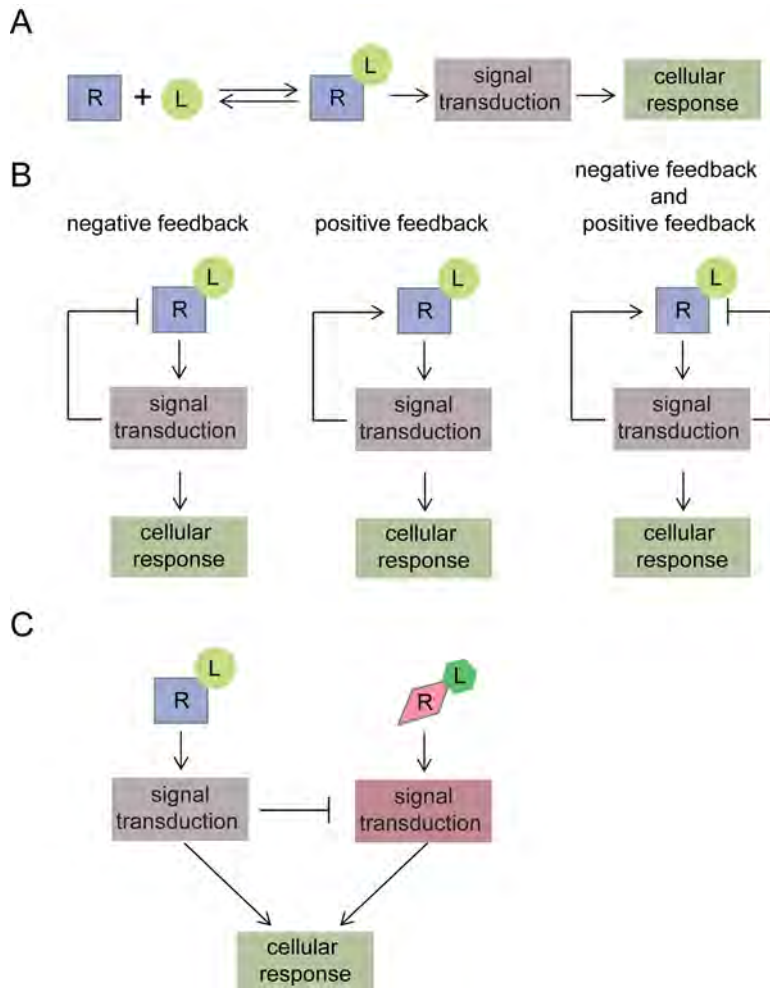


Figure 1. Simplified diagram illustrating receptor mediated signalling. A) Ligand binding to the receptor activates the signal transduction cascade thereby initiating transcriptional regulation of specific target genes resulting in a cellular response. B) The input of a signal transduction cascade can be coupled to the output by positive and negative feedback mechanisms resulting in spatial and temporal dynamics of the system C) Intracellular crosstalk between signalling outputs can affect the outcome of the signal transduction cascades. This example shows that activation of one-signal transduction pathway results in negative regulation of the other. Activation of one pathway resulting in positive regulation of the other is possible but not shown in this diagram. In actual signal transduction networks A, B and C can be combined to trigger the desired cellular response.

Being sessile by nature, plants are continuously challenged by changing environmental conditions such as temperature, light and moisture, but also by biotic stress agents such as pathogens. One question that arises is how a cell is able to distinguish these multiple inputs and how different signalling pathways

are able to operate and regulate gene expression simultaneously yet trigger the required cellular response. Certainly, a given specificity is ensured by receptors only capable of perceiving and transducing signals from a limited set of ligands. Both receptor as well as ligand needs to be present to initiate a signal transduction cascade. Mutations in a gene coding for the receptor can result in the absence of a functional receptor protein leading to impaired signal transduction. Absence of ligand can be caused by a defect of the biosynthesis genes, which are responsible for producing the ligand. Impaired signalling can result in a constitutively active signalling pathway (negative feedback) or a general reduction of signalling activity (positive feedback). However, pathway components can be shared and positive and negative regulation of signal transduction is interlinked, e.g., activation of one pathway can result in attenuation of the other (Fig. 1C). In this respect, different signal transduction pathways seem to operate cooperatively rather than individually.

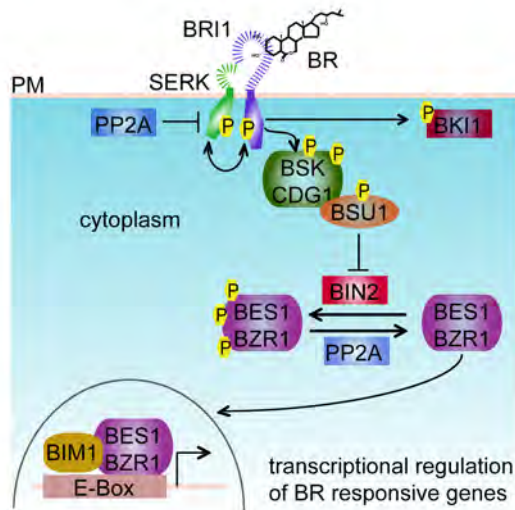


Figure 2. The BRI1 signal transduction cascade, according to Ye et al. (2011). Binding of BR to the extracellular LRR domain of BRI1 results in the phosphorylation and dissociation of BK11 from the BRI1 kinase domain thereby enabling the interaction between BRI1 and SERK proteins and the subsequent phosphorylation of BSKs (Wang and Chory, 2006; Jaillais et al., 2011). Besides BSKs, BRI1 also phosphorylates constitutive differential growth 1 (CDG1) and CDG1-like 1 (CDL1) (Kim et al., 2011). Phosphorylation of BRI Suppressor 1 (BSU1) by BSKs, CDG1 and CDL1 leads to dephosphorylation and inactivation of brassinosteroid insensitive 2 (BIN2) (Mora-García et al., 2004; Kim et al., 2011). In absence of BR, BRI1 signalling is negatively regulated by BIN2, which phosphorylates Brassinazole-Resistant1 (BZR1) and BRI1-EMS suppressor 1 (BES1) transcriptional regulators thereby preventing their translocation to the nucleus (Yin et al., 2002; Sun et al., 2010; Yu et al., 2011). Inactivation of BIN2 results in the dephosphorylation of BZR1 and BES1 thereby enabling translocation of BES1/BZR1 to the nucleus where they can interact with other transcriptional regulators (e.g. BES1-interacting Myc-like 1; BIM1) to regulate expression of BR responsive genes. The protein phosphatase 2A (PP2A) plays a dual role in BR signalling by dephosphorylating BZR1 and BRI1. Phosphorylation of BRI1 promotes the degradation and inactivation of BRI1 whereas BZR1 dephosphorylation positively regulates BR signalling (Di Rubbo et al., 2011; Tang et al., 2011; Wu et al., 2011).

For example, in the model plant *Arabidopsis thaliana*, the *de-etiolated 2* (DET2) gene, which is part of the brassinosteroid (BR) biosynthesis pathway (Li et al., 1996; Fujioka et al., 1997; Li and Chory, 1997), was originally implicated in the regulation of light-signalling based on phenotypical observations. When grown in the dark, *det2* mutants exhibit characteristics of light grown plants such as hypocotyl growth inhibition, cotyledon expansion, primary leaf initiation and accumulation of anthocyanins. In addition, *det2* mutants show significant up regulation of light-regulated genes (Chory et al., 1991). Light grown *det2* mutants show altered morphogenesis such as a dwarfed stature and dark-green leaves, reduced male fertility as well as delayed senescence and flowering (Chory et al., 1991; Chory et al., 1994). The pleiotropic phenotype of *det2* mutant plants indicated that signalling of at least two pathways is impaired. Indeed, later studies demonstrated that BR signalling negatively regulates the expression of genes involved in light signalling, this crosstalk is mediated via BR responsive transcriptional regulators (Luo et al., 2010; Sun et al., 2010; Oh et al., 2012; Wang et al., 2012). BRs, which are essential hormones for growth and development in plants, are perceived by the brassinosteroid insensitive 1 receptor (BRI1) (Clouse and Sasse, 1998). *bri1* receptor mutants exhibit, similar to BR biosynthesis mutants, developmental phenotypes such as a dwarfed stature, impaired photomorphogenesis, fertility defects, and reduced root growth (Clouse et al., 1996; Clouse and Sasse, 1998; Wang et al., 2001). BRI1 is a member of the leucine -rich repeat receptor like kinase (RLK) superfamily (Li and Chory, 1997). With more than 600 members, plant RLKs form one of the largest gene families in *Arabidopsis*. Plant receptor like kinases (RLKs), which are structurally similar to the RTKs in animal systems, have diverse functions (Shiu and Bleecker, 2001; Shiu et al., 2004). For example, Clavata 1 (CLV1) is involved in meristem development (Clark et al., 1993; Clark et al., 1997), ERECTA in organ elongation (Torii et al., 1996), HEASA in floral organ abscission (Jinn et al., 2000), and the flagellin sensitive 2 (FLS2) and elongation factor Tu (EFR) receptors are involved in defence responses (Gomez-Gomez and Boller, 2000; Zipfel et al., 2006). Analogous to animal systems (Lemmon and Schlessinger, 2010) receptor heterodimerisation is important for RLK mediated signalling in plants. For example BRI1-Associated Kinase 1 (BAK1), which is another member of the RLK super family, has been originally identified by its interaction with the BRI1 receptor in a yeast two-hybrid screen. *bak1* mutants resemble a weak allelic *bri1* mutant phenotype with a semi-dwarfed stature and reduced sensitivity towards exogenously applied BRs (Nam and Li, 2002). In addition, the *bak1* mutant enhances the phenotype of weak allelic *bri1* mutants thereby genetically confirming the involvement of SERK3 in BR signalling (Li et al., 2002; Nam and Li, 2002). BAK1 (hereafter SERK3) is a member of the somatic embryogenesis receptor like kinase (SERK) family of RLKs. SERK receptors have

not been reported to bind any ligand themselves; instead they are believed to function as non-ligand binding co-receptors (reviewed in Chinchilla et al., 2009). Recently it has been shown that BRI1 mediated signalling (Fig. 2) completely depends on the presence of SERK co-receptors (Gou et al., 2012).

SERK co-receptors function in different signalling pathways

The SERK co-receptor family consists of a class of five homologous members (SERK1-5). They all contain 5 extracellular LRR domains, followed by a proline-rich (SPP) domain, which is characteristic for the SERK family, a transmembrane domain and an intracellular kinase domain (Hecht et al., 2001). Genetic analysis of the SERK genes resulted in a complex pattern of phenotypes (Fig. 3). SERK1 functions as co-receptor of excess microsporocytes 1/extra sporogenous cells (EMS1/EXS) in tapetum formation together with SERK2. Presence of either SERK1 or SERK2 is sufficient for normal pollen development indicating that they act redundantly (Albrecht et al., 2005; Colcombet et al., 2005). A suppressor screen of the abscission mutant *nevershed* has also revealed a role for SERK1 in abscission (Lewis et al., 2010). Co-immunoprecipitation experiments showed that BRI1 and SERK3 are part of the SERK1 receptor complex (Karlova et al., 2006). SERK1 acts redundant with SERK3 in BR signalling as shown by the enhanced BR insensitivity of the *serk1serk3* double mutant when compared to the *serk3* single mutant (Albrecht et al., 2008; Gou et al., 2012). The insensitivity of the *serk1serk3* double mutant towards BRs can be rescued by overexpression of BRI1 EMS suppressor 1-D (BES1-D), a downstream transcription factor of BRI1, indicating that this phenotype is indeed BR related. Other members of the SERK receptor family did not further increase the insensitivity of the *serk1serk3* double mutant towards exogenously applied BRs (Albrecht et al., 2008). SERK4 is also implicated as co-receptor of BRI1 by its ability to rescue a *bri1-5* mutant and its interaction with BRI1 *in vivo* as shown by co-immunoprecipitation experiments. *serk4* single mutants do not have a phenotype, while the *serk3serk4* double mutant shows a dwarfed phenotype different from the strong *bri1* cabbage phenotype; *serk3serk4* mutants show early senescence symptoms while the *bri1* mutants do not (He et al., 2007). SERK3 and SERK4 are also implicated in defence and pathogen triggered cell death (Chinchilla et al., 2007; Postel et al., 2010; Roux et al., 2011). The spontaneous cell death phenotype of the *serk3serk4* double mutant (He et al., 2007) is not triggered by pathogens as it already occurs in a sterile environment. *serk1* does not further enhance the spontaneous cell death phenotype of the *serk3serk4* double mutant indicating that this process is mainly affected by SERK3 and SERK4 (Du et al., 2012). Besides BR related development SERK co-receptors also affect developmental processes unrelated to BR signalling. For example, the *serk1serk3serk4* triple mutant shows in contrast to *bri1* null and biosynthesis

mutants a reduced expression of genes involved in auxin transport, cell cycle and differentiation, and development (Du et al., 2012). Altogether, with the exception of SERK5, individual SERK co-receptors act partially redundant in at least three different biological processes. As more than one pathway is affected already in a single *serk* mutant, phenotypical analysis of SERKs is complicated, a difficulty which is further enhanced in double and triple mutants.



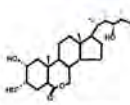



co-receptors	ligand perceiving receptor	biological process
SERK1	?	abscission 
SERK1 SERK2	EXS/EMS?	male fertility 
SERK1 SERK3 SERK4	BRI1	BR signaling 
SERK1 SERK3 SERK4	?	development 
SERK3 SERK4	FLS2 EFR PEPR1	defense 
SERK3 SERK4	?	cell death 
SERK5	?	?

Figure 3. SERK co-receptors function in different signalling pathways. Most of the SERK co-receptors function redundantly in multiple different signalling pathways, from which most of the main ligand perceiving receptors are unknown. SERK1 functions in abscission, SERK1 and SERK2 in male together with cells EMS1/EXS. SERK1, SERK3, SERK4 are involved in brassinosteroid signalling as co-receptors of BRI1, and in BR independent developmental processes. SERK3 en SERK4 are as co-receptors of FLS2 and EFR involved in defence against bacterial pathogens and cell death. SERK3 is also implicated as co-receptor of PEPR1 in chitin response. SERK5 is until now not clearly linked to any of the processes named above

Sub-cellular localization of BRI1 and SERK

The BRI1 protein is localised at the plasma membrane but can also be found in pre-vacuolar compartments and the early endosome/ trans Golgi network (Friedrichsen et al., 2000; Geldner et al., 2007; Viotti et al., 2010). A central mechanism, which can be employed to control the signalling output of a ligand perceiving receptor, is via endocytosis and trafficking (Sorkin and von Zastrow, 2002; Birtwistle and Kholodenko, 2009; Molfetta et al., 2010; Beck et al., 2012). In animal systems for example, ligand occupied epidermal growth factor receptors (EGFR) can be routed for degradation by specific interactions with GTPases and ubiquitin ligases while unoccupied ones are recycled back into the plasma membrane (Herbst et al., 1994; Marmor and Yarden, 2004). The non-ligand binding co-receptor of EGFR, ERBB2 alters specific phosphorylation sites at the kinase domain of EGFR thereby preventing its association with ubiquitin ligases and subsequent degradation of the activated receptor complex (Hartman et al., 2012). Hence, the co-receptors can stabilise the activated receptor complex thereby prolonging the signal.

In plants, endocytosis is also employed to regulate cellular processes. For example, the boron transporter Requires High Boron 1 (BOR1) is internalised and routed for degradation at high boron concentrations while at low concentrations BOR1 remains localised at the plasma membrane (Takano et al., 2005).

Attenuation of the signal by enhanced endocytosis has been proposed for BRI1; however at present it remains unclear if BRI1 adopts different endocytotic routes depending on its activation state (Irani et al., 2012) or by association with SERK co-receptors. In cowpea protoplasts co-expression of BRI1-CFP with yellow fluorescently tagged SERK1 and SERK3 resulted in an enhanced endosomal localization of BRI1. The same study also demonstrated that distinct populations of receptors and co-receptors localised together or separately (Russeinova et al., 2004). In defence signalling, flagellin induced endocytosis of the FLS2 receptor was reduced in the *serk3* mutant background (Chinchilla et al., 2007). The subcellular trafficking of FLS2 appears to be dynamic and differs depending on its activation state (Beck et al., 2012).

Whether SERK co-receptors affect trafficking and endocytosis of main ligand perceiving receptors and consequently the signalling output remains to be elucidated. However, the examples above do illustrate that receptor mediated signalling can be directed through different endosomal compartments adding a spatial factor by which the signalling output can be affected. The emerging picture from this is that signal transduction is not only dependent on the type of molecular components of a signalling pathway but also rely on the subcellular localization and concentration of these components (Kholodenko, 2006).

SERKs as modulators of the signalling output

SERK co-receptors do not perceive any ligand, yet clearly modulate the signalling output of main ligand perceiving receptors. For example, transphosphorylation between BRI1 and SERK3 is essential for increasing the kinase activity of BRI1 (Wang et al., 2008). One way to achieve this increased activity is to alter the binding affinity of BRI1 for BRs. Such a mechanism was described for the auxin perceiving receptor transport inhibitor response 1 (TIR1) where different combinations of heterodimers result in altered binding affinities (Calderon Villalobos et al., 2012). However, the dissociation constant between BRI1 and BL remains unaltered in a *serk3* mutant background (Kinoshita et al., 2005). This indicates that SERK co-receptors affect the signal of BRI1 after ligand binding. In addition, phosphorylation of the BRI1 associated kinase (BSK), a member of the Receptor Like Cytoplasmic Kinase (RLCK) superfamily and downstream target of BRI1, is mediated by BRI1 and not SERK3 (Tang et al., 2008). This suggests that it is unlikely that SERK co-receptors modify the BRI1 signalling activity by activating BSKs. In FLS2 mediated signalling SERK3 enhances the signalling output as well (Chinchilla et al., 2007; Roux et al., 2011). The affinity between FLS2 and flagellin is unaltered in a *serk3* mutant background (Chinchilla et al., 2007). Hence, in both BRI1 and FLS2 mediated signalling SERK3 appears to regulate the signal transduction after ligand binding. In FLS2 mediated signalling SERK3 enhances the signal by interacting with RLCK family member Botrytis Induced Kinase 1 (BIK1), a downstream target of FLS2 (Lu et al., 2010). This indicates that the way by which SERK3 enhances the signal of the main receptor might differ between BRI1 and FLS2 mediated signalling. Because SERK3 is a co-receptor for BRI1 and FLS2 it was suggested that SERK3 is a potential trade-off point between defence and development (Albrecht et al., 2012; Vert and Chory, 2011). In that scenario, SERK3 was postulated to be rate limiting i.e. there is not sufficient co-receptor for BRI1 and FLS2 to operate simultaneously. However, although activation of the BRI1 pathway leads to inhibition of pathogen triggered immunity (PTI) signalling, SERK3 is not rate limiting between these two signalling pathways (Albrecht et al., 2012). In other words, even when defence and BR signalling operate at the same time, there is enough SERK3 co-receptor available for FLS2 and BRI1 to maintain signalling. This points towards a mechanism where SERK co-receptors do not function as decisive nodes between different signalling pathways.

Mathematical modelling as a tool to study biological systems

The understanding of biological systems can be enhanced by using mathematical modelling (Klipp and Liebermeister, 2006). Already in the 1950s, a pioneering model by Alan Turing described morphogenesis and pattern formation based on reaction-diffusion equations (Turing, 1952). Turing, a British mathematician, who is most famous to the general public for his involvement in breaking the code of the Enigma machine and developing the Turing test, proposed that substances traveling in waves with different rates can result in the formation of specific patterns. In the reaction-diffusion model, signalling molecules are defined as chemical substances (morphogens), which can trigger a specified cellular response depending on local concentrations. The interaction and reaction rate between two morphogens is stated to follow catalytic behaviour according to Michaelis-Menten kinetics (Michaelis and Menten, 1913), which is based on the law of mass action i.e. the reaction rate depends on the initial concentration of the reactants. To date, the concepts of morphogens and Turing patterns (reaction-diffusion patterns) are used to describe biological processes such as pigment patterns on zebra fish and seashell, but also shoot apical meristem (SAM) development of plants (Meinhardt, 2008; Kondo et al., 2009; Kondo and Miura, 2010; Fujita et al., 2011).

The choice which mathematical model to use, depends on the question posed and the scale at which information is available (Band et al., 2012). In general, there are two ways to model a biological system i.e. bottom up (network) and top down (analyse the behaviour of a system). Bottom up, or mechanistic modelling, aims to predict emergent behaviour of the biological system by underlying molecular mechanisms such as gene network interactions, hormone signalling and metabolic interactions. Top down or “black box” modelling aims to describe a phenomenon mathematically, without the model being necessarily based on biological considerations. Models expanding towards cellular and tissue levels often use mechanistic approaches to capture interactions and relations between neighbouring cells or relate outputs of a gene regulatory network to a physiological response using phenomenological considerations. There is a myriad of techniques to enable bottom up and top down modelling approaches, ranging from ones low in detail (e.g. boolean networks) to highly detailed descriptions (e.g. ordinary or stochastic differential equations), from deterministic (Boolean, ordinary differential equations) to stochastic, and from static non-spatial to spatiotemporal models. These techniques can all be used to gain more insight of a biological system. For example, Boolean based models were used to study floral organ development (Espinosa-Soto et al., 2004), circadian rhythms (Akman et al., 2012) or large scale microarray data sets (Genoud et al., 2001). Boolean logics defines gene expression in two states on (1) and off (0) resulting in a qualitative view on the network (Akutsu et al., 1999). By assigning ordinary differential equations (ODE)

to each node intermediate values between 0 and 1 can be obtained (Di Cara et al., 2007). A combined approach of Boolean and ODE based modelling can be used to perform a semi quantitative analysis of the activation state of different components in the network (Fig. 4). Such an approach was used to evaluate the crosstalk between BRI1 and auxin signal transduction networks mediated by the gene Bravis Radix X (BRX; Sankar et al., 2011).

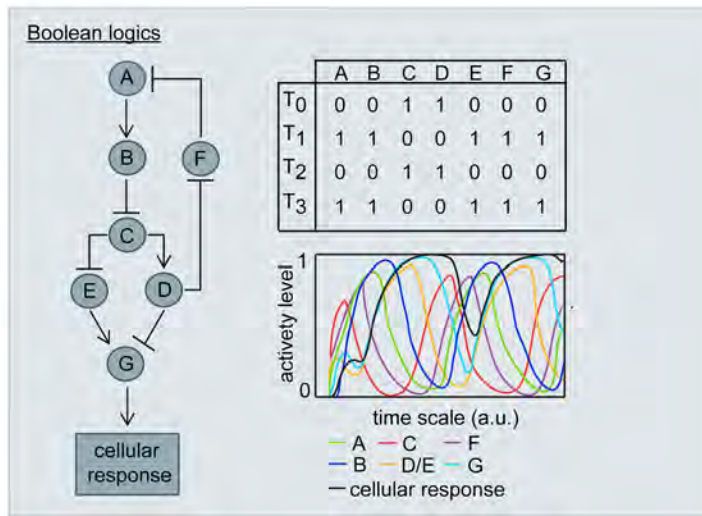


Figure 4. Modelling signal transduction networks using Boolean logics. The example presented in this figure is modified from Shankar et al. (2011). Left panel shows a simplified network scheme, including negative feedback, which can be modelled using Boolean logics (top right panel). The network starts at time point T_0 , at this moment no activation of B has occurred, C is active (1) the other pathway components are inactive (0). Activation of A at time point T_1 results in activation of B at time point T_2 leading to the inactivation of C, inactivation of D, activation of E, leading to activation of F and activation of G and consequent inactivation of A. By assigning ordinary differential equations to each node, intermediate activity levels between inactive (0) and active (1) can be computed (bottom right panel). The time scale at which this occurs is in arbitrary units (a.u.).

To incorporate quantitative information ODE based models following Michaelis-Menten or Hill kinetics are often used. Such an approach was applied in animal systems to study the effect of internalization dynamics on EGFR signalling and regulation based on the amount of receptor occupied by ligand and the ratio between the rate of internalization of occupied versus unoccupied receptor molecules. Ligand stimulus resulted in a rise in receptor-ligand concentration, followed by a decay caused by receptor internalization and depletion of extracellular ligand. When simulating an irregular ligand pulse *in silico*, the shape and magnitude of the pulse was faithfully reproduced if endocytotic down-regulation was incorporated, but not in absence of ligand induced endocytosis (Shankaran et al., 2007). Hence, *in silico* simulations showed improved accuracy

of the EGFR system by endocytotic downregulation of ligand occupied receptors. Mechanistic models based on ligand and receptor availability can also be combined with phenomenological models. For example, ligand binding and heterodimerization of EGFR was calculated according to mass action kinetics and coupled to a physiological response using phenomenological model considerations thereby linking the effect of receptor expression levels to cellular phenotypes (Shankaran et al., 2006).

In Arabidopsis, ODE based models have been employed to describe the dynamics of gene expression during floral organ formation, floral organ patterning, root development, crosstalk and transcriptional feedback (Liu et al., 2010; van Mourik et al., 2010; Middleton et al., 2012; van Mourik et al., 2012; Muraro et al., 2013). These examples point out how mathematical modelling can help to study complex biological systems. However, the use of actual receptor and ligand concentrations as starting point is hardly applied in the field of Arabidopsis research.

SCOPE OF THE THESIS

SERK co-receptors can function simultaneously and partly redundant in multiple signalling pathways. To study how SERK co-receptors are distributed between different signalling pathways, and how individual SERK proteins quantitatively affect the output of one specific signalling pathway by a change in the physiological response, are important questions to answer. For this, the use of quantitative modelling can be very helpful. One of the best-studied signal transduction cascades in Arabidopsis is the BR mediated BRI1 signalling pathway, which makes it amendable for modelling approaches. The focus of this study is to evaluate how SERK co-receptor members affect the signalling output of the BRI1 pathway. For this, we set out to use a mathematical modelling approach in which actual BRI1 and SERK receptor concentrations are incorporated by combining mechanistic with a physiological growth model based on phenomenological considerations (Fig. 5). In such an approach, the pathway can be treated as a “black box” (modelled via a top-down approach) while the input (i.e. ligand binding to the receptor) is modelled according to mass action kinetics (bottom-up). To achieve this goal quantitative confocal imaging, biochemical and genetic approaches were employed to establish a mathematical model revealing mechanistic details of the BRI1 signalling pathway.

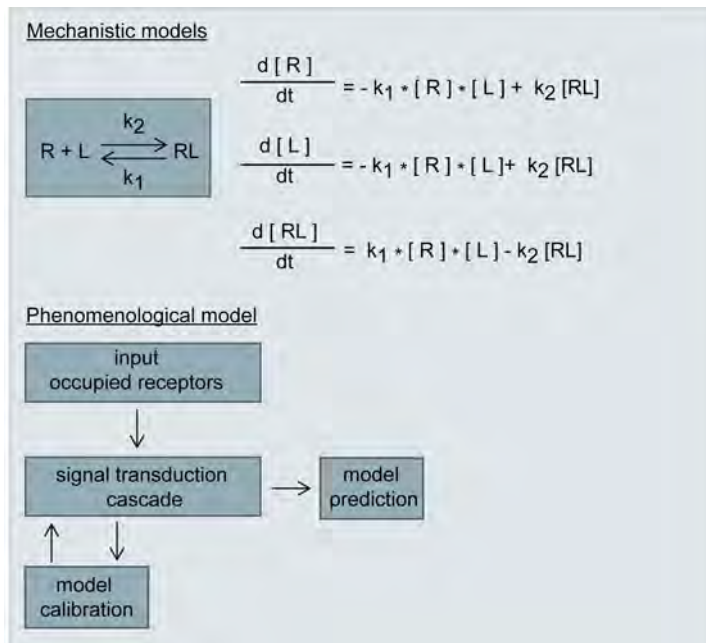


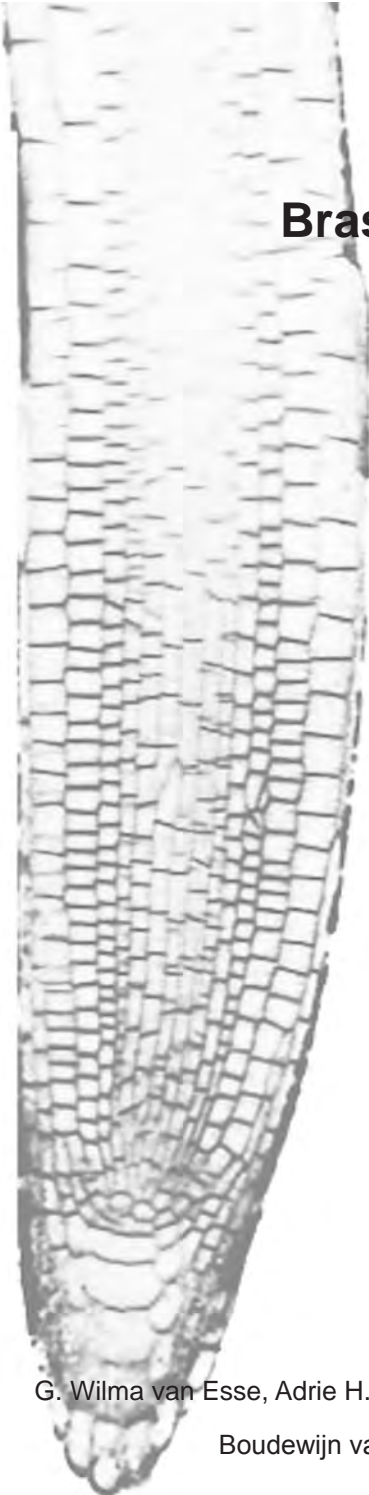
Figure 5. Mechanistic and phenomenological modelling approaches to study signal transduction. Mechanistic models can be employed to gain a quantitative view on the network, incorporating actual or relative concentration values. The mechanistic model in the figure exemplifies how ligand (L) binding to a receptor (R) results in a receptor ligand complex (RL), which can be modelled using ODEs. Phenomenological models are descriptive which can be used to couple the output of a signal transduction cascade to a complex biological response. In such an approach, only initial interaction such as ligand binding to the receptor are taken into account while the downstream signal transduction cascade is considered as a “black box” and not explicitly incorporated. Instead, only a few core components such as ligand and receptor concentrations are used as input for the phenomenological model which links the input to the physiological response. Unknown parameters can be estimated by calibrating the model to a known reference set. Model predictions show change in physiological response when the input is altered.

CONTENTS OF THIS THESIS

Brassinosteroids (BR) are plant specific hormones which are essential for growth and development. In **Chapter 1** the BR signal transduction pathway, which comprise the brassinosteroid insensitive 1 (BRI1) receptor and the somatic embryogenesis receptor like kinase (SERK) co-receptors, is introduced. SERK co-receptors function in multiple signalling pathways, for this reason it is of interest to know how SERK proteins affect the output of one signal transduction pathway quantitatively (scope of the thesis). What was still lacking was a quantitative modelling approach to study how SERK co-receptors affect BR mediated signalling. For this we set out to employ a combination of mechanistic and phenomenological modelling. Data sets incorporating local protein concentration, ligand receptor binding affinity and the different pathway components are essential to facilitate modelling of BRI1 mediated signalling via SERK co-receptors. In **Chapter 2** the number of BRI1, SERK1, and SERK3 molecules was quantified in roots of 5 day old Arabidopsis seedlings. To enable quantification of proteins at the subcellular level confocal imaging was employed to approximate the number of fluorescently tagged protein molecules in living Arabidopsis root cells. Results indicate that, with exception of the quiescent centre and columella cells, the BRI1 receptor density is constant throughout the whole root meristem. In addition, we also quantified the number of SERK1 and SERK3 co-receptor in meristem epidermal cells. It appears that these numbers are within the same order of magnitude as the number of BRI1 molecules at the plasma membrane. In **Chapter 3** the number of BRI1 receptors occupied by ligand was calculated and used to link the biochemical properties of the main receptor with root growth and hypocotyl elongation. The use of receptor - ligand concentrations and properties as a starting point represents a novel approach within the plant systems biology field. This strategy resulted in a number of unexpected findings, to our knowledge not previously described in the plant receptor field. First, a rather low number of BRI1 receptors is needed to initiate a physiological response. Second, BRI1 receptor activity appears to be controlled by positive and negative regulators or ligand availability rather than the receptor concentration. In **Chapter 4** the BRI1 model was extended by including SERK1 and SERK3. Here, the biochemical properties of the BRI1 receptor are linked to root growth or hypocotyl elongation under the assumption that BRI1 signalling only occurs in the presence of the co-receptors. *In silico* simulations indicate that BRI1 mediated signalling is not affected when the majority of SERK1 and SERK3 operate in other signalling pathways. In addition, the model correctly predicts that roots of the *serk1serk3* double mutant are almost completely insensitive towards BR while hypocotyls are not. This suggests either signalling by BRI1 alone or a different co-receptor usage between roots and shoots. Taken together, it is now possible to simulate how a wide range of proteins

affect the signalling of the main receptor. This offers a starting point to further study BR mediated signalling via a mechanistic modelling approach. In **Chapter 5** the mobility of BRI1 and SERK *in planta* is evaluated using fluorescence recovery after photobleaching (FRAP). Results indicate that BRI1 and SERK *in planta* have a rather low mobility in cells of meristematic zone, suggesting that BRI1 and SERK3 are restricted in the lateral movement. This points towards a mechanism where plasma membrane BRI1-SERK3 hetero-oligomeric complexes are present prior to ligand binding.

In **Chapter 6** the *serk1* and *serk3* single and double mutants are studied using transcriptional analysis. It appears that more than 50% of the genes differentially regulated in the *serk1serk3* double mutant is related to BRI1 signalling. A number of genes involved in primary and secondary metabolism are differentially regulated in the *serk1serk3* double mutant. This would yet add another novel biological process involving SERK co-receptors. In **Chapter 7** a general discussion is provided on the data obtained from modelling BRI1 mediated signalling and how modelling and quantitative imaging techniques can be combined to study signalling in plants.



Chapter 2

Quantification of the Brassinosteroid Insensitive 1 receptor *in planta*

G. Wilma van Esse, Adrie H. Westphal, Ramya Preethi S. Catherine Albrecht,

Boudewijn van Veen, Jan Willem Borst and Sacco C. de Vries

Plant Physiology 156 (4), 1691-1700 (2011)

ABSTRACT

In plants, green fluorescent protein (GFP) is routinely used to determine the subcellular location of fusion proteins. Here, we show that confocal imaging can be employed to approximate the number of GFP labelled protein molecules present in living *Arabidopsis* root cells. The technique involves calibration with soluble GFP to provide a usable protein concentration range within the confocal volume of the microscope. As a proof of principle we quantified the Brassinosteroid Insensitive 1 (BRI1) receptor fused to GFP, under control of its own promoter. The number of BRI1-GFP molecules per root epidermal cell ranges from 22,000 in the meristem, 130,000 in the elongation zone to 80,000 in the maturation zone, indicating that up to 6 fold differences in BRI1 receptor content exist. In contrast, when taking into account differences in cell size, BRI1-GFP receptor density in the plasma membrane is kept constant at 12 receptors μm^{-2} in all cells throughout the meristem and elongation zone. Only the quiescent centre and columella cells deviate from this pattern and have 5-6 receptors μm^{-2} . Remarkably, root cell sensitivity towards brassinosteroids appears to coincide with uniform meristem receptor density.

INTRODUCTION

The Brassinosteroid Insensitive 1 (BRI1) receptor is the main ligand perceiving receptor of brassinosteroids (BRs) in plants (Li and Chory, 1997; Wang et al., 2001). There are several BRs known in *Arabidopsis*, of which 24 (epi)-brassinolide (BL) has the highest affinity for BRI1 (Wang et al., 2001) and binds to the extracellular ligand binding (island) domain of the BRI1 receptor (He et al., 2000). Activation of BRI1 kinase results in autophosphorylation and transphosphorylation of targets such as BKI1 (Wang et al., 2006) and BAK1 (Nam and Li, 2002; Wang et al., 2005). Eventually, downstream targets such as the transcriptional regulators BZR1 (Wang et al., 2002) and BES1 (Yin et al., 2002) are activated. In general, both ligand concentration as well as receptor availability determine sensitivity and signalling output. In animal cells, receptor availability is regulated by various processes such as endocytosis (Sorkin and von Zastrow, 2002; Warren and Landgraf, 2006), degradation and recycling (Molfetta et al., 2010) and positive or negative feedback mechanisms (Freeman, 2000). In *Arabidopsis* roots, BRI1 mediated BL signalling promotes primary root growth at low exogenous BL concentrations, whereas higher concentrations are strongly inhibitory (Müssig et al., 2003). This suggests that BL signalling is indeed dependent on ligand concentration. It is less evident to what extent BRI1 receptor availability is important. BRI1 strong alleles exhibit severe phenotypes such as extreme dwarfism, altered morphogenesis, reduced fertility and full insensitivity to BRs (Clouse, 1996; Wang et al., 2001). However, *bri1* null mutants are recessive suggesting that 50% reduction in BRI1 level is not detrimental to total signalling activity. Overexpression of the *BRI1* gene results in longer leaves and petioles as well as an increased number of binding sites (Wang et al., 2001). The *BRI1* gene is considered to be ubiquitously expressed (Friedrichsen et al., 2000) and the protein is found at the plasma membrane (PM) (Geldner et al., 2007), in the early endosome/trans Golgi network (EE/TGN) and in the prevacuolar compartment (PVC) (Viotti et al., 2010). BRI1 receptor availability (i.e. the number of receptors at the PM) is so far not addressed at the organ nor at the cellular level. For this, a quantitative microscopic method suitable for use in intact plant cells is required. Quantitative methods based on confocal laser scanning microscopy (CLSM) techniques have provided insight in the amount and sub-cellular localisation of proteins (Verveer and Bastiaens, 2008). Confocal imaging is applicable for plant membrane, nuclear and cytosolic proteins (Mathur, 2007; Berg et al., 2008) and is used in yeast (Wu and Pollard, 2005) and animal cells (Sugiyama et al., 2005; Goldsbury et al., 2007) to quantify fluorescently tagged proteins. In plants, fluorescence-based quantification techniques have been used to determine protein level in whole tissue samples (Halfhill et al., 2005) and in extracts using ELISA (Richards et al., 2003) or intact cells using flow cytometry (Lu et al., 2007).

However, quantification of proteins at the subcellular level in intact plants has not been described.

Here we describe the use of confocal imaging to estimate the number of BRI1-GFP receptors at the PM of living *Arabidopsis* root cells. The method first correlates the fluorescence intensity inside a confocal volume of root cells to that of a calibrated amount of GFP in a confocal volume of a solution. This allowed us to extrapolate the fluorescence intensity obtained from 2-dimensional images of root cells to the number of BRI1-GFP molecules per cell. It also allowed an estimate of the distribution of receptors between PM and internal membrane compartments. Recently it was reported that in *Arabidopsis*, the inhibitory effect of BL on root growth primarily resides in meristem cells (González-García et al., 2011) with epidermal cells being most important in perceiving the ligand (Hacham et al., 2011). These studies demonstrated that BRI1-mediated BL signalling reduced the root meristem stem cell division rate in addition to preventing expansion of matured root cells. Our results indicate that root meristem epidermal cells responding to BL have a remarkably constant BRI1 receptor density of about 12 BRI1 molecules μm^{-2} .

RESULTS

Quantitative confocal microscopy

To determine the number of BRI1-GFP molecules per cell by confocal microscopy, the pBRI1::BRI1-GFP line described in Geldner et al. (2007) was employed. This line (referred to here as BRI1-GFP line 1) contains an equal amount of the BRI1-GFP protein when compared to endogenous BRI1 protein and shows only a mild overexpression phenotype. Root meristem epidermal cells located between 3 and 10 cells from the quiescent centre (QC) were chosen as an example (Fig. 1A). This was based on size uniformity, average expression level, location close to the root surface and a small vacuole that enables determination of PM and intracellular fluorescence separately. Measurements at the PM were performed at anticlinal cell walls because the periclinal walls are always shared with another cell type. The initial approach was to record z-stack images using Nyquist sampling. However, while these images provide spatial information, it resulted in incremental lower fluorescence intensity due to bleaching (Supplemental Fig. S1) thus rendering it unsuitable for quantification purposes. Instead, 2-dimensional confocal images were acquired using only a single scan of roots expressing BRI1-GFP, which minimised signal loss due to bleaching. As can be seen in Figure 1, BRI1-GFP localises at the PM as well as in the cytoplasm. The region of interest (ROI) from which the fluorescence intensity at the PM is derived is 1.1 μm . This equals

the full width of the Gaussian fit of the fluorescence intensity over the anticlinal cell wall (Fig. 1D) and the two adjacent PMs. However, this area includes signals from the PM as well as from intracellular membrane compartments, presumably from the TGN/EE network or the ER in close proximity to the PM (Aker and de Vries, 2008). The theoretically calculated width of the cell wall and two PMs as it appears in the microscope (Elgass et al., 2009) Supplemental File S1) is 790 nm, which confirms that in the analysed area the majority of fluorescence intensity measured is PM derived (Fig. 1D).

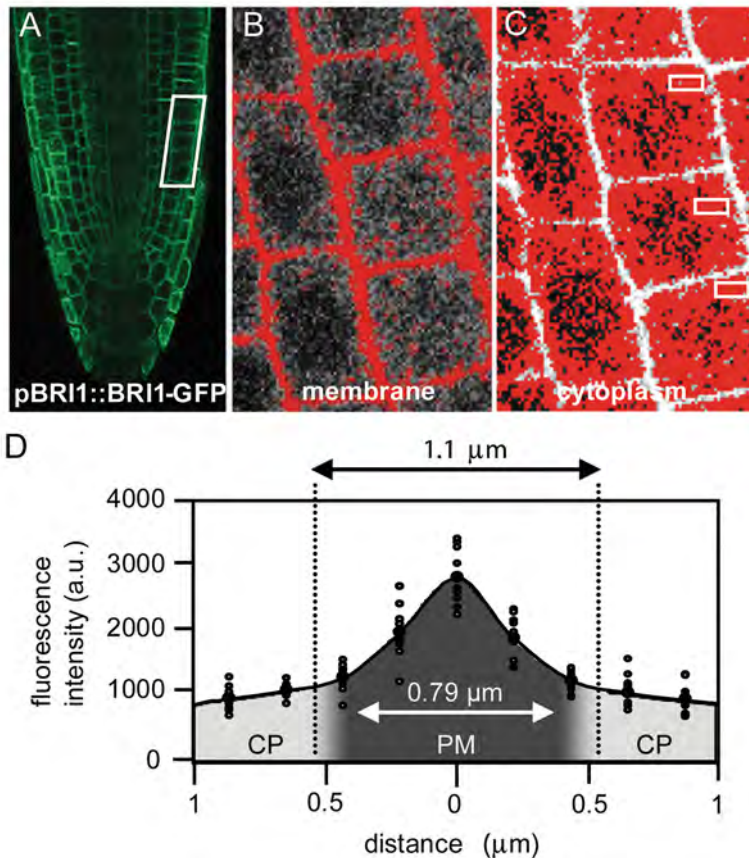


Figure 1. Fluorescence intensity measurements in root cells. A) Image of the root meristem of a 5 day old seedling of BRI1–GFP line 1. The marked area indicates the epidermal cells for which the fluorescence of the anticlinal cell walls was recorded. B) Magnification of root epidermal cell PMs as deconvoluted by the Image-Pro Plus software. C) Magnification of root epidermal cells for determination of the cytoplasmically located BRI1–GFP molecules. The small rectangles represent areas for which the fluorescence intensity was recorded. D) Gaussian fit of fluorescence intensity over the anticlinal cell wall as centred on the middle lamella is 1.1 μm in width and includes both adjacent PMs at a distance of 0.79 μm from each other (dark grey area within the Gaussian fit). For the area labelled as PM, the fluorescence intensity includes that present in the cytoplasm assuming a uniform distribution up to the PM.

To approximate the contribution of intracellular membrane compartments to the fluorescence intensity measured in the Gaussian fit over the PM, the ratio between fluorescence intensity at the PM (Fig. 1B) and in the cytoplasm (Fig. 1C) was determined. The nucleus and the vacuole were not taken into account in the measurements. Assuming a uniform distribution of BRI1-GFP containing vesicles in the cytoplasm (Fig. 1C) ratio imaging showed that 38 ± 1 % ($n \geq 50$ roots #150 cells) of the fluorescence intensity originates from intracellular membrane compartments (See Supplemental File S1 for calculations). In each measurement, the ratio between the fluorescence intensity observed in the ROI at the PM and in the cytoplasm was taken into account to correct for the contribution of intracellular membrane compartments to the fluorescence intensity assigned to the PM. A calibration curve consisting of free GFP in solution was generated to correlate with fluorescence intensity in a confocal volume (Fig. 2A). Assuming an equal fluorescence intensity between free GFP in solution and in the cytoplasm, the concentration in the analysed ROI and subsequently the receptor density could be calculated (Formula 1 ; Supplemental file S1).

$$R_{\text{BRI1}} = \left(\frac{V_{\text{app}} \cdot C_{\text{app}} \cdot N_{\text{a}}}{2} \right) \cdot \left(100 - \text{BRI1}_{\text{cyto}} \right) \quad (1)$$

in which R_{BRI1} is number of BRI1-GFP receptors at the PM, V_{app} is the apparent volume in μm^3 , C_{app} is the apparent concentration in μm^3 , $\text{BRI1}_{\text{cyto}}$ is the percentage of cytoplasmic localized BRI1-GFP in the ROI and N_{a} is Avogadro's constant.

Since the fluorescence intensities are derived from a two-dimensional confocal image we refer to the measured GFP concentration as an apparent concentration. Taking into account that the imaged area consists of two PM and vesicles in close proximity of the PM, the BRI1-GFP receptor density in root meristem epidermal cells was calculated to be 12 ± 1 receptors μm^{-2} PM. This corresponds to 9,000 BRI1-GFP receptors per cell in the PM. A similar approach was applied to calculate the number of BRI1-GFP receptors in intracellular compartments, only in this instance the fluorescence intensity measurements in the cytoplasm (Fig. 1C) were used as the starting point (See Supplemental file S1 for calculations). The volume of the cytoplasm was calculated by subtracting the volume of the nucleus (Willemse et al., 2008) and vacuole (Seguí-Simarro and Staehelin, 2006) from the volume of the entire cell. Results show that in root meristem epidermal cells there are 12,800 BRI1-GFP receptors localised in intracellular compartments in addition to the 9,000 receptors present in the PM, resulting in a total of approximately 22,000 BRI1-GFP molecules per cell.

Quantitative confocal microscopy can distinguish between different levels of GFP-tagged receptors

To ensure that the quantitative fluorescence imaging method as described above is capable of distinguishing cells expressing different amounts of receptors, several approaches were employed. For comparative purposes, receptor density at the PM was used rather than the total amount of receptors present to rule out differences due to changes in subcellular distribution. First, the number of BRI1-GFP molecules was determined in root meristem epidermal cells of another BRI1-GFP line (referred to here as BRI1-GFP line 2) in which BRI1-GFP expression is significantly higher and showing an overexpression phenotype (Friedrichsen et al., 2000; Geldner and Robatzek, 2008). Using quantitative confocal microscopy the BRI1-GFP receptor density in root meristem epidermal cells of 5 day old seedlings of BRI1-GFP line 2 is 34 ± 3 receptors μm^{-2} , approximately 3 times higher than the BRI1-GFP line 1 (Fig. 2B). The difference in expression level was verified by quantitative Western blotting (Supplemental Fig. S3). Next, the BRI1-GFP receptor density in root meristem epidermal cells of a T1 hemizygous line of BRI1-GFP line 1 was found to be half of the homozygous line (Fig. 2B). To test system independency, the number of BRI1-GFP receptors μm^{-2} PM was also determined in root meristem epidermal cells using two different confocal microscopes, a LSM510/Confocor 2 and a LSM510-META (both Carl Zeiss). The results obtained showed no significant differences in receptor values (Supplemental Fig. S4).

Finally, the receptor density of SERK1-YFP and SERK3-GFP, corresponding to the two non-ligand binding co-receptors of BRI1 (Nam and Li, 2002; Karlova et al., 2006; Albrecht et al., 2008; Li et al., 2008), was determined in root meristem epidermal cells using pSERK1::SERK1-YFP and pSERK3::SERK3-GFP lines. For quantification of SERK1-YFP a new calibration curve was generated, now using YFP instead of GFP. Quantitative confocal microscopy revealed that SERK1-YFP receptor density is 24 ± 2 receptors μm^{-2} and that of SERK3-GFP is 5 ± 1 receptors μm^{-2} (Fig. 2B). Gene expression studies (Birnbaum et al., 2003; Nawy et al., 2005) showed that SERK1 expression is indeed higher and SERK3 expression is lower compared to BRI1 in root meristem epidermal cells. Taken together, we conclude that the quantitative confocal microscopy method as described here faithfully reports changes in PM receptor density and is applicable to different receptors.

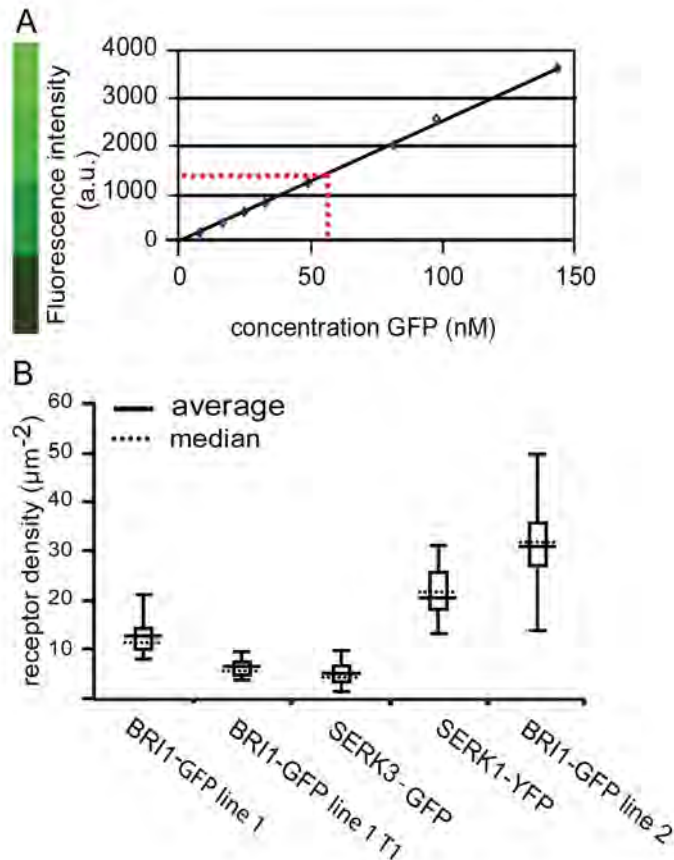


Figure 2. Calculation of the receptor density in root meristem epidermal cells. A) Typical calibration curve of GFP in solution. The mean pixel intensity increases linearly with the concentration of GFP. The red dashed lines represent the GFP concentration that was determined for a confocal volume present in root epidermal cells. Only measurements that fell within the linear part of the graph as shown here were used. B) Receptor density as determined in different plant lines. The box and whisker plots indicate the upper (75 %) and lower (25 %) quartiles and the highest and lowest value measured. Data evaluation for each measured receptor density was done using a one-way ANOVA using Bonferroni test ($\alpha = 0.05$). All values differ significantly when compared to BRI1-GFP line 1.

Quantification of the BRI1 receptor in different cell types

The next step was to provide a receptor density map of BRI1-GFP in other cell types in the root meristem, the elongation and maturation zone (Fig. 3). Unfortunately, fluorescence intensities derived from GFP molecules present in more internally located cell types can be influenced by scattering and absorption effects (Fricker et al., 2006). Therefore, fluorescence intensity measured in various cell types in the root meristem was compared with published gene expression data (Birnbaum et al., 2003; Naway et al., 2005). The results indicate that there is a close correlation between gene expression and fluorescent protein concentration (Supplemental Fig. 5). Signal attenuation due to scattering and absorption

apparently has a minor influence on our results. However, we have restricted our measurements to the upper cell layers not exceeding a distance of 45-50 μm from the cell surface.

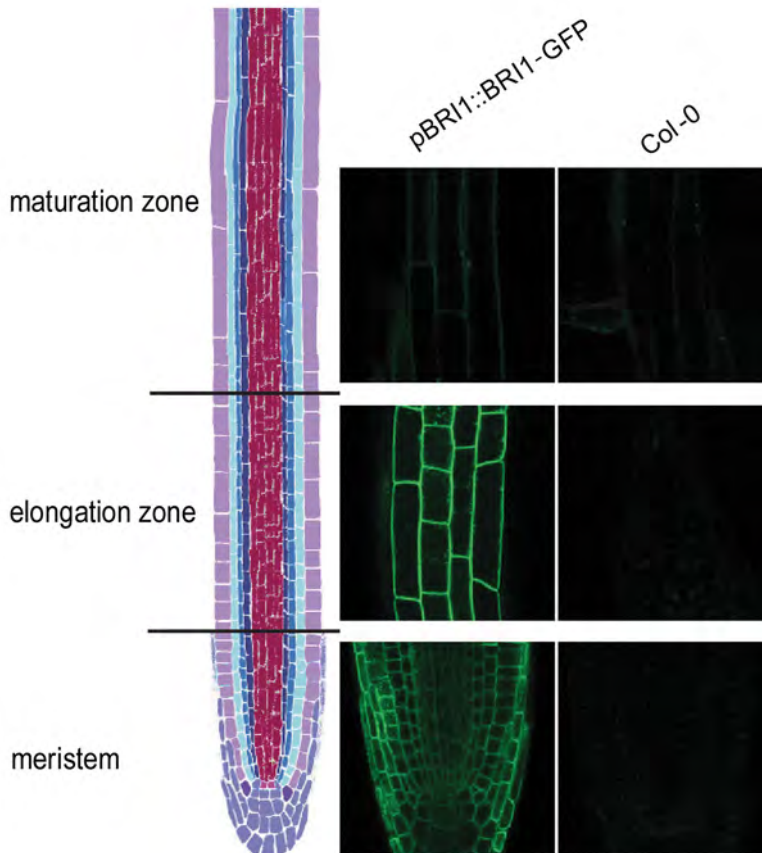


Figure 3. BRI1-GFP line 1 expression pattern in 5 day seedling roots. On the left a schematic overview of the different zones is presented. The images in the middle show BRI1-GFP expression in the different zones of the root. The root meristem is a median section and for the elongation and maturation zone only epidermal cells are shown. The images on the right represent the same areas but now in a wild type (Col-0) root.

In the root meristem, BRI1-GFP line 1 PM receptor density remains constant at about 12 receptors μm^{-2} in root epidermal, cortex and endodermis cells (Table 1) with a similar distribution between PM and intracellular compartments. In leaf epidermal cells BRI1-GFP is present at about 10 receptors μm^{-2} . In lateral root cap cells BRI1-GFP density rises to about 16 receptors μm^{-2} but is significantly lower in columella and QC cells at 5 and 6 receptors μm^{-2} respectively. In contrast to the other cell types, the receptor density of the QC cells was recorded from their joined periclinal walls. This was corroborated by the intermediate receptor density observed in their anticlinal walls joined with those of the different stem

cell populations just above the QC. These data show that adjacent membranes can differ at least 1.5 to 2 fold in receptor density. In the transition and elongation zone epidermal cells, receptor density remained constant at approximately 12 receptors μm^{-2} . Only in the fully expanded epidermal cells in the maturation zone a strong reduction of receptor density was observed. In these cells GFP fluorescence intensity is reduced to almost the level of the autofluorescence background (Table 1). Therefore, receptor density could only be estimated to be about 2 receptors μm^{-2} with a correspondingly large standard deviation. However, due to their 6-fold increase in size (Table 2), the total number of receptors per epidermal cell remains higher (130,000 to 80,000) than in the meristem. This is confirmed by semi-quantitative Western blot analysis indicating that the amount of BRI1-GFP is slightly higher in the maturation zone when compared to the meristem (Supplemental Fig. S3C).

Verification of quantitative confocal microscopy by Western blotting

To obtain an independent estimate of the number of BRI1-GFP molecules per root, quantitative immunological detection of GFP in total root protein extracts from the BRI1-GFP line 1 was employed. The results show that roots of 5 day old *Arabidopsis* seedlings contain 2.1 ± 0.8 pmol gram^{-1} fresh weight (FW) BRI1-GFP (Fig. 4).

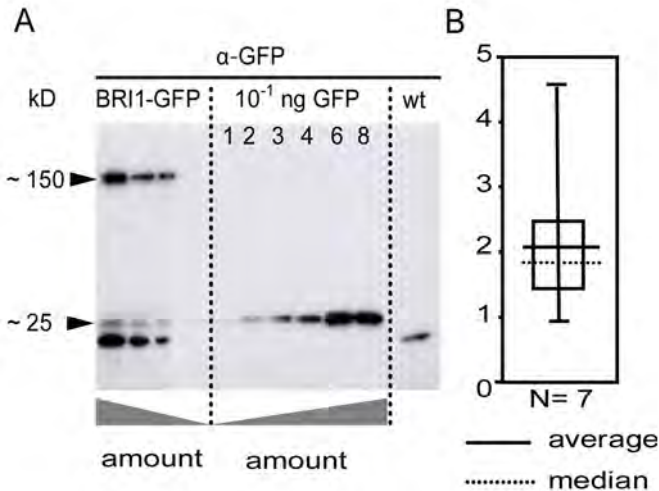


Figure 4. Semi-quantitative Western blotting of root proteins of roots of 5 day old BRI1-GFP line 1 seedlings. A) Decreasing amounts of total root proteins probed with anti-GFP antiserum. The band at 25 kD corresponds to free GFP split from the BRI1-GFP proteins during extraction and is included in the amount of BRI1-GFP protein calculated. Only scans for which the intensity fell within the linear part of the calibration curve were used for estimating the concentration of BRI1-GFP. B) The average concentration of BRI1-GFP is 2.1 ± 0.8 pmol gram^{-1} root material.

To estimate the number of BRI1-GFP receptors per root from quantitative confocal microscopy, several approximations were made; a 5 day old root when cut just below the hypocotyl has a fresh weight of 0.18 ± 0.04 mg and each cut root has $9,300 \pm 2,000$ cells. The number of cells in the root of a 5 day old seedling was calculated using published data (Supplemental Tables S1-2) as well as measurements described in this paper (Table 1). Details concerning the calculations can be found in Material and Methods and Supplemental File S2 and S3. The total number of cells in each of the different cell types shown in Table 2 and the estimated number of receptors per cell were then calculated and predict that a 5 day old BRI1-GFP line 1 root contains 3.8 ± 1.8 pmol gram⁻¹ of BRI1-GFP (Supplemental File S2, S3). This value is about two-fold higher than the value of 2.1 ± 0.8 pmol gram⁻¹ as determined by Western blotting. The difference is likely due to the uncertainty in estimating the amount of BRI-GFP in the maturation zone and in internal cell layers. However, we conclude that both numbers are close enough to validate the use of quantitative confocal microscopy as described here.

Table 1. Number of BRI1-GFP receptors in root epidermal cells and in different cell types in the root meristem

	receptor density ¹ (μm^{-2})	number of receptors cell ⁻¹	% BRI1 in cytoplasm ¹
root meristem			
epidermis	12 \pm 1 ^a	22,000 \pm 1,500	57 \pm 2 ^a
cortex	12 \pm 1 ^a	18,000 \pm 2,000	54 \pm 4 ^a
endodermis	12 \pm 1 ^a	12,100 \pm 900	41 \pm 4 ^b
lateral root cap cells	16 \pm 2 ^a	52,000 \pm 9,100	64 \pm 3 ^a
columella	5 \pm 1 ^b	10,800 \pm 1,900	58 \pm 6 ^a
quiescent centre	6 \pm 1 ^b	6,700 \pm 1,000	62 \pm 5 ^a
elongation zone			
epidermis			
transition/elongation	11 \pm 1 ^a	130,000 \pm 1,100	N.D. ²
epidermis			
elongation/maturation	5 \pm 1 ^a	100,000 \pm 17,000	N.D.
maturation zone			
epidermis	2 \pm 0.5 ^b	80,000 \pm 15,000	N.D.
Leaf			
epidermis	10 \pm 1 ^a	N.D.	N.D.

¹All values are shown with a 95 % confidence interval, with N > 45 cells using at least 20 different roots. Data evaluation for each measurement was done with a one-way ANOVA using Bonferroni test ($\alpha = 0.05$). a indicates no difference, b indicates a difference from the root meristem epidermal cells.

²N.D. = not determined. The cytoplasm in the epidermal cells of the elongation and maturation zones falls within the Gaussian width of the cell wall and therefore could not be determined separately.

BRI1 receptor density and biological significance

In root epidermal cells BRI1 receptor density is maintained at a constant level from the meristem up to the maturation zone (Table 1, Fig. 5). To elucidate whether maintenance of BRI1 receptor density may have functional significance, it is required to know which root cells respond to BL. Two recent studies reveal that cells in the root meristem are primarily responsible for the observed inhibitory effects of BL and overexpression of the BRI1 receptor (González-García et al., 2011; Hacham et al., 2011). There is a clear reduction in the number of meristem cells by approximately 40 % after treatment of wild-type roots to 4 nM of BL while root growth is reduced by about 30% in a BRI1 overexpression line (González-

García et al., 2011), identical to the BRI1-GFP line 2 used here. Under the conditions employed in our work the same reduction in meristem cell number as well as in root growth reduction was observed (Supplemental Fig. S6). The direct target cells of BL signalling were identified as belonging to the stem cell niche, including the QC, affecting both division rate and elongation (González-García et al., 2011) and extending into the elongation zone primarily affecting cell expansion (Hacham et al., 2011). Interestingly the second study points to the same epidermal cells we used here as “example” cells for BRI1-GFP quantification (Fig. 1A) as the ones that are responsible for regulating the entire effect of BRI1-mediated signalling in root meristems. Remarkably, the BRI1 receptor density, rather than the total number of receptors per cell is kept constant in all cells identified as direct targets of BL signalling in the meristematic zone of the root in both independent studies (Table 1, Fig. 5). At present no experimental strategy in plants is available to independently change BRI1-GFP receptor density while leaving the total number of active receptors and the cell size unaltered.

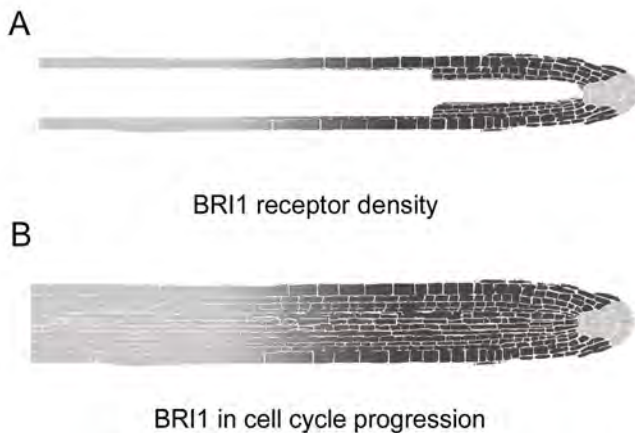


Figure 5. Graphic representation of receptor density in a BRI1-GFP line 1 root. A) Actual numbers are represented as a grey scale from dark (12 receptors μm^{-2}) to light (3 receptors μm^{-2}) Only cell types in which the measurements were performed are shown. B) Schematic presentation of an Arabidopsis root where the dark grey area indicates BRI1-mediated control of cell cycle progression according to González-García et al. (2011).

Table 2. Cell sizes measured in roots of 5 day old seedlings. Measured cell length and width of various cells in a 5 day old wild type seedling

	length ¹ (μm)	width ¹ (μm)	surface membrane (μm ²)
root meristem			
epidermis	8.1±0.4	9.8±0.5	767±2
cortex	8.0±0.4	8.5±0.5	698±2
endodermis	7.7±0.3	6.1±0.4	565±2
pericycle	8.6±0.5	5.1±0.3	557±2
vascular	11.7±0.6	5.5±0.3	714±3
lateral root cap cells	15.4±1.1	9.5±0.5	1139 ±3
columella	14.9±1.7	5.3±0.4	845±4
quiescent centre	6.1±0.3	6.6±0.6	512±3
transition zone			
epidermis	27.2±2.8	13.0±0.9	2098±9
cortex	19.2±2.8	13.7±1.8	1647±7
endodermis	18.9±2.9	8.1±0.2	1222±3
pericycle	N.D. ²	N.D.	N.D.
vascular	N.D.	N.D.	N.D.
elongation zone			
epidermis	75.0±9.6	14.8±1.2	5273±24
cortex	65.7±11.4	18.4±1.1	5273±26
endodermis	47.6±11.1	8.6±1.3	5729±20
pericycle	58.4±10.8	5.5±0.5	2809±18
vascular	N.D.	N.D.	N.D.
maturation zone			
epidermis	231.5±23.7	15.9±0.9	12,795±49
cortex	156.6±20.2	19.1±3.5	11,969±36
endodermis	97.9±8.7	9.4±1.7	5483±11
pericycle	N.D.	N.D.	N.D.
vascular	N.D.	N.D.	N.D.

¹All values are shown with a 95 % confidence interval, with N ≥ 10 cells using at least 5 different roots.

²N.D. = not determined.

DISCUSSION

In this work we have employed quantitative confocal imaging as a non-destructive method to determine the number of fluorescently tagged protein molecules in a plant cell. The results show that root cells of 5 day old *Arabidopsis* seedlings have a variable number of BRI1-GFP receptors in their PM, ranging from 22,000 in meristem epidermal cells to 130,000 in epidermal cells in the elongation zone. Interestingly, BRI1-GFP receptor density is kept constant at 12 receptor molecules μm^{-2} of PM in most of the root meristem and the distribution of receptors between the PM and in intracellular membrane compartments is about equal.

Traditionally, biochemical techniques such as Western blotting and LC-MS/MS are used to determine the concentration of individual proteins (Barnidge et al., 2003; Kito and Ito, 2008; Heidebrecht et al., 2009; Charette et al., 2010). Quantitative confocal microscopy offers the advantage of revealing spatial information in a non-destructive manner (Sugiyama et al., 2005; Goldsbury et al., 2007; Verveer and Bastiaens, 2008; Wu et al., 2008). This is especially important when dealing with proteins such as membrane receptors that are continuously recycled. In our study we have used the BRI1 receptor as a proof of principle. BRI1 is the main ligand perceiving receptor for brassinosteroids (BRs) in *Arabidopsis* (Wang et al., 2001) and is considered to be universally expressed in all cells and organs in *Arabidopsis* (Friedrichsen et al., 2000; Birnbaum et al., 2003; Nawy et al., 2005). A reduction in BL concentration due to mutation of BR biosynthesis genes or in BL perception due to reduced BRI receptor activity leads to severe growth related phenotypes implicated as a result of the failure to control expansion (Chory et al., 1991; Clouse, 1996; Clouse and Sasse, 1998; Noguchi et al., 1999; Wang et al., 2001). Conversely, ectopic overexpression of the BRI1 receptor, even to a modest level, leads to exaggerated stature of plants (Geldner et al., 2007). Surprisingly, although expressed in almost all cells, BRI1 activity appears to be required only in epidermal cells of *Arabidopsis* shoots (Savaldi-Goldstein et al., 2007), implying that a direct link between receptor presence and amount and response to ligands may not be straightforward. Part of this could be caused by the presence of negative regulators of BRI1 activity such as the BKI1 protein (Wang et al., 2006) and positive regulators such as the BAK1 (Li et al., 2002; Nam and Li, 2002) and SERK1 (Karlova et al., 2006; Albrecht et al., 2008) co-receptors or two receptor like cytoplasmic kinases designated as BR-signalling kinase 1 (BSK1) and BSK2 (Tang et al., 2008).

The number of BRI1 receptors per cell found in our studies is in line with the amounts reported for PM located hormone receptors in animal cells. For example, the number of human epidermal growth factor receptors (EGFR or ErbB1) ranges from 50,000 receptors cell^{-1} in HeLa cells (Berkers et al., 1991) to 1.4×10^7 in human squamous carcinoma cell lines (Cowley et al., 1986). In animal (Sawano

et al., 2002; Tranchant et al., 2010) and bacterial (Besschetnova et al., 2008) cells it is accepted that receptor density is decisive for signal enhancement and attenuation. For example, endocytosis, recycling and degradation of EGFR depends on the presence of ligand, composition of the signalling complex (Wiley, 2003; Warren and Landgraf, 2006) and receptor density (Sawano et al., 2002). Receptor density is therefore essential for ligand (in)dependent signal propagation (Sawano et al., 2002), autocrine signalling (DeWitt et al., 2001), EGFR distribution and determining the ratio between high and low affinity receptors (Kuszynski et al., 1993). In plant cells it is unknown if the total number of receptors per cell or receptor density is important for signalling activity. An added complexity in plants is the wide variation in cell size within the same organ due to gradual expansion of differentiated cells produced by the meristems. It was therefore of interest to find in this study that BRI1 receptor density, rather than the total number of receptors per cell, is essentially constant throughout the entire root meristem and only becomes reduced in expanding and mature cells. This would imply that with the exception of QC and columella cells, root meristematic cells would be the ones more sensitive to respond to BL when compared to the expanding mature cells. There are a number of indications that this is indeed the case. The growth promoting effect of BRs is high in seedlings and young plants (Müssig et al., 2003), whereas optimal BR signalling was found to be required for proper cell cycle progression in the root meristem (González-García et al., 2011). In that elegant study it was further shown that BR signalling also promoted stem cell differentiation. The fact that we observed a marked reduction in BRI1 receptor density in the normally rarely dividing QC cells may be a reflection of such a broad control mechanism. Furthermore, nuclear localisation of BZR1 and BES1, two transcription factors that are up-regulated after BRI1 activation, is primarily detected in the nuclei of epidermis cells in the root meristem and elongation zone rather than in the maturation zone (Ryu et al., 2007; Ryu et al., 2010). Taken together, it appears that in those cells in the root meristem that exhibit active BRI1-mediated BR signalling, BRI1 receptor density is kept at a constant value, regardless of differences in cell size. We propose that, as in animal cells, BRI1 receptor density is an important element in BRI1 mediated BL signalling. Mathematical modelling has proven to be a powerful tool to understand and interpret the complexity of the EGFR pathway (Neves and Iyengar, 2002; Hsieh et al., 2010). Our results presented here can provide a starting point for modelling studies of the BRI1 signalling pathway in *Arabidopsis*.

EXPERIMENTAL PROCEDURES

Plant Growth Conditions and plant lines

Arabidopsis thaliana plants (ecotype Columbia (Col-0)) were used throughout as wild type. Wild type plants expressing BRI1 (AT4G39400) fused to GFP under its own promoter here referred to as BRI1-GFP line 1 were provided by N. Geldner (Geldner et al., 2007). The higher BRI1-GFP expressor line, here referred to as BRI1-GFP line 2 was provided by J. Chory (Friedrichsen et al., 2000) respectively. Seeds were surface sterilised and germinated on half strength Murashige and Skoog medium (Duchefa, Haarlem, the Netherlands) supplemented with 1% Sucrose (Sigma-Aldrich chemie, Steinheim, Germany), 0.1 % MES (Sigma-Aldrich) and 0,8 % agar. For Western blotting experiments the MS medium was supplemented with 1,2% agar. The seedlings were grown vertically under fluorescent light at 22 °C, with 16-h-light/8-h-dark photoperiods. Genotyping was performed by PCR using the following primer combination: Forward (AGCACGCAAACTGCGGATTAGCGA)/ Reverse (TTTGATGCCGTTC TTTTGCTTGTC). The pSERK1::SERK1-YFP line (SERK1; AT1G71830) was in the rescued *serk1serk2serk3* triple mutant background. Genotyping of the line was done using the following primer combinations: forward (CGTGACAACAGCAGTCCGTGGCACCATCGG) / reverse (CCGGACACGCTGAACTTG) for the SERK1-YFP insert *serk1* forward (GCTGCTCCTGCAATAGCCTTTGCTTGGTGG / reversed (CCCTTTTAATCGAACCATAGCAC), *serk2* forward (CGGCTAGTAACTGGGCCGCATAGATCC)/ reverse (GGTGATGCACTGCACAGTTTGAGAGC), *serk3* forward (GCACTGAAAAACAGTTTAGC)/ reverse (GATGCAGGAAGGGGAGTCAACTTGGTG) for the mutant background. The *serk2-2* (SAIL nr. 119-G03) T-DNA tagged allele was identified in the Syngenta Arabidopsis insertion library. The *serk1-1* (SALK_044330), *serk3-1* (SALK_034523) or *bak1-3* (Rusznova et al., 2004, Kemmerling et al., 2007) were obtained from the Signal Collection at the Salk Institute (Alonso et al., 2003). The pSERK3::SERK3-GFP line (SERK3; AT4G33430) was in wild type background, genotyping of the line was done using the following primer combination: forward (AGCTGATGGTACTTTAGTGG)/reverse (TTTGATGCCGTTC TTTTGCTTGTC). Except when noted in the text, all plants used for quantitative microscopy were homozygous for the inserted transgenes.

Production and quantification of GFP

The enhanced GFP (eGFP) was cloned into a pTYB expression vector (Hink et al., 2003) after which the eGFP protein was purified according to manufactures protocol (New England Biolabs, <http://www.neb.com>). The eGFP and eYFP concentration were determined by measuring the absorption at 488 and 514 nm respectively. For calculations of the GFP concentration using the absorption measurements at 488 nm, a molar extinction coefficient of $55,000 \text{ M}^{-1}\text{cm}^{-1}$, was used (Schmid and Neumeier, 2005). For calculations of the YFP concentration a molar extinction coefficient of $84,000 \text{ M}^{-1}\text{cm}^{-1}$ was used (Schmid and Neumeier, 2005). The concentration and purity of the stock solution confirmed by Coomassie staining after SDS-PAGE electrophoresis using a range from 0.75 μg to 9 μg bovine serum albumin (BSA, Pierce, Rockford, USA) as reference compound (Supplemental Fig. S7).

GFP and YFP standard curves

For the GFP or YFP standard curve, dilutions of GFP or YFP were made in a PBS solution of pH 7.2, which is similar to the pH in the cytoplasm (Moseyko and Feldman, 2001). 200 μL of different dilutions of GFP were transferred to a 96 wells plate (Whatman, Maidstone, UK) with borosilicate bottom. To prevent adherence of the fluorophore to the glass plate, each well was pre-coated with BSA (Sigma-Aldrich) by incubation for 10 minutes with 10 mg ml^{-1} BSA followed by three washes with PBS (pH 7.2).

Fluorescence Microscopy

Roots of 5 day old Arabidopsis seedlings expressing BRI1-GFP were imaged with a CONFOCOR2/LSM510 and LSM 510-META confocal microscope (Zeiss, Jena, Germany) equipped with a 40x water objective (NA 1.2) and an Argon ion laser. The Argon laser was used for excitation of GFP and YFP at 488 nm and 514 nm respectively, and a He/Ne laser was used to excite FM4-64 at 543 nm. GFP fluorescence emission was detected with a band-pass filter 505-550 nm, while YFP fluorescence was filtered with a 530-600 band-pass filter. FM4-64 fluorescence was detected with a band-pass filter 600-650. The optical slices were acquired in confocal mode (1 Airy unit) with an average of 4 scans. The pinhole diameter was adjusted to a slice thickness of $\sim 0.9 \mu\text{m}$. All z-stacks were generated using a slice thickness of $\sim 0.45 \mu\text{m}$ thereby fulfilling Nyquist sampling criteria. For each confocal system used, the linear range of the detector and the effect of bleaching were evaluated (Supplemental Fig. S2). Bleaching of GFP and YFP can occur upon long exposure time or high intensity laser power. To limit bleaching effects all images used for quantification were taken within 45 seconds from the moment the root was exposed to the laser. The mean pixel intensity in the cytoplasmic

area and at the PM was measured separately using Image-Pro Plus software (MediaCybernetics, <http://www.mediacy.com>). A Low pass filter, pass 1 strength 2 was used to lower the background noise in the images. All fluorescence intensities measured were corrected for autofluorescence by subtracting the fluorescence intensity measured in wild type lines in the corresponding tissue and cell type. In order to correlate the fluorescence intensity in the root tissue with the GFP calibration curve, the confocal settings and data analysis were kept the same for all images obtained during an experiment. The same protocol was followed to quantify SERK1-YFP, only in that case YFP instead of GFP was used to generate the calibration curve. Each quantitative imaging session was accompanied by a parallel calibration curve to avoid differences due to experimental conditions.

Protein purification and Western blot analysis.

To obtain a protein extract, roots of 5 day old seedlings were ground in liquid nitrogen and thawed in extraction buffer containing 50 mM Tris, pH 7.5, 150 mM NaCl, 1% Triton X-100, and a protease inhibitor cocktail (Roche, <http://www.roche.com>) after which the samples were incubated on ice for 30 minutes. The extraction buffer was added in a 1:1 w/v ratio based on the weight of the ground material. The extract was centrifuged at 4 °C for 10 minutes at 200 x g (MSE Micro Centaur, London, UK). The total protein concentration in the extract was determined using a BSA protein assay (Pierce). The proteins in the extract were denaturated by boiling for 5 minutes in sample buffer containing 60 mM TRIS/HCl pH 6.8, 2% w/v SDS, 10 % glycerol w/v, 0.2 % bromophenol blue and 20 % v/v β -mercaptoethanol. The GFP reference was boiled in the same denaturation solution. Subsequently, 100, 50 and 25 ng of total protein and a range from 0.1 to 0.8 ng of GFP reference standard was loaded on a 10 % SDS-polyacrylamide gel and transferred to a PVDF membrane (Millipore, Badford, USA) by wet electroblotting (Mini-Protean II system; Bio-Rad). The BRI1-GFP and GFP reference were probed using anti-GFP-HRP antibody (Miltenyi Biotec, Bergisch Gladbach, Germany). HRP was detected using the ECL plus detection kit (GeHealthcare, Little Chalfort, Buckinghamshire, UK) according to manufacturer's instructions. The surface area and intensity of each band was determined using Image-Pro Plus software. Only scans for which the intensity fell within the linear part of the calibration curve were used.

Fresh weight determination

To determine the fresh weight, roots of 5 day old seedlings were cut just below the hypocotyls and weighed on a microbalance (Sartorius microbalance) immediately after cutting to prevent drying out of the roots. For each measurement (n = 5) at least 15 roots were used.

Determination of cell size and cell number per root

Cell sizes were measured in the meristem, elongation zone and maturation zone of 5 day old wild type *Arabidopsis* seedlings using images obtained with confocal microscopy (CONFOCOR2/LSM510) and Nomarski light microscope (LEICA,) using a 40x and a 20x objective respectively (Supplemental Fig. S8). For confocal microscopy, roots were stained for 5 minutes with 0.02 mM FM464 (Invitrogen), rinsed and mounted in dH₂O. To approximate the average thickness and size of the cells, z-stack images of the roots with a maximum slice thickness of 1 µm were acquired. To visualise roots using the Nomarski light microscope, samples were mounted in chloral hydrate solution containing 1 M chloralhydrate and 25 % v/v glycerol. All cell sizes were measured using Image-Pro Plus software. The number of cells in the cross section (Doerner, 1993; Kwaaitaal and de Vries, 2007), the number of cells in the transition zone and elongation zone (Verbelen et al., 2006) and the number of primordial cells (Malamy and Benfey, 1997; Dubrovsky et al., 2009) have been determined previously. The number of cells in the meristem was determined here.

ACKNOWLEDGEMENTS

The work that has been carried out is part of the WUR IP/OP systems biology research program, in collaboration with Jaap Molenaar and Hans Stigter. We are most grateful to Walter van Dongen for providing the purified YFP stock solution used in this study and Dolf Weijers for critically reading this manuscript.

SUPPLEMENTAL FILES

Supplemental File 1

Calculation of the apparent volume

In order to determine the receptor density, i.e. the number of BRI1 receptors per μm^2 PM, standard parameters such as the confocal volume and the volume of the analysed area needed to be determined. The pinhole diameter of the LSM510 was set at a slice thickness of $\sim 0.9 \mu\text{m}$, equivalent to a value of 1 AU. To confirm this value, the slice thickness (z) was approximated by calculating the Full Width Half Maximum (FWHM) in the axial direction (Wilhelm et al., 2003). The emission wavelength was 509 nm, the excitation wavelength was 488 nm, while the numerical aperture (N.A.) of the lens is 1.2. Since we used a 40x water lens, the refractive index of the immersion liquid is equal to the refractive index of water.

$$\text{FWHM}_{\text{det,axial}} = \sqrt{\left(\frac{0.88 \cdot \lambda_{\text{em}}}{n - \sqrt{n^2 - \text{NA}^2}} \right)^2 + \left(\frac{\sqrt{2} \cdot n \cdot \left(\text{AU} \cdot \frac{1.22 \cdot \lambda_{\text{ex}}}{\text{NA}} \right)}{\text{NA}} \right)^2}$$

$$\text{FWHM}_{\text{det,axial}} = \sqrt{\left(\frac{0.88 \cdot 0.51}{1.33 - \sqrt{1.33^2 - 1.2^2}} \right)^2 + \left(\frac{\sqrt{2} \cdot 1.33 \cdot \left(1 \cdot \frac{1.22 \cdot 0.488}{1.2} \right)}{1.2} \right)^2} = 0.98 \mu\text{m}$$

In which:

λ_{em} = emission wavelength

λ_{ex} = excitation wavelength

n = refractive index of the immersion liquid

NA = numerical apertures of the objective

AU = pinhole diameter in arbitrary units

The volume of the analysed area of $1 \mu\text{m}^2$ PM was calculated by multiplying the surface area of the ROI by the slice thickness (z). In case of the PM area, for example, the length (l) of the imaged area is $1 \mu\text{m}$. The thickness (d) of the imaged area is $1.1 \mu\text{m}$, this value corresponds to the full width of the Gaussian fit over the imaged area (Fig. 1B). Since the volume of the analysed area is derived from the ROI in the 2-d image as well as the slice thickness, we refer to this volume as the apparent volume (V_{app}).

$$V_{\text{app}} = l \cdot d \cdot z = 1 \cdot 1.1 \cdot 0.98 = 1.07 \mu\text{m}^3 = 1.07 \cdot 10^{-15} \text{ liter}$$

Calculation of the percentage of BRI1-GFP in intracellular membrane compartments

To calculate the number of BRI1-GFP that resides in cytoplasmic vesicles, the fluorescence intensity was measured in the cytoplasm (I_{cyto}) of epidermis cell in the root meristem. These cells were chosen because they have a small vacuole which allows measurement of the fluorescence intensity in the cytoplasm only. All the fluorescence intensities were corrected for autofluorescence measured in wild type lines if necessary, after which the concentration of BRI1-GFP in the cytoplasm could be calculated. Because the concentration is calculated using fluorescence intensities derived from a 2-d image we refer to this as apparent concentration (C_{app}). The volume of the cytoplasm was approximated by subtracting the volume of the vacuole ($49 \mu\text{m}^3$) and the nucleolus ($19 \mu\text{m}^3$) from the volume of the cell which is $1350 \mu\text{m}^3$ in the example. The volume of the vacuole (Seguí-Simarro and Staehelin, 2006) and nucleolus (Willemse et al., 2008) were derived from literature. The number of BRI1-GFP molecules in the cytoplasm of meristem epidermis cells can be calculated via:

$$R_{\text{BRI1}/\text{cyto}} = C_{\text{app}} \cdot V_{\text{app}} \cdot N_{\text{a}} \cdot \frac{\text{volume cytoplasm}}{V_{\text{app}}}$$

$$R_{\text{BRI1}/\text{cyto}} = 16 \cdot 0.98 \cdot 6.023 \cdot 10^{23} \frac{1281}{0.98} = 12,800 \text{ receptors in the cytoplasm}$$

Calculation of the BRI1 receptor density

The receptor density was calculated by multiplying V_{app} with the apparent concentration of BRI1-GFP (C_{app} , in the example 77 nM), which is calculated using the calibration curve (Fig. 2A) and Avogadro's constant (N_{a}). In all cells analysed it is assumed that the BRI1-GFP fluorescence is derived from both

PM (Elgass et al., 2009). To correct for the fact that the imaged area consist of two PM and vesicles in close proximity of the PM the number is divided by two and multiplied by the fraction of BRI1 that is estimated to reside on the PM in the selected ROI ($100 - BRI1_{cyto}$). For the epidermis cells in the elongation and maturation zone it was assumed that the percentage BRI1-GFP in the cytoplasm is similar to the amount of BRI1 in the cytoplasm in epidermis cells in the meristem.

$$R_{BRI1/PM} = \left(\frac{V_{app} \cdot C_{app} \cdot Na}{2} \right) \cdot \left(100 - BRI1_{Cyto} \right) = \left(\frac{1.1 \cdot 10^{-15} \cdot 77 \cdot 10^{-9} \cdot 6.022 \cdot 10^{23}}{2} \right) \cdot 0.43$$

$$R_{BRI1/PM} = 11 \text{ BRII receptors}$$

This calculation approach however, is only applicable to cells in the elongation and maturation zone and for leaf epidermal cells, where the cytoplasm is completely pressed against the PM due to the large vacuole. Therefore, all fluorescence derived from the vesicles in close proximity of the PM was already taken along in the ROI in the intensity measurements. For cells with a smaller vacuole (e.g. epidermal cells in the root meristem) the area around the PM does not include all BRI1-GFP molecules residing in intracellular membrane compartments. For example, if I_{cyto} is 750 arbitrary units (a.u.), I_{PM} is 1850 a.u. The autofluorescence in the PM area is already filtered out in the Image-Pro Plus analysis and the wild type autofluorescence in the cytoplasm is 125 a.u. The contribution of BRI1-GFP molecules that reside in intracellular located membrane vesicles to the fluorescence intensity measured in the ROI was approximated via:

$$BRI1_{Cyto} = \frac{I_{cyto} - I_{wt}}{\left((I_{cyto} - I_{wt}) + \left(\left(\frac{I_{PM}}{2} \right) - I_{wt} \right) \right)} \cdot 100\%$$

$$BRI1_{Cyto} = \frac{750 - 125}{\left((750 - 125) + \left(\frac{1850}{2} \right) \right)} \cdot 100\% = 40\%$$

Calculation of the number of BRI1 receptors per cell

The number of receptor molecules per cell was determined by multiplying the apparent concentration of BRI1-GFP at the PM (C_{app}) that was calculated using the calibration curve with Na and the V_{app} -cell of the PM. The V_{app} -cell of the PM is the volume of the PM as it is imaged. This value is calculated using the length (l),

with (w), height (h) and the full width (FW) value of the Gaussian fit over the PM in the radial direction.

$$R_{\text{BRI1}}/\text{cell} = \frac{((1 + \text{FW}) \bullet (w + \text{FW}) \bullet (h + \text{FW}) - (1 - \text{FW}) \bullet (w - \text{FW}) \bullet (h - \text{FW})) \bullet C_{\text{app}} \bullet N_{\text{a}}}{2}$$

For example, the number of BRI1 receptors in an epidermis cell in the elongation zone is calculated as follows.

$$V_{\text{app-cell}} = (75 + 1.1) \bullet (14.8 + 1.1) \bullet (17 + 1.1) - (75 - 1.1) \bullet (14.8 - 1.1) \bullet (17 - 1.1)$$

$$R_{\text{BRI1}}/\text{cell} = \frac{V_{\text{app-cell}} \bullet 77 \bullet 10^{-9} \bullet 6.022 \bullet 10^{23}}{2} = 130,000$$

For cells in the root meristem the number of BRI1 receptors per cell was approximated by adding the number of receptors calculated in the cytoplasm to the number of receptors at the PM.

Calculation of the apparent thickness of the PM

To verify that the analysed area consist mostly of PM derived signal, the apparent thickness of the PM was calculated according to Elgass et al., 2009. Briefly, the microscopes' point spread function, which equals ω (Z), is calculated using a Z0 of 68 nm and a Z resolution of 250 nm after which the convolution ω_{con} could be calculated. The apparent thickness of the PM was calculated using a value of 10 nm for real thickness of one PM and 100 nm for the cell wall (Elgass et al., 2009). Since our measurements are performed at the anticlinal cell wall, we assume that the PM is slanted with an angle of 60 degrees (Elgass et al., 2009).

Calculation of the microscope dimensions

$$\omega_0 = \frac{Z}{2 \bullet \text{NA}} = \frac{250}{2 \bullet 1.2} = 104\text{nm}$$

$$Z_0 = \frac{\pi \bullet \omega_0^2}{\lambda} = \frac{\pi \bullet 104^2}{509} = 68\text{nm}$$

Calculation of the point spread function

$$\omega(Z) = \omega_0 \left[1 + \left(\frac{Z}{Z_0} \right)^2 \right]^{1/2} = 104 \left[1 + \left(\frac{250}{68} \right)^2 \right]^{1/2} = 396.11 \text{ nm}$$

Calculation of the convolution

$$\omega_{\text{con}} = \sqrt{\omega_{\text{ideal}}^2 + \omega(Z)^2} = \sqrt{10 \text{ nm}^2 + 396 \text{ nm}^2} = 396.23 \text{ nm}$$

Calculation apparent thickness

$$\omega_{\text{final}} = (\omega_{\text{con}} + \text{cell wall thickness}) + (0.557 \cdot \lambda)$$

$$\omega_{\text{final}} = 396.23 + 100 + (0.577 \cdot 509 \text{ nm}) = 790 \text{ nm}$$

In which the factor 0.557 times λ is added to correct for the angle of 60 degrees by which the PM in the anticlinal cell wall can be slanted (Elgass et al., 2009).

Supplemental File 2**Approximation of the number of cells per root**

To estimate the number of BRI1 receptors per root using quantitative confocal microscopy, the number of cells per root had to be determined. The number of cells in the root meristem, elongation and maturation zone was calculated using available literature (Supplemental Table S1 – S2) as well as data generated in this work (Table 1). For the transition zone it was assumed that the number of cells in the cross section was equal to the number of cells in a comparable section of the elongation zone. The number of epidermal cells in the root meristem in the longitudinal direction was calculated by dividing $208 \pm 7 \mu\text{m}$ ($n = 20$), which is the length of the root meristem by the average cell size (Table 2) of this zone. For the cortex, endodermis, pericycle and vascular cells in the root meristem the same approach is taken. The number of epidermal cells in the longitudinal direction of the transition zone, the total length of the transition zone ($320 \mu\text{m}$) and elongation zone ($330 \mu\text{m}$) are derived from literature (Verbelen et al., 2006) The transition zone contains 17 epidermal cells from which the first 6 have the same cell size after which they elongate to a length of $30 \mu\text{m}$. For all other cell types it was assumed that the first 6 cells have the same cell size as in the root meristem. The number cells in the transition zone was approximated by dividing the length of the remaining part of the transition zone by the average length of the cell in this zone (Formula S1). A similar approach has been taken to determine the number of cells in the elongation and maturation zone (Formula S2 and S3). The length of the maturation zone was determined by subtracting the length of the root meristem, transition zone and elongation zone from $1.32 \pm 0.05 \text{ cm}$ ($n = 30$), being the average root length of a 5 day old seedling in our growth system. For the pericycle and vascular cells it was assumed that the cell length corresponds to the average length of the endodermis and epidermis cells respectively. The total number of cells in each zone (Supplemental Table S3) is obtained by multiplying the number of cells in the longitudinal direction with the number of cells in the cross section (Ncs). Based on these data, the total number of cells in a 5 d root was estimated to be 9300.

Formula S1: Number of cells in the transition zone

$$N = \left(\frac{\text{total length transition zone} - (6 \bullet \text{cell size root tip})}{\text{cell size transition zone}} \right) \bullet Ncs$$

Formula S2: Number of cells in the elongation zone

$$N = \left(\frac{\text{length elongation zone}}{\text{cell size length elongation zone}} \right) \bullet Ncs$$

Formula S3: Number of cells in the maturation zone

$$N = \left(\frac{\text{root length} - (\text{length root tip} + \text{length transition zone} + \text{length elongation zone})}{\text{cell size maturation zone}} \right) \bullet Ncs$$

Approximation of the amount of BRI1-GFP per root

In order to correlate the confocal microscopy data to the Western blot data the amount of BRI1-GFP per root was estimated based on the confocal microscopy measurements. To that end, the number of BRI1 receptors was calculated per cell type for each zone of the root separately (Formula S4, Supplemental File S3). As an example the calculations are shown for root meristem epidermal cells. Using the fresh weight of the root, which is determined to be 0.18 ± 0.04 mg per seedling the total amount of BRI1-GFP per root in pmol g^{-1} could be approximated (Formula S5).

Formula S4: Calculation of the number of BRI1-GFP receptors per cell file based

$$R_{\text{BRI1}}/\text{cell type} = N_{\text{cells}} \cdot [R_{\text{BRI1/cell}}] = 492 \cdot 21700 = 1.1 \cdot 10^7 \quad \text{BRI1 molecules}$$

In which:

$R_{\text{BRI1/cell type}}$ = Total number of BRI1 receptors per cell type per zone

N_{cells} = Number of cells of a certain cell type

$R_{\text{BRI1/cell}}$ = Number of BRI1 receptors in this cell type

Formula S5: Calculation of the number of BRI1-GFP receptors per root using the microscopy data

$$R_{\text{BRI1}}/\text{root} = \frac{\sum R_{\text{BRI1/cell type}}}{N_a} \cdot \frac{1}{m_r} \cdot 1 \cdot 10^{12} = \frac{4.1 \cdot 10^8}{6.023 \cdot 10^{23}} \cdot \frac{1}{18 \cdot 10^{-5}} \cdot 1 \cdot 10^{12} = 3.8 \text{ pmol g}^{-1}$$

In which:

$R_{\text{BRI1/root}}$ = Concentration in pmol g^{-1} BRI1-GFP per root

N_a = Number of Avogadro

M_r = Weight in g of a 5 day old Arabidopsis root

Supplemental File 3

Estimation of the amount of BRI1-GFP in pmol/g in roots of 5 day old Arabidopsis seedlings based on the quantitative confocal microscopy measurements

Legend value other cell type used
value approximated

root meristem

	length (µm)	width (µm)	Capp (nM)	Vapp-cell (µm ³)	number of cells	BRI1 per cell	total BRI1 molecules
Epidermis	8	10	62	847	492	21700	1.1E+07
Cortex	8	9	58	769	198	18000	3.6E+06
Endodermis	8	6	56	622	205	12100	2.5E+06
Pericycle	9	5	56	612	276	12700	3.5E+06
Vascular	12	6	56	788	340	17500	6.0E+06
Total							2.6E+07

transition zone

	length (µm)	width (µm)	Capp (nM)	Vapp-cell (µm ³)	number of cells	BRI1 per cell	total BRI1 molecules
Epidermis	8	10	62	847	120	21700	2.6E+06
Cortex	8	9	58	769	55	18000	9.8E+05
Endodermis	8	6	56	622	57	12100	6.9E+05
Pericycle	9	5	56	612	79	12700	1.0E+06
Vascular	12	6	56	788	104	17500	1.8E+06
Total							7.1E+06

	length (µm)	width (µm)	Capp (nM)	Vapp-cell (µm ³)	number of cells	BRI1 per cell	total BRI1 molecules
Epidermis	28	13	77	2271	180	52594	9.5E+06
Cortex	19	14	77	1812	127	41962	5.3E+06
Endodermis	19	8	77	1352	129	31304	4.0E+06
Pericycle	19	6	77	1144	198	26493	5.2E+06
Vascular	28	6	77	1188	250	27515	6.9E+06
Total							3.1E+07

elongation zone zone

	length (µm)	width (µm)	Capp (nM)	Vapp-cell (µm ³)	number of cells	BRI1 per cell	total BRI1 molecules
Epidermis	75	15	77	5803	91	130000	1.2E+07
Cortex	66	18	77	5808	45	134505	6.1E+06
Endodermis	48	9	77	3005	63	69600	4.4E+06
Pericycle	66	5	77	3384	98	78375	7.7E+06
Vascular	77	5	77	3916	113	90696	1.0E+07
Total							4.0E+07

maturation zone

	length (µm)	width (µm)	Capp (nM)	Vapp-cell (µm ³)	number of cells	BRI1 per cell	total BRI1 molecules
Epidermis	220	16	16	16364	1103	78755	8.7E+07
Cortex	157	19	16	13107	698	63152	4.4E+07
Endodermis	98	9	16	6040	1116	29104	3.2E+07
Pericycle	157	5	16	7788	1163	37526	4.4E+07
Vascular	220	5	16	10836	1876	52222	9.8E+07
Primordia	8	10	62	847	70	5100	3.6E+05
Total							3.1E+08

Number of BRI1-GFP receptors in an average cell in a root of a 5 day old seedling

	total BRI1 molecules			
	per zone			
root meristem	2.6E+07			
transition zone	7.1E+06			
	3.1E+07			
elongation zone zone	4.0E+07			
maturation zone	3.1E+08			
Total BRI1-GFP	4.1E+08	mol	mol/gram	pmol/gram
receptors per root		6.8E-16	3.8E-12	3.8
Average per cell	44071			
(divided by 9300)				

SUPPLEMENTAL FIGURES AND TABLES

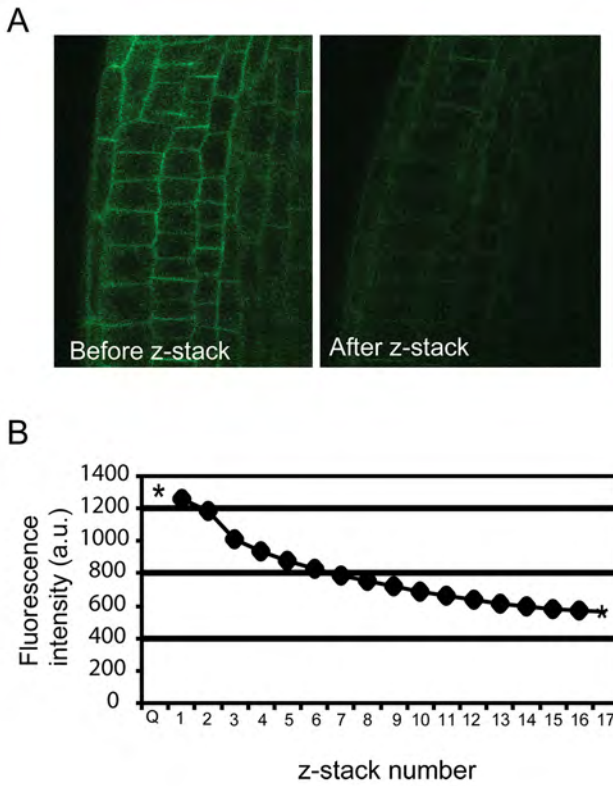


Figure S1. Bleaching occurs during z-stack imaging. A) Root epidermal cells imaged at the height of the QC before and after z-stacks. B) Fluorescence decrease due to z-stack imaging. The first image (Q) was taken at the position of the QC, after which the z-slices were taken starting from 8.5 mm above the original focal plane down again to the same QC position. The curve shows the decrease in fluorescent intensity in each z-stack. The * at position Q indicates the fluorescence intensity recorded for a group of root epidermal cells before z-stack imaging. The * after position 17 represents the remaining intensity at position Q after z-stack imaging.

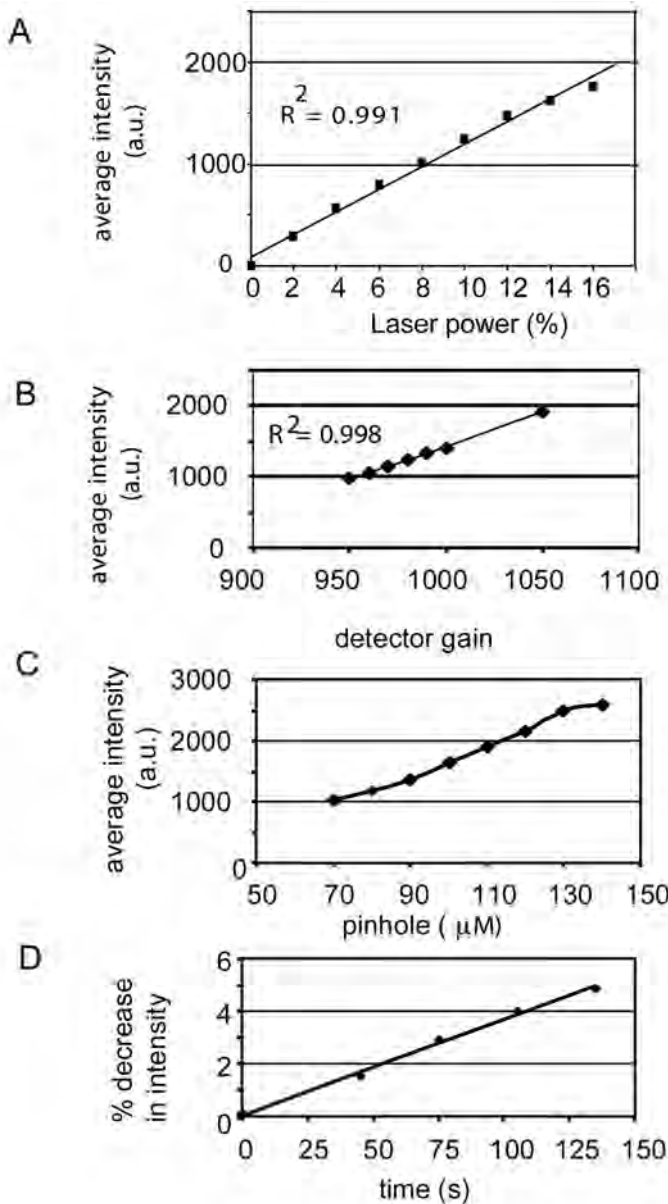


Figure S2. Calibration of the LSM 510 confocal microscope. A) The average fluorescence intensity increases linearly with increased laser power and detector gain. B) Similar results were obtained for the amplifier gain and measurements. Measurements were only performed at the midpoint of the linear range. C) The average fluorescence intensity does not increase linearly with opening of the pinhole. Therefore the pinhole setting was not changed after recording the calibration curve for each set of experiments. D) The percentage decrease in fluorescence intensity due to bleaching.

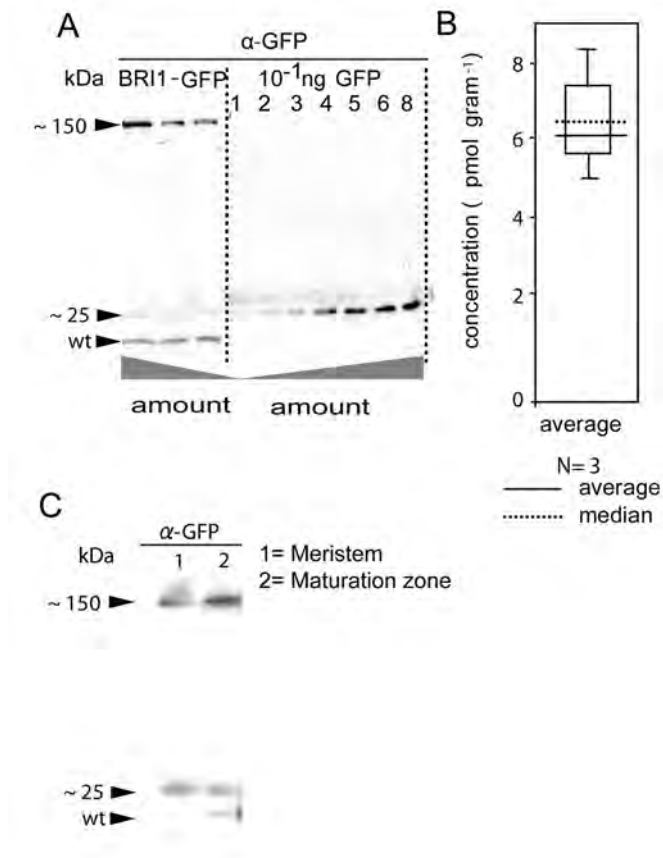


Figure S3. Semi-quantitative Western blotting of BRI1-GFP line 2. A) An amount of 100, 50 and 25 ng total root protein extract of 5 day old seedlings expressing BRI1-GFP line 2 are probed with anti-GFP antiserum. Free GFP split from the BRI1-GFP proteins, visualised by the band at 25 kDa, is included in the amount of BRI1-GFP protein. Only scans for which the intensity fell within the linear part of the calibration curve were used for estimating the concentration of BRI1-GFP. B) The average concentration of BRI1-GFP line 2 is 5.8 ± 0.6 pmol gram⁻¹ root material C) Semi quantitative Western comparing the BRI1-GFP amount in the meristem with the maturation zone. Equal amounts of total protein are loaded.

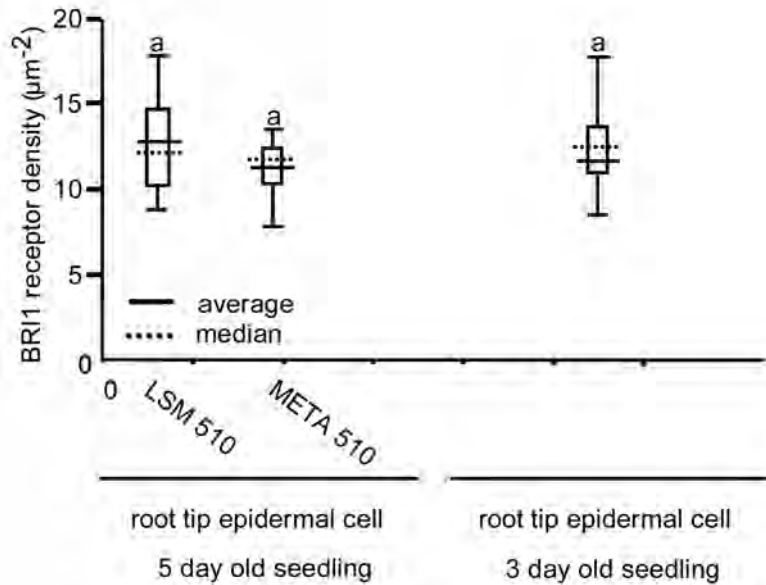


Figure S4. Receptor density determined in meristem epidermal cells of 5 day old BRI1-GFP line 1 seedlings using two different confocal microscope systems and 3 day old seedlings. The Confocor2/LSM510 is at the Microspectroscopy Centre, Wageningen University and the LSM510-META is the instrument used at the Wageningen Light Microscopy Centre. Data evaluation for each measured receptor density was done using a one-way ANOVA using Bonferroni test ($\alpha = 0.05$), a indicates no difference in receptor density measured at different the confocal microscope systems and between 5 day old and 3 day old seedlings.

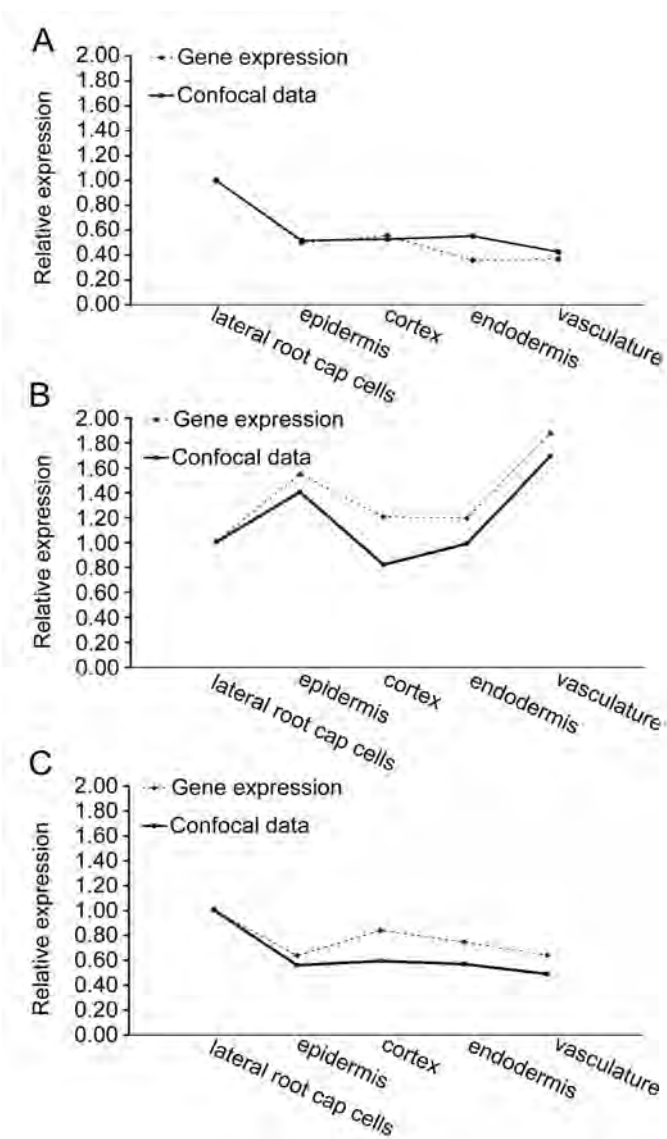


Figure S5. Relative amounts of fluorescence intensities compared to gene expression data. The gene expression data was derived from Birnbaum et al. (2003) and Nawy et al. (2005). All values were compared towards the lateral root cap cells. Measurements were performed on root meristem cells expressing BRI1-GFP (A), SERK1-YFP (B) and SERK3-GFP (C).

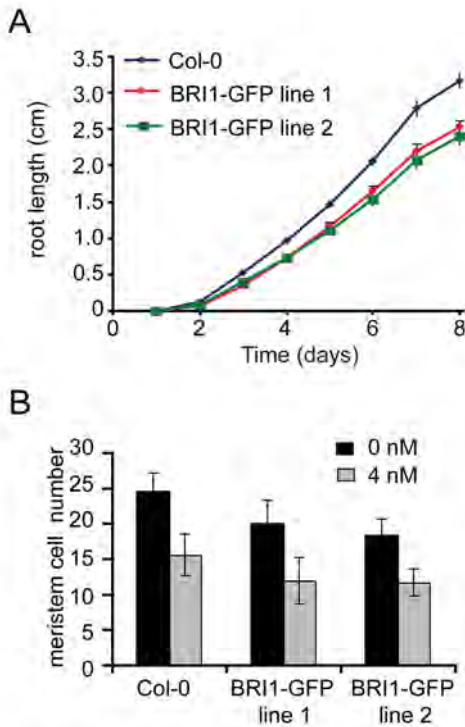


Figure S6. BRI1 overexpression in Arabidopsis roots. A) A reduction of the root length in BRI1-GFP line 1 and BRI1-GFP line 2 is observed. B) The number of epidermal cells in the meristem is reduced after stimulation with BL in wild type lines as well as in BRI1-GFP line 1 and BRI1-GFP line 2.

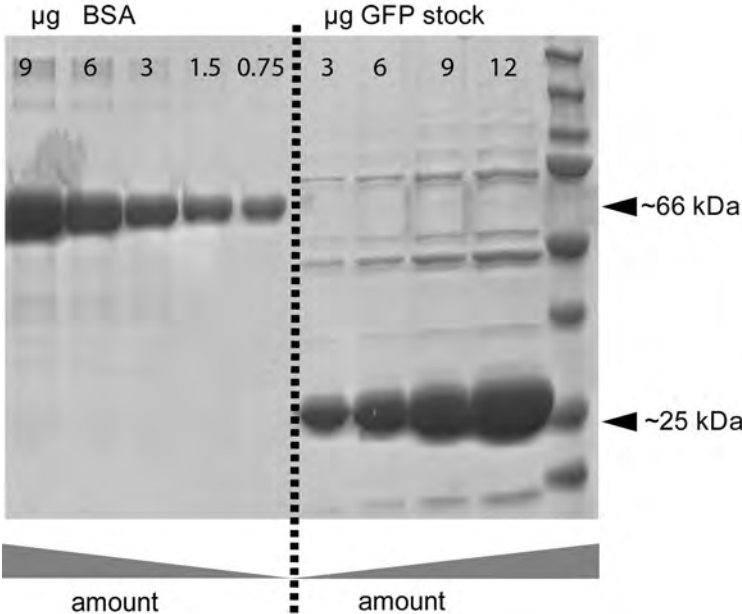


Figure S7. Confirmation of the concentration of the GFP stock. Coomassie staining after SDS-PAGE of GFP used to compare the band intensities of the GFP stock solution with 0.75-9 µg BSA.

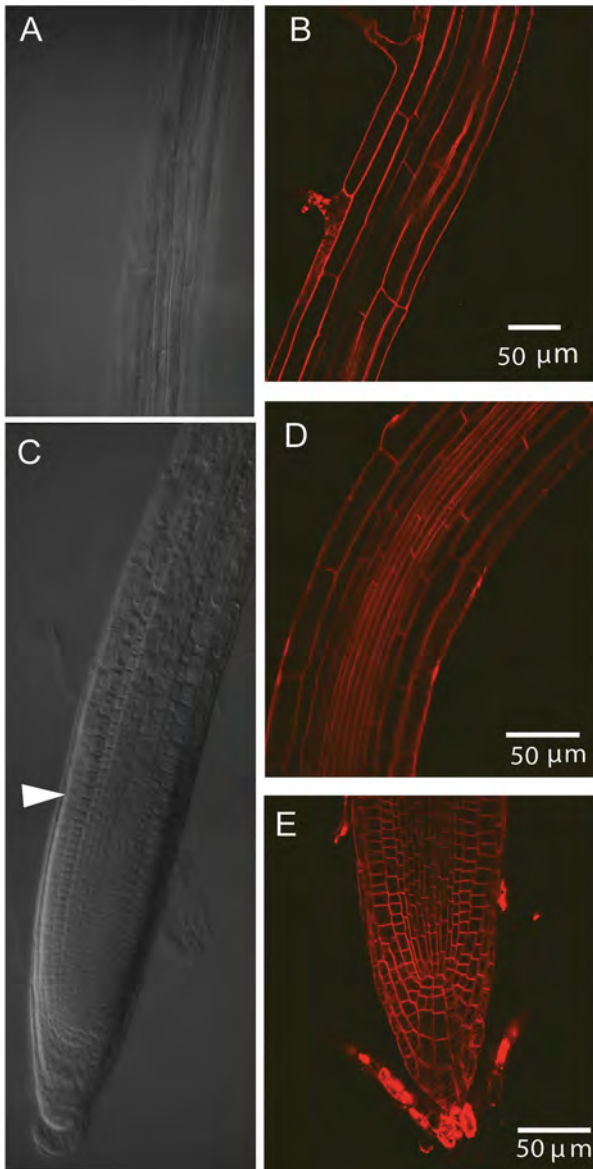


Figure S8. Cell size measurements in 5 day seedling roots. A) Images obtained using the Nomaski light microscope, used for measuring the length of the epidermis cells in the maturation zone. B) Number of cells and total length in the meristem, the white arrowhead indicates the end of the meristem and beginning of the transition zone. (C-E) FM464 stained roots visualised using the confocal microscope. Images were taken in the maturation zone (C), elongation zone (D) and root meristem (E).

Table S1. Number of cells in the cross section of a 5 day old *Arabidopsis* seedling

Cell type	Root tip	Elongation zone	Maturation zone	References
epidermis	20	20	20	(Kwaaitaal and de Vries, 2007)
cortex	8	9	9	(Kwaaitaal and de Vries, 2007)
endodermis	8	9	9	(Kwaaitaal and de Vries, 2007)
pericycle	12	14	15	(Kwaaitaal and de Vries, 2007)
vascular	20	25	34	(Kwaaitaal and de Vries, 2007)
primordia			35	(Malamy and Benfey, 1997)

Table S2. Number of cells in the longitudinal section in roots of 5 day old *Arabidopsis* seedlings

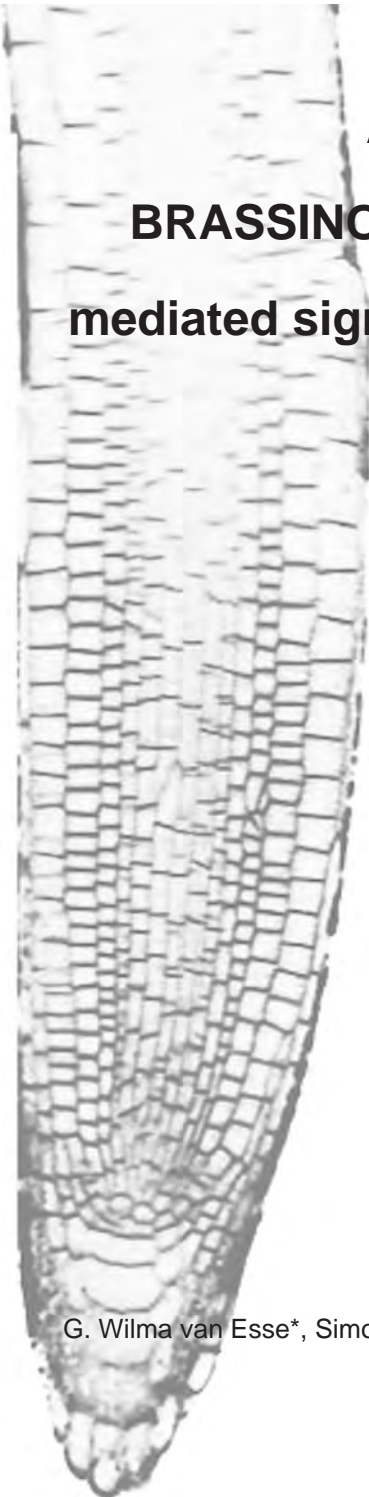
Cell type	Root meristem	Transition zone	Elongation zone	Maturation zone	References
epidermis	25	16	4	52	This Chapter and (Verbelen et al., 2006)
cortex	25	20	5	78	(Verbelen et al., 2006)
endodermis	16	21	7	124	(Verbelen et al., 2006)
pericycle	23	20	7		(Verbelen et al., 2006)
vascular	17	14	5		(Verbelen et al., 2006)
lateral root cap	12				(Doerner, 1993)
quiescent centre	4				(Doerner, 1993)
columella	10				(Doerner, 1993)
primordia				2	(Dubrovsky et al., 2009)

Table S3. Number of cells per root

Cell type	Root	Transition	Elongation	Maturation
	meristem	zone	zone	zone
epidermis	492	300	91	1103
cortex	198	182	45	698
endodermis	205	186	63	1116
pericycle	276	277	98	1163
vasculature	340	354	113	1876
lateral root cap	12			
quiescent centre	10			
columella	4			
primordia				70
total per zone	1538	1299	410	6026
total per root	9270			

Chapter 3

A mathematical model for **BRASSINOSTEROID INSENSITIVE1-** mediated signalling in root growth and hypocotyl elongation



G. Wilma van Esse*, Simon van Mourik*, Hans Stigter, Colette A. ten Hove,

Jaap Molenaar and Sacco C. de Vries

Plant Physiology 160 (1), 523-532 (2012)

*These authors contributed equally

ABSTRACT

Brassinosteroid signalling is essential for plant growth and development. In *Arabidopsis*, brassinosteroids (BRs) are perceived by the BRI1 receptor. Root growth and hypocotyl elongation are convenient downstream physiological outputs of BR signalling. A computational approach was employed to predict root growth solely on the basis of BRI1 receptor activity. The developed mathematical model predicts that during normal root growth, few receptors are occupied with ligand. The model faithfully predicts root growth as observed in *bri1* loss-of-function mutants. For roots it incorporates a stimulatory and two inhibitory modules, while for hypocotyls a single inhibitory module is sufficient. Root growth as observed when *BRI1* is overexpressed can only be predicted assuming a decrease occurred in the BRI1 half maximum response values. Root growth appears highly sensitive to variation in BR concentration and much less to reduction in BRI1 receptor level, suggesting that regulation occurs primarily by ligand availability and biochemical activity.

INTRODUCTION

Brassinosteroids (BRs) play a key role in plant growth and development. In *Arabidopsis* BRs are perceived by the plasma membrane located receptor kinase brassinosteroid insensitive 1 (BRI1). Detailed models (He et al., 2000; Wang et al., 2006; Jaillais et al., 2011; Ye et al., 2011) of BR signalling describe the binding of BR to the extracellular leucine-rich repeat (LRR) domain of BRI1 followed by activation of the receptor through autophosphorylation (Wang and Chory, 2006). Subsequently, BRI1 phosphorylates BRI1-kinase inhibitor 1 (BKI1) resulting in the release of BKI1 from the intracellular BRI1 kinase domain (Jaillais et al., 2011). BKI1 restricts association between BRI1 and another LRR-receptor like kinase (LRR-RLK), the BRI1-associated kinase 1 (BAK1) (Li et al., 2002; Nam and Li, 2002). The release of BKI1 from the kinase domain of BRI1 enables transphosphorylation between BRI1 and BAK1 (Wang et al., 2008) initiating a phosphorylation and dephosphorylation cascade mediated by cytoplasmic BR signalling kinases (BSKs) (Kim et al., 2009). This cascade results in the transcriptional regulation of BR-responsive genes (Sun et al., 2010; Wu et al., 2011; Yu et al., 2011) mediated by the BZR1 and BES1/BZR2 transcriptional regulators (Wang et al., 2002; Yin et al., 2002). The protein phosphatase 2A (PP2A) regulates at least two different steps in the BRI1 signalling pathway, dephosphorylation and degradation of BRI1 after activation (Wu et al., 2011) and dephosphorylation of BKI1 thereby promoting its translocation to the nucleus (Tang et al., 2011). Thus, both negative (BKI1, PP2A) and positive (BAK1 and BSK) regulators exist in the pathway (Supplemental Fig.S1). Disruption of BR signalling results in complex phenotypes such as extreme dwarfed stature, impaired photomorphogenesis, fertility defects and impaired root growth (Clouse, 1996; Wang et al., 2001). BRs stimulate root growth at low ligand concentrations and are strongly inhibitory at high ligand concentrations (Müssig et al., 2003). Overexpression of *BRI1*, a reduction of BRI1 activity by mutation, or exogenously applied ligands all result in an arrest in cell cycle progression in the root meristem (González-García et al., 2011). Hence, BRI1 mediated brassinosteroid signalling may not only affect root growth by promoting cell elongation (Szekeres et al., 1996; Müssig et al., 2003) but also by affecting cell division. In *Arabidopsis* roots, the meristem and elongation zone are very sensitive to changes in BR concentration, with the epidermis playing a major role in translating the BR signal into a root growth response (Hacham et al., 2011). Remarkably, BRI1 receptor density in wild type roots remains almost constant in the meristematic region (Chapter 2). To help understand the complex cellular responses to BRI1-mediated BR signalling, a mathematical model is beneficial. Modelling was previously employed to describe radial patterning of the vascular bundles in shoots, which is controlled by polar auxin transport and BR signalling (Ibañes et al., 2009; Fabregas et al., 2010) and

to help understand the role of the *BREVIS RADIX (BRX)* gene in BR and auxin signalling (Sankar et al., 2011).

The aim of this work is to develop a mathematical model to link BRI1 receptor activity directly to a downstream physiological response. Therefore, wild type *Arabidopsis* root growth was used based on its reproducible and quantifiable response to BR signalling activity. Sufficient biochemical parameters such as the BRI1 dissociation constant (Wang et al., 2001) and the BRI1 concentration (Chapter 2) are now available for this purpose. The developed model includes one stimulatory and two inhibitory modules. For validation, roots were used in which BRI1 receptor activity was either increased by expressing an extra BRI1 copy or decreased by using strong and weak *bri1* mutant alleles. Computer-generated model simulations show that the growth behaviour of the *bri1* mutant roots can be faithfully predicted in terms of BRI1 receptor occupancy level. Interestingly a model structure with only one inhibitory response faithfully predicts the hypocotyl elongation response, previously reported to primarily rely on cell elongation (Gendreau et al., 1997). We conclude that mathematical modelling of the BRI1 plant signalling pathway helps to explain complex physiological responses in both roots and hypocotyls.

RESULTS

BRI1 receptor occupancy

Receptor occupancy is a widely used estimated parameter to describe signalling activity (Brent, 2009). To accurately predict BRI1 occupancy at physiological ligand concentrations, a good estimate of BRI1 receptor and BR ligand concentration is required. BRI1 is capable of binding the most active BR, 24-epibrassinolide (BL) but also 22-homobrassinolide (HBL) and the bioactive precursor castasterone (Wang et al., 2001), the latter two being approximately five-fold less active. The endogenous level of castasterone is about 0.03-0.05 ng g⁻¹ FW or 0.06-0.1 nM assuming an equal distribution throughout the inside and outside of the cells. In roots, only trace amounts of BL and HBL are detected (Bancos et al., 2002; Shimada et al., 2003). It is not known where the natural pool of BRs exist; if this is exclusively outside of the cells, it is reasonable to assume that physiological levels can be about ten-fold higher i.e. up to approximately 1 nM. To accurately predict BRI1 receptor occupancy at physiological ligand concentration, all root growth experiments described here were performed using seedlings pre-cultured in the presence of brassinazole (BRZ), a potent inhibitor of BR biosynthesis (Asami et al., 2000). To ensure that the stimulatory and inhibitory effects of BRs on root growth entirely depend on the exogenous supply of ligand, BRZ remained present in the medium throughout the experiments. With this experimental setup we were able to monitor a clear stimulatory effect of exogenously applied BL on root growth with concentrations up to 1 nM (Fig. 1A). For comparison, the stimulatory effect of BL is hardly visible when wild type roots are treated without the presence of BRZ (Supplemental Fig. S2), confirming previous reports (Müssig et al., 2003; González-García et al., 2011). To estimate BRI1 occupancy under these physiological ligand concentrations, several assumptions had to be made based on literature. First, the highest affinity ligand is BL (Wang et al., 2001). Therefore, the model only considers BL binding to BRI1. Second, BL is bound at the island domain of BRI1 (He et al., 2000) in a ratio of one molecule to one monomer (Hothorn et al., 2011; She et al., 2011). Presently it is not clear whether monomers, homodimers or heterodimers (Russeinova et al., 2004) represent the active state. The third assumption is that the affinity of BRI1 for BL does not change between monomeric, homodimeric or heterodimeric state. For the BL dissociation constant, values ranging between 7.4-15 nM (Wang et al., 2001) and 55 nM (Caño-Delgado et al., 2004) have been reported, so simulations were done at a comparable range of values. Fourth, the BRI1 receptor concentration is estimated at 62 ± 4 nM in wild type seedling roots (Chapter 2). The fifth assumption is that BRI1 receptor concentration remains constant during receptor activation and as long as required to record a downstream physiological effect (Geldner et al., 2007).

With these assumptions, the concentration of ligand occupied BRI1 receptors can be described as a steady state equilibrium between free receptor and free ligand.

$$[BRI1\ BL] = \frac{[BRI1_{free}] \cdot [BL_{free}]}{K_d} \quad (1)$$

In accordance with the first three assumptions this equilibrium is subject to the mass balance:

$$\begin{aligned} [BRI1\ BL] + [BRI1_{free}] &= [BRI1_{tot}] \\ [BRI1\ BL] + [BL_{free}] &= [BL_{tot}] \end{aligned} \quad (2)$$

By combining equation 1 and 2, and the condition that without ligand there is no signalling, the number of BRI1 molecules occupied by ligand can be calculated analytically as:

$$[BRI1\ BL] = \frac{K_d + [BRI1_{tot}] + [BL_{tot}] - \sqrt{(K_d + [BRI1_{tot}] + [BL_{tot}])^2 - 4 \cdot [BRI1_{tot}] \cdot [BL_{tot}]}}{2} \quad (3)$$

Here, $[BRI1\ BL]$ is the amount of BRI1 receptor occupied by ligand, K_d the dissociation constant, $[BRI1_{tot}]$ the total amount of BRI1, and $[BL_{tot}]$ the total amount of BL. To calculate the BRI1 receptor occupancy, a concentration of 1 nM and 10 nM BL was used in the calculations, in line with the root growth stimulatory and inhibitory modes (Fig. 1A). From equation 3 it follows that ligand occupancy of the BRI1 receptor at physiological, stimulatory BL concentration is less than 1% and at full inhibitory mode not more than 15% (Supplemental Fig. S3).

Relationship between BRI1 receptor occupancy and root growth

A model was developed to describe root growth in terms of ligand-dependent receptor occupancy. The model structure with the best predictive power has one stimulatory module and two inhibitory modules (Equation 4). Which biological entities represent the inhibitory modules is presently not clear. As discussed in the previous section, the receptor-ligand concentration is considered constant over time, as are the half maximum response values in the pathway. However, BRI1 dependent and independent root growth are unknown functions of time. This gives the following root growth model:

$$\frac{dR(BRI1_{tot}, BL_{tot}, t)}{dt} = r(0, 0, t) + \frac{e_{max}(t) \cdot [BRI1BL]}{k_1 + [BRI1BL]} \frac{k_2}{k_2 + [BRI1BL]} \frac{k_3}{k_3 + [BRI1BL]} \quad (4)$$

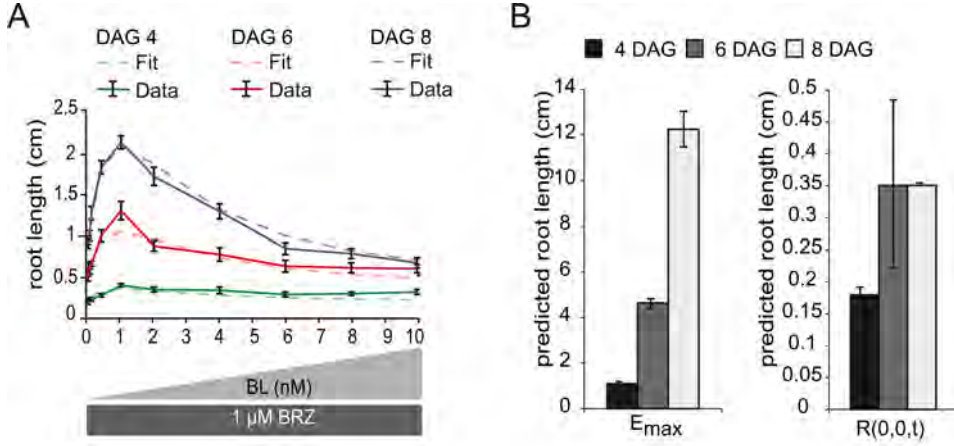


Figure 1. BRI1 receptor occupancy is linked to root growth. A) Visualisation of root promoting and inhibitory effect of BL on root growth at 4, 6 and 8 days after germination (DAG). The medium was supplemented with 1 μ M BRZ, after which increasing amounts of BL were added. Error bars represent \pm SEM, $n \geq 30$ roots per data point, measured in three independent replicates. The model is able to fit the predicted root length with the experimental dataset. B) Model predictions of E_{max} and $R(0,0,t)$ at 4, 6 and 8 DAG. The model was fit to the measured root length of seedlings at 4, 6 and 8 DAG.

Here $r(0,0,t)$ is the root growth at time t in the absence of BRI1 mediated signalling, $e_{max}(t)$ the maximum possible root growth when no inhibitory mechanisms are present, and k_1, k_2 and k_3 are the half maximum response values (k values). Integrating equation 4 over time gives the root length at time t :

$$R(BRI1_{tot}, BL_{tot}, t) = R(0,0,t) + \frac{E_{max}(t) \cdot [BRI1BL]}{k_1 + [BRI1BL]} \frac{k_2}{k_2 + [BRI1BL]} \frac{k_3}{k_3 + [BRI1BL]}, \quad (5)$$

with:

$$E_{max}(t) = \int_0^t e_{max}(\tau) d\tau, \quad R(0,0,t) = \int_0^t r(0,0,\tau) d\tau, \quad (6)$$

in which τ is the integration variable representing the time over which is integrated, going from 0 to t . The model structure in equation 5 can be fitted precisely to the biological data (Fig. 1A). $E_{max}(t)$ and $R(0,0,t)$ are regarded as free parameters that are changed over time (Fig. 1B). According to the Akaike (AIC) and Bayesian (BIC) information criteria (Klipp et al., 2009) several model structures explain the data equally well. To select the best model, the predictive power with respect to the *bri-116* null mutant was also taken into account. Of all tested model structures there was only one with a better prediction, however with higher AIC and BIC scores (Supplemental File S1, Table S1, Fig. S4, S5 and S6). Models with only one module, or with a single inhibitory module had significantly higher

AIC and BIC scores, clearly indicating a minimal necessary model complexity (See Supplemental File S1 and Table S1).

Plants treated with BRZ display similar phenotypes as *deetiolated 2* (*det2*) mutants (Nagata et al., 2000). The *det2* mutant has been reported to contain less than 10% of the wild type levels of BRs (Fujioka et al., 1997). Therefore, the model assumes that there is still a small amount of endogenous BRs (≤ 0.1 nM in the extracellular compartment) present despite the BRZ treatment. However, the stimulatory effect of BL on root length is only observed in roots depleted from endogenous BL using BRZ. The model can explain this observation by fitting the root length of seedlings treated with BL only. Assuming a physiological BL level of 1 nM only the inhibitory effect of BL on root growth is observed (Supplemental Fig. S7).

The model parameters $RL(0,0,t)$, $E_{max}(t)$ at discrete t , as well as k_1 , k_2 and k_3 were calibrated with the actual measured root lengths in wild type plants after treatment with BL in increasing amounts. Roots of different ages do not have the same sensitivity to brassinosteroids. Therefore, calibration was done on root lengths of wild type seedlings at 4, 6 and 8 days after germination (DAG). For this, a controlled random search (CRS) parameter fitting procedure was conducted (Price et al., 1976), that found the same minima as a hybrid algorithm consisting of two runs of the MATLAB Genetic Algorithm, a global search algorithm, followed by the MATLAB gradient based search algorithm *lsqnonlin* (Supplemental File 2, Table S2).

Model validation reveals new insights into BRI1 mediated root growth

bri1 mutant roots typically exhibit enhanced resistance towards BL. For modelling purposes this is considered as a reduced concentration of active BRI1. It was therefore of interest to validate our model by varying the BRI1 receptor concentration. The model was first calibrated based on the wild type root length assays, after which the BRI1 receptor concentration was theoretically reduced stepwise to 0 (Fig. 2A). The model predicts that a two-fold reduction will not have a severe effect on root growth, neither at BL concentrations below 1 nM nor at high BL concentration. This is obviously in line with the recessive nature of *bri1* loss-of-function alleles, corroborated here by the experimental evidence showing no difference between wild type seedlings and a segregating population of the *bri1-116* mutant (Fig. 2B). Similar results were obtained for the *bri1-201* mutant (Supplemental Fig. S8). Further theoretical reduction in receptor concentration to 0 nM BRI1 yields roots that are predicted to become completely insensitive towards BL (Fig. 2A). The model also predicts that the root length at 0 nM BRI1 will be about 20% of wild type (Fig. 2A), which is exactly what is observed for real *bri1-116* roots (Fig. 2B).

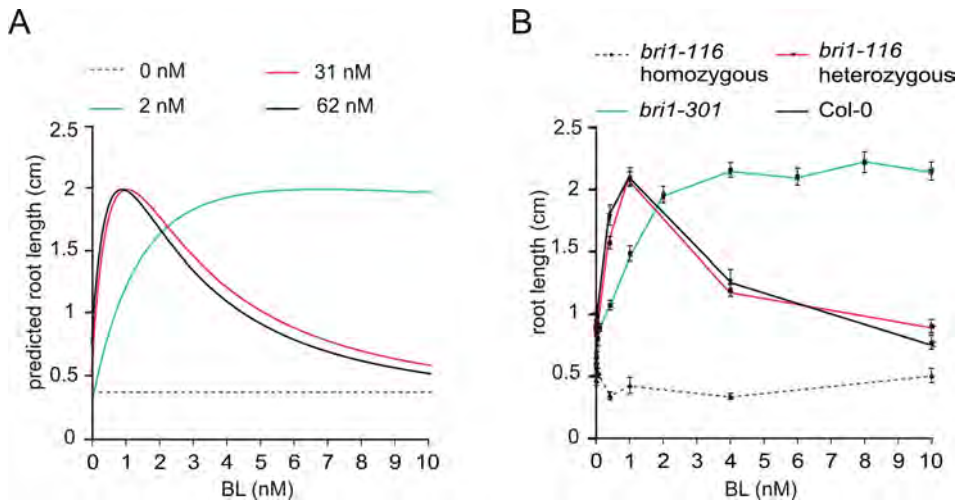


Figure 2. Experimental validation of the mathematical model. A) Model predictions of the root length when only the BRI1 receptor concentration and ligand concentrations are altered. At 62 nM, the model predicts the wild type (Col-0) root length, 31 nM represents the heterozygous *bri1-116* line and the 2 and 0 nM represent respectively the *bri1-301* and the homozygous *bri1-116* lines. B). Experimental verification of the model predictions using wild type, *bri1-116* heterozygotes, *bri1-116* homozygotes and *bri1-301* homozygotes. Error bars represent \pm SEM, $n \geq 30$ roots per data point, measured in three independent replicates.

Interestingly, the model predicts that at an active BRI1 receptor level of about 1-3% of wild type, there is a more severe effect on the inhibition of root growth when compared to the stimulation of root growth. Although it requires much more ligand to obtain the stimulatory effect, eventually such roots will exhibit the same growth as wild type while at high ligand concentrations they exhibit insensitivity (Fig. 2A). This pattern is experimentally demonstrated using the weak *bri1-301* mutant. *bri1-301* harbours a two-nucleotide change (GG-AT) resulting in a Gly989Ile conversion that causes reduced sensitivity towards BL (Xu et al., 2008). When *bri1-301* is exposed to BL in the presence of BRZ there is a stimulatory effect on root growth (Fig. 2B), while roots are insensitive to BL at higher BL concentrations. Assuming a 30-fold decrease in activity of the BRI1 receptor in *bri1-301*, the model output (Fig. 2A) agrees well with the experimental data (Fig. 2B). Similar results were obtained when the root length of seedlings at 4 and 8 DAG was predicted (Supplemental Fig. S9). A striking observation is that below 3 nM BL, wild type root growth is highly sensitive to variation in BL concentration but not very sensitive to moderate reduction in the amount of BRI1 receptor. This suggests that under physiological conditions BR signalling activity depends on ligand availability rather than on receptor density.

As a final validation of the model, the response of the roots towards the less potent ligand HBL was simulated by decreasing the K_d between BRI1 and BL. The

resulting predictions indicate that the slope of the root growth curves and the ligand concentration at which maximum root growth is observed are altered, the eventual root lengths are the same for both BL and HBL (Supplemental Fig. S10 A and B). The model predictions were experimentally corroborated using HBL (Supplemental Fig. S10 C and D).

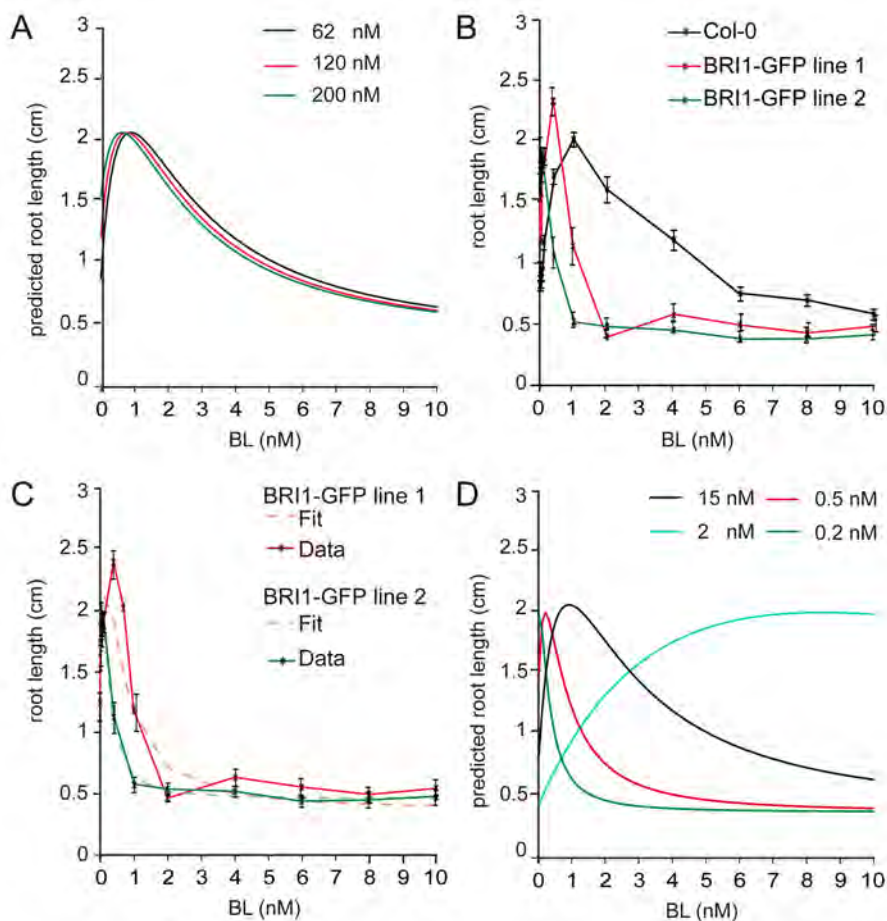


Figure 3. The BRI1-GFP lines are more sensitive to BL. A) Model prediction for the behaviour of a BRI1-GFP line. B) Root length assay of BRI1-GFP line 1 and 2 containing respectively 2 and 3 times more BRI1. The effect of the additional BRI1 copy is more severe than what the model predicts. All points in the graph are shown \pm SEM, $n \geq 30$ roots per data point measured in three independent replicates. C) The model is able to fit the results of the BRI1-GFP lines. All parameters were fit to the BRI1-GFP lines and wild type (Col-0) lines separately. The BRI1 concentrations used for modelling are 62 nM for wild type, 120 nM for BRI1-GFP line 1 and 200 nM for BRI1-GFP line 2. D) The behaviour of BRI1-GFP lines can only be modelled when k_1 , k_2 , and k_3 are altered when compared to the wild type lines. The following values for k_1 , k_2 , and k_3 were used for modelling: 2 nM for wild type, 0.5 nM BRI1-GFP line 1, 0.2 nM BRI1-GFP line 2, and 15 nM for *bri1-301*. The maximum root length E_{max} , and the minimum root length $R(0)$ were respectively 12 and 0.35 cm.

BRI1 kinetics is altered in BRI1-GFP lines

According to the model prediction, an increase of BRI1 receptor should only have a minor effect on root growth (Fig. 3A). To verify this, commonly used BRI1-GFP lines in wild type were used. Surprisingly, actual root growth of BRI1-GFP line 1 and 2 is already inhibited at 0.4 nM and 0.1 nM BL respectively (Fig. 3B). These lines have about two times (120 nM) and three times (200 nM) more BRI1 receptor when compared to wild type line (Chapter 2). In particular for BRI1-GFP line 2, hardly any stimulatory effect is seen while even in the presence of BRZ the roots indeed grow faster than wild type (Geldner et al., 2007). Alternative model structures (Supplemental File S2) were not able to explain the enhanced BL sensitivity observed in the BRI1-GFP lines. These results suggest that there may be an additional component in the pathway not detected in wild type seedling roots. Most likely, upon introduction of another copy of the BRI1 receptor, a normally present rate-limiting component is out-titrated, making these roots almost constitutively sensitive to the ligand. In the model, this would result in a reduction of the k values. To test this hypothesis, we ran the model (Equation 5) now calibrating the system to the BRI1-GFP lines instead of wild type. A good fit was obtained between the model and the actual data set (Fig. 3C). However, this is only obtained when k values are decreased by at least a factor of 4 (Fig. 3D). Therefore, our model unexpectedly reveals that BR signalling in the BRI1-GFP lines is altered in a way that cannot simply be explained at the level of initial ligand-receptor interaction (Supplemental File S3; Fig. S11). Interestingly, an increase in the k values to 15 nM results in a similar trend as observed in the *bri1-301* line (Fig 2B, Fig. 3D). This suggests that the 30-fold reduction of receptor activity predicted for the *bri1-301* line (Fig. 2A and B) could also be due to a failure to interact with a positive regulator. In modelling terms this is the same as a reduction in the total number of functional BRI1 receptors.

Modelling of hypocotyl elongation

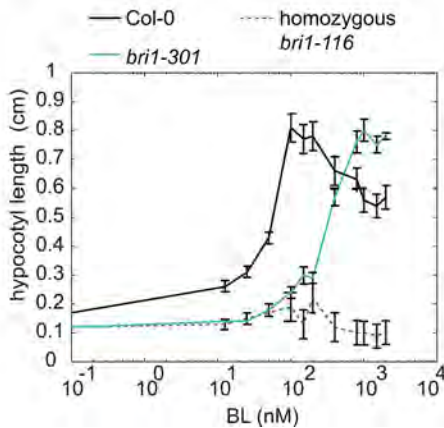
To determine if the developed model is generally applicable to other BRI1-related developmental processes, hypocotyl elongation was used as an alternative physiological read-out. In the presence of BRZ, a clear stimulatory effect of BL on hypocotyl elongation can be observed while inhibition of hypocotyl elongation is observed at 1 μ M BL (Fig. 4A, Supplemental Fig. S12). Different model structures (Supplemental File S2, Table S3, Fig. S13) were evaluated using the same criteria as described for model comparison for the root growth.

Strikingly, only one inhibitory module was sufficient to explain the experimental data, in contrast with the root where two are required. The following model structure was selected, based on a low AIC and BIC score, as well as a good prediction with respect to the *bri-116* null mutant:

$$H(BR11_{tot}, BL_{tot}, t) = H(0,0,t) + \frac{E_{max}(t) * [BR11BL]}{k_1 + [BR11BL]} \frac{k_2}{k_2 + [BR11BL]} \quad (7)$$

Here $H(0,0,t)$ is the measured hypocotyl length at time t in the absence of BRI1 mediated signalling $E_{max}(t)$ the maximum possible hypocotyl length when no inhibitory mechanisms are present, k_1, k_2 and k_3 are the k values. Similar to the root, the model parameters $H(0,0,t)$, $E_{max}(t)$, k_1, k_2 and k_3 were calibrated to the measured hypocotyl lengths in wild type plants, under variation of the BL level. The model was validated using homozygous *bri1-116* and *bri1-301* mutants (Fig. 4B). The BL concentration to which hypocotyls respond is about 10-fold higher when compared to roots. This is in agreement with previous observations showing that the endogenous BR concentration is higher in shoots (Shimada et al., 2003) and requires more exogenous BL (Gou et al., 2012). This implies that in hypocotyls BRI1 receptor occupancy is much higher or the K_d of BRI1 is much lower when compared to the root. A good prediction of the hypocotyl length was only obtained when the K_d was increased from 7.4 nM to almost 1 μ M (Fig. 4B, Supplemental Fig. S12) while a comparable BRI1 receptor density was found in leaf epidermal cells (Chapter 2). Thus, BRI1 has a much lower affinity for BL in the hypocotyl or accessibility to exogenous BL is impaired.

A



B

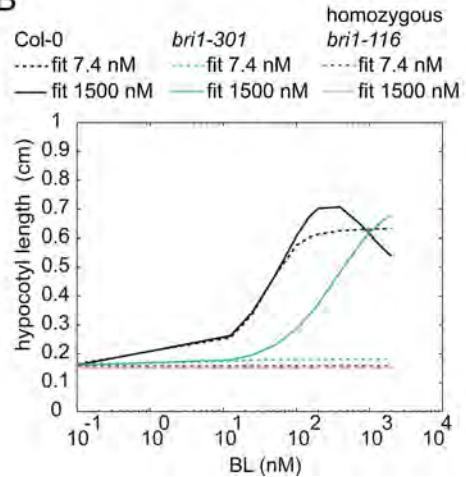


Figure 4. BRI1 receptor occupancy linked to hypocotyl elongation. A) Hypocotyl lengths at different BL concentrations when 1 μ M BRZ is added to the medium. Seedlings were grown for 5 days in the dark after which the hypocotyl length was measured. All points in the graph are shown \pm SEM, $n \geq 15$ hypocotyls per data point measured in three independent replicates. B) A good fit and prediction of the model described in equation 7 was possible when assuming a K_d between 750 and 3000 nM, a total BRI1 concentration of 62 nM for wild type (Col-0) and 0 nM for *bri1-116*. Whereas in *bri1-301* roots a 30-fold reduction in BRI1 activity was predicted, *bri1-301* hypocotyls required only a 6-fold reduction. The graphs show a fit at a K_d value of 7.4 and 1500 nM respectively.

DISCUSSION

This work describes a mathematical approach in which BRI1 receptor activity, expressed as receptor occupancy, is used to model root growth and hypocotyl elongation in *Arabidopsis*. The model parameters employed were tuned on wild type root growth and required a stimulatory and two inhibitory modules. The *in silico* root growth predictions of *bri1* mutants fitted well with the experimental data. A good prediction of *bri1* mutant hypocotyl elongation required a stimulatory and only a single inhibitory module besides an approximately hundred-fold higher BRI1 dissociation constant. Impaired as well as enhanced BRI1 signalling results in shorter roots and reduced hypocotyl elongation. For roots, it was recently proposed that this effect is due to a decrease in meristem size via control of cell cycle progression as well as a reduction in elongation (González-García et al., 2011). This hypothesis is in line with our observation that the best fit and prediction of root growth is obtained when incorporating one stimulatory module and two inhibitory modules. It is attractive to propose that these two inhibitory modules reflect cell expansion and cell division, but no evidence is presently available to support this idea. Hypocotyl elongation is thought to be affected only through cell expansion. It is therefore of interest to note that the use of a single inhibitory module gave the best fit between BRI1-mediated BR signalling and hypocotyl elongation. Clearly, our model is applicable to BR-controlled responses in general.

In *Arabidopsis*, there are various mathematical models that describe plant architecture in terms of auxin signalling. These models are used to study the effect of polarised auxin transport resulting in local auxin maxima to evaluate root growth or auxin mediated signalling on the shoot apex (Grieneisen et al., 2007; Laskowski et al., 2008; Vernoux et al., 2011). Kinetic models of auxin mediated signal transduction have resulted in the identification of genes involved in auxin/ ethylene/cytokinin crosstalk and the effect of auxin/ cytokinin cross talk in cell fate determination (Liu et al., 2010; Muraro et al., 2011). In case of brassinosteroid signalling, mathematical modelling is applied to evaluate auxin/ brassinosteroid cross talk (Ibañez et al., 2009; Sankar et al., 2011). Boolean logics have been used to analyse auxin and brassinosteroid gene networks, which led to new insights in the role of the *BREVIX RADIX* (*BRX*) gene in BR and auxin signalling (Sankar et al., 2011). In shoots radial patterning of vascular bundles is controlled by auxin polar transport and BR signalling. Ibañez *et al* (2009) used mathematical modelling combined with quantitative biological data. Their model uses the appearance of DR5::GUS expression as readout for auxin maxima whereas detailed studies of the vascular bundle patterning on various auxin transporter and *bri1* mutants was used to evaluate the effect on radial patterning. However, to our knowledge none of the modelling studies in *Arabidopsis* so far completed have employed biochemical activity of a key component as starting point. Therefore, the mathematical

description of BRI1-mediated BR signalling in root growth as described here represents a novel approach in plant modelling.

At physiological concentration, ligand availability rather than receptor concentration apparently determines BRI1-mediated BR signalling activity in roots. In addition, less than 1% of the total number of BRI1 receptors is occupied by ligand under these conditions. This does not appear to be unusual, as it is reported for many animal systems as well. Epidermal growth factor (EGF) binding to its receptor (EGFR) triggers a full cellular response when less than 1% of the receptors is occupied (Wiley et al., 1989; Uyemura et al., 2005; Teramura et al., 2006). In EGFR mediated signalling, ligand-independent signal propagation is important (Verveer et al., 2000) and thought to be occurring at increased receptor density (Sawano et al., 2002). Clustering of receptors is important in autocrine signalling (DeWitt et al., 2001), while the ratio between high and low affinity EGF receptors in the plasma membrane also assumes a large number of non-ligand binding receptors (Kuszynski et al., 1993). It has been proposed that EGFR affinity for EGF is reduced due to negative cooperatively (Macdonald and Pike, 2008; Alvarado et al., 2010), resulting in more single occupied homodimers at low ligand concentration, and double occupied homodimers at high ligand concentration (Macdonald et al., 2008). EGFR is capable of regulating distinct biological processes, depending on the ligand and its concentration (Krall et al., 2011). In this model, the presence of a large number of unoccupied receptors could function as a mechanism to differentiate between downstream pathways served in the hour-glass model of EGF (Citri and Yarden, 2006; Warren and Landgraf, 2006). In the case of BR signalling in Arabidopsis root cells, it is not clear whether unoccupied BRI1 receptors contribute to a physiological response. It was therefore of interest to find that the switch between activation and inhibition of root growth depends on the BRI1 occupancy level. This implies that, like EGFR, BRI1 might function as a core regulator capable of activating multiple target proteins resulting in the activation of different genes dependent on the activated target.

Endocrine signalling pathways in animals often employ receptor availability in target cells as a means to regulate responses. Given our previous observation that BRI1 receptor density is kept constant throughout the root meristem (Chapter 2), it is unlikely that differential receptor density is an important mechanism in BR signalling. Our modelling suggests that at least a 10-30 fold reduction in BRI1 concentration is required to markedly change the BR signalling output. Taken together, ligand availability appears to be a more restrictive factor. In this respect it is of interest to note that brassinosteroids appear to be largely immobile. This is based on the observation that cell type specific expression in epidermal cells of BR synthesis can rescue the stature phenotype, while expression in vascular cells does not (Savaldi-Goldstein et al., 2007). A similar scenario was developed

for the root meristem, where again the importance of the epidermis was noted as an important source of BR signalling activity (Hacham et al., 2011). Because all of the cells in shoots and in roots have BRI1 receptors, it was suggested that other diffusible BR pathway related signals exist (Savaldi-Goldstein et al., 2007). Unexpectedly, simulation experiments revealed that the properties of BR signalling are altered in commonly used BRI1-GFP reporter lines. The extra copy of the BRI1 gene results in a higher ligand sensitivity of the roots than predicted. To explain this, we propose that a negative regulator is out-titrated rendering the roots almost constitutively sensitive to BRs. Alternatively, the GFP tag on the C-terminal end of BRI1 may interfere with the interaction with downstream targets, similar to what has been demonstrated for BAK1 (SERK3), one of the BRI1 co-receptors (Ntoukakis et al., 2011). In modelling terms both mechanisms would result in a change in half maximum response values. Interestingly, this is corroborated by the mathematical model that demonstrates that these values are indeed altered in the BRI1-GFP reporter lines. The *bri1-301* mutant has a reduced sensitivity towards BRs (Xu et al., 2008), and is unable to transphosphorylate BAK1 (Kang et al., 2010). This indicates that the *bri1-301* protein is hampered in its interaction with a positive regulator of the BRI1 signalling pathway, as predicted by our model. Recently, it has been reported that the early events in BRI1 signalling almost completely depend on the activity of the SERK co-receptor family (Gou et al., 2012). The model of BRI1 mediated BR signalling presented here is a starting point for more extended mathematical models to fit existing and new components of the BRI1 signalling pathway in a precise cellular context.

EXPERIMENTAL PROCEDURES

Plant lines and growth conditions

Arabidopsis thaliana plants (ecotype Columbia (Col-0)) were used in all growth assays for calibrating the mathematical model. The *bri1* null mutants *bri1-116* (Li and Chory, 1997) and *bri1-201* (Bouquin et al., 2001), the weak allele *bri1-301* (Xu et al., 2008) and two transgenic *BRI1-GFP* lines (Friedrichsen et al., 2000; Geldner et al., 2007) were used to verify the mathematical model. For more details on the plant lines used and genotyping information see Supplemental File S4. Freshly harvested seeds were surface-sterilised for 10 minutes in 10% (v/v) bleach in ethanol after which the seeds were washed 3 times with ethanol and dried before plating. The seedlings were grown vertically under fluorescent light with 16-h-light/8-h-dark photoperiods on half strength Murashige and Skoog medium (Duchefa, Haarlem, the Netherlands) supplemented with 1% Sucrose (Sigma-Aldrich chemie, Steinheim, Germany), 0,1% MES (Sigma-Aldrich) and 0,8% agar. To equalise germination, the plates were kept in the dark at 4°C for two days before they were placed into the light. For the root growth assays the germinating medium was supplemented with 1 μ M or 5 μ M BRZ (ICT) and various concentrations of 24-BL (Sigma-Aldrich) or HBL (Sigma-Aldrich). For wild type lines, no significant difference between 1 μ M and 5 μ M BRZ was observed (Supplemental Fig. 11). For the hypocotyl assays, the germinating medium was supplemented with 1 μ M BRZ and supplemented with various concentrations of BL. Hypocotyl lengths were measured after 5 days growth in the dark. For all assays, at least 3 independent replicates were performed measuring 5-10 roots or hypocotyls per assay ($n \geq 15$ roots or hypocotyls in total). All values are shown \pm the standard error of mean (SEM), error bars indicate SEM.

Software and modelling

The model was programmed in MATLAB, version 7.8 (MathWorks). The model parameters $RL(0,0,t)$, $E_{\max}(t)$, k_1 , k_2 and k_3 were calibrated on wild type root length of seedlings at 4, 6 and 8 DAG under varying BL concentrations. E_{\max} and $R(0,0,t)$ are two functions of time. Per time point t they are regarded as free parameters. More details on the parameter estimation method can be found in Supplemental file S1. A K_d value of 7.4 nM (Wang et al., 2001) was used for all modelling experiments. To obtain an optimal fit between the mathematical model and the biological data set several models were explored. More details about the different models tested and the criteria for model selection can be found in Supplemental File S1 and S2. Estimates of endogenous BRI1 and BL levels are discussed in Supplemental File S4.

ACKNOWLEDGEMENTS

The authors thank Joanne Chory for providing *BRI-GFP* line 2 and the *bri1-116* mutant, Niko Geldner for providing *BRI1-GFP* line 1, John Mundy for providing the *bri1-201* line and Yonghong Wang for providing the *bri1-301* line.

SUPPLEMENTAL FILES

Supplemental file 1

Model structures

The model part that describes the relation between receptor activity and growth is largely phenomenological. In order to see what complexity is needed to describe this pathway, the following model structures were compared with respect to model complexity, data fit and predictive power:

Model 1. single stimulation, double inhibition (equation 5 in used for modelling root growth in main manuscript)

$$R(BRI1_{tot}, BL_{tot}, t) = R(0, 0, t) + \frac{E_{max}(t) \cdot [BRI1BL]}{k_1 + [BRI1BL]} \cdot \frac{k_2}{k_2 + [BRI1BL]} \cdot \frac{k_3}{k_3 + [BRI1BL]}.$$

Model 2. double stimulation, double inhibition

$$R(BRI1_{tot}, BL_{tot}, t) = R(0, 0, t) + \frac{E_{max}(t) \cdot [BRI1BL]}{k_1 + [BRI1BL]} \cdot \frac{[BRI1BL]}{k_4 + [BRI1BL]} \cdot \frac{k_2}{k_2 + [BRI1BL]} \cdot \frac{k_3}{k_3 + [BRI1BL]}.$$

Model 3. double stimulation, single inhibition

$$R(BRI1_{tot}, BL_{tot}, t) = R(0, 0, t) + \frac{E_{max}(t) \cdot [BRI1BL]}{k_1 + [BRI1BL]} \cdot \frac{[BRI1BL]}{k_2 + [BRI1BL]} \cdot \frac{k_3}{k_3 + [BRI1BL]}.$$

Model 4. single stimulation, single inhibition (equation 7 used for modelling hypocotyl elongation in main manuscript)

$$R(BRI1_{tot}, BL_{tot}, t) = R(0, 0, t) + \frac{E_{max}(t) \cdot [BRI1BL]}{k_1 + [BRI1BL]} \cdot \frac{k_2}{k_2 + [BRI1BL]}.$$

Model 5. single stimulation

$$R(BRI1_{tot}, BL_{tot}, t) = R(0, 0, t) + \frac{E_{max}(t) \cdot [BRI1BL]}{k_1 + [BRI1BL]}.$$

Model 6. single inhibition

$$R(BRI1_{tot}, BL_{tot}, t) = R(0, 0, t) + \frac{E_{max}(t) \cdot k_1}{k_1 + [BRI1BL]}.$$

Model 7. triple stimulation, double inhibition

$$R(BRI1_{tot}, BL_{tot}, t) = R(0, 0, t) + \frac{E_{max}(t) \cdot [BRI1BL]}{k_1 + [BRI1BL]} \cdot \frac{[BRI1BL]}{k_2 + [BRI1BL]} \cdot \frac{[BRI1BL]}{k_3 + [BRI1BL]} \cdot \frac{k_4}{k_4 + [BRI1BL]} \cdot \frac{k_5}{k_5 + [BRI1BL]}.$$

Model 8. double stimulation, triple inhibition

$$R(BRI1_{tot}, BL_{tot}, t) = R(0, 0, t) + \frac{E_{max}(t) \cdot [BRI1BL]}{k_1 + [BRI1BL]} \cdot \frac{[BRI1BL]}{k_2 + [BRI1BL]} \cdot \frac{k_3}{k_3 + [BRI1BL]} \cdot \frac{k_4}{k_4 + [BRI1BL]} \cdot \frac{k_5}{k_5 + [BRI1BL]}.$$

Model 9. triple stimulation, triple inhibition

$$R(BRI1_{tot}, BL_{tot}, t) = R(0, 0, t) + \frac{E_{max}(t) \cdot [BRI1BL]}{k_1 + [BRI1BL]} \cdot \frac{[BRI1BL]}{k_2 + [BRI1BL]} \cdot \frac{[BRI1BL]}{k_3 + [BRI1BL]} \cdot \frac{k_4}{k_4 + [BRI1BL]} \cdot \frac{k_5}{k_5 + [BRI1BL]} \cdot \frac{k_6}{k_6 + [BRI1BL]}.$$

Model 10. single stimulation, triple inhibition

$$R(BR1_{tot}, BL_{tot}, t) = R(0, 0, t) + \frac{E_{max}(t) \cdot [BR1BL]}{k_1 + [BR1BL]} \frac{k_2}{k_2 + [BR1BL]} \frac{k_3}{k_3 + [BR1BL]} \frac{k_4}{k_4 + [BR1BL]}$$

Model 11. triple stimulation, single inhibition

$$R(BR1_{tot}, BL_{tot}, t) = R(0, 0, t) + \frac{E_{max}(t) \cdot [BR1BL]}{k_1 + [BR1BL]} \frac{[BR1BL]}{k_2 + [BR1BL]} \frac{[BR1BL]}{k_3 + [BR1BL]} \frac{k_4}{k_4 + [BR1BL]}$$

Here $R(0, 0, t)$ is the root length at time point t without BR signalling, $E_{max}(t)$ is the maximum root length at time point t , $[BR1BL]$ is the concentration of BR1 occupied by ligand and k_1, k_2, k_3, k_4, k_5 and k_6 are the half maximum response values. For all models it was assumed that there is still a small amount (0.1 nM of total BRs, simplified to BL only) present in the roots after addition of BRZ.

The different model structures were compared using the Akaike information criterion (AIC) and the Bayesian information criterion (BIC).

$$AIC = S(\theta) + 2p + \frac{2p(p+1)}{n-p-1} \quad (S1)$$

$$BIC = S(\theta) + p \log(n) \quad (S2)$$

These two error criteria are based on the weighted residual sum of squares $S(\theta)$ obtained from the parameter estimation (Supplemental File S2), the total number of parameters to be estimated (p) and the number of data points (n). The main difference between the AIC and BIC criterion is that the BIC penalises the number of free parameters p more (Klipp et al., 2009).

In the roots, models with only one module (models 5 and 6), or with less than two inhibitory modules (models 3, 4 and 11) have a significantly higher AIC and BIC scores, as well as a higher fitting error, clearly indicating a minimal necessary model complexity (Supplemental Table S1). Incorporation of at least one stimulatory module and two inhibitory modules is optimal for modelling the effect of BL on root growth. Incorporation of more than 2 stimulatory or more than 2 inhibitory modules (models 7, 8 and 9) can give similar AIC and BIC numbers as models 1 and 2. To make a well-founded model selection, the predictive power with respect to the *bri-116* null mutant was also taken into account. From the models 1, 2, 7, 8 and 9, model 1 gives the best prediction and was therefore selected.

In the hypocotyl, only one inhibitory module is required for a good fit (Supplemental Table S3). Models with one module in total still have significantly higher AIC and BIC scores. Similar to the situation in roots, the predictive power was taken into account for model selection. The differences between the models are smaller than for the models tested for the root data. However, since model 4 has the second lowest AIC score and the best prediction, this model was selected.

Supplemental File 2

Parameter estimation

The unknown parameters R (0,0,t), $E_{\max}(t)$, and the k values are estimated using a controlled random search algorithm (CRS; Price et al., 1976) and a hybrid algorithm consisting of two runs of the MATLAB global search algorithm called Genetic Algorithm, followed by the MATLAB gradient based search algorithm lsqnonlin. Both algorithms yielded similar parameter estimates (Table S2). Here the object function and the CRS method are discussed.

The maximum likelihood estimate in equation [4] is obtained by minimising the object function:

$$S(\theta) = \sum_i \left(\frac{R(BRI1_{tot}, BL_{tot}(i), t, \theta) - R_i}{\sigma_i} \right)^2, \quad (S3)$$

where i is the index over the BL concentrations, $R(BRI1_{tot}, BL_{tot}(i), t, \theta)$ the predicted root lengths at time t for concentrations $BL_{tot}(i)$ based on the initial parameter vector θ , R_i the measured root lengths, and σ the standard deviation of assumed normally distributed noise on the data points. The main idea behind this algorithm is that, starting with an initial collection of parameter vectors, CRS repeatedly draws a new parameter vector that replaces a vector in the collection if its corresponding data fit is better. The CRS method starts by taking a random set of n_Q parameter vectors inside a search domain D and continues by computing the corresponding values of the object function. The bounds of D represent the *a priori* limits for the parameters. From this list of n_g vectors, a new vector is chosen using the rule

$$\theta_{new} = 2\bar{\theta}_{rand} - \theta_{rand} \quad (S4)$$

where θ_{rand} is a random vector from the list, and $\bar{\theta}_{rand}$ is the average of a random subset of p vectors in the list. To ensure that the new vectors are selected with equal preference over the logarithmic space, [S4] is modified element wise to

$$S(\theta_{new}) < \max(S(\theta)) \quad (S4)$$

If $S(\theta_{new}) < \max(S(\theta))$, and $\theta_{new} \in D$, the parameter vector with the maximum object function is replaced by the new one:

$$\theta | \{S(\theta) = \max(S(\theta))\} \rightarrow \theta_{new}$$

By repeating this, the worst fitting parameter vectors are removed continuously and replaced by ones with a better fit. Eventually, the points will form a cloud that gets denser and denser. The algorithm stops when

$$\max(S(\theta)) \leq s_C \cdot \min(S(\theta)) \quad (\text{S5})$$

with s_c the stop criterion. So the worst fit has an at most $100(s_C - 1)$ % larger S value than that of the best fit. We used the following values: $s_c = 1.0001$, $n_o = 800$, and $D = [10^{-3}, 10^3]$ for each parameter.

Supplemental File 3**The k values are altered in BRI1-GFP reporter lines.**

The model is not able to predict the behaviour of the BRI1-GFP reporter lines. Only a decrease in the half maximum response values can explain the increased sensitivity of these lines. There are two possible causes for an altered half maximum response value. First, a rate limiting component can be out titrated, thereby making these lines hypersensitive to the ligand. Second, there can be a higher residual BL concentration after BRZ treatment in the BRI1-GFP reporter lines, when compared to the wild type lines. The latter will result in a stronger response of the lines towards exogenously applied BL. To ensure that this is not due to a higher level of leftover endogenous BL after BRZ treatment, measurements were repeated with a BRZ concentration of 5 μM instead of 1 μM (Fig. S11). Although this further reduced the root length of the BRI1-GFP reporter lines, the model was still not able to predict the behaviour of the BRI1-GFP reporter lines. Therefore, predicted decrease in k value in these lines is likely due to shortage of a negative regulator.

Supplemental File 4

Supplemental Materials and Methods

Plant lines and growth conditions

In the root growth assays, the homozygous *bri1-116* and *bri1-201* lines were scored on the cabbage phenotype on 20-day-old seedlings. To evaluate if there was a difference between wild type and the heterozygous pool of *bri1-116* and *bri1-201*, only the non-cabbaged plants were taken into account. As proof of principle, individual plants ($n \geq 25$ plants) were genotyped to confirm the plant was homozygous or heterozygous for the mutation. Genotyping was performed by PCR using the following primer combinations: *bri1-201* mutant forward (TCAAGCTTCTGTAAACAA) or *bri1-201* wild type forward (GCTTCTTTCTCTCTGTAAAC)/ BRI1-LRR reversed (GGAGATTGATTGCGAGAAAGATCCAG). Genotyping of the *bri1-116* line was done by PCR amplification using the following primer combination: forward (CGAATCACTCGCGTTGTGAGTAACAAC)/ reversed (CCAACTCCGCCTCTTTCTTTCTCC) followed by a cleaved amplified polymorphism (CAP) marker digest of the PCR fragment using *PmeI* (New England Biolabs).

Approximation of endogenous BL levels

In wild type *Arabidopsis* the endogenous castasterone concentration has been reported to be 0.03-0.05 ng g⁻¹ fresh weight in roots (Bancos et al., 2002; Shimada et al., 2003). To correlate these values to a BR concentration in mol l⁻¹ the following data were used; a root of a 5-day-old seedling cut just below the hypocotyl weighs 0.18 ± 0.3 (SEM) mg (Chapter 2), and contains 95.7 ± 0.3 (SEM)% moisture. For determination of the moisture content in 5 day old seedling roots, fresh roots were weighted on pre-dried and weighted aluminium dishes (Sartorius microbalance). The samples were dried for at least 15 hours in a pre-warmed oven at 100-110 °C. To ensure that the roots did not absorb moisture after drying, roots were cooled down in a desiccator for 1 hour at room temperature. The weight of the dried roots was determined immediately after removal from the desiccator. At least 300 roots were used for each measurement ($n = 5$). Assuming that the ligand concentrations in a seedling root are within the same range as published (Bancos et al., 2002; Shimada et al., 2003), it was estimated that a wild type root of an *Arabidopsis* seedling contains 0.06-0.1 nM BL.

BRI1 receptor availability in Arabidopsis roots

Recently it has been reported that the BRI1-GFP receptor density in BRI1 reporter line 1 is 12 receptors μm^{-2} (Chapter 2). The BRI1-GFP reporter line contains exactly the same amount of BRI1-GFP as native BRI1 as has been demonstrated by Western blot analysis (Geldner et al., 2007). Thus, this line contains in total 24 receptors μm^{-2} , when the amount of wild type receptor present is taken into account. Using this data, three different lines with three different receptor concentrations are available, the wild type line containing 12 receptors μm^{-2} , BRI1-GFP line 1 with 24 receptors μm^{-2} , and BRI1-GFP line 2 containing 44 receptors μm^{-2} . This corresponds to a concentration of respectively 62 nM, 120 and 200 nM BRI1, taking into account BRI1 receptors at the plasma membrane and in the endosomal vesicles close to the plasma membrane. It was assumed that the total BRI1 concentration in the hypocotyl is similar to that in the root.

SUPPLEMENTAL FIGURES AND TABLES

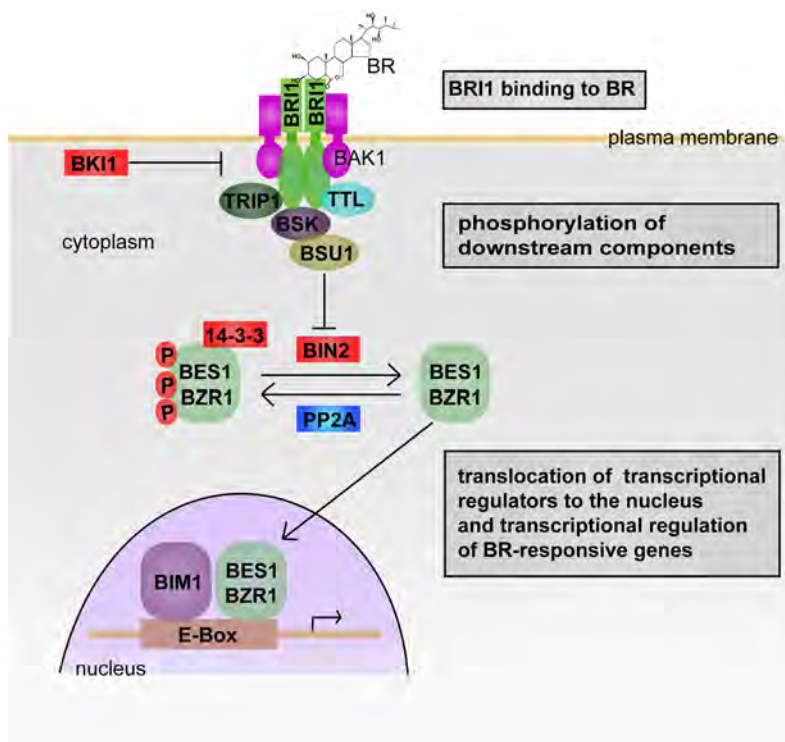


Figure S1. Schematic representation of BRI1 mediated BR signalling. Binding of BR to the BRI1 receptor results in the dissociation of BKI. Subsequently, BRI1 phosphorylates and activates BAK1 resulting in phosphorylation of downstream targets such as BSKs, Arabidopsis TGF- β receptor-interacting protein-1 (TRIP-1) and transthyretin-like protein (TTL). The phosphorylated BSKs enable interaction with BSU1, which inhibits BIN2 kinase while PP2A dephosphorylates BZR1 and possibly BES1. This cascade results in the accumulation of dephosphorylated BES1/BZR1 in the nucleus, where they can interact with other transcriptional regulators (e.g. BES1-interacting Myc-like 1; BIM1) to regulate the expression of various BR responsive genes. Model according to Ye et al., (2011).

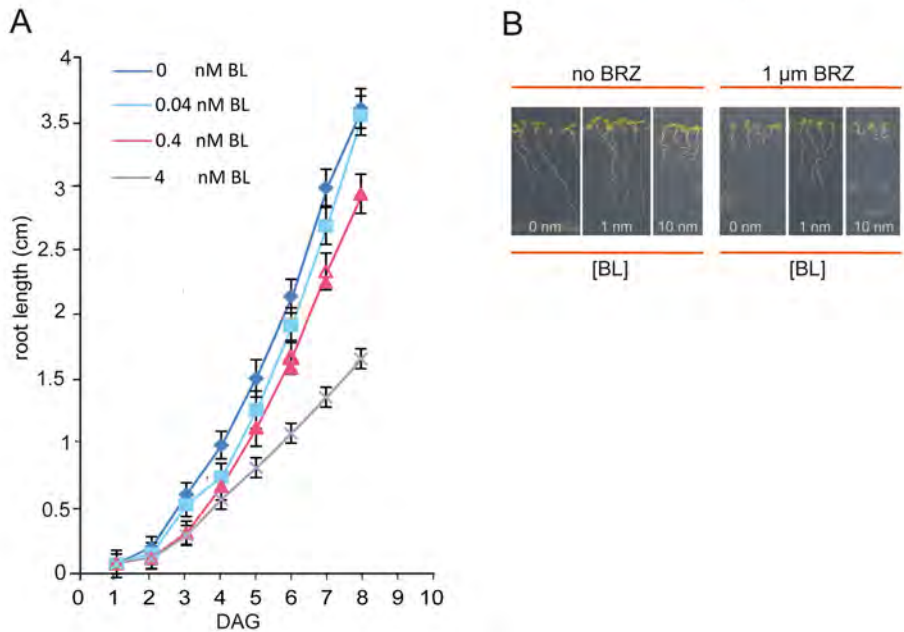


Figure S2. Root length assay on wild type lines in the absence of BRZ. A) Difference in growth in days after germination (DAG) of wild type seedlings after application of various concentrations BL. The stimulatory effect of BL is hard to visualise when BRZ, a biosynthetic inhibitor for BRs, is not added to the medium. B) Seedlings treated with BL (left panel) or BL and BRZ (right panel). Representative roots are shown at 8 DAG. After application of BRZ, a clear stimulatory effect of BL on root growth is observed.

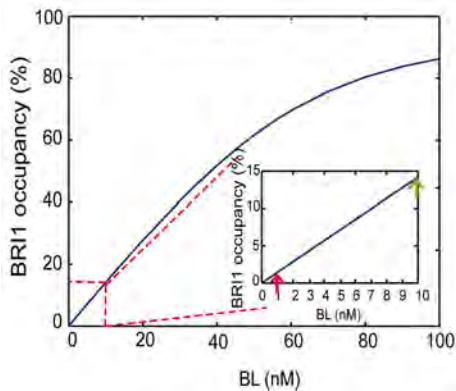


Figure S3. BRI1 receptor occupancy levels at physiological ligand concentration. At root growth stimulatory ligand concentrations around 1 nM the BRI1 receptor occupancy is less than 1% (indicated by the red arrow). The root growth is completely inhibited at a BL level of 10 nM. At this concentration around 14% of the total number of BRI1 receptors is occupied (green arrow).

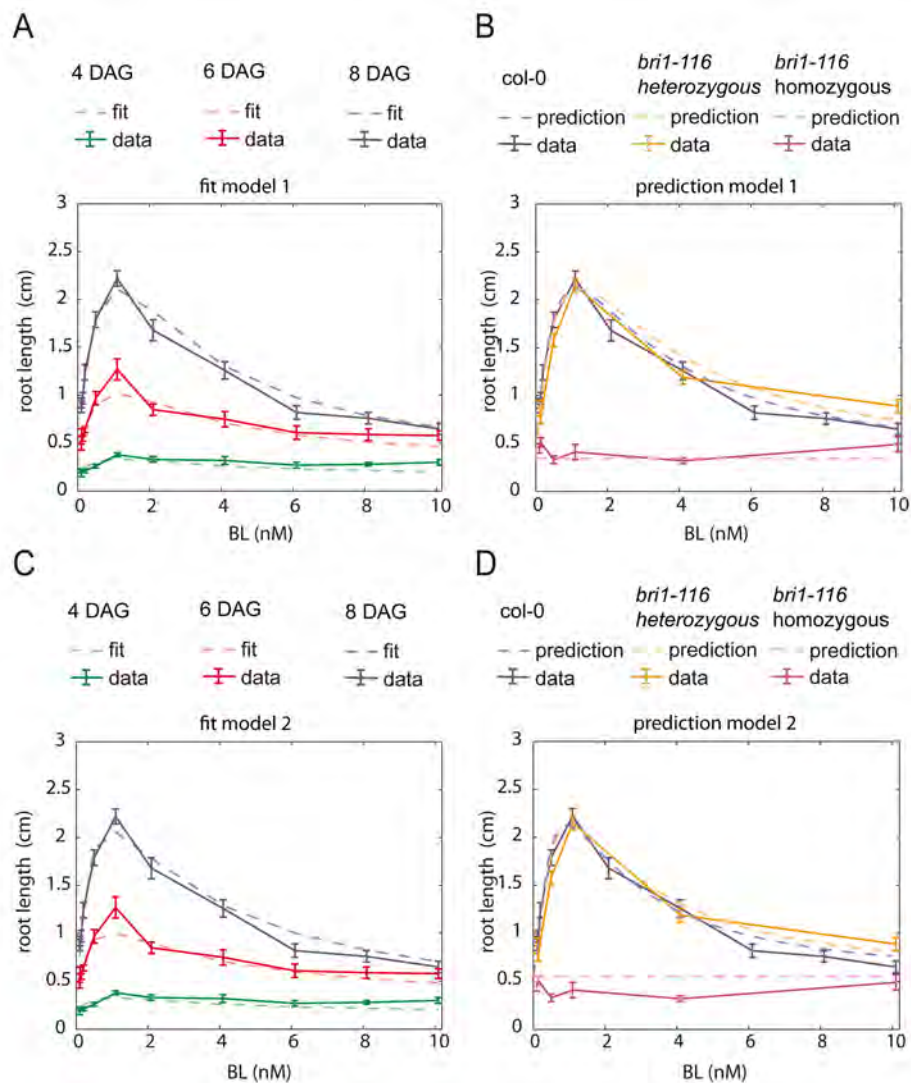


Figure S4. Model fit and predictions model number 1 and 2. Fit of model 1 (A) and 2 (C) to the root length of seedlings at 4, 6 and 8 days after germination. Model 1 consists of one stimulatory module and two inhibitory modules, model 2 has two stimulatory modules and one inhibitory module (B and D). Model 1 (B) gives a reliable prediction of the root length at 8 DAG of *bri1-116* null mutants and *bri1-116* heterozygous lines whereas model 2 (D) predicts a slightly higher value.

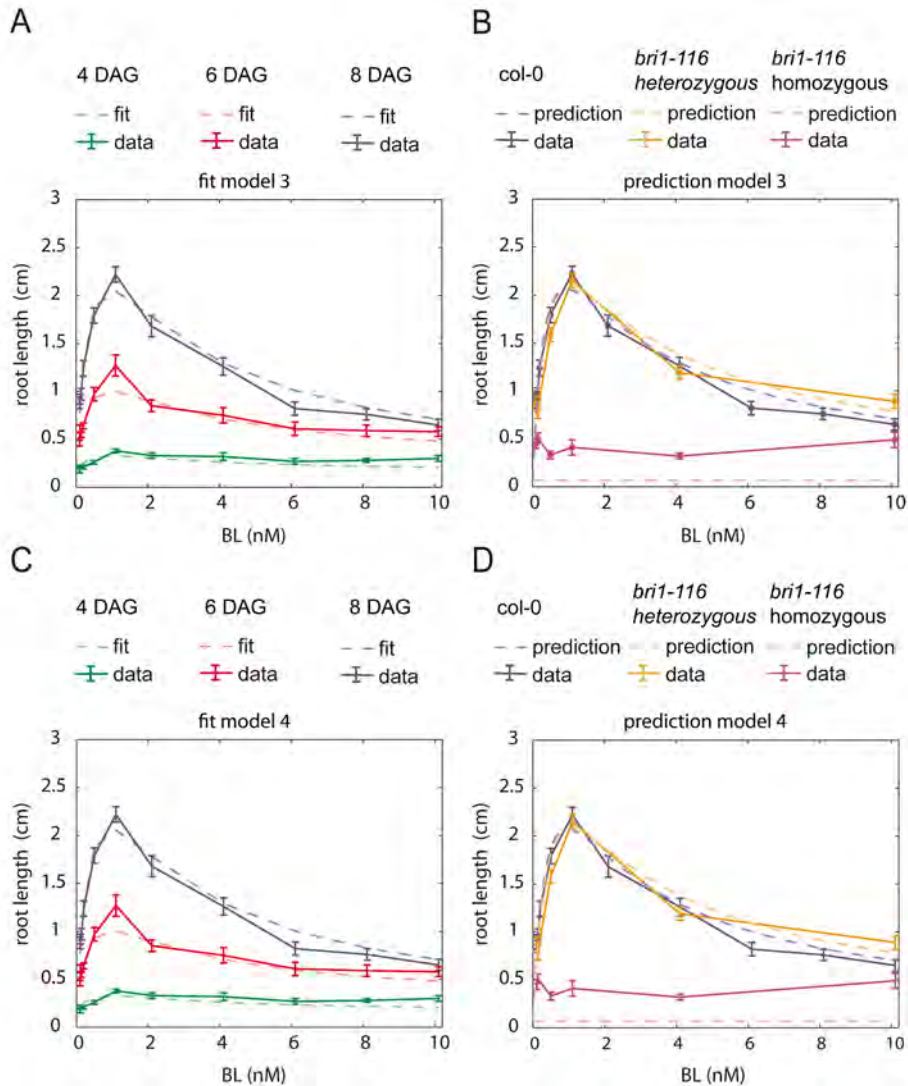


Figure S5. Model fit and predictions model number 3 and 4. Fit of model 3 (A) and 4 (C) to the root length of seedlings at 4, 6 and 8 days after germination. Model 3 consists of two stimulatory modules and one inhibitory module, model 4 has one stimulatory module and one inhibitory module. Models 3 (B) and 4 (D) give a reliable prediction of the root length at 8 DAG of *bri1-116* heterozygous lines. The root length of *bri1-116* null mutants at 8 DAG could not be predicted with models 3 and 4.

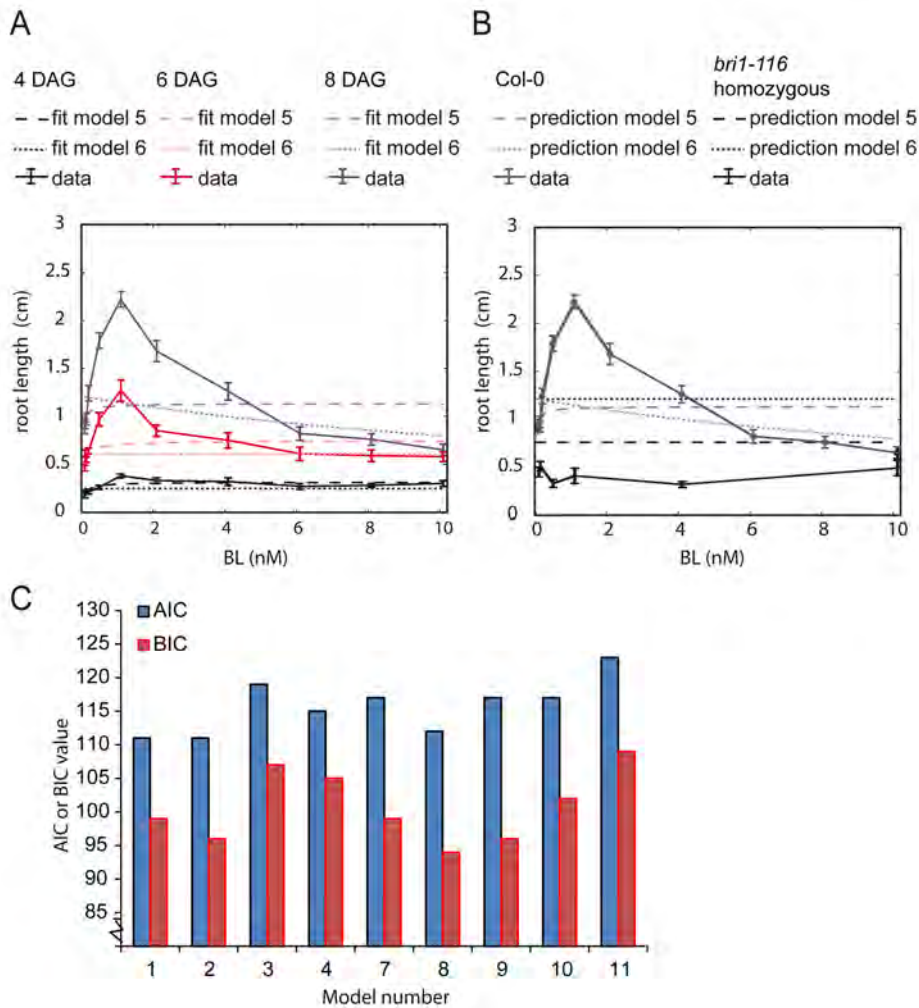


Figure S6. Modelling stimulation as well as inhibition is essential for a good fit and prediction of root length. A) Fit of models 5 and 6 to the root length of seedlings at 4, 6 and 8 days after germination (DAG). Model 5 consists of one stimulatory module, model 6 has one inhibitory module. B) Neither model 5 nor model 6 was able to predict the root length of wild type (Col-0), *bri1-116* null mutants and *bri1-116* heterozygous lines. C) Akaike information criterion (AIC) and the Bayesian information criterion (BIC) values when models 1-4 and 7-11 are fitted to root length of seedlings at 4,6 and 8 DAG.

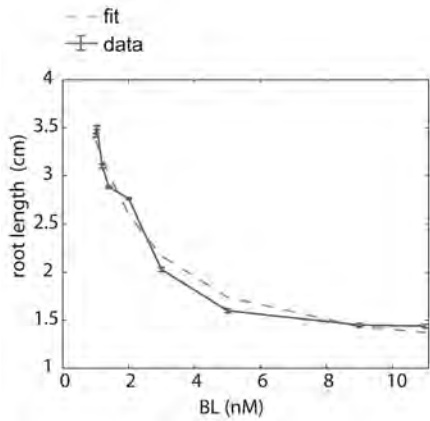


Figure S7. Fit between model 1 and wild type after BL stimulation in the absence of BRZ. Fit between the model and experimental data set assuming an endogenous BR level of 1 nM BL. Error bars \pm SEM; $n \geq 15$ root measured in three independent replicates.

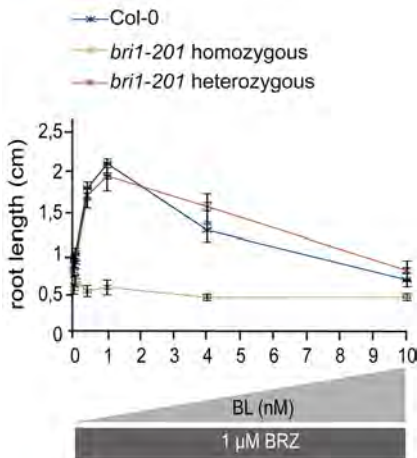


Figure S8. Root length assays on heterozygous and homozygous *bri1-201* null mutants.

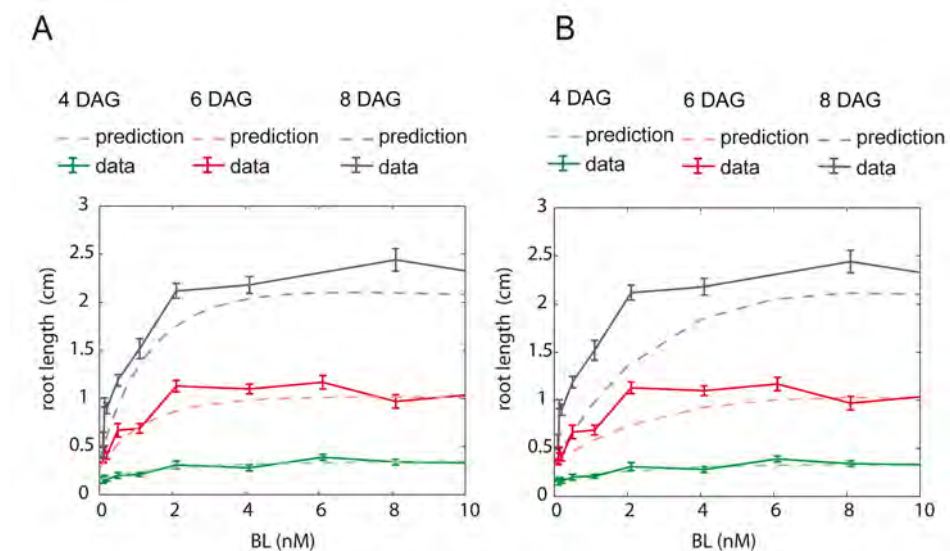


Figure S9. Root length of *bri1-301* at 4 and 6 and 8 days after germination. A) Model predictions versus experimental data at 4, 6 and 8 days after germination. The model is calibrated on wild type (Col-0) lines. Prediction of the *bri1-301* line is done by assuming that the total number of BRI1 receptors actively signalling is 2 nM. B) Similar results as in (A) are obtained when the half maximum response values, k_1 , k_2 and k_3 are increased to 15 nM.

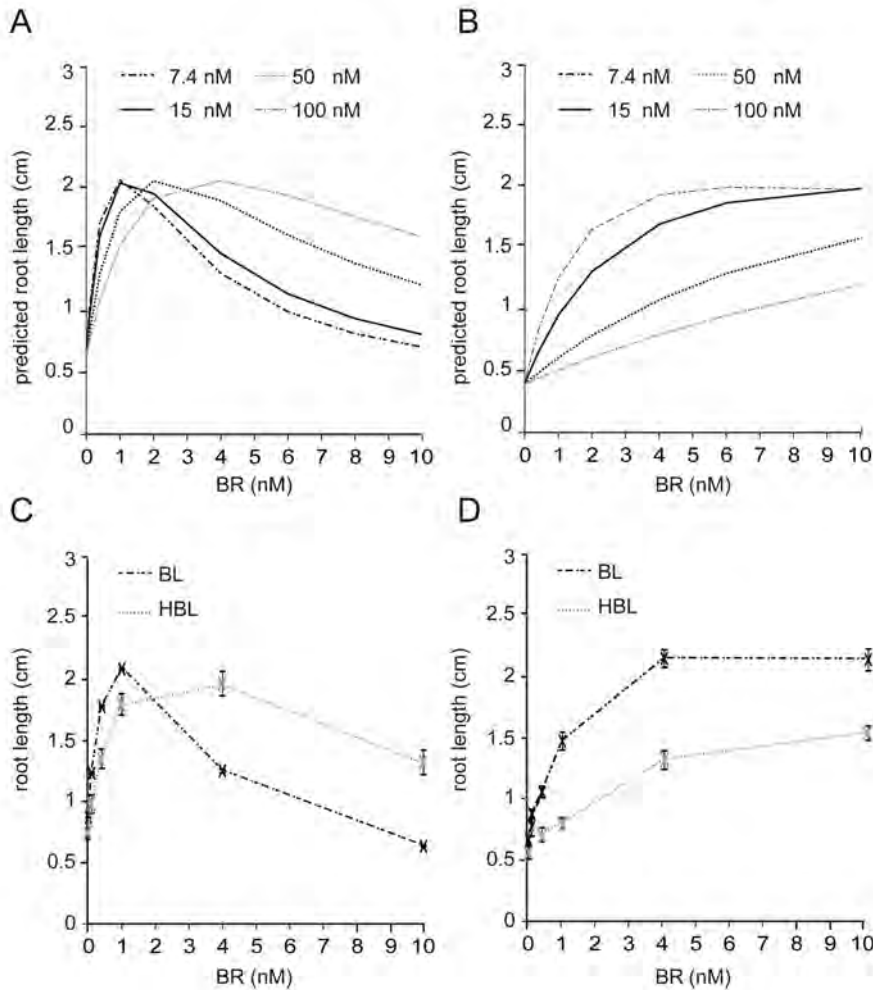


Figure S10. Model predicts root growth in response towards less potent ligand. A and B) The root growth of 8-day old wild type (Col-0; A) and *bri1-301* (B) seedlings when stimulated with a less potent ligand as predicted by *in silico* experiments. The Kd is altered from 7.4 till 100 nM. (C and D) Actual root growth when wild type (C) or *bri1-301* (D) roots are grown on the less potent ligand HBL compared to root growth on BL. Error bars \pm SEM, $n \geq 20$ roots per data point, measured in three independent replicates.

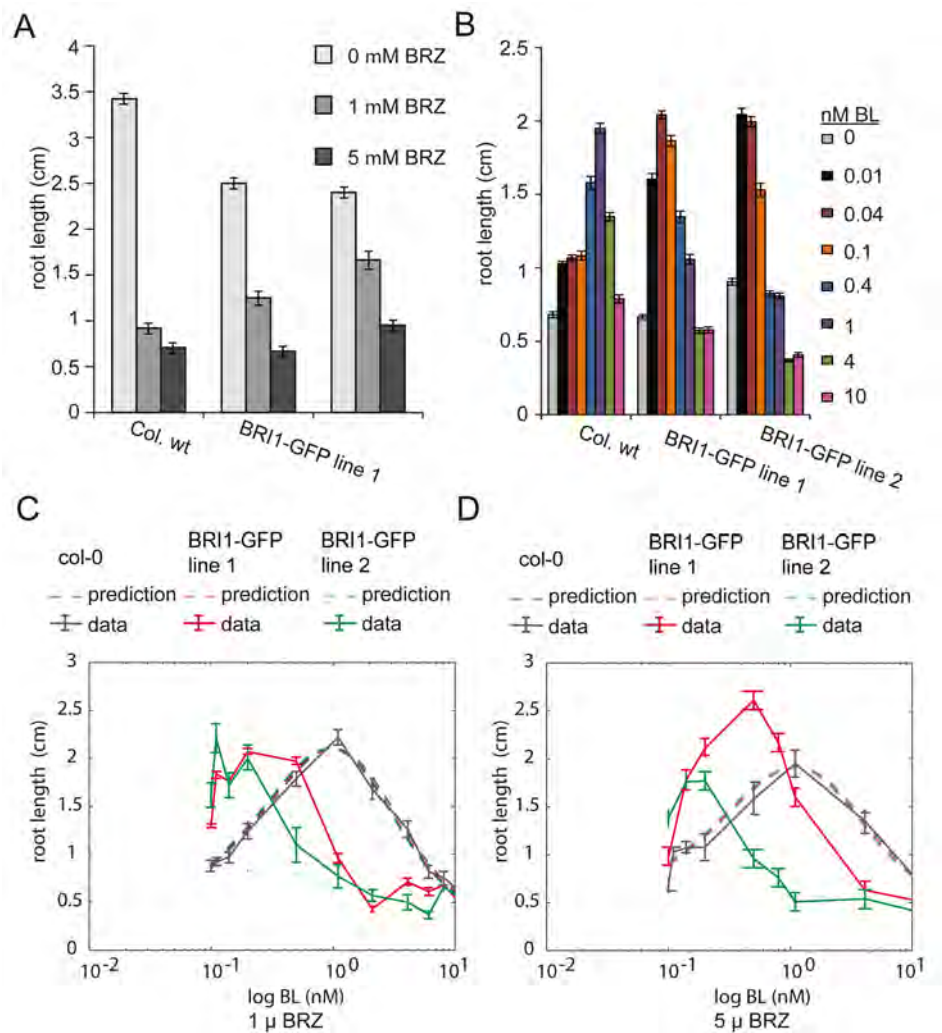


Figure S11. Root growth assays on BRI1-GFP reporter lines in presence of 5 μ M BRZ. A) BRI1-GFP reporter lines are less sensitive towards BRZ when compared to wild type (Col-0). B) In the presence of 5 μ M BRZ the BRI1-GFP reporter lines remain hypersensitive to BL, causing a rapid increase in root length at 0.04 nM BL (BRI1-GFP line 1) and 0.01 nM BL (BRI1-GFP line 2) after which the effect of BL on the root length is strongly inhibitory. C and D) Fit of the model on the BRI1-GFP reporter lines when the assay is performed on 1 μ M BRZ (C) and 5 μ M BRZ (D).

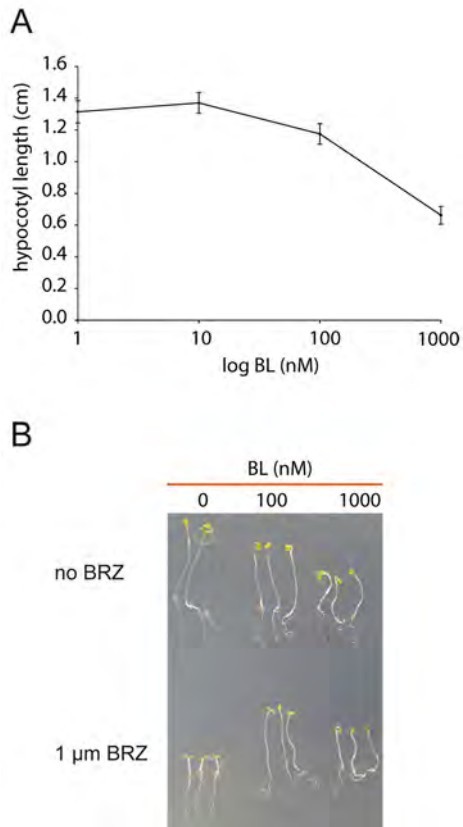


Figure S12. Hypocotyl length assay using wild type when there is no BRZ in the medium. A) Difference in hypocotyl length after application of various concentrations BL. Seedlings were grown for 5 days in the dark. Error bars \pm SEM, $n \geq 15$ hypocotyls per data point, measured in three independent replicates. B) Seedlings treated with BL (top panel) or BL and BRZ (bottom panel). Representative hypocotyls are shown at 5 days growth in the dark. After application of BRZ, a clear stimulatory effect of BL on hypocotyl growth is observed.

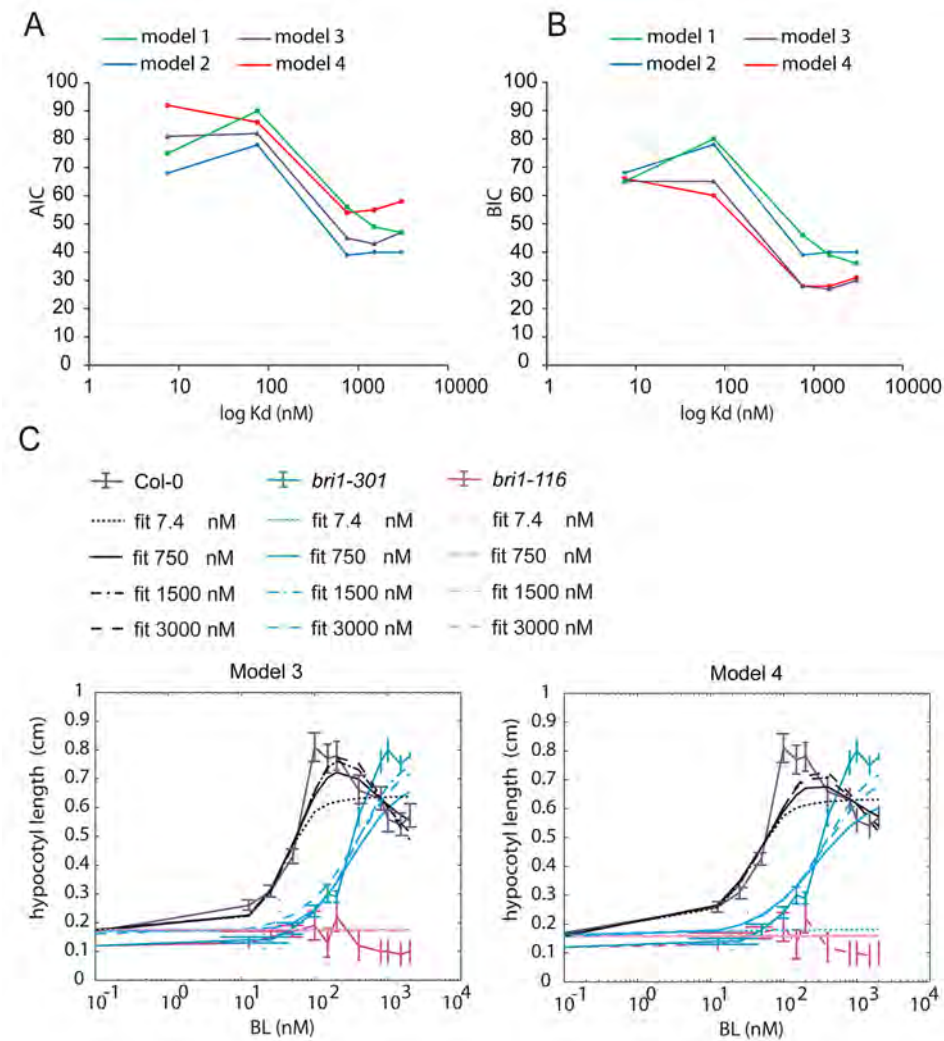


Figure S13. Model fit and predictions on hypocotyl length. A and B) Akaike information criterion (A) and the Bayesian information criterion (B) when model structures 1-4 are fitted on hypocotyl length. The best fit is obtained for model structures 3 and 4 when increasing the Kd to at least 750 nM. (C and D) Fits of model 3 (C) and 4 (D) under varying Kd values.

Table S1. Comparison between different model structures using root length as readout.

Model nr.	Modules		S(θ^*)	AIC	BIC	Predicted root length of <i>bri1-116</i> null mutant at 8 DAG (cm)
	Stimulatory	Inhibiting				
1	1	2	85	111	99	0.35
2	2	2	81	111	96	0.61
3	2	1	93	119	107	0.08
4	1	1	93	115	105	0.07
5	1	0	533	552	544	0.76
6	0	1	641	659	651	1.1
7	3	2	82	117	99	0.64
8	2	3	77	112	94	0.67
9	3	3	78	117	96	0.69
10	1	3	87	117	102	0.44
11	3	1	93	123	109	0.08

Calibration was done on root length of seedlings at 4, 6 and 8 days after germination (DAG). Prediction of the root length of *bri1-116* null mutant was done for roots at 8 DAG. The actual root length of a *bri1-116* null mutant at 8 DAG is 0.45 ± 0.05 cm ($n \geq 15$ roots, value \pm SEM).

AIC = Akaike information criterion

BIC = Bayesian information criterion

S(θ^*) = least sum of squared errors

Table S2. Comparison between CRS and MATLAB genetic algorithm (GA) combined with Isqnonlin.

	4 DAG		6 DAG		8 DAG	
	GA +		GA +		GA +	
	CRS	Isqnonlin	CRS	Isqnonlin	CRS	Isqnonlin
E_{max} (cm)	1.05±0.08	1.07±0.01	4.60±0.26	4.55±0.01	12.21±0.85	11.90±0.05
R (0,0,t) (cm)	0.18±0.01	0.18±0.00	0.35±0.13	0.34±0.00	0.35±0.00	0.35±0.00
k₁	2.03±0.16	1.97±0.00				
k₂	1.95±0.08	1.98±0.01				
k₃	1.96±0.13	1.98±0.00				

Values ±STDEV, n = 5 runs

E_{max} = the maximum possible root length when no inhibitory mechanisms are present

R(0,0,t) = the root length at time 0 in the absence of BRI1 mediated signalling

k₁, k₂ and k₃ are the half maximum response values

CRS = controlled random search

GA + Isqnonlin = MATLAB genetic algorithm followed by Isqnonlin

Table S3. Comparison between different model structures using hypocotyl length as readout.

Predicted root						
Modules				length of <i>bri1-116</i>		
				null mutant at 8		
Model nr.	Stimulatory	Inhibiting	S(θ^*)	AIC	BIC	DAG (cm)
1	1	2	30	52	35	0.16
2	2	2	22	55	28	0.18
3	2	1	22	44	27	0.18
4	1	1	34	49	38	0.16
5	1	0	92	101	95	0.16
6	0	1	738	747	741	0.32
7	3	2	22	73	29	0.18
8	2	3	22	74	30	0.18
9	3	3	22	110	31	0.18
10	1	3	30	63	37	0.16
11	3	1	22	55	28	0.18

Calibration was done on hypocotyl length of seedlings grown for 5 days in the dark. The actual hypocotyl length of a *bri1-116* null mutant grown for 5 days in the dark is 0.14±0.01 cm (n ≥ 15 hypocotyls, value ± SEM).
AIC = Akaike information criterion
BIC = Bayesian information criterion
S(θ^*) = least sum of squared errors

ADDENDUM

CHAPTER 3

Wilma van Esse, Sacco de Vries and Simon van Mourik

ADDENDUM

**A mathematical model for BRASSINOSTEROID INSENSITIVE1-mediated
signaling in root growth and hypocotyl elongation**

van Esse et al., Plant Physiology 160 (1), 523-532 (2012)

This addendum discusses five points that might be less clear to the reader of this paper. These points comprise the general choice of model structure in equation (4), the equality of parameters k_1 , k_2 , and k_3 , the choice of regarding $R(0,0,t)$ as a parameter, model validation by using the *bri1-301* mutant, and the axes labels in Figure 1B. In addition, an erratum is provided.

Model structure

Equation (4) states that BRI1 mediated root growth is the product of two functions, one depending only on time, and one depending only on BRI1 mediated signaling. The BRI1 signal transduction cascade is an intricate network of interacting processes, each with a different timing. Therefore the separation of timing and BRI1 mediated signal into two different functions implicates a simplification that can be a posteriori justified by the quality of the data fit and the validation results. This was not explicitly mentioned in the paper.

Parameter values

Parameters k_1 , k_2 , and k_3 were all found to be equal to 1.98 (a.u.). It is therefore tempting to conclude that the model complexity can be reduced a priori by assuming that $k_1 = k_2 = k_3$. Moreover, one might think that this may be seen from the data set, or that different values will result in a multimodal response curve. This is however not the case. To illustrate this, we simulated the response function

$$\text{Response} = \frac{k_1 [\text{BRI1 BL}]}{k_1 + [\text{BRI1 BL}]} \frac{k_2}{k_2 + [\text{BRI1 BL}]} \frac{k_3}{k_3 + [\text{BRI1 BL}]}$$

for the case in which $k_1 = k_2 = k_3 = 1$, and for the case in which this is not true (Fig. A1). The response curves have very similar forms that cannot be distinguished based on the data set in Fig. 1A (main manuscript), and are both unimodal. Therefore, this model simplification can in principle only be made after fitting the data. Employing three k values instead of one provides more flexibility in future analyses, and might lead to a better fit of the data.

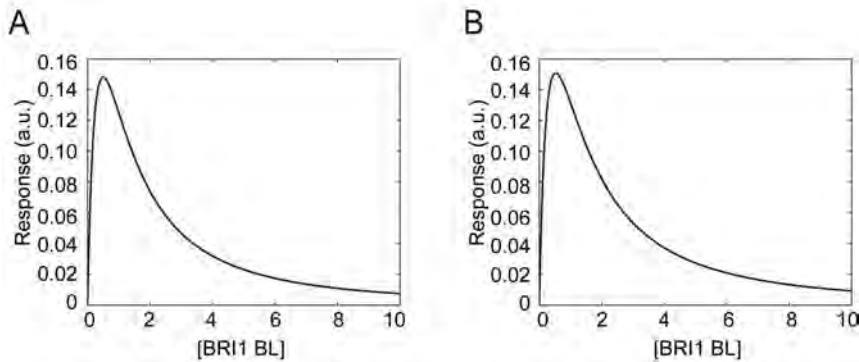


Figure A1. Response curves for $k_1=k_2=k_3=1$ (A), and for $k_1=0.6$, $k_2=1.2$, and $k_3=1.8$ (B).

$R(0,0,t)$ as a parameter

From Fig. 1A in van Esse et al. (2012) it appears that BRI1-independent root length, $R(0,0,t)$, can be directly observed from the data set, namely by the root length at $BL=0$. This would alleviate the need of regarding it as a fitting parameter (Fig 1B). However, it was pointed out in the text that even after BRZ treatment a small endogenous level of BL is assumed to be present. This means that the root lengths displayed at $BL=0$ in Fig 1A are larger than $R(0,0,t)$ due to residual BRI1 signalling. How much larger depends on the fitting parameters $E_{\max}(t)$, k_1 , k_2 , and k_3 . Therefore, $R(0,0,t)$ cannot be inferred directly from the data, and was therefore retrieved via data fitting for $t=4$ DAG, 6 DAG, and 8 DAG. The three discrete values of $R(0,0,t)$ obtained this way were used for all BL concentrations and further predictions.

Validation

The validation of the *bri1-301* weak allelic mutant in Fig. 3D is incomplete, since the reduced receptor activity was modeled by assuming a concentration of 2 nM of active receptors. The *bri1-301* protein has no or very little residual kinase activity, is fully insensitive towards BL but has only a weak morphological phenotype suggesting partial kinase-independent biological activity (Xu et al. 2008). However, the exact number remains unknown. Although the model clearly captures the typical features of the measured response curve, a complete validation would require quantitative determination of residual kinase activity of the *bri1-301* mutant receptor.

Figure 1B

Figure 1B in the main manuscript showed 'predicted root length' on the vertical axes. This can be confusing for two reasons. First, the values are estimated by data fitting, and second, 'root length' here refers to length as a dimension rather than the model output $R(BRI, BL, t)$. Therefore, Fig 1B is revised (Fig A1B), by displaying the time on the horizontal axes, and the parameters on the vertical axes.

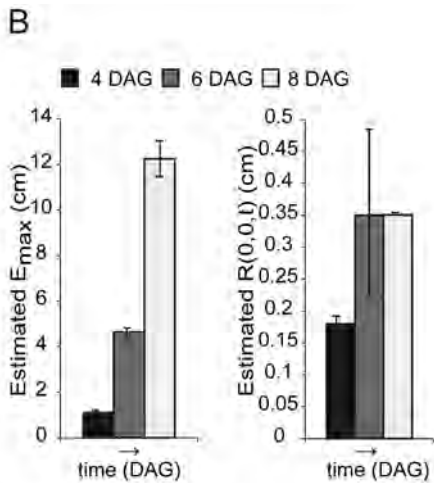


Figure A1B. Revision of Fig. 1B in the main manuscript.

Erratum

The figure legends in the main manuscript mention that SE is based on 30 roots. However, this is only the case for wild type at 8 DAG. For the other experiments, all root growth assays were measured in three independent biological replicas of 5-10 roots per experiment, giving a $n \geq 15$ roots. This was reported correctly in the Materials and Methods section but not in the figure legends.

We thank prof.dr. Bela Mulder, AMOLF Amsterdam and Wageningen University for pointing out the unclarities in our paper.

Chapter 4

A mathematical model for the co-receptors SERK1 and SERK3 in BRI1 mediated signalling



G. Wilma van Esse*, Simon van Mourik*, Catherine Albrecht,

Jelle van Leeuwen, Sacco C. de Vries

(Submitted)

*These authors contributed equally

ABSTRACT

Brassinosteroids (BRs) are key regulators in plant growth and development. The main BR perceiving receptor in *Arabidopsis* is Brassinosteroid Insensitive 1 (BRI1). Seedling root growth and hypocotyl elongation can be accurately predicted using a model for BRI1 receptor activity. Genetic evidence shows that non ligand-binding co-receptors of the Somatic Embryogenesis Receptor-like Kinase (SERK) family are essential for BRI1 signal transduction. A relatively simple biochemical model based on the properties of SERK loss-of-function alleles explains complex physiological responses of the BRI1 mediated BR pathway. The model uses BRI1-BR occupancy as the central estimated parameter and includes BRI1-SERK interaction based on mass action kinetics and accurately describes wild type root growth and hypocotyl elongation. Simulation studies suggest that the SERK co-receptors primarily act to increase the magnitude of the BRI1 signal. The model predicts that only a small number of active BRI1-SERK complexes are required to carry out BR signalling at physiological ligand concentration. Finally, when calibrated with single mutants, the model predicts that roots of the *serk1serk3* double mutant are almost completely BL-insensitive, while the double mutant hypocotyls remain sensitive. This points to residual BRI1 signalling or to a different co-receptor requirement in shoots.

INTRODUCTION

The classic biochemical model for the transduction of an extracellular signal involves ligand binding by a receptor after which the signal is transduced to a downstream target. The main ligand binding receptors often employ co-receptors that can enhance endocytosis (Sorkin and von Zastrow, 2002; Molfetta et al., 2010), interactions with downstream targets or the binding affinity between the ligand and the main receptor (Gakamsky et al., 2005; Hubbard and Miller, 2007). In plants, various signal transduction pathways in defence, development and programmed cell death employ co-receptors to transduce an extracellular signal (Li, 2010; Calderon Villalobos et al., 2012). An important class of signalling hormones involved in growth and development are brassinosteroids (BRs), plant steroid hormones with structural similarity to animal steroid hormones (Bajguz and Tretyn, 2003). In Arabidopsis, the main ligand perceiving receptor for BRs is the Brassinosteroid Insensitive 1 (BRI1) receptor. Impaired BR signalling either by a reduction of BRI1 receptor level or BR availability results in severe growth and developmental phenotypes such as a dwarfed stature, impaired photomorphogenesis, fertility defects, and impaired root growth (Clouse, 1996; Wang et al., 2001). For its signalling activity, BRI1 interacts with members of the Somatic Embryogenesis Receptor-like Kinase (SERK) family that function as non-ligand binding co-receptors (Li and Nam, 2002; Li et al., 2002; Russinova et al., 2004). In Arabidopsis, four of the five members of the SERK family are reported to have partially redundant functions and act in various signalling pathways via their interaction with different ligand binding Receptor-like Kinases (RLKs). SERK1 is known to be involved in male sporogenesis together with SERK2 and in brassinosteroid (BR) signalling together with SERK3 (also known as BAK1) and SERK4 (also known as BKK1) (Albrecht et al., 2008). SERK3 functions in defence (Chinchilla et al., 2007; Heese et al., 2007) and together with SERK4 in a BR independent cell death pathway (He et al., 2007) and defence (Roux et al., 2011). While the SERK co-receptors serve both BR dependent and independent signalling pathways, BRI1 mediated BR signalling was recently shown to be completely dependent on three of the SERK co-receptors, SERK1, 3 and 4 (Gou et al., 2012). SERK3 is the only member of the SERK family in which the single mutant shows a BRI1 related phenotype (Albrecht et al., 2008).

A major difficulty arising from the genetic analyses of the SERK genes is that individual genes appear to participate in multiple pathways, a difficulty enhanced further in double and triple mutant combinations. For example, the strong root phenotype observed in a *serk1-1serk3-1serk4-1* triple mutant (Gou et al., 2012) is only in part the result of an impaired BR-unrelated pathway (Du et al., 2012). For these reasons, the question how individual SERK proteins quantitatively affect the output of one specific signalling pathway, and consequently the resulting

change in the physiological response, is important to help elucidate the role of these receptors. Here, we use a mathematical modelling approach in combination with experimental validation focussing on the role of SERK1 and SERK3 in the BRI1 signalling pathway. BR signalling is one of the best-understood signal transduction cascades in Arabidopsis with respect to biochemical interactions and downstream responses (Ye et al., 2011; van Esse et al., 2013) (Fig. 1). In addition, quantitative information on BRI1-BL binding affinity, and BRI1 and SERK receptor concentrations are available (Wang et al., 2001; Chapter 2), which is essential for modelling. Recently, we developed a quantitative model to explain and predict how root and hypocotyl growth depend on the BRI1 receptor and BL ligand concentration. With the mass action kinetics on which the biochemical part of the model is based, phenotypes of *bri1* mutants could be correctly predicted (Chapter 3).

In this work the model is extended to include the contribution of the co-receptors SERK1 and SERK3 to BL dependent BRI1 activity (Fig. 1). For this, root length and hypocotyl elongation of *serk1* and *serk3* single and double mutants were used as physiological readouts of BRI1 activity. The predictive power of the resulting model was tested by a leave-one-out cross-validation. *In silico* simulations show that in roots the signal perceived by BRI1 is transduced by a complex consisting of BRI1 with either SERK1, SERK3 or both while in the hypocotyl BRI1 signalling requires another SERK member, all in line with the experimental observations (Gou et al., 2012). Previously it has been postulated that SERK3 enhances the phosphorylation of BRI1 thereby quantitatively increasing the signalling output (Wang et al., 2008). The model presented here correctly reflects this observation by predicting that the prime activity of the SERK co-receptors is to increase the physiological output.

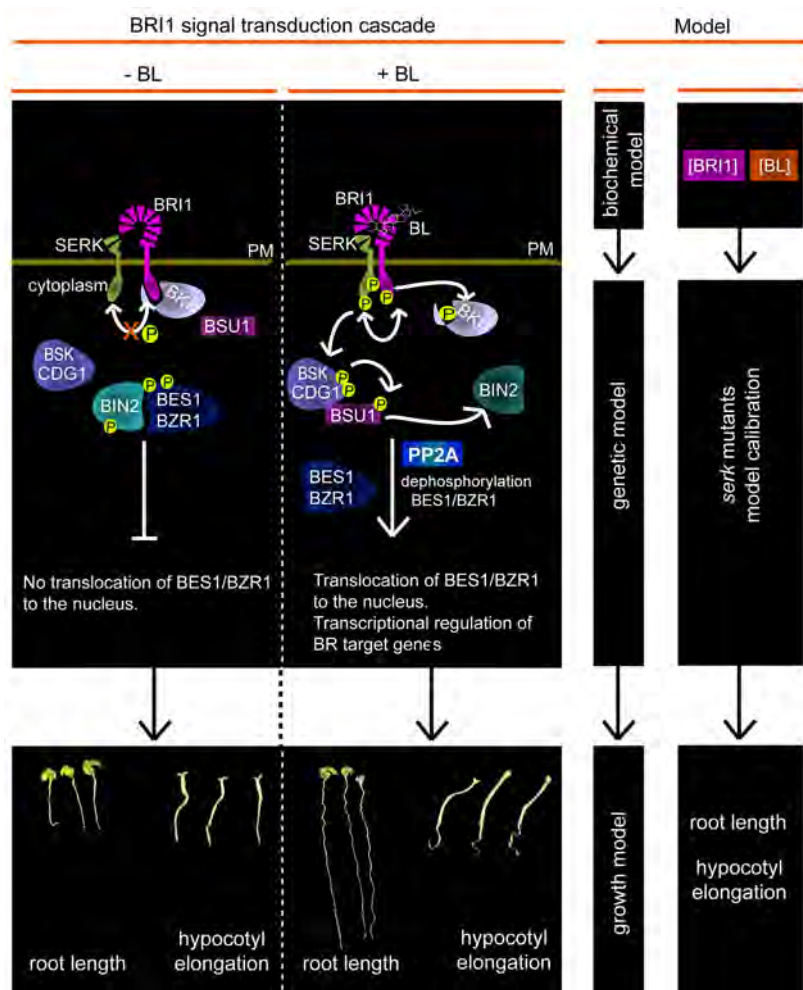


Figure 1. Modelling oligomeric receptor complexes. In the left hand panel a brief scheme of the BRI1 pathway is shown (redrawn after Ye et al., 2011). In the absence of BL, the kinase activity of unbound BRI1 receptor is restricted by negative regulators such as the BRI1 kinase inhibitor 1 (BKI1). BL binding to BRI1 results in transphosphorylation between BRI1 and SERKs which leads to the phosphorylation of BR signalling kinases (BSKs) and constitutive differential growth 1 (CDG1). The phosphorylated BSKs, CDG1 subsequently interact with BRI1 Suppressor 1 (BSU1) phosphatase promoting its interaction with BIN2. Inactivation of BIN2 by BSU1 results in the dephosphorylation and activation of the BR transcriptional regulators brassinazole-resistant1 (BZR1) and BRI1-EMS suppressor 1 (BES1). The middle and right hand panels summarise the modelling approach. The biochemical model describes BL dependent BRI1 activation (Chapter 3). Using genetically identified components the model is now extended using mutated SERK1 and SERK3 co-receptors as an example. This way, the input data from the biochemical model, modified by the co-receptors and combined into a growth model are linked to the physiological readout in the form of root growth and hypocotyl elongation.

RESULTS

Mathematical model

The mathematical model consists of a biochemical and a root growth part. The growth model is largely based on phenomenological considerations and couples the output of BRI1 signalling to root growth. To determine the contribution of the SERK1 and SERK3 co-receptors to overall BRI1 mediated BR signalling, the stimulatory and inhibitory effect of BL on root growth of the *serk1-3* and *serk3-2* single and double mutants was measured (Fig. 2). To highlight the stimulatory effect of exogenous BL, the BR biosynthesis inhibitor brassinazole (BRZ) was used throughout. The *serk1-3serk3-2* mutant has only a minor stimulatory response towards exogenously applied BL (Fig. 2B). No inhibitory effect of BL on root growth was observed, even in the absence of BRZ (Supplemental Fig. S1). This indicates that roots of the *serk1-3serk3-2* double mutant are almost completely insensitive towards BL. The biochemical model (Supplemental File S1A) describes three types of receptor combinations responsible for BRI1 mediated signalling in roots i.e. [BRI1], [BRI1 SERK1] and [BRI1 SERK3]. All three only transduce the signal when BL is bound to BRI1. To incorporate the co-receptors into the existing model describing BR activated BRI1-mediated signalling (Chapter 3) several assumptions were made: The first is that BRI1 binds to SERK proteins in a 1:1 ratio. The second is that the protein concentrations of BRI1 (62 nM), SERK1 (120 nM) and SERK3 (30 nM) in wild type seedling roots Chapter 2) remain constant over time. The third assumption concerns the amount of SERK3 and SERK1 interacting with BRI1 at saturating ligand levels. While the precise stoichiometry is unknown, a 2:1:1 ratio is assumed between BRI1, SERK1 and SERK3 in functional complexes (Supplemental File S1). In wild type seedlings no more than 10 % of the total number of SERK3 co-receptors is required in brassinosteroid signalling at a saturating ligand concentration (Albrecht et al., 2012), so at most 3 nM of SERK3, 3 nM of SERK1 and 6 nM of BRI1 are simultaneously active in signalling. Fourth, the affinity of BRI1 for BL remains unaltered in *serk* mutants. This is based on the findings of Kinoshita et al. (2005) reporting that the K_d between BRI1 and BL of 7.4 nM (Wang et al., 2001) remains unaltered in the absence of BAK1 (SERK3). Finally, although Arabidopsis plasma membrane localised proteins are relatively immobile (Martinière et al., 2012), spatial inhomogeneity is not explicitly modelled.

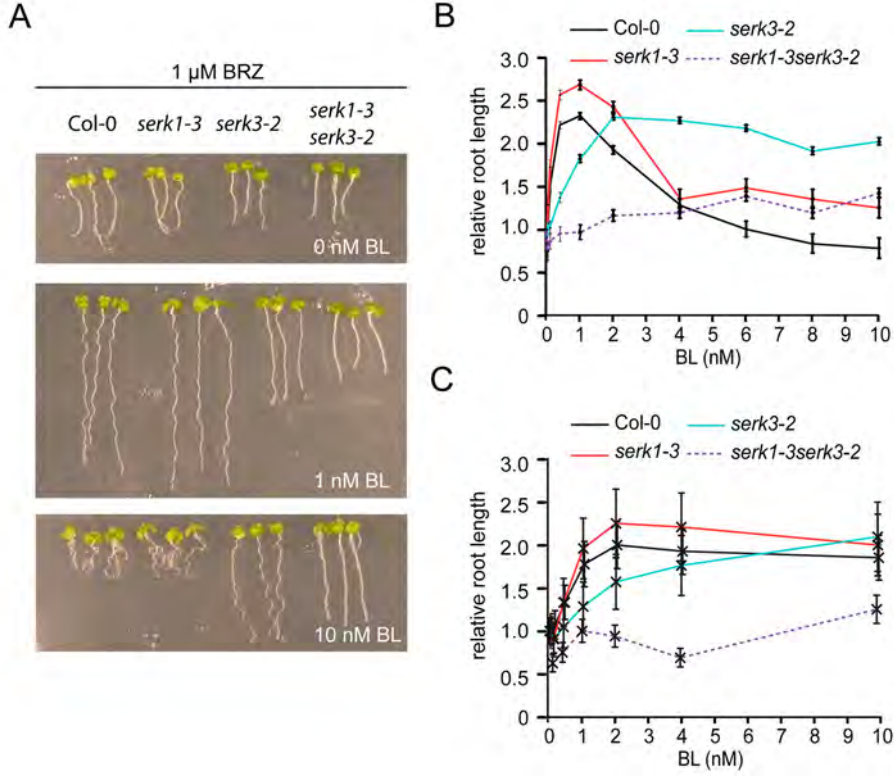


Figure 2. Root length of *serk* mutants in response to BL. A) Root length of wild type seedlings, *serk1-3* and *serk3-2* single and double mutants at 0 nM BL (top panel), 1 nM BL (middle panel) and 10 nM BL (bottom panel). All assays were performed in the presence of 1 μ M brassinazole (BRZ). B) Root growth assays of the *serk1-3* and *serk3-2* single and double mutants compared to wild type at different BL concentrations. Root lengths are measured at 8 DAG and plotted relative to the BRZ treated control. The *serk1-3* single mutant does not have a clear BL dependent phenotype, whereas the *serk3-2* mutant never reaches the wild type root length and does not show any inhibition in response to BL. The *serk1-3serk3-2* is almost completely unresponsive towards BL. C) Root lengths relative to the BRZ treated control at 4 DAG. For all measurements $n \geq 15$ roots, error bars \pm SEM.

The main hypothesis in the biochemical model is that the formation of functional complexes consisting of BRI1, SERK1, SERK3 and BL follow mass action laws. The signal (σ) induced by BL binding to BRI1 is modelled as:

$$\sigma = \alpha_1 C_1^a + \alpha_2 C_2^a + \alpha_3 C_3^a \quad (1)$$

Here C_1^a , C_2^a , and C_3^a denote [BRI1], [BRI1 SERK1], and [BRI1 SERK3]. The term C_1^a represents all responses towards exogenously applied BL not covered by SERK1 and SERK3. Parameters α_1 , α_2 , and α_3 are proportionality constants that reflect the contribution of the different complexes to the signal strength of BRI1.

Due to the inclusion of the co-receptors the growth model is now modelled as a combination of two separate mechanisms

$$R(\sigma, t) = R_0(t) \cdot (1 + f(\sigma, t)) \quad (2)$$

with $R(\sigma, t)$ the root length at time t (days after germination, DAG), $f(\sigma, t)$ the root length as a result of BRI mediated signalling, and $R_0(t)$ the root length independent of BRI1 mediated signalling or response towards BRs. Scaling of $R_0(\sigma, t)$ gives the root length due to BRI1 signalling relative to the root length independent of BRI1 signalling. The output of the growth model is then root length relative to the BRZ treated control instead of absolute values (Fig. 2B). For this, the parameter $R_0(t)$ is scaled out of the equation:

$$y(\sigma, t) = \frac{R(\sigma, t)}{R_0(t)} = 1 + f(\sigma, t) \quad (3)$$

where $y(\sigma, t)$ is the increase in root length as relative to the BRZ treated control. The function $f(\sigma, t)$ is based on phenomenological considerations, and consists of one activating and two inhibiting modules:

$$f(\sigma, t) = E(t) \frac{\sigma}{\alpha_4 + \sigma} \frac{1}{\alpha_5 + \sigma} \frac{1}{\alpha_6 + \sigma} \quad (4)$$

Here $E(t)$ is a time dependent growth factor, followed by a module that represents the stimulatory effects of BR signalling on root growth and a second module for the inhibitory effects. The half maximum response values for the growth model (k values) are denoted as α_4 , α_5 and α_6 . The form of function $E(t)$ is unknown and is therefore regarded as a free parameter which is allowed to change between different time points. The unknown model parameters such as the k values (α_4 , α_5 , α_6) and $E(t)$ were estimated by minimizing the fitting error between the model output and measured root length data. Different structures of $f(\sigma, t)$ were compared using the Akaike (AIC) and Bayesian (BIC) information criteria and a four-fold cross validation. The first two reflect the trade-off between a good fit with the data and complexity, and the third one measures the prediction error that is possibly due to over- or under-fitting (Supplemental File S1 B and C). In total, 13 functions for $f(\sigma, t)$ were tested, ranging from one activating or inhibiting module to three activating and three inhibiting modules and all relevant combinations in between. Model structure 1 (one activating and 2 inhibiting modules) scored best with respect to root growth (Supplemental Table S1) as well as hypocotyl elongation (Supplemental Table S2) and was therefore selected.

The response to BL treatment is minor at 4 DAG when compared to 6 and 8 DAG (Fig. 2B and C). For this reason, the model cannot fit the relative root growth

response curves at 4, 6 and 8 simultaneously (Supplemental Fig. S2). However, growth at 4 DAG can be computed separately (Supplemental Fig. S3). Therefore, only the difference between wild type and the *serk1* and *serk3* mutants in terms of relative response in root length at 6 and 8 DAG is used for model selection, calibration and validation.

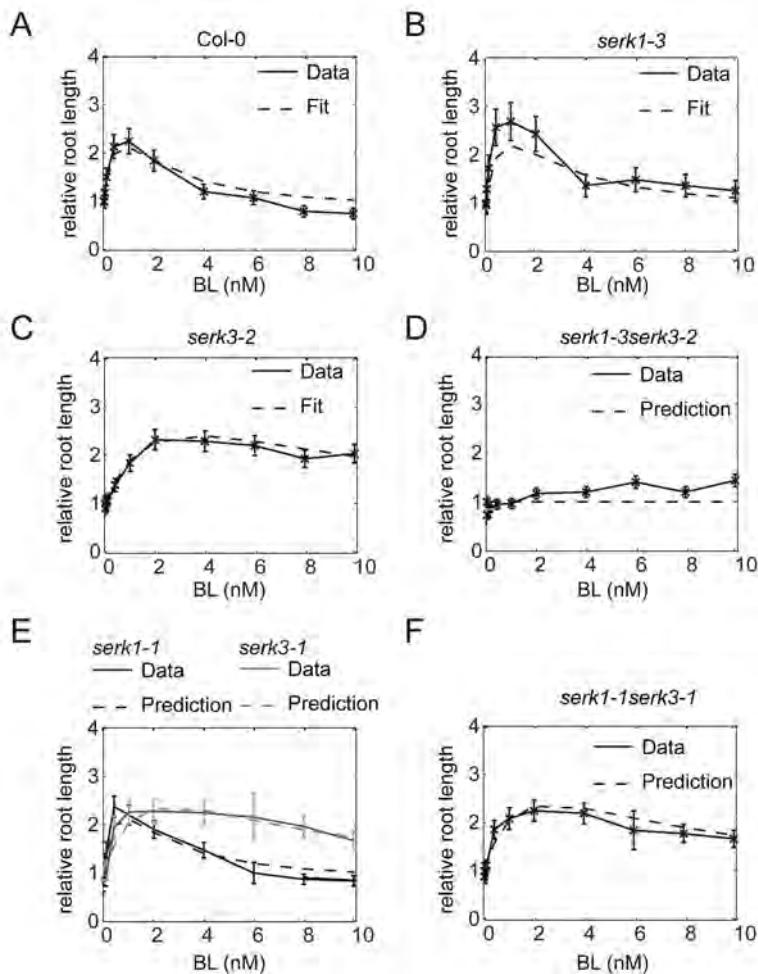


Figure 3. Model fit and prediction of relative root growth response for wild type and *serk* mutants. All measured root lengths are plotted relative to the BRZ treated control. A-C) Model calibration on the relative root length of the wild type, *serk1-3* and *serk3-2* mutant at 6 and 8 days after germination (DAG). Only results of 8 DAG are shown. D) The model is now validated by predicting the relative root growth response of *serk1-3serk3-2* double mutant seedlings at 8 DAG. E-F) Model predictions for the relative root length of the *serk1-1* and *serk3-1* single (E) and *serk1-1serk3-1* double mutants (F). For all experiments $n \geq 15$ roots measured in three independent replicates, error bars \pm SEM, assays were performed in the presence of 1 μ M BRZ.

Model calibration and validation

Root growth assays of the *serk1-3* and *serk3-2* single mutants were included in the model calibration data set to train the model on the effect of SERKs on BRI1 receptor activity. The model is able to fit the relative root growth pattern of wild type and the *serk1-3* and *serk3-2* single mutants while predicting the relative root length of the *serk1-3serk3-2* double mutant (Fig. 3 A-D). The *serk3-2* mutant is a true null loss-of-function allele. There is a slight discrepancy between the model predictions and actual data for the root growth response of the *serk1-3serk3-2* double mutant (Fig. 3D). This could be due to a minor contribution of SERK2 or SERK4 in BR signalling only occurring in the absence of SERK3 (Jeong et al., 2010; Du et al., 2012) or to trace signalling mediated by the BRI1 receptors alone. Leave-one-out cross-validation consisting of calibration on relative root growth of the single *serk* mutants and wild type shows a small predictive error (Supplemental Fig. S4). To further test the predictive power of the model, the relative root growth response of the *serk1-1* and *serk3-1* single and *serk1-1serk3-1* double mutant towards BL was simulated. The *serk3-1* mutant is a weak mutant which still harbours low levels of SERK3 transcript (Gou et al., 2012). Small prediction errors were obtained when assuming that there is between 10 and 20% SERK3 activity left in the *serk3-1* mutant background (Supplemental Fig. S5). Under this assumption, the model accurately predicts the behaviour of the *serk1-1serk3-1* double mutant (Fig. 3 E and F).

As a final validation the model was used to predict hypocotyl elongation relative to the BRZ treated control. The trends of the relative hypocotyl elongation of the wild type, *serk1-3* and *serk3-2* single and the *serk1-3serk3-2* double mutant were predicted correctly for all cross-validations (Fig. 4, Supplemental Fig. S6). The model correctly predicts that in the hypocotyl there is still a marked response of the *serk1-3serk3-2* double mutant towards BL. This suggests that there is either a difference in co-receptor usage by BRI1 between the roots and hypocotyl or a substantial contribution by BRI1 alone.

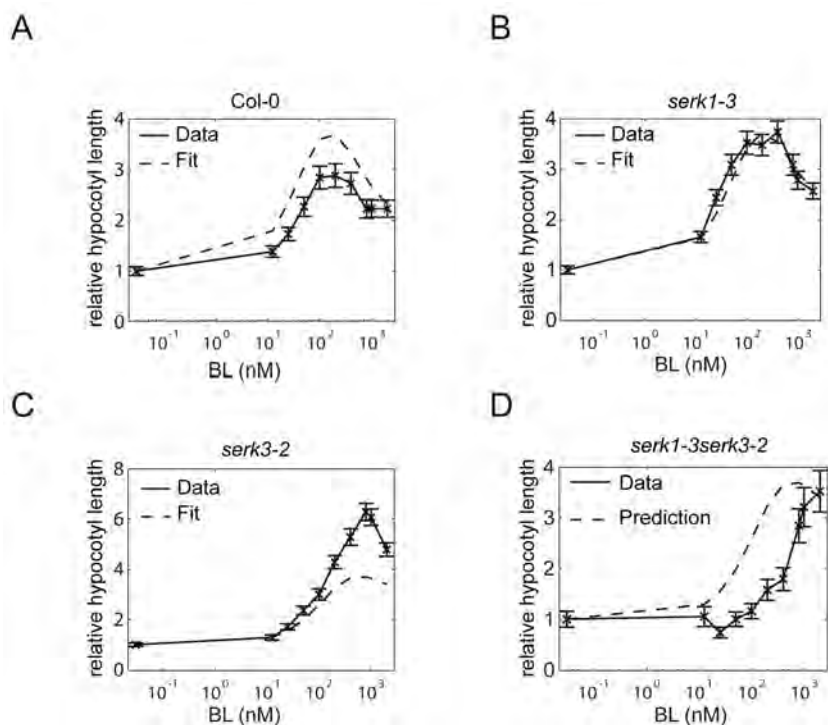


Figure 4. Model fit and prediction of relative hypocotyl elongation for wild type and *serk* mutants. All measured hypocotyl lengths are plotted relative to the BRZ treated control. A-C) Calibration on the hypocotyl elongation of the *serk1-3serk3-2* double mutant. All hypocotyl lengths were measured at 5 DAG, seedlings were grown in the dark. B) The model is validated by predicting the relative hypocotyl elongation of the *serk1-3serk3-2* double mutant. Error bars \pm SEM, $n \geq 30$ hypocotyls measured in three independent replicates.

Co-receptors act by changing the maximum output of BR signalling

Next, the model was used to address the question how the co-receptors affect the signal (σ) after BL binding to BRI1. We focussed on the absence of SERK3 because the *serk1-3serk3-2* strong loss-of-function mutants are less informative due to the almost complete absence of signalling activity. Simulations predict that one possible explanation for the reduced σ is a reduction in the concentration of BRI1 (Supplemental Fig. S7A). For example, the amount of BRI1 receptor should be about 30-fold less in the *serk3-2* mutant background when compared to the wild type background in order to result in the trend observed in the *serk3-2* mutant (Supplemental Fig. S7A). However, quantitative confocal microscopy experiments demonstrate that the amount of BRI1-GFP in the PM is hardly changed in the *serk3-2* background (Supplemental Fig. S7B-C) suggesting that reduction of the total number of BRI1 receptors molecules is not a mechanism by which co-receptors attenuate the signal. It has been postulated that SERK3 acts by increasing the activity of the BRI1 receptor to achieve full signalling output

(Wang et al., 2008), and therefore we tested whether our model could reflect this possibility. Indeed, predicting the behaviour of σ in the absence of SERK3 shows that the σ_{\max} will drop about 6-fold and is close to zero in the double *serk1-3serk3-2* mutant (Fig. 5). Therefore, we propose that in wild type roots, SERKs primarily act by increasing the σ_{\max} of BRI1, in line with the experiments shown by Wang et al. (2008).

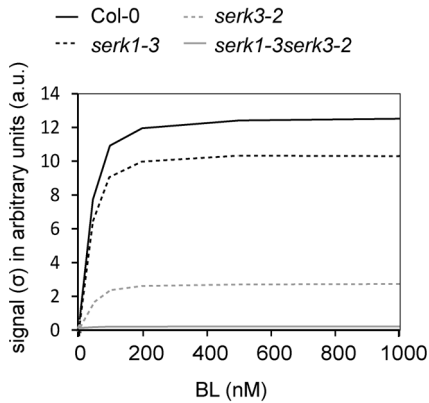


Figure 5. Prediction of BRI1 signalling output in the absence of SERK co-receptors. The signal intensity of BRI1, σ is predicted in the presence or absence of SERK1 and SERK3. The signal transduced in *serk3-2* and *serk1-3* mutants is computed by plotting $\alpha_3 C_3^a$ (σ SERK3) and $\alpha_2 C_2^a$ (σ SERK1). For the signal in the *serk1-3serk3-2* mutant the term $\alpha_1 C_1^a$ was computed, representing the residual responses to BL.

BRI1 signalling operates with only a minor amount of co-receptors

SERK1 and SERK3 function as co-receptors in various signalling pathways by interacting with different main ligand perceiving receptors. If these pathways operate at the same time this implies that the co-receptors are distributed amongst them. For this reason, it is of interest to know how co-receptor dosage affects BRI1 mediated BR signalling. Therefore this possibility was incorporated into the model by the mass balance equation (2) in Supplemental File S1A. Based on the amount of SERK3 co-immunoprecipitated by BRI1 at saturating ligand level (assumption 3 in Results section), the model predicts that only about 0.05 nM of SERK1 and SERK3 (0.04 and 0.16% of the total amount respectively) is used in BR signalling at a physiological ligand concentration of 1 nM BL (Supplemental File 1 and Supplemental Table S3). Even after increasing the percentage of both SERK1 and SERK3 used by other pathways to 85% the model is still able to predict BRI1 mediated root growth (Table 1). This corroborates the finding that FLS2 mediated flg22 signalling uses up to 70% of SERK3 without affecting BR signalling (Albrecht et al. 2012).

Table 1. Effect on model prediction of changing the amount of SERK1 and SERK3 employed by non BRI1-related pathways

Amount of SERK in other pathways		Prediction Error*
Root		
	10 %	63
	85 %	64
Hypocotyl		
	10 %	175
	85 %	174

In normal conditions, it is assumed that 10% of the SERK1 and SERK3 co-receptors is employed in non BRI1-related pathways (Supplemental File S1A). This yields a low prediction error of the model (Supplemental Table S1). A prediction error deviating more than 10% from the optimal value is considered to be significantly different.

*Average prediction error over four leave-one-out cross-validations.

Testing different biochemical model structures

So far, biochemical model 1 was employed, assuming the occurrence of preformed BRI1-SERK complexes. Such a mechanism has been reported for several RLKs in mammalian systems (Gadella and Jovin, 1995; Lemmon and Schlessinger, 2010). Alternative mechanisms, where BRI1 binds BL before recruiting SERK3 co-receptors have also been proposed (Wang et al. 2005). The structure of the extracellular domain of BRI1 in the presence or absence of BL does not show substantial changes and does not provide a clear indication for either mechanism (Hothorn et al., 2011). Therefore, it was tested if the root growth model is able to distinguish between the different biochemical models (Supplemental File S1A). The results show that the order of [BL BRI1 SERK] complex formation does not affect the prediction error (Table 2). Next, differences in the stoichiometry were tested. A model in which the complexes consist of heterodimers (1 molecule of BRI1 and 1 of SERK) results in a lower prediction error when compared to a model with tetrameric complexes with 2 BRI1 molecules and 2 SERKs (Table 2). Changing the ratio between BRI1:and SERK from 1:1 to 1:4 also does not significantly alter the prediction error. Taken together, we conclude that physiological data such as growth readouts have low predictive value for biochemical models.

Table 2. Comparison of different biochemical model structures using root length as readout

	Stoichiometry	
	BRI1:SERK1:SERK3	Prediction Error*
Biochemical model 1	1:1	63
	1:2	67
	1:4	69
	2:2	105
Biochemical model 2	1:1	67
	1:2	65
	1:4	74
	2:2	106

Biochemical model 1 assumes a pre-assembly between BRI1, SERK1 and SERK3 in absence of ligand while biochemical model 2 assumes only an interaction in presence of ligand (Supplemental File S1A). The Table shows the prediction errors of biochemical model 1, biochemical model 2 and the effect of changing the stoichiometry between BRI1, SERK1 and SERK3. A deviation of 10 % in prediction error from the optimal value is considered to be significantly different.

*Average prediction error over four leave-one-out cross-validations.

DISCUSSION

In this work we have extended a model for BR signalling mediated by the ligand-binding BRI1 receptors with the associated non ligand-binding co-receptors of the SERK family. The resulting model can be used to incorporate downstream components of the main pathway identified by forward genetics or biochemical means. As an example the reduced root growth and increased ligand insensitivity observed in single *serk* mutants was linked to the signalling output of a biochemical receptor model. The model accurately predicts relative root and hypocotyl growth in double *serk* mutant and wild type seedlings and agrees well with existing experimental data presented here and elsewhere. The validated model presented here can now be used to incorporate additional BR pathway components and offers the opportunity to include quantitative elements in an otherwise genetic model.

The identification of members of the SERK family that act redundantly in different signalling pathways (He et al., 2007; Li, 2010; Du et al., 2012; Gou et al., 2012; Kim et al., 2013) has underscored the importance of a class of non-ligand binding receptors in plant signalling pathways. In BRI1-mediated BR signalling, there is no evidence that SERK3 indeed directly influences the ligand-binding properties (Kinoshita et al., 2005), a finding that seems to rule out a role as a classical co-receptor as used in comparable animal signalling systems. Moreover, there appears to be no change in structure of the ligand-binding domain of BRI1 after incubation with BL but a ligand-induced platform was proposed to occur in BRI1 allowing interaction with SERK3 (Hothorn et al., 2011). Yet, the SERKs clearly modulate and are necessary for sustained BRI1-mediated signalling (Wang et al., 2005). Regardless of the precise biochemical mechanism, this would qualify them as true co-receptors. Recently, it was shown that SERK3, also functioning as a co-receptor for the flagellin-triggered Flagellin sensitive 2 (FLS2) signalling pathway is not rate-limiting between both BR and flg22 pathways and in fact most of the SERK3 proteins can be recruited by FLS2 without affecting BRI1-mediated root growth (Albrecht et al., 2012). However, it is unclear what the precise role of these receptors is. One possibility is that they act to narrow down the broad BR signal affecting a multitude of developmental events such as cell division, cell elongation, cell death and cell differentiation (Chinchilla et al., 2007; Heese et al., 2007; Albrecht et al., 2008; Lewis et al., 2010; González-García et al., 2011; Hacham et al., 2011) and that their effects on fertility and on immunity are downstream effects of alterations in such basic cellular pathways. However, genetic evidence does not support that option, mainly because the phenotypes encountered mimic precisely the phenotype of a loss of function in the main receptor or are weak mutants showing the entire array of phenotypes. On top of that, it becomes evident that a single member of the SERK family can simultaneously affect different pathways.

This property in some cases can be traced back to individual residues in the SERK3 protein (Schwessinger et al., 2011). For these reasons, we decided to develop a more mathematical approach to provide a better quantitative insight into the role of the SERK family.

In the complete absence of the co-receptors the maximal signal transduced by BRI1 is significantly reduced. The most obvious explanation for this effect is therefore that SERKs act by transducing the signal from the ligand-binding receptor to the downstream targets. Evidence for this role is that mutual transphosphorylation between BRI1 and SERK3 was found to be essential for enhancing BR signalling *in vivo* (Wang et al., 2008). In FLS2 mediated signalling, SERK3 enhances the signal by interacting with Botrytis Induced Kinase 1 (BIK1), a member of the Receptor Like Cytoplasmic Kinase (RLCK) superfamily and downstream target of FLS2. In the absence of SERK3, FLS2 is unable to phosphorylate BIK1 (Lu et al., 2010). Similarly, BRI1 Substrate Kinases (BSKs), that are also members of the RLCK superfamily, are a substrate of BRI1 and are activated by upon BL binding to BRI1. However, *in vitro* kinase assays have demonstrated that BRI1 and not SERK3 phosphorylates BSKs (Tang et al., 2008). This indicates that a mechanism by which SERK3 enhances BRI1 signalling via specific phosphorylation of BSKs is not likely.

BRI1 signalling is regulated by the presence of positive (BSKs) and negative (BRI1 associated kinase 1, BIK1) regulators. The protein phosphatase 2A (PP2A), stimulates BRI1 signalling by dephosphorylating the downstream BRI1 transcriptional regulator brassinazole-resistant 1 (BRZ1) but is also required for the degradation of BRI1 via dephosphorylation of the activated receptor (Di Rubbo et al., 2011; Tang et al., 2011; Wu et al., 2011). Attenuation of the BRI1 signal is regulated by phosphorylation of specific serine and threonine residues (Oh et al., 2012). Thus, there appears evidence for a role of the SERKs as amplifiers of the entire signalling pathway, rather than having a specific effect on only one element. The modelling presented here is indeed able to predict the alterations described for the role of the SERK receptors in BR signalling. Although not addressed in the present study, the model could also be useful for other pathways that use different main ligand-perceiving receptors employing SERK proteins. Simulations also demonstrate that in roots the signal transduced by BRI1 is mainly affected by BRI1 in complex with SERK1 or SERK3. However, when simulating hypocotyl elongation in absence of SERK1 and SERK3 the model predicts correctly that there is still a significant BL induced increase in hypocotyl elongation. This implies that in the hypocotyl there is either a larger contribution of BRI1 alone, or alternatively, another SERK member compensate for the loss of SERK1 and SERK3 in hypocotyl tissue. In Arabidopsis seedlings, signal transduction by BRI1 is completely abolished in absence of SERK1, SERK3 and SERK 4 (Gou et al.,

2012), making that member a likely candidate. In that respect, the interaction of BRI1 with different co-receptors might reflect a mechanism that regulates the sensitivity of a cell or tissue for BRs depending on the family members present. However, there are clearly limitations to what can be understood about the underlying biochemical model predicted by the model based on physiological readout. Our modelling results emphasise that one type of co-receptors can be employed for various pathways simultaneously. This was based on the fact that remarkably low numbers of the SERK proteins are needed to sustain BR signalling. This predicts that a high level of separation must exist between the different receptor complexes active in the same cell. SERK3 has been implicated as a means to provide cross-talk between different pathways (Vert and Chory, 2011). In one study it appeared that SERK3 was rate-limiting between BRI1 and FLS mediated signalling (Belkhadir et al., 2012) while we showed that in wild type conditions this does not appear to be the case. Therefore, a role of SERK proteins as direct mediators in receptor cross talk seems unlikely (Albrecht et al., 2012). In general, there are several mechanisms by which co-receptors can alter the activity of the main receptor. In mammalian systems for example, the T-Cell co-receptors CD4 and CD8 are positive regulators that enhance the interaction between the T-cell receptor (TCR) and its ligand (Gao et al., 2002; Berg and Sewell, 2011) whereas the non-ligand binding glucocorticoid receptor (GR) isoform β is a dominant negative regulator of the ligand perceiving GR α (Kino et al., 2009). Similar mechanisms have been reported for several other steroid receptors such as the estrogen receptor β (ER β), peroxisome proliferator-activated receptor (PPAR α) and PPAR γ and the thyroid hormone receptor α (TR α) and the epidermal growth factor receptor (EGFR). In plants, co-receptors are also employed to alter the signalling properties of the main ligand perceiving receptor. Recently, it has been shown that efficient binding of the auxin receptor TIR1 to its ligand requires co-receptors (Calderon Villalobos et al., 2012). In this respect, it is proposed that combinations of TIR1 with different co-receptors result in ligand perceiving complexes with distinct auxin binding affinities. Such a mechanism would enhance the concentration range of the hormone, thereby contributing to the complexity of the auxin response (Calderon Villalobos et al., 2012). Similarly, overexpression of ERBB2, the non-ligand binding co-receptor of EGFR, does not result in receptor hyper-autophosphorylation. Instead, ERBB2 regulates the ubiquitin ligase c-Cbl through altering the phosphorylation patterns on the EGFR-HER2 heterodimer thereby protecting the heterodimer from ligand induced ubiquitination and degradation (Hartman et al., 2012). As a consequence, the EGFR-ERBB2 heterodimer is stabilised, resulting in sustained signalling. In line with these animal receptor models, we propose that the action of the SERK co-receptors in BRI1-mediated BR signalling is to transiently stabilise ligand-

induced active receptor complexes as a means to increase signalling strength. Whether this same action applies to other SERK-employing pathways remains to be determined. We believe that the modelling approach as described here can help to distinguish between the action of SERK members in the various pathways and to provide a more comprehensive framework of the multitude of signalling occurring simultaneously in plant cells.

EXPERIMENTAL PROCEDURES

Plant lines and growth conditions

Arabidopsis thaliana wild type plants (ecotype Columbia (Col-0)), *serk1-3* (GABI-KAT line 448E10) and *serk3-2* or *bak1-4* (SALK_116202) single and the *serk1-3serk3-2* double mutants, all in the wild type background, were used in all growth assays. For model validation, the *serk1-1* (SALK_544330), *serk3-1* or *bak1-3* (SALK_034523) single and double mutant were used. For fluorescent microscopy, wild type seedlings expressing BRI1-GFP under its own promoter (Geldner et al., 2007) were crossed with the *serk3-2* mutant. Root growth and hypocotyl elongation assays were performed as described previously (Chapter 3).

Software and modelling

All computational and modelling procedures were performed within the MATLAB® environment (see Supplemental File S1 and Chapter 3. Out of the different models tested, throughout the manuscript biochemical model 1 and physiological model 1 are used unless specified otherwise. For all simulations, root lengths relative to the BRZ treated control were used.

Analysis of fluorescence distribution of BRI1-GFP in wild type versus *serk3-2* background

Roots of 3 to 5 day old seedlings containing BRI1-GFP in wild type or *serk3-2* background were imaged using a CONFOCOR2/LSM510 confocal microscope (Zeiss, Jena, Germany) equipped with a 40x water objective (NA 1.2) and an Argon ion laser. Imaging was performed as described previously Chapter 2. Briefly, the Argon laser was used for excitation of GFP at 488 nm after which GFP fluorescence emission was detected with a band-pass filter 505-550 nm, the pinhole diameter was adjusted to a slice thickness of ~ 0.9 µm. All images were taken within 45 seconds from the moment the root was exposed to the laser to limit bleaching effects. Images were analysed using Image-Pro Plus software (MediaCybernetics, <http://www.mediacy.com>). The mean intensities of about 7 roots measuring 5 cells per roots were measured in two independent replicates.

ACKNOWLEDGEMENTS

This work is part of the Wageningen University and Research Centre IP/OP systems biology research program. The authors thank Niko Geldner for providing the *BRI1-GFP* line in wild type background, the Arabidopsis Biological Resource centre for providing us the *serk1* and *serk3* mutant seeds and Eric Boer and Jaap Molenaar for fruitful scientific discussions on the manuscript.

SUPPLEMENTAL FILES

File S1. Mathematical model description

The mathematical model consists of two parts, a biochemical model and a growth model. The biochemical model incorporates actual ligand, BRI1 receptor and SERK1 and SERK3 co-receptor concentrations. To simulate the effect of altering the ligand, BRI1, SERK1 or SERK3 concentrations on organ growth the outcome of the biochemical model is coupled to organ growth using a phenomenological model structure. The mathematical equations and details on the modelling are described in this supplemental file.

BRI1 receptor and SERK co-receptor availability in Arabidopsis roots

The BRI1 receptor and the SERK1 and SERK3 co-receptor densities in root epidermal cells of 5 day old Arabidopsis seedlings are respectively 12, 24 and 5 receptors μm^{-2} (Chapter 2). For BRI1, this corresponds to a concentration of 62 nM (Chapter 2). For SERK1 this amounts to 120 nM and for SERK3 30 nM. It is assumed that in the hypocotyl the total BRI1, SERK1 and SERK3 receptor concentrations are similar to the ones in the root.

File S1A. Biochemical models

This section describes the details of the modelling approaches of different biochemical hypotheses. In total, 3 different biochemical model structures are tested. In all structures, BRI1 mediated signalling is induced when the ligand BL binds to BRI1. The standard model (biochemical model 1) assumes that BRI1, SERK1 and SERK3 interact in a ratio of 2:1:1, and complex formation between BRI1 and SERK1 or SERK3 can already occur in absence of the ligand. Biochemical model 2 assumes that interaction between BRI1 and SERK3 only occurs after BL binding to the BRI1 receptor. In biochemical model 3 the stoichiometry between BRI1, SERK1 and SERK3 is changed.

Biochemical model 1: Standard model The standard model represents the main hypothesis that BRI1-SERK complexes are activated upon binding with BL. The following notation is used: $x_1 = \text{BRI1}$, $x_2 = \text{BL}$, $x_3 = \text{SERK1}$, and $x_4 = \text{SERK3}$. The model incorporates the possibility that x_3 and x_4 can also be part of other receptor complexes. The following complexes are formed:

$$C_1 = x_1$$

$$C_2 = [x_1 x_3] = \gamma_1 x_1 x_3$$

$$C_3 = [x_1 x_4^n] = \gamma_2 x_1 x_4^n$$

$$C_4 = \gamma_3 x_3$$

$$C_5 = \gamma_4 x_4.$$

(1)

Here n is 1 (representing 1 SERK molecule and 1 BRI1 molecule) unless otherwise specified, and the γ 's the binding affinities. The second right hand terms represent the assumption that the complexes are formed via a mass action law. Complexes C_1 , C_2 and C_3 are involved in BRI1 mediated signalling. BRI1-BL binding occurs independently of BRI1-SERK binding. Therefore, BRI1-BL binding is modelled separately, and x_2 is discarded for now. This gives the mass balance

$$x_1^T = C_1 + C_2 + C_3$$

$$x_3^T = x_3 + nC_2 + C_4$$

$$x_4^T = x_4 + nC_3 + C_5,$$

(2)

with x^T the total concentrations. From mass balance (2) the concentrations of the complexes can be predicted for plants in which x^T is changed (and known). For this, γ should be known. Since the γ 's represent the binding affinities which are independent of x^T , they have to be estimated for only one x^T . The value of γ is estimated in two steps.

First, the following conditions are based on wild type measurements with $x^T = [62 \ 10^3 \ 120 \ 30] \text{ nM}$. At saturating ligand concentrations of $1 \ \mu\text{M}$ no more than 10 % of the total amount of SERK3 co-receptor is associated with BRI1 (Albrecht et al., 2012). This is around 5 % of the total number of available BRI1 resulting in:

$$C_2 = 0.05x_1^T = a_1x_1^T \quad 5 \% \text{ of BRI1 is in complex with SERK1}$$

$$C_3 = 0.05x_1^T = a_2x_1^T \quad 5 \% \text{ of BRI1 is in complex with SERK3}$$

$$C_4 = 0.1x_3^T = a_3x_3^T \quad 10 \% \text{ of SERK1 is in complex with other factors}$$

$$C_5 = 0.1x_4^T = a_4x_4^T \quad 10 \% \text{ of SERK3 is in complex with other factors.}$$

(3)

From this, x is solved. Inserting (3) into (2) results in the following equation for the monomer concentrations:

$$\begin{pmatrix} x_1 \\ x_3 \\ x_4 \end{pmatrix} = - \begin{pmatrix} a_1 + a_2 - 1 & 0 & 0 \\ na_1 & a_3 - 1 & 0 \\ na_2 & 0 & a_4 - 1 \end{pmatrix} \begin{pmatrix} x_1^T \\ x_3^T \\ x_4^T \end{pmatrix}. \quad (4)$$

In short, $x = Ax^T$. Now that x is estimated, y is obtained by inserting (3) into (1). When the y 's are calculated, the concentrations of the complexes can now be computed for plant lines with different x^T concentrations, by solving the mass balance (2) for x , and insert x into (1), which gives the concentrations of the complexes C . The complex concentrations were computed by solving the mass balance using the `lsqnonlin` algorithm in Matlab.

Simulating growth response when SERK1 and SERK3 are employed in other pathways

FLS2 mediated signalling can use up to 70% of the total amount of available SERK3 without affecting BR signalling (Albrecht et al., 2012). For this reason, C_4 and C_5 were increased to 85 %. The following parameters were inserted into (3):

$$x^T = [62 \ 10^3 \ 120 \ 30] \text{ nM}$$

$$C_2 = 0.05 x_1^T$$

$$C_3 = 0.05 x_1^T$$

$$C_4 = 0.85 x_3^T$$

$$C_5 = 0.85 x_4^T.$$

Under this condition, the model predicts the relative root growth response towards BL accurately (Table 1).

Binding of BL

Using the assumptions that BL only binds to BRI1, that BRI1-BL binding is independent of the binding of SERK to BRI1 and the fraction of BRI1 that is bound to BL can be derived via the following mass balance

$$x_1^T = x_1 + [x_1 \ x_2]$$

$$x_2^T = x_2 + [x_1 \ x_2]$$

$$K_d^{-1} x_1 x_2 = [x_1 \ x_2]. \quad (5)$$

It follows that the amount of BRI1 bound to BL is

$$[x_1 \ x_2] = \frac{K_d + x_1^T + x_2^T - \sqrt{(K_d + x_1^T + x_2^T)^2 - 4x_1^T x_2^T}}{2}. \quad (6)$$

The percentage of BRI1 receptors bound to BL is

$$\frac{[x_1 \ x_2]}{x_1^T}, \quad (7)$$

and hence the fractions of complexes bound to BL are

$$C^a = \frac{[x_1 \ x_2]}{x_1^T} C. \quad (8)$$

Here C^a are the concentrations of activated complexes that constitute signalling.

Biochemical model 2: BL binds to BRI1, after which BRI1 interacts with SERK

This model implies that the association between BRI1 and SERK depends on the binding between BRI1 with BL. To account for the competition between SERK1 and SERK3 to be in complex with BL, the mass balance (2) is extended with

$$[x_1 \ x_2] = [x_1 \ x_2]^f + [x_1 \ x_2]^f \gamma_1 x_3^n + [x_1 \ x_2]^f \gamma_2 x_4^n. \quad (9)$$

Here $[x_1 x_2]^f$ denotes the free BRI1-BL complexes, and $[x_1 x_2]$ the solution in (6). The conditions (3) are adjusted. According to the model, complexes C_2 and C_2 only exist in activated form. Therefore the conditions apply only to the activated complexes

$$\begin{aligned}
C_2^a &= [x_1 \ x_2 \ x_3] = [x_1 \ x_2]^f \gamma_1 x_3^n = a_1 x_1^T \\
C_3^a &= [x_1 \ x_2 \ x_4] = [x_1 \ x_2]^f \gamma_2 x_4^n = a_2 x_1^T.
\end{aligned} \tag{10}$$

The binding of BR11 with BL occurs independently of SERK, and is described by (6) using mass balance (5). The mass balance for x_1 , x_2 , and x_4 becomes

$$\begin{aligned}
x_1^T &= C_1 + [x_1 \ x_2] \\
x_3^T &= x_3 + nC_2^a + C_4 \\
x_4^T &= x_4 + nC_3^a + C_5.
\end{aligned} \tag{11}$$

From (11), x_1 , x_2 , and x_4 can be solved as follows:

$$\begin{pmatrix} x_1 \\ x_3 \\ x_4 \end{pmatrix} = - \begin{pmatrix} -1 & 0 & 0 \\ na_1 & a_3 - 1 & 0 \\ na_2 & 0 & a_4 - 1 \end{pmatrix} \begin{pmatrix} x_1^T \\ x_3^T \\ x_4^T \end{pmatrix} - \begin{pmatrix} [x_1 \ x_2] \\ 0 \\ 0 \end{pmatrix}. \tag{12}$$

Thereafter, y_3 and y_4 are computed as before, via inserting C_4 and C_5 in (3) into (1). To compute y_1 and y_2 , the condition (9) is inserted into (10) to eliminate the unknown $[x_1, x_2]^f$, which gives the following equations

$$\begin{aligned}
\gamma_1 x_3^n &= \frac{\beta_1 \beta_2 (1 + \gamma_2 x_4^n)}{1 - \beta_1 \beta_2} \\
\gamma_2 x_4^n &= \frac{\beta_2 \beta_3 (1 + \gamma_1 x_3^n)}{1 - \beta_2 \beta_3},
\end{aligned} \tag{13}$$

with

$$\begin{aligned}
\beta_1 &= a_1 x_1^T \\
\beta_2 &= \frac{1}{[x_1 \ x_2]} \\
\beta_3 &= a_2 x_1^T \\
\beta_4 &= \frac{\beta_2^2 \beta_3 \beta_1}{(1 - \beta_1 \beta_2)(1 - \beta_2 \beta_3)}.
\end{aligned}$$

This can be solved analytically as

$$\gamma_2 = \frac{\beta_2 \beta_3 (1 + \frac{\beta_1 \beta_2}{1 - \beta_1 \beta_2})}{x_4^n (1 - \beta_2 \beta_3) (1 - \beta_4)}$$

$$\gamma_1 = \frac{\beta_1 \beta_2 (1 + \gamma_2 x_4^n)}{x_3^n (1 - \beta_1 \beta_2)}.$$

Biochemical model 3: BRI1-SERK form tetramer complexes

This model states that the main functional complexes are [BRI1 BRI1], [BRI1 BRI1 SERK1 SERK1] and [BRI1 BRI1 SERK3 SERK3], which signal when all two BRI1 are bound to BL. The functional complexes are

$$C_1 = [x_1 \ x_1] = \gamma_5 x_1^2$$

$$C_2 = [x_1 \ x_1 \ x_3 \ x_3] = \gamma_1 x_1^2 x_3^2$$

$$C_3 = [x_1 \ x_1 \ x_4 \ x_4] = \gamma_2 x_1^2 x_4^2. \quad (16)$$

The mass balance then reads

$$x_1^T = 2C_1 + 2C_2 + 2C_3$$

$$x_3^T = x_3 + 2C_2 + C_4$$

$$x_4^T = x_4 + 2C_3 + C_5. \quad (17)$$

The conditions for C_1 , C_2 and C_3 now become

$$2C_1 = a_5 x_1^T = 0.08 x_1^T \quad 8\% \text{ of BRI consists of BRI dimers not in complex with SERK}$$

$$2C_2 = a_1 x_1^T$$

$$2C_3 = a_2 x_1^T. \quad (18)$$

The conditions for C_4 and C_5 remain the same as before. The mass balance (17) is combined with (18) to compute x :

$$\begin{pmatrix} x_1 \\ x_3 \\ x_4 \end{pmatrix} = - \begin{pmatrix} a_1 + a_2 + a_5 - 1 & 0 & 0 \\ a_1 & a_3 - 1 & 0 \\ a_2 & 0 & a_4 - 1 \end{pmatrix} \begin{pmatrix} x_1^T \\ x_3^T \\ x_4^T \end{pmatrix}. \quad (19)$$

File S1B. Growth model

In this section, the signalling constituted by the activated BRI1-SERK complexes is linked to organ growth via a growth model. Whereas the receptor activation kinetics is modelled bottom up, based on specific biochemical suppositions, the relation between receptor activation and phenotype development is modelled top down, based on phenomenological considerations. The BRI1 mediated signal that regulates organ growth consists of contributions from the three activated complexes

$$R(\sigma, t) = R_0(t) \cdot (1 + f(\sigma, t)) \quad (20)$$

with α_i free model parameters that have to be estimated. Root growth is modelled as a combination of two separate mechanisms

$$\sigma = \alpha_1 C_1^a + \alpha_2 C_2^a + \alpha_3 C_3^a, \quad (21)$$

with $R(\sigma, t)$ the root length on time t , $f(\sigma, t)$ the root length via regulation of BRI1 mediated signalling, and $R_0(t)$ the root length of BRZ treated seedlings. Scaling of (21) gives the root length due to application of BL relative to the root length of BRZ treated seedlings:

$$y(\sigma, t) = \frac{R(\sigma, t)}{R_0(t)} = 1 + f(\sigma, t). \quad (22)$$

The function $f(\sigma, t)$ that relates BRI1 signalling to root length is built up from two types of modules, activating and inhibiting, e.g.,

$$f(\sigma, t) = E(t) \frac{\sigma}{\alpha_4 + \sigma} \frac{1}{\alpha_5 + \sigma} \quad (23)$$

Here $E(t)$ is a time dependent growth factor, $\frac{\sigma}{\alpha_4 + \sigma}$ is an activating module, and $\frac{1}{\alpha_5 + \sigma}$ an inhibiting module, representing activating and inhibiting influences

of signalling on root growth. In total 13 functions $f(\sigma, t)$ were tested, ranging from 1 activating or inhibiting module to 3 activating and 3 inhibiting modules and all relevant combinations in between.

Data scaling

The scaling in (23) requires the data be scaled with $R_0(t)$, which is the root length corresponding to BL=0. However, in the BL response experiments there is always a little amount of BL left after BRZ treatment, so the precise value of $R_0(t)$ cannot be measured directly. Therefore, $R_0(t)$ is estimated with help of the model. The small rest amount of BL corresponds to a small signal $\tilde{\sigma}$, so $R(\tilde{\sigma}, t) = R_0(t) + f(\tilde{\sigma})$ according to (21). Therefore, the data are not scaled with $R_0(t)$ but with $R(\tilde{\sigma}, t)$:

$$y(\sigma, t) = \frac{R(\sigma, t)}{R(\tilde{\sigma}, t)}. \quad (24)$$

The model output is scaled accordingly:

$$y(\sigma, t) = \frac{R(\sigma, t)}{R(\tilde{\sigma}, t)} = \frac{1 + f(\sigma, t)}{1 + f(\tilde{\sigma}, t)}. \quad (25)$$

File S1C. parameter optimization and model selection

Parameter optimization

The parameters are optimised in the same way as reported in Chapter 3. The χ^2 criterion

$$S(\theta) = \sum_i \left(\frac{y(\theta)_i - y_{d,i}}{\sigma_i} \right)^2 \quad (26)$$

is minimised. Here $y(\theta)$ denotes the model prediction, y_d the measured data, σ the standard deviation of the measurement noise, and i ranges over measured data points.

Model selection

The plausibility of the different models is tested by fitting them to experimental data, and by assessing their predictive power with three different methods. In the first two methods the model fits of the different model structures were compared using the Akaike Information Criterion (AIC) and the Bayesian Information Criterion (BIC)

$$AIC = \min S(\theta) + 2p + \frac{2p(p+1)}{n-p-1}$$

$$BIC = \min S(\theta) + p \log(n) \quad (27)$$

Here p is the number of parameters, and n the number of data points. The third method consists of a four-fold cross-validation, with error criterion (26) defined as the prediction error, averaged over the four predictions.

SUPPLEMENTAL FIGURES AND TABLES

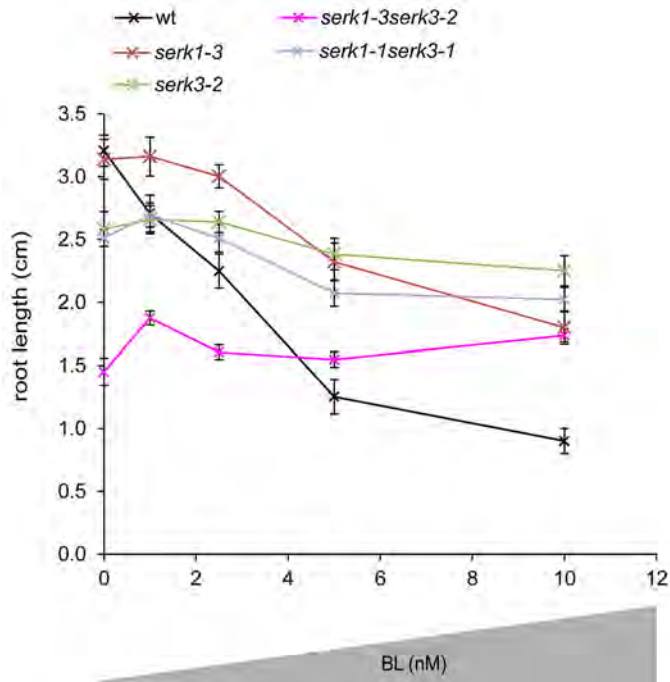


Figure S1. Root length assays of *serk1-3* and *serk3-2* mutants in absence of BRZ. In absence of BRZ, roots of the *serk1serk3* double mutant are completely insensitive to exogenously applied BL. For all measurements $n \geq 15$ roots measured at 8 days after germination (DAG) in three independent replicates, error bars \pm SEM.

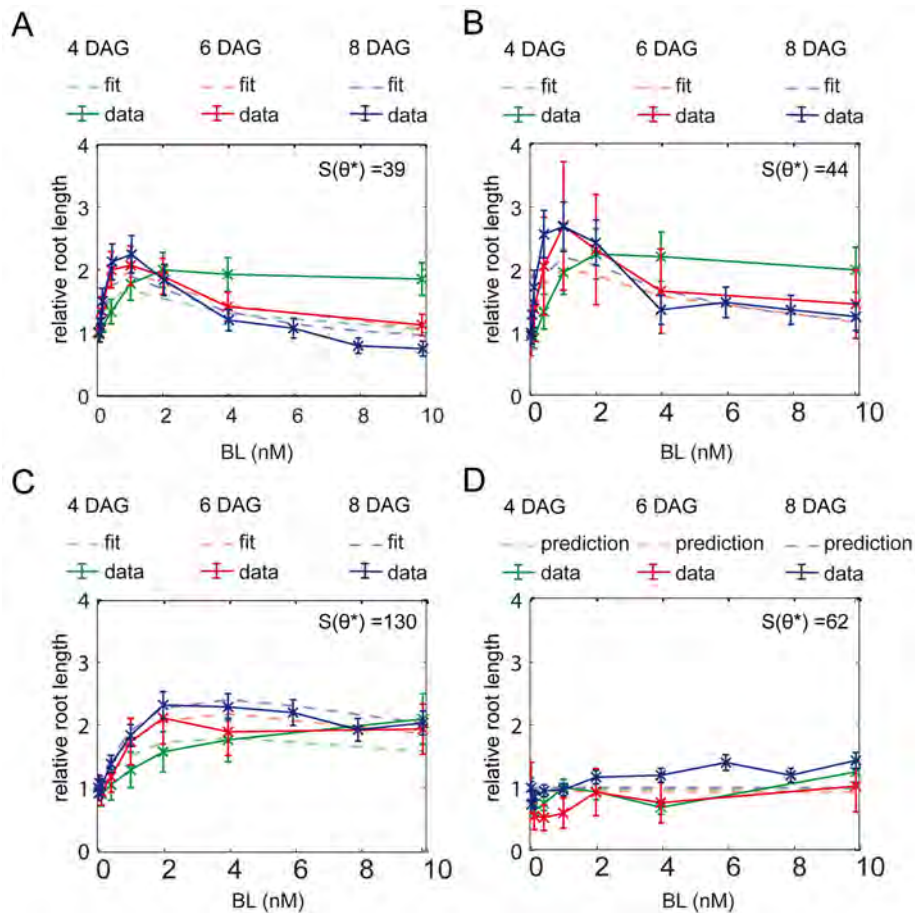


Figure S2. Model calibration on relative root lengths of seedlings at 4, 6 and 8 DAG simultaneously. The model can accurately fit with the relative root length at 6 and 8 DAG simultaneously but not with the relative root length at 4, 6 and 8 DAG. Figure shows fit and actual data set at 4, 6 and 8 DAG for Col-0 wild type (A) and the *serk1-3* (B) *serk3-2* (C) and *serk1-3serk3-2* (D) mutants. Error bars \pm SEM, $n \geq 15$ measured in three independent replicates.

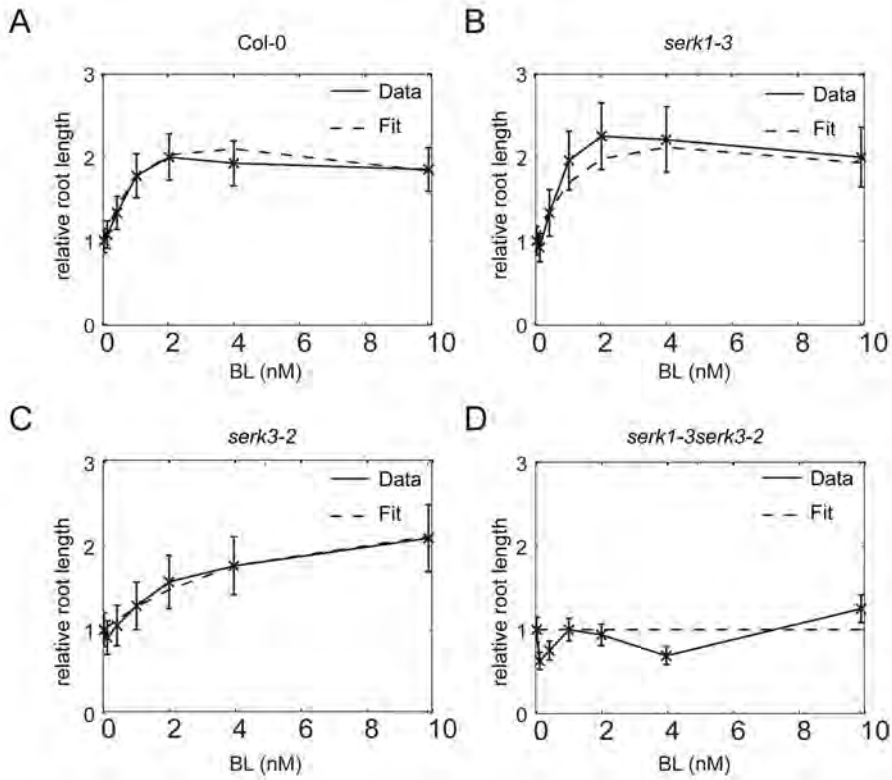


Figure S3. Model calibration on relative root lengths of seedlings at 4 DAG. Figure shows fit of the model on relative root length of seedlings at 4 days after germination (DAG). Error bars experimental data set are \pm SEM, $n \geq 15$ measured in three independent replicates.

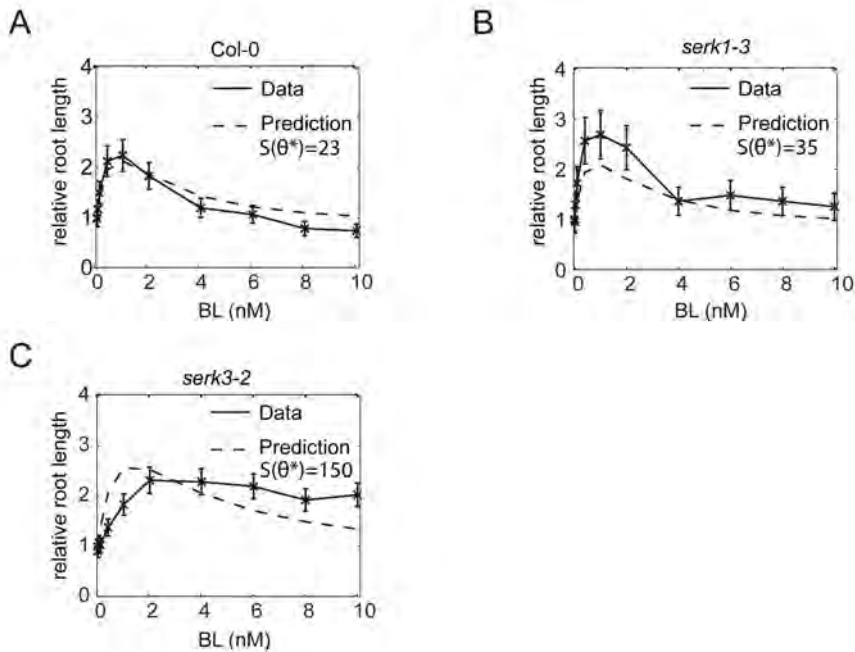


Figure S4. Leave-one-out cross-validation for modelling root growth. (A) After calibration on the *serk1-3*, *serk3-2* and *serk1-3serk3-2* double mutant root growth of wild type seedlings was predicted. (B) Model calibration on wild type, *serk3-2* and *serk1-3serk3-2* while predicting root growth of the *serk1-3* mutant (C) Model calibration on wild type, *serk1-3* and *serk1-3serk3-2* while predicting root growth of the *serk3-2*. All data shows root growth relative to BRZ treated control at 8 days after germination. $S(\theta^*)$ denotes the prediction error.

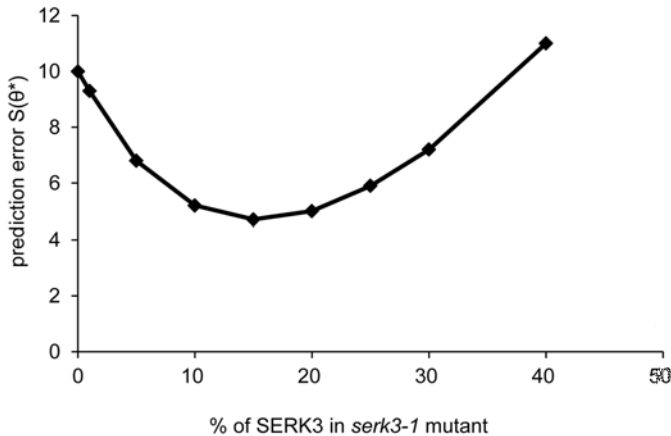
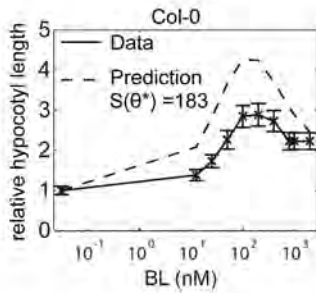
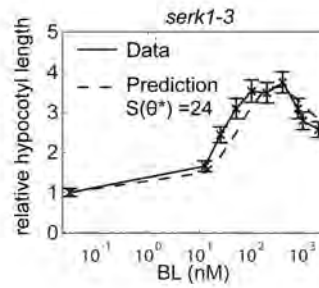


Figure S5. The model is robust against alterations in the amount of SERK3 transcript in *serk3-1* background. The % of SERK3 protein left in the *serk3-1* mutant is plotted against the sum of squared errors $S(\theta^*)$ that represents the error between the model predictions and actual data. $S(\theta^*)$ denotes the prediction error, a lower $S(\theta^*)$ indicates a better resemblance between the model predictions and experimental data. The model shows the best prediction when assuming that there is between 10-20 % of SERK3 protein still present in the *serk3-1* background.

A



B



C

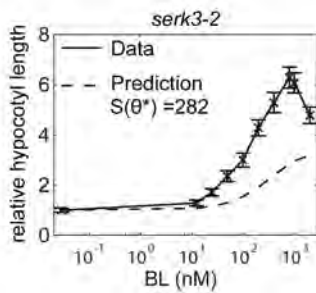


Figure S6. Leave-one-out cross-validation for modelling hypocotyl elongation. Figure shows prediction and actual data sets of relative hypocotyl lengths for wild type (A), *serk1-3* (B) and *serk3-2* (C) mutants. All predictions were done using a K_d of 1500 nM. $S(\theta^*)$ denotes the prediction error. Error bars \pm SEM, $n \geq 30$ measured in three independent replicates.

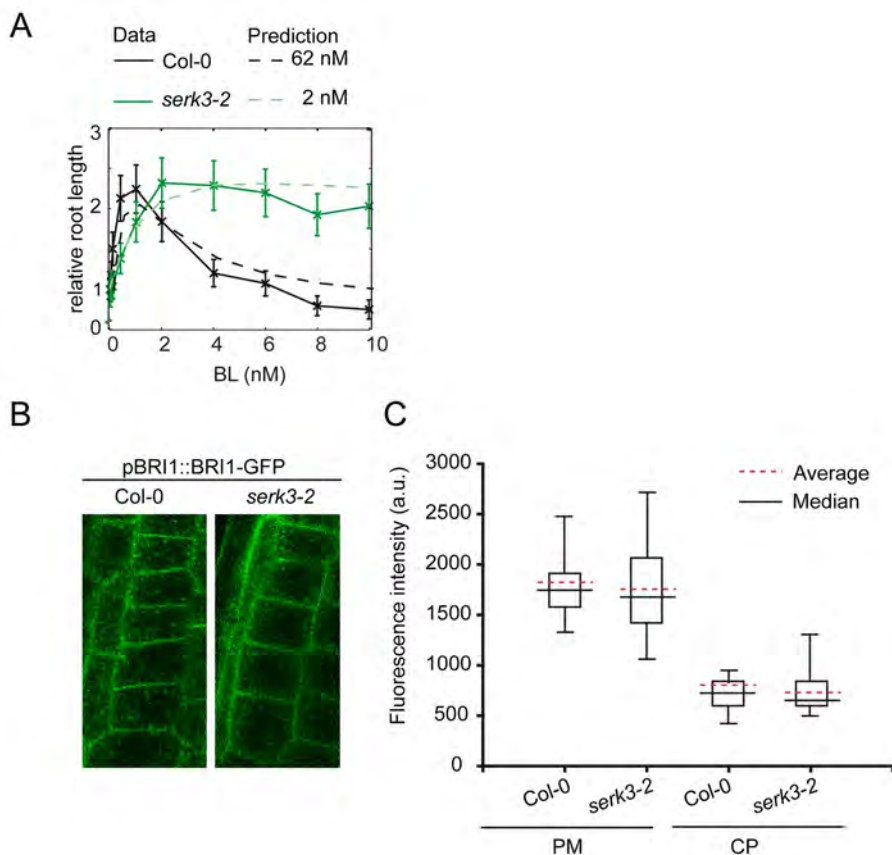


Figure S7. Trend observed in the *serk3-2* mutant is not due to a reduced BRI1 level. A) Effect of the active number of BRI1 receptors on root growth which is for modelling purposes considered as a reduced concentration BRI1. Model calibration was done on wild type, *serk1-3*, *serk3-2* and *serk1-3serk3-2* double mutant. Model predictions for a BRI1 concentration of 62 (wild type) and 2 nM are shown. The trend in the *serk3-2* mutant is similar to the trend observed when the active BRI1 concentration is 2 nM. B) Confocal images showing the BRI1-GFP expression in wild type and *serk3-2* background. Representative images are shown. C) Comparison of the BRI1-GFP fluorescence intensity in wild type and *serk3-2* background. The fluorescence intensity of BRI1-GFP in the *serk3-2* background is hardly changed when compared to the wild type background indicating that the observed trend in (A) is due to a reduced BRI1 receptor activity rather than the total BRI1 concentration. For root length assays $n \geq 30$ roots measured in three independent replicates, values \pm SEM. For fluorescence microscopy $n \geq 7$ roots # 5 Cells per root (35 cells in total) measured in two independent replicates. PM= plasma membrane CP = cytoplasm.

Table S1. Comparison of different growth model structures using root length as readout

model structure	modules		model selection criteria*		
	stimulatory	inhibiting	AIC	BIC	PE
1	1	2	79	75	63
2	2	2	82	77	63
3	2	1	92	87	75
4	1	1	90	87	80
5	1	0	197	195	100
6	0	1	379	377	129
7	3	2	85	79	62
8	2	3	83	77	61
9	3	3	85	77	55
10	1	3	79	74	57
11	3	1	94	89	79
12	0	2	382	379	129
13	0	3	384	380	129

AIC = Akaike information criterion. For definitions see Supplemental File S1C

BIC = Bayesian information criterion. For definitions see Supplemental File S1C

PE = Prediction Error. The average weighted squared prediction error of four leave-one-out cross-validations

Calibration was done using the relative root length of wild type, *serk1-3*, *serk3-2* and *serk1-3serk3-2* seedlings at 6, and 8 days after germination (DAG) as training set. All criteria of the growth model structures were computed using biochemical model structure 1 (Supplemental File S1A).

*Model 1 was selected based on a low score of three criteria and having the simplest model structure. Increasing the complexity by adding an extra inhibitory (models 8-10) or stimulatory module (model 2,3, 7-9) does not considerably improve the score.

Table S2. Comparison of different growth model structures using hypocotyl elongation as readout

model structure	modules		model selection criteria*		
	stimulatory	inhibiting	AIC	BIC	PE
1	1	2	220	213	175
2	2	2	224	214	171
3	2	1	224	217	214
4	1	1	223	218	192
5	1	0	707	703	247
6	0	1	1807	1804	449
7	3	2	227	216	182
8	2	3	228	216	169
9	3	3	232	217	168
10	1	3	224	215	168
11	3	1	228	219	216
12	0	2	1810	1805	449
13	0	3	1814	1806	449

AIC= Akaike information criterion. For definitions see Supplemental File S1C

BIC= Bayesian information criterion. For definitions see Supplemental File S1C

PE= Prediction Error. The average weighted squared prediction error of four leave-one-out cross-validations

Calibration was done using the relative root length of wild type, *serk1-3*, *serk3-2* and *serk1-3serk3-2* seedlings at 6, and 8 days after germination (DAG) as training set. All criteria of the growth model structures were computed using biochemical model structure 1 (Supplemental File S1A).

*Model 1 was selected based on a low score of three criteria and having the simplest model structure. Increasing the complexity by adding an extra inhibitory (models 8-10) or stimulatory module (model 2,3, 7-9) does not considerably improve the score.

Table S3. Predicted amount of ligand occupied BRI1 interacting with SERK in wild type background

Biochemical model	Col-0			
	BL (nM)	[BRI1 BL] (nM)	[BRI1 BL SERK1] (nM)	[BRI1 BL SERK3] (nM)
1	0	0.02	0.00	0.00
	0.1	0.10	0.01	0.01
	0.4	0.35	0.02	0.02
	1	0.83	0.05	0.05
	2	1.63	0.09	0.09
	4	3.22	0.18	0.18
	10	7.92	0.44	0.44
2	0	0.05	0.00	0.00
	0.1	0.13	0.01	0.01
	0.4	0.37	0.02	0.02
	1	0.84	0.05	0.05
	2	1.64	0.09	0.10
	4	3.22	0.18	0.20
	10	7.89	0.45	0.48

Biochemical model 1: BL binds to [BRI1 SERK]

Biochemical model 2: BL binds to BRI1, after which BRI1 interacts with SERK

Growth model 1 is used consisting of one stimulatory and two inhibitory modules

Model assumes that there is a still some BL left after BRZ treatment. The 0 nM BL in the Table represents the amount of complex still present after BRZ treatment assuming that there is ≤ 0.1 nM BL in a BRZ treated seedlings.



Chapter 5

Monitoring BRI1 and SERK3 mobility in Arabidopsis roots by Fluorescence Recovery after Photobleaching

G. Wilma van Esse, Antsje Nollens, Bart Geverts,
Simon van Mourik, Jan Willem Borst and Sacco C. de Vries

ABSTRACT

Members of the Somatic Embryogenesis Receptor like Kinase (SERK) co-receptor family associate with different ligand perceiving receptors such as brassinosteroid insensitive 1 (BRI1) and flagellin sensitive 2 (FLS2). Current models suggest fast recruitment of SERK co-receptors towards FLS2 or BRI1 upon ligand binding. However, in plasma membranes (PM) lateral movement of proteins is often restricted. How mobility of proteins is affected is of interest especially in signal transduction cascades where receptor hetero-oligomerization at the PM often forms a key point in activation of downstream targets. In plants, an additional complexity is the presence of the cell wall that further restricts movement of PM localised proteins. Therefore, the measurement of lateral protein movement in protoplasts usually results in an overestimate of the diffusion coefficient. The aim of this work is to determine the mobility of BRI1 and SERK3 employing fluorescence recovery after photobleaching (FRAP) in Arabidopsis root cells active in BR signalling. Results indicate that PM localised BRI1 and SERK3 have low diffusion coefficients in root meristematic cells suggesting that the (lateral) mobility of BRI1 and SERK3 is limited.

INTRODUCTION

The association of proteins into complexes is an important step in cellular signal transduction cascades (Chen et al., 2003). The cell in which the proteins reside can be viewed as an enclosed area in which proteins can diffuse freely. However, proteins are usually restricted to a certain cellular compartment and often move inhomogeneously (Ritchie et al., 2005). In particular PM localised proteins can be restricted in their movement due to e.g. the presence of lipid rafts, which can compartmentalise proteins (Lingwood et al., 2009; Owen et al., 2012). As protein interactions are essential to signal transduction, it is of interest to know the mobility of proteins and how fast downstream target proteins can be reached. In Arabidopsis, the lateral mobility of PM localised proteins is restricted by the presence of the cell wall. This limitation in movement is not necessarily due to direct interaction of the protein with cell wall components, but can also be due to PM/cell wall constraints (Martinière et al., 2012). BRI1 and SERK1, two PM localised receptor like kinases, have a significant higher mobile fraction and diffusion coefficient *in planta* compared to protoplasts (Kwaaitaal et al., 2011). Current models of BR signalling propose a mechanism where ligand binding to BRI1 induces the hetero-oligomerization between BRI1 and SERK3 (Li et al., 2002; Wang et al., 2005). SERK3 (also referred to as BAK1) is employed as co-receptor in different signalling pathways. For example, upon ligand binding the FLS2 receptor rapidly interacts with SERK3 inducing downstream phosphorylation events (Chinchilla et al., 2007; Schulze et al., 2010). In hormone signalling, maximal phosphorylation of SERK3 is already observed within 60-120 seconds after BL stimulation (Schulze et al., 2010). Co-immunoprecipitation experiments indicate that there is a significant increase in amount of SERK3 associating with BRI1 at 10 and 90 minutes after ligand application (Albrecht et al., 2012). To enable a fast response on a diffusion-based model, SERK3 and BRI1 should not be restricted in their lateral mobility. This work aims to evaluate the mobility between BRI1 and SERK3 *in planta* using Fluorescence Recovery after Photobleaching (FRAP). The diffusion coefficients of BRI1-GFP and SERK3-GFP *in planta* as measured here are highly variable between 0.009 and 0.11 $\mu\text{m}^2\text{s}^{-1}$. These values are far below the 10 $\mu\text{m}^2\text{s}^{-1}$, which is the value for free lateral diffusion of PM receptors in mammalian systems (Meissner and Haberlein, 2003; Bacia et al., 2006). This indicates that the plant RLKs BRI1 and SERK3 are restricted in their movement *in planta*. For this reason, we propose that BRI1 and SERK3 are already in close proximity at the PM, possibly in plasma membrane domains, as pre-formed complexes or both.

RESULTS AND DISCUSSION

BRI1-GFP and SERK3-GFP mobility in protoplasts

FRAP experiments were performed to determine the diffusion coefficients and mobile fractions of BRI1-GFP and SERK3-GFP in protoplasts derived from *Arabidopsis* mesophyll cells. After one minute a complete recovery of BRI1-GFP at the plasma membrane (PM) was observed (Fig. 1). The diffusion coefficient and the mobile fraction of BRI1-GFP in protoplast is respectively $0.38 \pm 0.08 \mu\text{m}^2\text{s}^{-1}$ and $49 \pm 8\%$. This is significantly lower compared to the measured values for SERK3-GFP, which has a diffusion coefficient of $0.55 \pm 0.07 \mu\text{m}^2\text{s}^{-1}$ and a mobile fraction of $78 \pm 5\%$ (Table 1). The measured mobile fraction and diffusion of BRI1-GFP in protoplast is within the same order of magnitude as previously reported (Ali et al., 2007; Kwaaitaal et al., 2011).

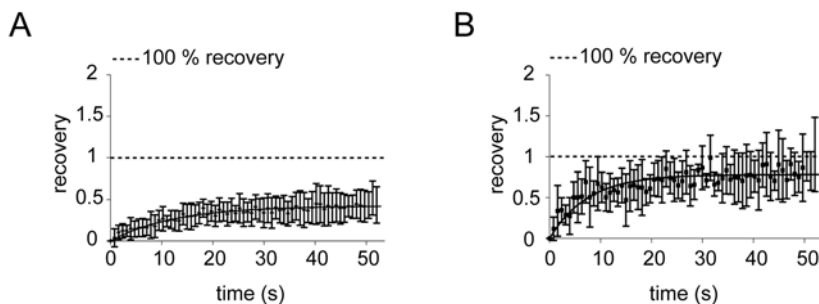


Figure 1. Fluorescence recovery curves of BRI1-GFP and SERK3-GFP in protoplasts. The data of BRI1-GFP (A) is an average of 9 independent experiments and the data of SERK3-GFP (B) is an average of 4 independent experiments. Error bars indicate standard deviation.

BRI1-GFP and SERK3-GFP mobility *in planta*

Next, FRAP measurements were performed in meristem cells of 5-day old seedling roots expressing BRI1-GFP. As a control KNOLLE-GFP was used. KNOLLE is a protein that is involved in the formation of the cell plate during cell division and showed a relative high mobility *in planta* (Boutte et al., 2010). The recovery of KNOLLE-GFP at the cell plate was completely restored after 3 min while hardly any recovery was measured at the PM of seedling roots expressing BRI1-GFP (Fig. 2A and B). For BRI1-GFP in the root meristem a diffusion coefficient of $0.009 \pm 0.002 \mu\text{m}^2\text{s}^{-1}$ and a mobile fraction of $28 \pm 2\%$ was found. For SERK3-GFP a mobile fraction of $78 \pm 3\%$ with a diffusion coefficient of $0.009 \pm 0.002 \mu\text{m}^2\text{s}^{-1}$ was obtained. Taken together, these data indicate that PM localised BRI1-GFP and SERK3-GFP are less mobile in meristem epidermal cells when compared to elongating cells and protoplasts (Table 1).

Table 1. Mobile fractions and diffusion coefficients of BRI1 and SERK3

	Tissue	Mf (%)	DC $\mu\text{m}^2\text{s}^{-1}$	N	Reference
BRI1-GFP	Protoplasts	70 \pm 17	2.2 \pm 0.7		Kwaaitaal et al. (2011)
		79 \pm 2.4	0.26 \pm 0.13	10	Ali et al. (2007)
		49 \pm 8	0.38 \pm 0.08	8	This work
	Meristem	28 \pm 2	0.009 \pm 0.002	15	This work
	Elongation zone	35 \pm 3	0.11 \pm 0.04	15	This work
	Root cells	10 \pm 10			Kwaaitaal et al. (2011)
SERK3-GFP	Protoplasts	78 \pm 5	0.55 \pm 0.07	4	This work
	Meristem	78 \pm 3	0.009 \pm 0.002	5	This work
	Elongation zone	58 \pm 2	0.08 \pm 0.02	5	This work

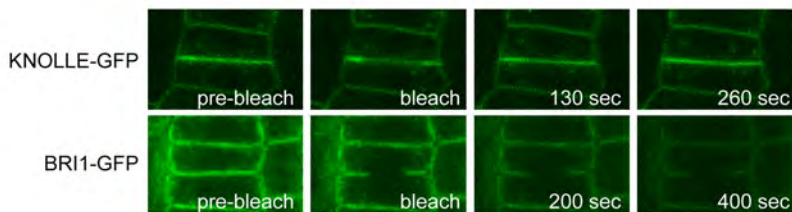
N = number of individual measurements.

Mf = mobile fraction

Dc = diffusion coefficients

Values are given \pm SEM

A



B

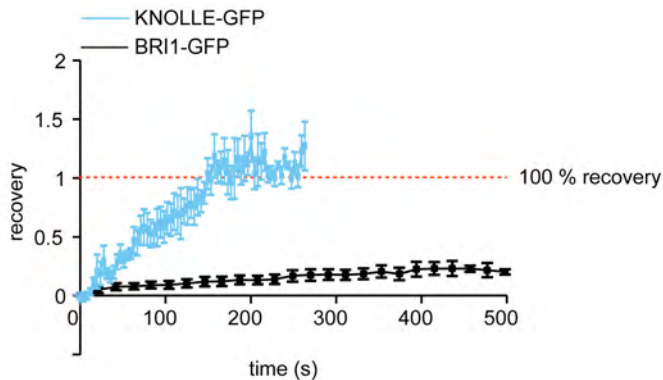


Figure 2. Bleach series of BRI1-GFP and KNOLLE-GFP in epidermal cells in root meristem. A) After approximately 3 min the fluorescence intensity at the PM from KNOLLE-GFP was restored while no such recovery was observed for BRI1-GFP even not after 400 seconds after the initially bleaching at the PM. B) Recovery-curves of KNOLLE-GFP (blue line) and BRI1-GFP (black line) in epidermal cells in the root meristem. Several independent replicates (KNOLLE-GFP: $n = 7$ and for BRI1-GFP: $n = 15$), were performed. In the graph the error bars indicate standard error of means (SEM).

BRI1-GFP protein is localised at the PM as well as in pre-vacuolar compartments and in early endosomes/ trans-Golgi network (Friedrichsen et al., 2000; Geldner et al., 2007; Viotti et al., 2010). Due to limitations of the spatial resolution of a confocal microscope it is not possible to discriminate between BRI1-GFP molecules residing in the PM or in cytosolic compartments located close proximity of the PM. Especially, in the root elongation zone it is hard to distinguish whether the measured diffusion rate and mobile fraction in roots cells correlates to lateral diffusion within the PM or to insertion from the ER/Golgi/TGN network localised in close proximity of the PM. For this reason, we determined the fluorescence intensity in the bleached area using Gaussian fits of the intensities measured in axial PM of meristem epidermal cells (Fig. 3). These cells were chosen because of their small vacuoles, making it possible to separately measure fluorescence of the cytoplasm. Surprisingly, in these cells the mobility of BRI1-GFP was reduced about a hundred-fold compared to cells within the elongation zone. This suggests that lateral mobility as well as insertion into the PM of fluorescent receptors is virtually non-existing. Assuming a comparable PM structure, this could imply that in elongating meristem cells the observed mobility is largely due to replenishment of receptors from within the cell. For SERK3-GFP insufficient measurements were done in order to confirm this trend.

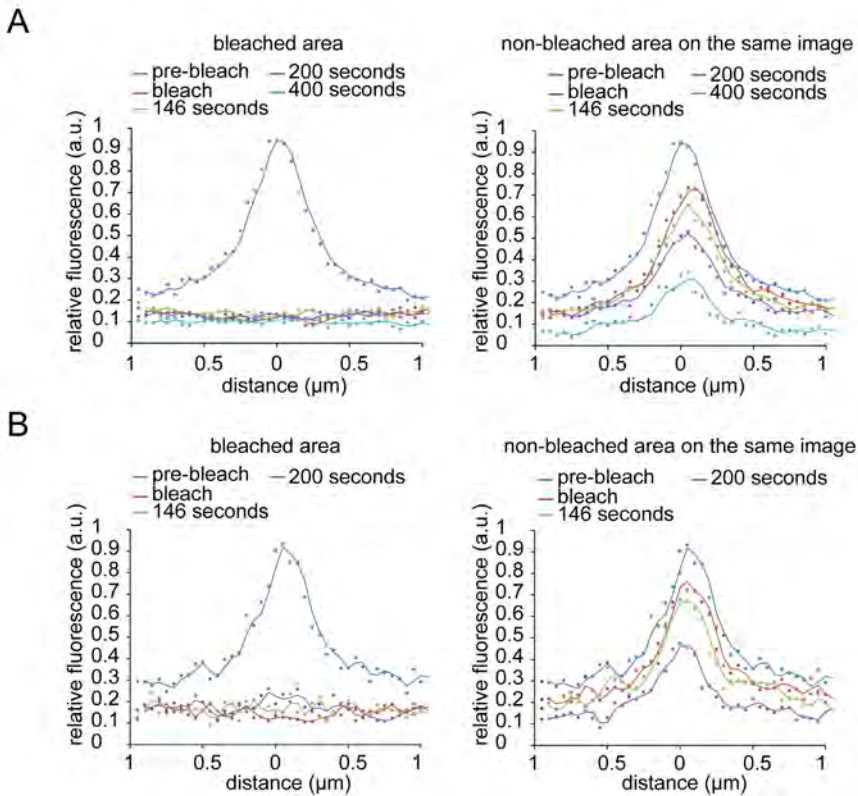


Figure 3. Gaussian fits drawn of fluorescent intensity over the anticlinal cell wall before and after photobleaching. The 0 is the middle point of two plasma membranes in a confocal image, between 1-0.5 μm is the fluorescence intensity in the cytoplasm next to the plasma membrane. A) Fluorescence intensity of BRI1-GFP at the bleached area (left) compared to the intensity at a non-bleached area of the PM (right). After 400 seconds, the fluorescence intensity at the non-bleached area (right panel) was reduced significantly due to scan bleaching, which occurs when the image is recorded. B) Same as in A, now for SERK3-GFP. $n = 5$ different roots measuring 20 fits per image ($n \geq 100$ data points).

Here we observed that a significant difference can occur in the diffusion coefficients of the same BRI1-GFP receptor in different cells of the root. Whereas relative immobility of PM located proteins was noted in a number of studies (Martinière et al. 2012) this work did not take into consideration possible differences due to cellular identity or location within a tissue. Epidermal cells of the meristematic zone of the root as well as elongating cells are reported to be active in BR signalling (Hacham et al. 2011; González-García et al. 2011). At present it is not possible to correlate the difference in mobility of BRI1-GFP to enhanced signalling activity. Potential caveats of using FRAP are the spatial limitation of the confocal microscope, so no definite answer is possible to the question whether lateral diffusion or insertion into the PM from the ER is the cause of the observed fluorescence recovery in elongating cells. In addition, technical difficulties such

as scan bleaching, low receptor fluorescence intensity at physiological relevant receptor level may result in an overestimate of the diffusion coefficient.

In conclusion, the observation of low BRI1 receptor mobility in meristematic root cells is in line with a model where a relatively small number of preformed BRI1-SERK3 receptor hetero-oligomers exist in the PM in the absence of the activating ligand. Clearly, other techniques such as single-molecule imaging are required to provide more definite evidence.

EXPERIMENTAL PROCEDURES

Plant lines

Arabidopsis thaliana ecotype Columbia-0 (Col-0) was used as wild type plant. For all FRAP experiments BRI1 (At4G39400), SERK3 (At4G33430) and KNOLLE (At1G08560) fused to green fluorescent protein (GFP) were used. All constructs were expressed under their own promoter in wild type background. The BRI1-GFP line was provided by J. Chory (Friedrichsen et al., 2000). KNOLLE-GFP was used as a positive control for the FRAP experiment based on the data of Boutté et al. (2010). Seed sterilization and plants growth was performed as described in Chapter 2. Protoplast isolation and transfection was done as described previously (Bücherl et al., 2010).

Confocal microscopy and FRAP measurements

Roots of *Arabidopsis* seedlings expressing BRI1-GFP, SERK3-GFP or KNOLLE-GFP and the protoplasts were imaged with a CONFOCOR2/LSM510 confocal microscope (Zeiss) equipped with a 40x water objective (numerical aperture 1.2) and an argon ion laser. The argon laser was used for excitation of GFP at 488 nm (laser output was set at 6.1 A), emission was detected with a band-pass filter at 505 to 550 nm. The measurement of BRI1-GFP and SERK3-GFP in protoplasts was performed in an 8-chamber slide containing 300 µL of the protoplast solution in a single chamber. For the bleach procedure 15 pulse iterations at 50% laser power at 488 nm was used. Images were taken up to 53 s after the bleach pulse. Roots were immobilised in 1x PBS (8 g NaCl, 0.2 g KCl, 1.44 g Na₂HPO₄, 0.24 g KH₂PO₄ in 1 L distilled H₂O) in a 2-chamber slide (pre-incubated with 0.1% poly-L-lysine for at least 1 hour) covered with a coverglass and a weight on top. KNOLLE-GFP was measured in the cell-plate of dividing cells in the root meristem of 5-day old *A. thaliana* plants. The bleach pulse was given with 20 iterations at 75% transmission at 488 nm, the recovery was followed up to 260 s. For BRI1-GFP and SERK3-GFP the excitation laser power was respectively 5% and 9 % at 488 nm. The images were taken with a 6x zoom, a scan time of 15.73 s and a cycle delay of 5 s. A fixed rectangular area of 60x15 pixels (4.5x1.1 µm) was bleached on the plasma membrane with 50 iterations at 45% transmission at 488 nm for both proteins. The recovery of the fluorescent signal was followed up to 499 s and 436 s, respectively for BRI1-GFP and SERK3-GFP. For FRAP measurements in the elongation zone the excitation laser power was set to 1% at 488 nm to reduce the scan bleaching. The images were taken with a 4x zoom and a scan time of 6.29 s. The bleach pulse was given with 15 iterations at 50% transmission at 488 nm for both proteins.

FRAP data analysis

Analysis of the FRAP data was done essentially as described previously (van Royen et al., 2009; Kwaaitaal et al., 2011). All fluorescence intensities were recorded in arbitrary units (a.u.) and corrected for autofluorescence in the wild type control according to:

$$I_{norm,t} = \frac{I_t - I_{background}}{(I_{t,scanbleach} - I_{background}) / (I_{0,scanbleach} - I_{0,background})}$$

where $I_{norm,t}$ is the normalized fluorescence intensity at time t , I_t is total intensity at time t , $I_{background}$ is the intensity in the wild type control, $I_{t,scanbleach}$ is the fluorescence intensity of an area with the same size as the bleached area for measuring the contribution of scan-bleaching, $I_{0,scanbleach}$ is the average fluorescence signal of the scan-bleaching before the bleaching procedure and $I_{0,background}$ is the average signal of the background before bleaching. The normalised fluorescence intensities are calculated according to:

$$I_{data,norm} = \frac{I_{norm,t} - I_{norm,bleach}}{I_{norm,0} - I_{norm,bleach}}$$

where $I_{data,norm}$ is the calculated normalised intensity, $I_{norm,bleach}$ is the normalised intensity just after the bleach, and $I_{norm,0}$ is the average normalised intensity before bleaching.

The mobile fraction is defined as:

$$F_m = \frac{I_{norm,end} - I_{norm,bleach}}{I_{norm,0} - I_{norm,bleach}}$$

where $I_{norm,end}$ is the normalised intensity after full recovery. The recovery data is fitted to a model describing two-dimensional diffusion according to the next formula:

$$I(t) = F_m(1 - e^{-kt})$$

where k is the recovery constant, which is related to the half-time of recovery as follows:

$$t_{1/2} = \ln(2) / k$$

For unrestricted two-dimensional diffusion, the diffusion coefficient (D_c) is related to the half-time of recovery ($t_{1/2}$) as follows:

$$D_c = \frac{A}{4 \times t_{1/2}} \mu m^2 s^{-1}$$

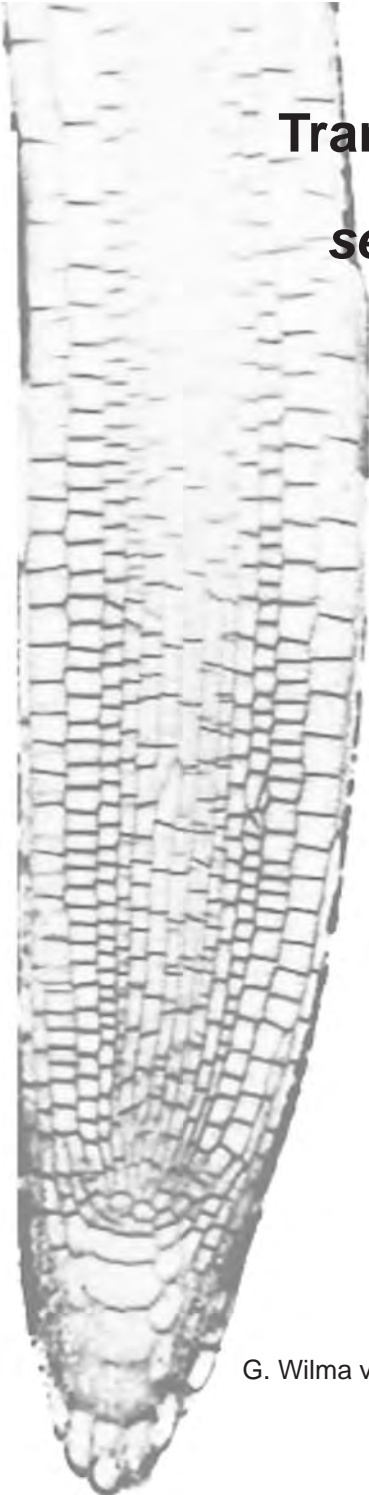
where A is the area of the bleached region. Note that the diffusion of 'out of focus' fluorescent molecules into the bleached area is not taken into account. This assumption only holds for membranes or very thin layers (Kwaaitaal et al., 2011). Curve fitting was performed using Microsoft Excel.

ACKNOWLEDGEMENTS

This work was financially supported by the Netherlands Consortium for Systems Biology (NCSB) which is part of the Netherlands Genomics Initiative / Netherlands Organisation for Scientific Research (SvM) and the IPOP systems biology initiative of Wageningen University (GWvE).

Chapter 6

Transcriptional analysis of *serk1* and *serk3* mutants



G. Wilma van Esse, Colette A. ten Hove, H. Peter van Esse,
Mark Boekschoten, and Sacco C. de Vries

In preparation for publication

ABSTRACT

Somatic embryogenesis receptor like kinases (SERK) are non-ligand binding co-receptors, that are able to combine with different ligand perceiving receptors such as Brassinosteroid Insensitive 1 (BRI1) and Flagellin Sensitive 2 (FLS2). Phenotypical analysis of *serk* single mutants is not straightforward because multiple pathways can be affected, while redundancy is observed for a single phenotype. For example, *serk1serk3* double mutant roots are insensitive towards brassinosteroids but have a phenotype different from *bri1* mutant roots. To decipher these effects, 4 day old *Arabidopsis* roots were studied using microarray analysis. 698 genes, involved in multiple biological processes, were found to be differentially regulated in *serk1-3serk3-2* double mutants. About half of these are related to BR signalling. The remainder appears to be unlinked to BRs and related to primary and secondary metabolism. In particular, it appears that suberin biosynthesis genes are down-regulated, suggesting a novel role of SERK-mediated pathways in secondary cell wall modification. The results show that the gene expression pattern of the *serk3-2* mutant is similar to that of *serk1-3serk3-2* roots. This confirms the existence of partial redundancy between SERK3 and SERK1 as well as the activity of a single co-receptor in multiple simultaneously active pathways.

INTRODUCTION

The five Somatic Embryogenesis Receptor Kinase (SERK) receptors in Arabidopsis are leucine rich repeat receptor like kinases (LRR-RLK) that are involved in various cellular processes (Hecht et al., 2001; Albrecht et al., 2008). No ligands have been reported to bind to the extracellular domain of the SERK receptors; current models assume they function as non-ligand binding co-receptors by heterodimerising with different ligand perceiving receptors (Chinchilla et al., 2009). SERK1, SERK3 (BAK1) and SERK4 (BKK1) function as co-receptor of BRI1, which is the main ligand perceiving receptor for brassinosteroids (BRs) in Arabidopsis (Wang et al., 2001; Li et al., 2002; Karlova et al., 2006; He et al., 2007). BRs are a class of plant specific steroid hormones involved in cell elongation, division and differentiation, photosynthesis, stress responses and senescence (Clouse and Sasse, 1998). Mutants that are unable to synthesise or perceive BRs have a dwarfed stature, impaired photomorphogenesis and fertility defects (Chory et al., 1991; Clouse et al., 1996; Clouse and Sasse, 1998). Recently, it was shown that BRI1 mediated BR signalling completely depends on its interaction with SERKs. However, with the exception of SERK3, single *serk* mutants do not give a morphological phenotype. Severe BR related phenotypes are only observed in double or triple mutants of different SERK combinations indicating that they act redundantly in BR signalling (Albrecht et al., 2008; Gou et al., 2012). An added complexity is that several members of the SERK family also serve in other signalling pathways such as plant immunity (Chinchilla et al., 2007; Heese et al., 2007; Roux et al., 2011), male fertility (Albrecht et al., 2005), BR independent cell death (He et al., 2007), abscission (Lewis et al., 2010) and root development (Du et al., 2012). This complicates the phenotypical analysis of *serk* mutants, especially in double and triple mutant combinations. Most studies performed so far are based on genetic and proteomic approaches. For example, a suppressor screen of the *nevershed* (*nev*) mutant, which does not show floral organ abscission, demonstrated that SERK1 functions as negative regulator of abscission (Lewis et al., 2010). SERK3 has been identified as co-receptor of BRI1 in a genetic screen for suppressors of a weak *bri1* phenotype and in a yeast two-hybrid screen (Nam and Li, 2002). SERK2 can also interact with BRI1, however exogenous application of BR only enhanced SERK2 phosphorylation activity but not the amount of SERK2 interacting with BRI1. This suggests that SERK2 may have a less pronounced role in BR signalling only revealed in unnatural situation such as over expression of SERK2 or exogenous application of BRs (Gou et al., 2012).

The BR related phenotype of *serk3* can be enhanced by *serk1* (Albrecht et al., 2008; Gou et al., 2012; Du et al., 2012) while *serk4* enhances the defence and cell death related phenotype of *serk3* (Roux et al., 2011, Chinchilla et al., 2007; Heese et al., 2007). Several genes involved in cell cycle and root meristem differentiation,

endodermis development and auxin transport were found to be repressed in *serk* mutants. Because the root phenotype in double and triple *serk* mutants was found to be different from that in strong *bri1* mutant alleles, it was concluded that so far unknown BR-independent pathways requiring the SERK proteins were affected (Du et al., 2012).

Profiling of the global transcriptional changes in *bri1* null mutants have revealed a complex regulatory network integrating brassinosteroid and light signalling pathways and showing multiple targets in the control of (root) development and cell elongation (Luo et al., 2010; Sun et al., 2010). This is in line with the proposed functions attributed to the BR signalling pathways.

To determine which BR-related and BR-unrelated processes are disturbed in *serk* mutants transcriptional analysis was applied. To simplify the interpretation, only *serk1* and *serk3* single and *serk1serk3* double mutants were used and the analysis restricted to roots rather than entire seedlings. Results show that a significant number of BR related genes are differentially regulated in the *serk1-3serk3-2* double mutant. In addition, transcriptional reprogramming occurred in the double mutants that appears to be unrelated to BR signalling and affects metabolic processes such as glycolipid and fatty acid metabolism. In particular, genes involved in suberin biosynthesis are down-regulated while glucosinolate biosynthesis genes are up-regulated in the *serk1-3serk3-2* double mutant.

Hierarchical cluster analysis (HCL) showed that in *serk3-2* a similar but less pronounced regulation occurred which was not detected in *serk1-3*. Apparently, SERK3 affects metabolic processes in a BR dependent and BR-independent fashion, which suggests that this single co-receptor serves even more pathways in a partially redundant mode together with other SERK proteins.

RESULTS

Magnitude of differential gene expression reflects *serk* mutant root phenotype

To determine which genes are differentially regulated in the *serk1* and *serk3* mutant lines RNA isolated from roots of wild type, *serk1-3* and *serk3-2* single and double mutant seedlings was hybridised to an Affymetrix GeneChip array (Hennig et al., 2003). In our initial analyses only genes differentially regulated more than two-fold with False Discovery Rate (FDR) of 1 % significance were considered. RNA was isolated from roots cut just below the hypocotyl at 4 days after germination (DAG), because at this time-point roots of the *serk3-2* single mutant already showed a reduction in root length (Fig. 1A and B). The phenotypes of the *serk* mutants have been described previously; *serk1-3serk3-2* has a severe reduction in root growth, which is minor in *serk3-2* and absent in *serk1-3* (Fig. 1 A and B, Supplemental Fig. S1 and S2) corroborating data previously presented (Du et al., 2012; Gou et al., 2012). Out of >26,000 genes analysed, only 4 and 42 genes were found to change expression in *serk1-3* and *serk3-2* mutant roots respectively (Supplemental Table S1 and S2). In *serk1-3serk3-2* roots 698 genes are differentially regulated (Supplemental Table S3) of which 29 are also differentially regulated over 2 fold in the *serk3-2* single mutant (Fig. 1C, Table 1). The majority of the 42 genes differentially regulated in the *serk3-2* single mutant display the same expression profile as in the *serk1-3serk3-2* double mutant (Fig. 1D). To assess whether any of the other 698 genes are also affected in single mutants an hierarchical cluster analysis (Eisen et al., 1998) was done. Interestingly, the expression profile of *serk3-2* is very similar to the *serk1-3serk3-2* double mutant and only differs in magnitude (Fig. 1E). In contrast, the *serk1-3* mutant does not display this profile, suggesting that in root development also on the transcriptional level loss of SERK1 only has a measurable effect in the absence of SERK3.

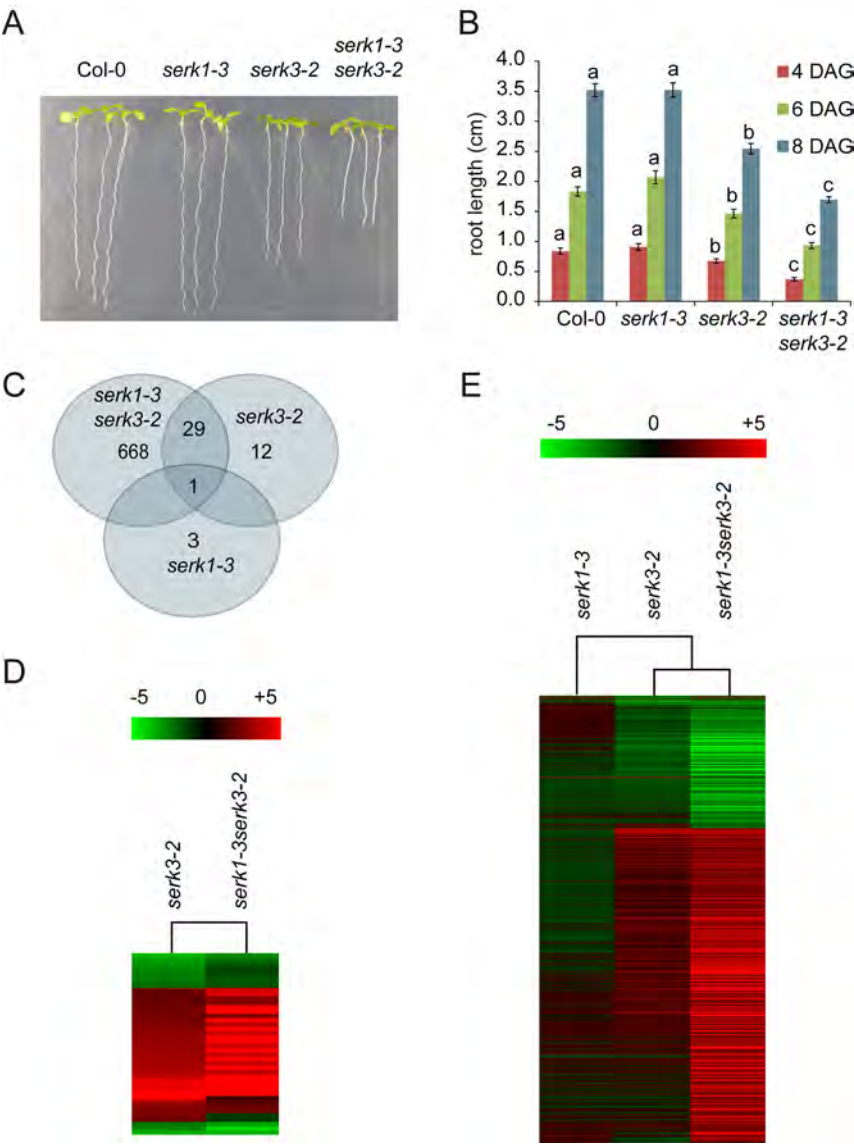


Figure 1. Morphological phenotype in *serk* mutants matches the magnitude of transcriptional response. A) Root length of *serk1-3*, *serk3-2* and *serk1-3serk3-2* mutants compared to wild type (Col-0) at 8 days after germination (DAG). B) Statistical evaluation of the root length of *serk1-3*, *serk3-2* and *serk1-3serk3-2* mutants at 4, 6 and 8 DAG. a, b, and c indicate statistical differences. Data evaluation was done with a one-way ANOVA using a Bonferroni test ($\alpha = 0.05$). C) Venn diagram showing the overlap in significantly differentially regulated genes between the *serk1-3serk3-2* double mutant and the *serk1-3* and *serk3-2* single mutants. D) Heat map comparing genes differentially regulated in the *serk3-2* and *serk1-3serk3-2* mutant. E). Hieratical cluster (HCL) analysis of all genes differentially regulated in the *serk1-3*, *serk3-2* single and *serk1-3serk3-2* double mutant. For all root length measurements error bars \pm SEM, $n \geq 20$ roots were measured in three independent replicates.

Table 1. Genes differentially regulated in the *serk3-2* single and *serk1-3serk3-2* double mutants

AGI	Other name	short gene model description	FC <i>serk3-2</i>	FC <i>serk1-3serk3-2</i>	remark
BR related genes					
AT4G12480	pEARL1	lipid transfer protein (LTP) family protein	4.63	18.0	BZR1 target
AT5G38940		manganese ion binding / nutrient reservoir	9.49	8.2	differentially regulated in <i>bri1-116</i>
AT2G24270	ALDH11A3	non-phosphorylating glyceraldehyde 3-phosphate dehydrogenase (NPGAP-DH)	2.35	11.1	BZR1 target
AT4G28530	anac074	NAC domain transcription factor family	-3.43	-3.5	differentially regulated in <i>bri1-116</i> , BZR1 target
AT1G68010	HPR	glycerate dehydrogenase/ poly(U) binding	2.94	5.6	differentially regulated in <i>bri1-116</i>
AT4G38770	PRP4	proline rich proteins, cell wall structure	3.42	5.1	BZR1 target
AT4G05180	PSII-Q	PSII polypeptide subunits	3.10	5.0	differentially regulated in <i>bri1-116</i> , BZR1 target
AT4G17245		zinc finger (C3HC4-type RING finger) family protein	4.81	4.9	differentially regulated in <i>bri1-116</i> , BZR1 target
AT1G74670	GASA6	Gibberellin-regulated family protein	2.03	4.3	BES1 target
AT3G56940	CRD1	DNA binding / magnesium-protoporphyrin IX monomethyl ester (oxidative) cyclase	3.05	4.1	differentially regulated in <i>bri1-116</i>
AT4G12800	PSAL	photosystem I subunit L	3.13	4.0	differentially regulated in <i>bri1-116</i>
AT3G16140	PSAH-1	photosystem I subunit H-1	3.56	3.8	differentially regulated in <i>bri1-116</i> , BZR1 target
AT1G03600	PSB27	photosystem II family protein	2.48	3.6	BES1/ BZR1 target
AT4G01050	TROL	hydroxyproline-rich glycoprotein family protein	2.04	2.7	differentially regulated in <i>bri1-116</i> , BZR1 target
AT1G31330	PSAF	photosystem I subunit F	2.32	2.6	differentially regulated in <i>bri1-116</i>
AT1G51400		photosystem II 5 kD protein	2.12	2.6	differentially regulated in <i>bri1-116</i> , BZR1 target
AT4G36430		peroxidase, putative	-3.67	-2.7	differentially regulated in <i>bri1-116</i>
Non-BR related genes					
AT3G16660		Pollen Ole e 1 allergen and extensin family protein	3.19	7.86	
AT4G04223		not assigned, unknown protein	2.71	7.71	
AT2G20835		not assigned, unknown protein	2.32	7.55	
AT5G65980		auxin efflux carrier family protein	3.75	7.04	
AT4G21250		Sulfite exporter TauE/SafE family protein	2.20	4.85	
AT5G19700		MATE efflux protein-related	3.01	4.84	
AT3G18890	TIC62	NAD(P)-binding Rossmann-fold superfamily protein; binding / catalytic/ coenzyme binding	2.04	4.20	
AT2G07600		pseudo gene, NADH dehydrogenase	3.33	3.96	
AT2G24710	GLR2.3	intracellular ligand-gated ion channel	2.82	3.95	
AT2G03260		ERD1/XPR1/SYG1 family protein	2.69	2.12	
AT2G21100		pathogen related-proteins	-2.26	-3.15	
AT1G53270		ABC transporter family protein	-2.69	-4.26	

AGI = Arabidopsis Genome Initiative gene identification number

Other name = common abbreviation for genes

FC = Fold change in the microarray experiment

Genes that are differentially regulated in *serk3-2* and *serk1-3serk3-2*

Expression of all SERK genes was followed in *serk3-2* and *serk1-3serk3-2* mutant roots. The *serk1-3* mutant carries a T-DNA insertion in the coding sequence of the SERK1 gene and therefore does not block the formation of the transcript. Surprisingly, SERK1 transcripts are significantly higher in the *serk1-3serk3-2* mutant (2.4 FC, FDR <0.01) and to a lesser extent SERK4 transcripts (1.6 FC, FDR 0.05). This possibly represents a compensatory mechanism for the loss of active SERK1 and SERK3 protein.

Genes differentially regulated in the *serk3-2* mutant are involved in various cellular processes such as photosynthesis, transport and protein degradation (Supplemental Table S2). To assess if these genes are part of a certain biochemical pathway an over-representation analysis (ORA) was performed (Backes et al., 2007). In the *serk3-2* mutant overrepresentation of photosynthesis and metabolic pathways was noted amongst the up-regulated genes whereas none was found in the down-regulated categories. In the double mutant, additional categories were found to be overrepresented, mainly involved in energy metabolism and in glucosinolate biosynthesis. In addition, down-regulated genes were found to be involved in secondary metabolite biosynthesis (Table 2). This suggests a link between SERK activity, BR signalling and chloroplast development. Light-grown roots have the capacity to develop chloroplasts (Kobayashi et al., 2012). BR signalling is correlated with the response to light; in the BR biosynthesis mutant *de-etiolated 2 (det2)* for example, increased expression of light responsive genes was observed (Chory et al., 1991; Song et al., 2009). Furthermore, BR induced transcriptional activation of BZR1 and BES1/BZR2 represses the expression of positive regulators of light signalling and induces expression of negative ones (Luo et al., 2010; Sun et al., 2010; Wang et al., 2012). Hence, reduced BR signalling could result in an increased expression of genes involved in photosynthesis.

Table 2. Over-representation analysis of differentially regulated genes in *serk1-3serk3-2* and *serk3-2* mutants

category	expected	observed	p-value
<i>serk3-2</i> up			
photosynthesis	0	5	3.6×10^{-08}
metabolic pathways	3	6	4.1×10^{-02}
<i>serk1-3serk3-2</i> up			
photosynthesis	2	26	2.1×10^{-25}
photosynthesis antenna proteins	1	14	1.5×10^{-15}
carbon fixation in photo-synthetic organisms	3	16	9.3×10^{-08}
metabolic pathways	51	79	9.3×10^{-08}
porphyrin and chlorophyll metabolism	2	8	5.5×10^{-04}
glyoxylate and dicarboxylate metabolism	1	6	2.1×10^{-03}
glucosinolate biosynthesis	1	4	1.5×10^{-02}
<i>serk1-3serk3-2</i> down			
glycerolipid metabolism	0	5	6.4×10^{-05}
glycerophospholipid metabolism	0	5	3.2×10^{-04}
phenylalanine metabolism	1	6	4.9×10^{-04}
biosynthesis of secondary metabolites	7	15	7.4×10^{-04}
phenylpropanoid biosynthesis	1	6	7.4×10^{-04}
fatty acid metabolism	0	3	5.0×10^{-03}
metabolic pathways	12	18	1.0×10^{-02}
limonene and pinene degradation	1	3	2.6×10^{-02}
stilbenoid, diarylheptanoid and gingerol biosynthesis	1	3	2.6×10^{-02}

Next, the genes differentially regulated in *serk3-2* and *serk1-3serk3-2* were compared with published datasets on (putative) targets of BZR1/BES1 and differentially regulated genes in the BR11 null mutant *bri1-116* (Sun et al., 2010; Yu et al., 2011) (Fig. 2A, Supplemental Fig. S3, Table S4, File S1). In total, 345 differentially regulated BR-related genes were observed in the *serk1-3serk3-2* mutant. This is a significantly higher number than would be expected by chance alone (119 genes) and indicates that the BR signalling process is significantly affected in roots of the *serk1-3serk3-2* mutants. The majority of the up-regulated photosynthesis related genes identified in the ORA are also BR related while a number of BR related metabolic processes appear to be significantly down-regulated (Table 3, Supplemental Table S5). The non-BR related up-regulated metabolic pathways mainly relate to genes involved in biosynthesis of secondary metabolites, glucosinolate biosynthesis, and glyoxylate and dicarboxylate metabolism (Table 4).

Table 3. Over-representation analysis of BR related genes differentially regulated in *serk1-3serk3-2* double mutant

category	expected	observed	p-value
<i>serk1-3serk3-2</i> BRI1 related up-regulated			
photosynthesis	1	24	6.3×10^{-25}
photosynthesis antenna proteins	1	14	3.9×10^{-17}
carbon fixation in photo-synthetic organisms	2	11	5.2×10^{-5}
metabolic pathways	41	60	5.2×10^{-5}
porphyrin and chlorophyll metabolism	1	6	3.8×10^{-3}
<i>serk1-3serk3-2</i> BRI1 related down-regulated			
glycerolipid metabolism	0	4	2.0×10^{-4}
glycerophospholipid metabolism	0	4	6.2×10^{-4}
phenylalanine metabolism	1	4	4.8×10^{-3}
biosynthesis of secondary metabolites	5	10	5.9×10^{-3}
phenylpropanoid biosynthesis	1	4	5.9×10^{-3}
metabolic pathways	8	13	1.1×10^{-2}

Table 4. Over-representation analysis of the non-BRI1 related genes up-regulated in *serk1-3serk3-2* double mutant

category	expected	observed	p-value
glucosinolate biosynthesis			
CYP79F2 BCAT4	0	4	6.4×10^{-5}
MAM1 CYP83A1			
glyoxylate and dicarboxylate metabolism			
AT5G38410 AT5G38430	0	4	1.6×10^{-4}
AT5G38420 ICL			
Metabolic pathways			
CH1 LDOX MAM1	10	19	1.8×10^{-4}
ADG1 AT3G54050 FNR2			
THIC AT1G32780 BCAT4			
AT5G38410 POR C AK3			
NPQ4 AT4G08780 AGT			
PRK AT5G38420 AT5G38430			
ICL			
carbon fixation photosynthetic organisms			
AT5G38410 PRK AT5G38430	1	5	3.2×10^{-4}
AT3G54050 AT5G38420			
biosynthesis of secondary metabolites			
CH1 AT3G54050 POR C	6	11	1.6×10^{-2}
LDOX AT1G32780 MAM1			
BCAT4 AK3 AT4G08780			
AGT CYP83A1			

Genes differentially regulated in the weak allelic *bri1-301* mutant

Macroscopically, *bri1-301* has a phenotype comparable to that of wild type seedlings while showing a reduced insensitivity towards exogenously applied BRs (Xu et al., 2008; Chapter 3). It is less evident whether roots of the *bri1-301* mutant already have a transcriptional phenotype at physiological ligand concentrations. Therefore, genes differentially regulated in the *bri1-301* mutant were compared to those affected in the *bri1-116* mutant and the *serk1*, *serk3* single and double mutants. In *bri1-301* roots only 4 genes are differentially regulated. This is significantly less when compared to the dataset available for the strong *bri1-116* mutant where 3531 genes (1.5 fold cutoff and FDR < 0.01) are affected (Sun et al., 2010). The *bri1-116* dataset obtained from literature was constructed using a lower cutoff and FDR value than use in our analyses. The rationale behind this was that BR regulated genes do not show extensive transcriptional responses (Deng et al., 2007). However, using a cutoff value of 1.5 fold change (FDR 0.01) did not increase the number of differentially regulated genes found in *bri1-301* in two independent experiments (Supplemental Table S6). HCL analysis using *bri1-301* and *serk3-2* and *serk1-3serk3-2* did not show a clear correlation due to the absence of a clear transcriptional profile in the *bri1-301* mutant (Fig. 2B). This is corroborated by HCL analysis at lower cut off values (1.5 fold FDR<0.01) and the HCL analysis between the differentially regulated genes in the *bri1-116* and *bri1-301* mutant which exhibit no clear correlation (Supplemental Fig. S4). In conclusion, although *bri1-301* roots are BR insensitive, hardly any effect in transcriptional response is observed.

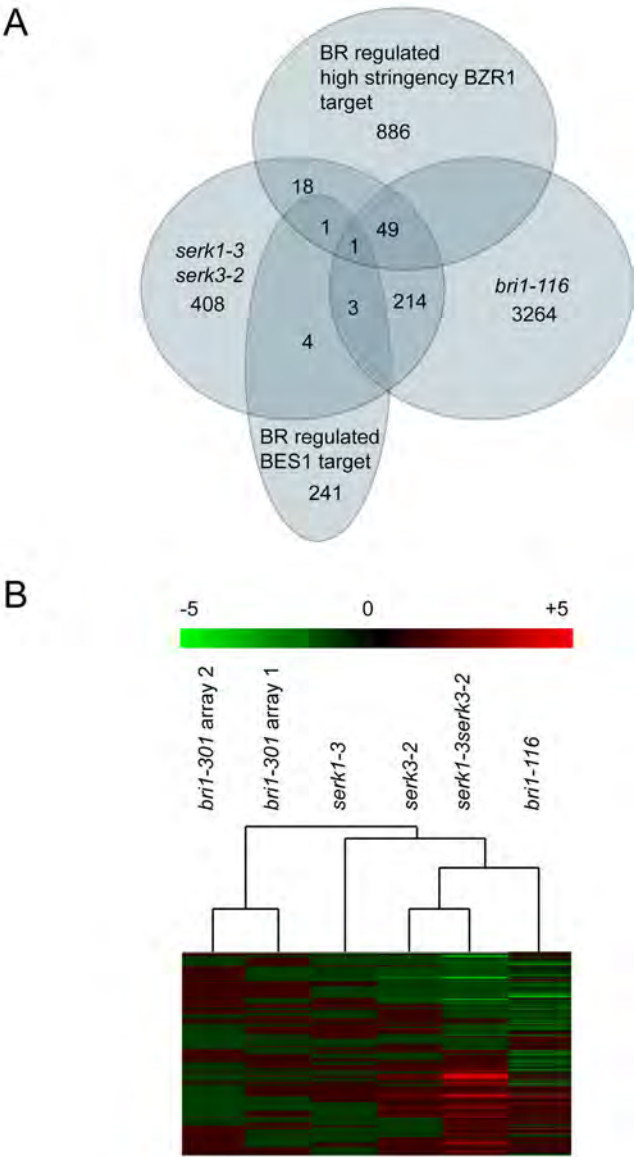


Figure 2. Comparison of differentially regulated genes in the *serk1-3serk3-2* mutant with BR-related genes. A) Venn diagram showing genes differentially regulated in the *bri1-116* mutant and known BR-related BES1 and BZR1 target genes compared to differential regulated genes in the *serk1-3serk3-2* double mutant. B) HCL analysis comparing genes differentially regulated in the *bri1-116* and *bri1-301* mutants with differentially regulated genes in the *serk3-2* and *serk1-3serk3-2* mutant. The two different arrays performed on *bri1-301* roots cluster together. Red = up-regulated, green = down-regulated. Data on BR-related BES1/ BZR1 target genes and genes differentially regulated in the *bri1-116* mutant was derived from Yu et al. (2011) and Sun et al. (2010).

Global transcriptional analyses of other SERK1 and SERK3 affected processes

SERK1 and SERK3 are important components in processes other than BR1 mediated signalling such as abscission, cell death and defence. Since these processes have been well studied, readily available data sets of global transcriptional changes are available in the Gene Expression Omnibus (GEO), The Arabidopsis Information Resource (TAIR) databases and current literature (Edgar et al., 2002; Zipfel et al., 2004; Denoux et al., 2008; Boudsocq et al., 2010; Lamesch et al., 2012; Niederhuth et al., 2013). Transcriptional changes due to the absence of functional Haesa (HAE) and Haesa-like (HSL2) receptor-like kinases and known abscission related genes derived from the TAIR data base were used as reference set for abscission related genes (Patterson, 2001; Sun and van Nocker, 2010; Gonzalez-Carranza et al., 2012; Niederhuth et al., 2013). *haehsl2* mutants fail to abscise their floral organs (Jinn et al., 2000; Cho et al., 2008; Stenvik et al., 2008). The defence related gene set consists mainly of genes that are differentially regulated upon flg22 treatment (Zipfel et al., 2004; Boudsocq et al., 2010; Denoux et al., 2008). Known cell death related genes were obtained from the TAIR database (Lamesch et al., 2012). This list was extended using differentially regulated genes in a *constitutive expresser of PR genes 5* (*cpr5*) mutant downloaded from the GEO data base (Edgar et al., 2002). CPR5 mutants have several phenotypes including spontaneous cell death, defects in cell division, cell expansion and cell wall biogenesis (Bowling et al., 1997; Kirik et al., 2001; Gao et al., 2011). Although none of these processes are described to occur in roots, the corresponding genes may nonetheless be differentially regulated. As previously mentioned *serk1-3serk3-2* has a reduced root length and fewer meristematic cells (Gou et al., 2012; Du et al., 2012, Supplemental Fig. S2). One possible cause for the meristem phenotype of *serk1-3serk3-2* is reduced cell cycle progression in the root meristem cells, similar to what has been postulated for the *bri1-116* mutant (González-García et al., 2011). In addition, it has been proposed that SERKs affect cell cycle and division via BR-independent processes (Du et al., 2012). Therefore, we also included previously described core cell cycle/ cell differentiation genes as well as known cell cycle and cell differentiation related genes in the TAIR database in our analysis (Vandepoele et al., 2002).

Table 5. Over-representation analysis on (known) SERK1 and SERK3 related processes

category			expected	observed	p-value
glucosinolate biosynthesis			0	4	6.4*10 ⁻⁵
CYP79F2	BCAT4				
MAM1	CYP83A1				
glyoxylate and dicarboxylate metabolism			0	4	1.6*10 ⁻⁴
AT5G38410	AT5G38430				
AT5G38420	ICL				
Metabolic pathways			10	19	1.8*10 ⁻⁴
CH1	LDOX	MAM1			
ADG1	AT3G54050	FNR2			
THIC	AT1G32780	BCAT4			
AT5G38410	POR C	AK3			
NPQ4	AT4G08780	AGT			
PRK	AT5G38420	AT5G38430			
ICL					
carbon fixation photosynthetic organisms			1	5	3.2*10 ⁻⁴
AT5G38410	PRK	AT5G38430			
AT3G54050	AT5G38420				
biosynthesis of secondary metabolites			6	11	1.6*10 ⁻²
CH1	AT3G54050	POR C			
LDOX	AT1G32780	MAM1			
BCAT4	AK3	AT4G08780			
AGT	CYP83A1				

observed is the number of genes identified in the specified category (m); refset is number of genes in reference set (k); expected is the of genes theoretically can be found by chance based on the size of the reference set, the number of differentially regulated genes (698 in *serk1-3serk3-2*) and the number of genes on the gene chip (27827), p values are calculated using a cumulative hypergeometric distribution

The reference sets obtained were compared to the transcriptional changes monitored in root tissue of the *serk1-3serk3-2* double mutant (For p-values see Table 5). Subsequently, it was determined whether previously unidentified, distinct biological processes are present in the overlapping differential gene sets shown in Figure 3. From the 209 core cell cycle genes in the reference sets, 5 genes were differentially regulated in absence of SERK1 and SERK3 (Fig. 3), indicating that cell cycle genes are not significantly affected in roots of the *serk1-3serk3-2* double mutant (Table 5). The cell cycle and cell differentiation related genes CYCLIN D1;1 (CYCD1;1), AT1G67270 are differentially up-regulated and, CLAVATA3/ESR-related 44 (CLE44), ERECTA-LIKE 2 (ERL2) and AT2G42220 are differentially down-regulated. CYCD1;1, which is in a wild type situation up-regulated at the start of cell division, is involved in the onset of cell proliferation during seed germination, resulting in a delayed germination in the *cycd1;1* mutants (Masubelele et al., 2005). In the *serk1-3serk3-2* mutant CYCD1;1 is down-regulated suggesting that the onset of cell division may be impaired. Altogether the analyses suggest that if cell division and cell differentiation is affected in absence of SERK1 and SERK3,

this is a rather subtle effect on a small number of core cell cycle genes. Similarly, only a small overlap was observed between genes involved in abscission, cell death and defence, and the differentially regulated genes in the *serk1-3serk3-2* double mutant (Fig. 3). For abscission and cell death related genes, no significant categories were identified in the ORA using GeneTrail. Comparison between the differentially regulated genes in *serk1-3serk3-2* root tissue with flagellin responsive genes suggested that there was a significant up-regulation of this biological process (Table 5). However, when performing an ORA using GeneTrail software on the 44 genes overlapping between these data sets it appears that they are mainly involved in secondary metabolism rather than a core defence processes. Noteworthy, a number of acetyl transferases were identified in the comparison between the abscission related data set and the differentially regulated genes in *serk1-3serk3-2* roots. For example, glycerol-3-phosphate-3-phosphate sn-2-acyltransferase (GPAT) 5 and fatty acid reductase (FAR) 4 and FAR5 are acetyl transferases essential for the biosynthesis of suberin (Beisson et al., 2007; Domergue et al., 2010). Together, these data corroborate the ORA on the gene set that is differentially regulated in the *serk1-3serk3-2* double mutant, where the non-BR related differentially regulated genes are mainly involved in secondary metabolism (Supplemental File S1, Table S5).





processes involving SERK1 and SERK3	reference data set source	tissue	total nr. of genes	differentially regulated in <i>serk1-3serk3-2</i> root tissue
 ? abscission	RNA seq. <i>hae hst2</i> abscission mutant (Niederhuth et al, 2013) abscission related genes (TAIR)	flower	410	FAR5 QRT2 GPAT5 AT3G22060 NHL10/YLS9 AT4G22090 GLIP4 AT3G15450 AT1G50590 FAR4 CEN2 AT1G58037 LBD26 AT5G63180 ORP4C SAG29 GH983/CEL3 AT1G67105 IPM1 AT5G42530 ACH1/NRT2 AT4G04223 GRP3S
?  BRI1 cell cycle defects	Core cell cycle genes (Vandepoele et al, 2002) cell cycle and cell differentiation related genes (TAIR)	seedling	209	CYCD1;1 AT1G67270 CLE44 ERL2 AT2G42220
 ? cell death	Microarray. <i>cpr5</i> mutant which exhibits spontaneous cell death (GEO database) cell death related genes (TAIR)	seedling	439	AT3G22060 NHL10/YLS9 AT3G51890 AT4G10500 AT5G67340 AZI1 RLP37 GLP9 SAG29 ATGPT2/GPT2 AT4G12490 CAT3/SEN2 TI1 EARL11
 FLS2 defence	flg22 responsive genes (Zipfel et al, 2004; Boudsocq et al, 2010; Denoux et al, 2008)	seedling	1354	AT1G14550 AT3G22060 NHL10/YLS9 GLIP4 AT3G15450 OBE1 AT5G40590 AT5G67340 AT1G29430 CAO/CH1 BAT5 AT1G33600 EXPA10 CBL10/SCABP8 AT1G53440 AT5G47610 GLK1/GPRI1 AT1G15260 EXPA1 AT2G35260 AT2G18300 EXPA8 RALFL34 BEE2/BEE2 CAL4/TCH3 DIR1 AT1G78170 CYP71B5 AT2G34930 AT1G55260 AT5G02760 ABR/PID ATML1 CAD9 CYP83A1 AT4G12490 AT3G48200 AT5G44580 SAUR68 THI2.2 LTP7 AT1G29670 GH3.3 AT1G55260

Figure 3. Global transcriptional analysis of known processes involving SERK1 and SERK3. Comparison of the global transcriptional responses during abscission, cell cycle and differentiation, cell death and defence with differentially regulated genes in the *serk1-3serk3-2* double mutant. Data on genes involved in abscission, cell cycle, cell death and defence was derived from literature or reference data set available in the GEO and TAIR database.

The suberin biosynthetic pathway is differentially regulated in *serk3* mutants

Based on both the ORA and study of known SERK3 related processes we propose that a small number of secondary metabolic pathways are affected in *serk3-2* and *serk1-3serk3-2* mutant roots. Interestingly, a number of genes found in the previous analyses point to a differential regulation of suberin biosynthesis. Suberin in roots and cutin in leaves are secondary wall modifications that help make plant organs “waterproof”. A comprehensive review on the current state of the art of both processes is available (Beisson et al., 2012). All other genes besides GPAT5 (AT3G11430) (Li et al., 2007; Beisson et al., 2012) known to be involved in suberin and cutin biosynthesis were therefore checked. Remarkably, 16 out of the 30 genes reported were differentially regulated in *serk1-3serk3-2* roots from which 11 were significantly down-regulated. The 14 genes that were not differentially regulated comprised mainly the genes known to be involved only in cutin biosynthesis (Fig. 4). This suggests that mainly suberin biosynthesis is affected in *serk* mutant

roots. Importantly, of the 11 genes known to be involved in suberin biosynthesis all but two are differentially regulated 2 fold (FDR < 0.01), indicating that suberin synthesis is significantly disrupted (Table 5). In total, 8 suberin biosynthesis genes are significantly down-regulated while one fatty acid reductase and one ABC transporter gene were significantly up-regulated. Altogether, these data suggest that suberin content may be reduced in roots of the *serk1-3serk3-2* double mutant. Although not initially reported as differentially regulated biological process in the *bri1-116* mutant (Sun et al., 2010) we also compared cutin and suberin biosynthesis genes to differentially regulated genes in the *bri1-116* mutant. In total, 5 suberin and 6 cutin biosynthesis genes are significantly down-regulated and one cutin biosynthesis genes is up-regulated in the *bri1-116* mutant (Supplemental Table S7). Apparently, cutin and suberin biosynthesis related genes are only mildly reduced in the *bri1-116* mutant but much more extensively in the *serk1-3serk3-2* double mutant. Altogether, suberin biosynthesis is affected when SERK3 is disrupted and this process is further affected when SERK1 is absent. However, to verify this hypothesis it is paramount that biological experiments are performed that corroborate the transcriptional data.

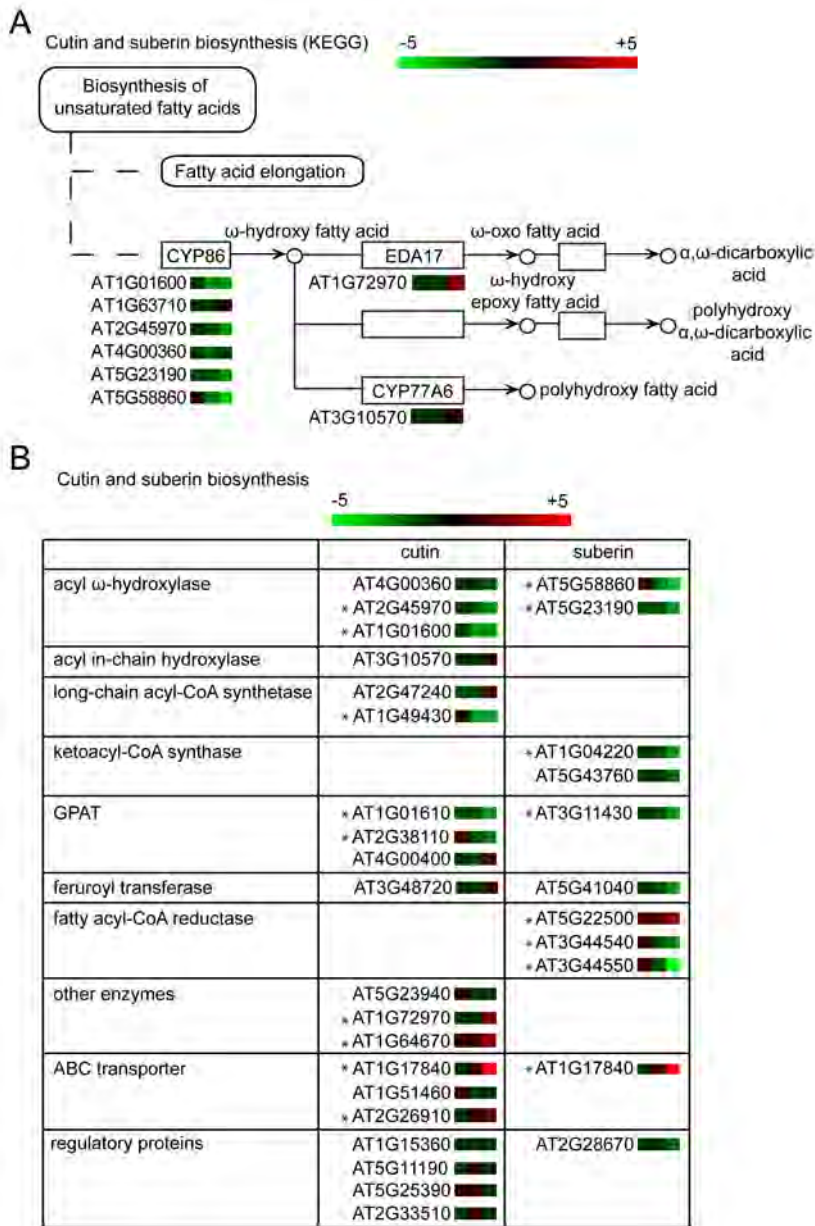


Figure 4. Suberin biosynthesis genes are differentially regulated in the *serk1-serk3-2* mutant. A) Biosynthesis pathway of suberin and cutin derived from the KEGG data base. B) Suberin and cutin biosynthesis related genes, table modified from Beisson et al. (2012). A and B) Expression of genes in indicated in the squares next to the Arabidopsis genome Arabidopsis Genome Initiative (AGI) identification number from left to right: first square is in the *serk1-3* mutant, middle square *serk3-2* mutant, and right square *serk1-serk3-2* mutant. Red indicates up-regulated genes, green down-regulated on a scale of 5 fold differentially regulated. Star (*) indicates genes more than 2 fold differentially regulated in the *serk1-serk3-2* double mutant (FDR<0.01).

DISCUSSION

In this study we employed a transcriptional analysis using microarrays to identify biological processes involving SERK1 and SERK3. This approach resulted in the identification of known BR related genes, indicating the robustness of the analysis. In addition, *serk1* and *serk3* mutants are impaired in secondary metabolic processes such as suberin biosynthesis, glyoxylate and dicarboxylate metabolism and glucosinolate metabolism. One major challenge in studying gene regulation of receptor mutants is that the effects may be indirectly caused by differential regulation of transcription factors downstream of the receptor. This is even further complicated by the interaction of SERK co-receptors with different main ligand perceiving receptors, thereby affecting multiple signalling pathways. It also raises the question if signal transduction mediated by SERK co-receptors can truly be separated using genetic approaches only.

Phenotypically, only *serk3* single mutants show a reduced root growth phenotype whereas *serk1* roots do not. In contrast, *serk1serk3* double mutants have a severe root growth phenotype (Du et al., 2012; Gou et al., 2012). Using microarray analysis only *serk3* and *serk1serk3* mutants display distinct transcriptional changes. Remarkably, the transcriptional profile of *serk1serk3* roots emulates the profile of the *serk3* mutant but displays transcriptional changes of a higher magnitude. Therefore, both on a phenotypic and transcriptional level, loss of SERK1 only affects root growth in the absence of SERK3. The presence of SERK1 does provide a certain robustness to the system since it can partially rescue a SERK3 mutant phenotype and ameliorate the transcriptional changes in this mutant. Similarly, in other tissues other combinations of SERKs may display similar profiles. Indeed, the rosette phenotype of the *serk1serk3* double mutant is more severe when compared to the *serk3* single mutant (Gou et al., 2012) and the defence phenotype of *serk3* is enhanced by *serk4* while the *serk4* single mutant does not have a phenotype (Chinchilla et al., 2007; Heese et al., 2007; Roux et al., 2011).

Preventing the production of functional SERK proteins resulted in increased transcription or reduced degradation of corresponding truncated mRNAs or in one case increased transcription of another member of the family. A similar phenomenon has been noted previously in the analysis of the SERK family (Jeong et al., 2010) and may suggest a form of feedback control.

From the root growth and BL insensitivity phenotype it is evident that roots of the *serk1-3serk3-2* double mutant exhibit a BR related phenotype. A significant number of photosynthesis related genes, differentially regulated in absence of SERK1 and SERK3, are also affected in *bri1* or a known target of BES1/BZR1. This is in line with the negative regulation of light responsive genes by BRI1 mediated BR signalling (Luo et al., 2010; Sun et al., 2010; Wang et al., 2012). BRI1 is also

known to be involved in cell cycle progression and cell differentiation in the root meristem (González-García et al., 2011; Hacham et al., 2011). Whether the strong root phenotype in *serk1serk3* is the result of aberrant cell cycle progression is not clear yet (Du et al., 2012). Few cell cycle genes were found to be altered in expression in *serk1serk3* suggesting that either the cell cycle and/or differentiation is not affected or is through a subtle effect on a small number of core cell cycle genes.

Genes that are neither listed as direct targets of BZR1/BES1 nor are affected in the *bri1-116* mutant (Sun et al., 2010) are classified as non-BR related in the present study. These genes are involved in metabolic processes such as biosynthesis of secondary metabolites, glucosinolate biosynthesis and glyoxylate and dicarboxylate metabolism. Disrupted glucosinolate biosynthesis is known to correlate to severe growth and developmental phenotypes and a disrupted hormone homeostasis (Bak and Feyereisen, 2001; Bak et al., 2001; Smolen and Bender, 2002; Tantikanjana et al., 2004). Although transcriptomics did not reveal a connection between brassinosteroids and glucosinolates, recently it has been postulated that BR signalling inhibits glucosinolate biosynthesis. The BR-deficient mutant *cpd* has an increased glucosinolate content while plants overexpressing the BR biosynthesis gene DWF4 exhibit a decrease in glucosinolate level. In addition, several glucosinolate biosynthesis genes are significantly down-regulated in the gain of BR function mutants *bes1-D*, *35sBZR1/bzr1-1D* (Guo et al., 2013). The same set of genes are affected upon defence responses (van de Mortel et al., 2012), down-regulated upon cytokinin treatment (Brenner et al., 2005) and involved in general hormone homeostasis (Chen et al., 2012). Therefore, the link between disrupted BRI1 mediated signalling in the *serk1-3serk3-2* double mutant and the up-regulation of glucosinolate biosynthesis genes cannot be excluded or verified based on these data.

BRI1 is also involved in cell elongation and differentiation. A number of genes found here appear related to BR-related cell wall modifications (Wolf et al., 2012), others, such as GPAT5, FAR4 and FAR5, are abscission related. These genes are essential for suberin biosynthesis, a process required in order to protect the abscission zone with a layer of suberin and lignin (Roberts et al., 2000). Suberin does not only function as protective barrier in abscission zones but also in root tissues (Beisson et al., 2012). Suberin, a cutin-like fatty acid and glycerol based polymer, forms part of the protective barrier against pathogens and the transport of water and solutes from the extracellular environment (Hofer et al., 2008; Baxter et al., 2009). To support this hypothesis all known suberin and cutin biosynthesis genes (Beisson et al., 2012) were investigated. Most are significantly down-regulated in roots of the *serk1-3serk3-2* double mutant. Whether indeed suberin content is affected in *serk3* and *serk1serk3* mutants remains to be elucidated.

To summarise, our transcriptional analysis has clearly revealed a role in aspects of BRI1-mediated BR signalling as well as pointing to an additional role of the SERK co-receptors in metabolic control.

EXPERIMENTAL PROCEDURES

Plant growth conditions

Arabidopsis thaliana ecotype Columbia (Col-0) was used as wild type reference. The *serk1-3* (GABI-KAT line 448E10) and *serk3-2* or *bak1-4* (SALK_116202) single and the *serk1-3serk3-2* double mutants, all in the wild type background, were used throughout this study. Seeds were surface sterilised using ethanol/ bleach (4:1 v/v) and germinated on half strength Murashige and Skoog medium (Duchefa, Haarlem, the Netherlands) supplemented with 1% Sucrose (Sigma-Aldrich chemie, Steinheim, Germany), 0.1 % MES (Sigma-Aldrich) and 0.8 % Daishin Agar (Sigma-Aldrich). Seedlings grown for RNA isolation were germinated on growth medium containing 1.2 % Daishin Agar. To equalise germination, the plates were kept in the dark at 4 °C for two days after which the seedlings were grown vertically under fluorescent light at 22 °C, with 16-h-light/8-h-dark photoperiods. For the root growth assays each measurement consisted of ≥ 20 roots measured in three independent replicates. For the meristematic phenotype characterization $n \geq 10$, for cell size measurements $n \geq 10$ measuring at least 3 cells per root all data was obtained in at least two independent replicates. All images of FM4-64 stained root meristems were taken using a CONFOCOR2/LSM510 (Zeiss, Jena, Germany) equipped with a 40x water objective (NA 1.2) and an Argon ion laser. A He/Ne laser was used to excite FM4-64 at 543 nm.

RNA isolation and sample preparation

Roots of 4-day old *Arabidopsis* seedlings were cut just below the hypocotyl and grounded in liquid nitrogen. Approximately 100 mg of grounded material was dissolved in 1 ml TRIzol reagent (Invitrogen, Carlsbad, CA, USA) and incubated for 5 minutes at room temperature. Next, 200 μ l of chloroform was added, the sample was homogenised, incubated for 2 minutes and centrifuged for 15 minutes at 4 °C. After phase separation isopropanol was added to the aqueous phase, which was subsequently incubated for 10 minutes at room temperature and further purified using an RNA easy Mini Kit (Qiagen, Venlo, the Netherlands). Before hybridization on the microarray, the RNA quality was tested using a bio analyzer. All samples used for microarray analysis were replicated three times in independent biological experiments and each replication consisted of ≥ 3000 seedlings.

Software for data analysis

The scanned Affymetrix arrays were analysed using Bioconductor packages (www.bioconductor.org; (Gentleman et al., 2004) integrated in the automated on-line MADMAX pipeline (<https://madmax.bioinformatics.nl>) (Lin et al., 2011). A quantile normalization was used to normalise the array data, expression estimates were

compiled with the RMA method using the empirical Bayes approach (Wu et al., 2004). The arrays were considered as sufficient high quality if: (1) the density and RNA degradation plots are not deviating, (2) the fitPLM images have < 10% of specks, (3) box plots representing the relative long expression (RLA) and normalised un-scaled standard errors (NURSE) should not deviate between the arrays. Probe sets which are differentially expressed were identified with linear models, using moderated t-statistics and empirical Bayes regularization for implementation of the standard errors (Smyth, 2004). Given the morphological differences between the *serk1serk3* double mutant and the wild type seedlings further analysis was done on genes which were 2 fold differentially regulated when compared to the wild type lines using a false discovery rate (FDR) of 1%. For comparison of the differentially regulated genes in the *bri1-301* line with differentially regulated genes in the *bri1-116* line (Sun et al., 2010) the same stringency values as used by Sun et al. (2010) were applied (FDR 1%, 1.5 FC). Gene trail software (Keller et al., 2008) was employed for the overrepresentation analysis of genes using a minimum of 3 genes identified per category and a FDR of 5% for correction of multiple testing (Benjamini and Hochberg, 1995). Differentially regulated genes were binned in different cellular processes using MAPMAN analysis (Thimm et al., 2004). HCL clustering was done with the TM4 microarray software suite (<http://www.tm4.org/mev/>) using default settings which apply a Pearson correlation as distance measure and an average linkage for clustering. For differentially regulated genes in the *bri1-116* lines data was derived from Sun et al. (2010) and downloaded from the GEO2R database, using the following GEO accession numbers GSE25134 using GSM 617578-617580 for wild type reference set, GSM 617575-617577 for *bri1-116*. For differentially regulated genes in the *cpr5* mutant GEO accession number GSE40322 was downloaded, using GSM991297-GSM991299 for wild type and GSM991294-GSM991296 for the *cpr5* mutant. Values for differentially regulated genes were derived from GEO2R using a Benjamin & Hochberg adjustment for multiple testing (False discovery rate) for calculation of the adjusted p-values (FDR values).

The p-values when comparing genes differentially regulated in the *serk1-3serk3-2* double mutant with known processes related to SERK1 and SERK3 were calculated using a cumulative hypergeometric distribution:

$$p = \sum_{x=0}^{m-1} \frac{\binom{k}{x} \binom{N-k}{n-x}}{\binom{N}{n}}$$

where N denotes the number of probes on the Affymetrix Gene Chip (27827), k is the size of the reference set, n is the number differentially regulated genes, m is the number of genes overlapping between the groups k and n. The hypergeometric distribution was computed using R version 3.0 (<http://www.R-project.org/>). The number of genes that can be expected to be identified by chance alone were calculated via:

$$N_{\text{expected}} = \frac{k \times n}{N}$$

ACKNOWLEDGEMENTS

We acknowledge Jenny Jansen for hybridizing the Affymetrix gene chips. Dolf Weijers, Bert de Rybel for advice on the data analysis. Zoltán Bochdanovits is acknowledged for critically reading this manuscript. This work has financially supported by the IP/OP systems biology program of Wageningen University (G.W.vE) and the Netherlands Proteomics Centre (C.A.tH).

SUPPLEMENTAL FILES

Supplemental file 1. Genes differentially regulated in *serk1-3serk3-2* compared to known BRI1 related genes

Calculation BR related genes in the *serk1-3serk3-2* double mutant

Genes differentially regulated in the *bri1-116* mutant and BES1/BZR1 target genes were derived from Sun et al. (2010) and Yu et al. (2010). Identified BZR1 binding regions were linked to the nearest neighboring genes using two independent statistical methods Tiling Analysis Software and TileMap. From this analysis, high and low confidence (stringency) BZR1 targets were defined i.e. high stringency BZR1 targets (3410 genes in total) are genes identified with two different statistical methods while low stringency BZR1 targets (4800 genes in total) are only identified by one.

In total, 3531 genes are differentially regulated in the *bri1-116* mutant, 955 genes are BR regulated high stringency BZR1 targets and 250 genes are BR regulated BES1 targets (Sun et al., 2010; Yu et al., 2011). From the 698 genes differentially regulated in the *serk1-3serk3-2* double mutant 290 are a known BR related BES1/BZR1 target or differentially regulated in the *bri1-116* mutant. Hence, 42 % of the genes differentially regulated in the *serk1-3serk3-2* double mutant is also differentially regulated in the *bri1-116* mutant or a known BR related BZR1/BES1 target. In addition, 112 genes which are differentially regulated in the *serk1-3serk3-2* double mutant are known as a non-BR regulated BZR1/BES1 target (48 genes in total) or as low stringency BZR1 target (64 genes in total). This is about 16% of the total number of genes differentially regulated in the *serk1-3serk3-2* double mutant. To assess which biological categories are BR related and non-BR related genes differentially regulated in the *serk1-3serk3-2* double mutant were divided into four different groups (Also indicated in Supplemental Table S4 and S5):
Group 1: BR responsive BES1/BSR1 target genes and differentially regulated in the *bri1-116* mutant

Group 2: non-BR regulated BES1/BSR1 target genes

Group 3: low stringency BZR1 targets

Group 4: genes not differentially regulated in *bri1-116* or known as BZR1/BES1 related

To assess which biological processes are differentially regulated in these groups an over representation analysis was done.

Group 1 (290 genes in total)

ORA on known BR responsive BES1/BZR1 target genes and genes differentially regulated in the *bri1-116* mutant and *serk1-3serk3-2* indicates that photosynthesis, photosynthesis of antenna proteins, metabolism, porphyrin and chlorophyll metabolism and carbonfixation in photosynthetic organisms are differentially regulated biological processes. Genes related to metabolism are also identified in the category photosynthesis indicating that these genes are related to photosynthesis rather than a general metabolic process.

Group 2 (48 genes in total)

ORA on genes differentially regulated in the *serk1-3serk3-2* double mutant and known BZR1/BES1 target genes which are not regulated by BR. In this group glycerol lipid metabolism, glycerolphospholipid metabolism and metabolic pathways are identified as differentially regulated biological processes.

Group 3 (64 genes in total)

Low stringency BZR1 targets. No differential biological processes are identified.

Group 4 (296 genes in total)

ORA on genes differentially regulated in the *serk1-3serk3-2* mutant but not in the *bri1-116* mutant or identified as BZR1/BES1 target. In this group genes related to glucosynolate biosynthesis, metabolic pathways, glyoxylate and dicarboxylate metabolism, carbonfixation in photosynthetic organisms, biosynthesis of secondary metabolites and fatty acid metabolism are differentially regulated.

The photosynthesis related genes identified in the ORA are mainly found in group 1. Therefore, we conclude that the photosynthesis genes identified in the ORA of differentially up-regulated genes in the *serk1-3serk3-2* double mutant (Table 1 in main text) are BR related. In addition, non BR related genes in groups 2 and 4 are metabolic processes such as glycerolipid and fatty acid metabolism are identified as biological categories. Hence, metabolism and biosynthesis of secondary metabolites may be due to SERK1 and SERK3 related processes other than BR signalling.

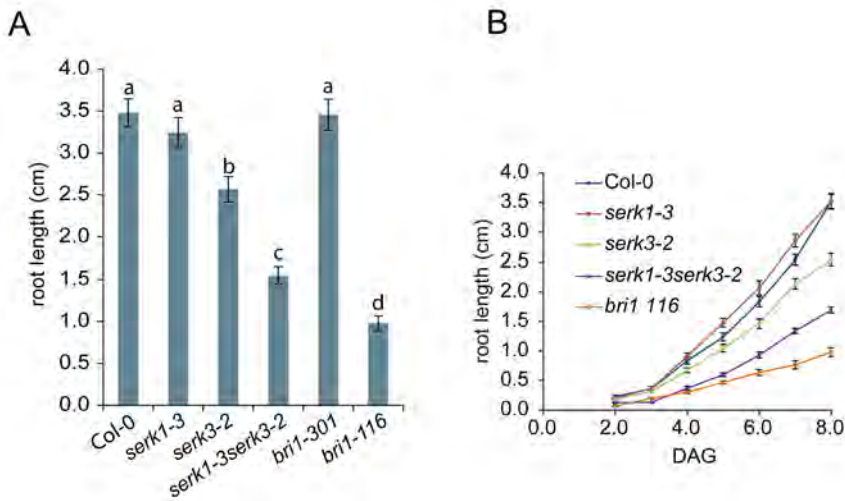


Figure S1. Root length of *serk* mutants compared to *bri1*-mutants. A) Root length phenotype of the *serk1-3*, *serk3-2*, *serk1-3serk3-2* compared to the wild type, *bri1-301* and *bri1-116* mutants. Letters a, b, and c indicate statistical differences, determined with a one-way ANOVA using an Bonniiferoni test ($\alpha = 0.05$). B) Comparison of the daily root growth of *serk1-3*, *serk3-2* and *serk1-3serk3-2* mutants with the *bri1-116* mutant and wild type. For (A) and (B) Error bars \pm SEM, $n \geq 20$ roots measured in three independent replicates.

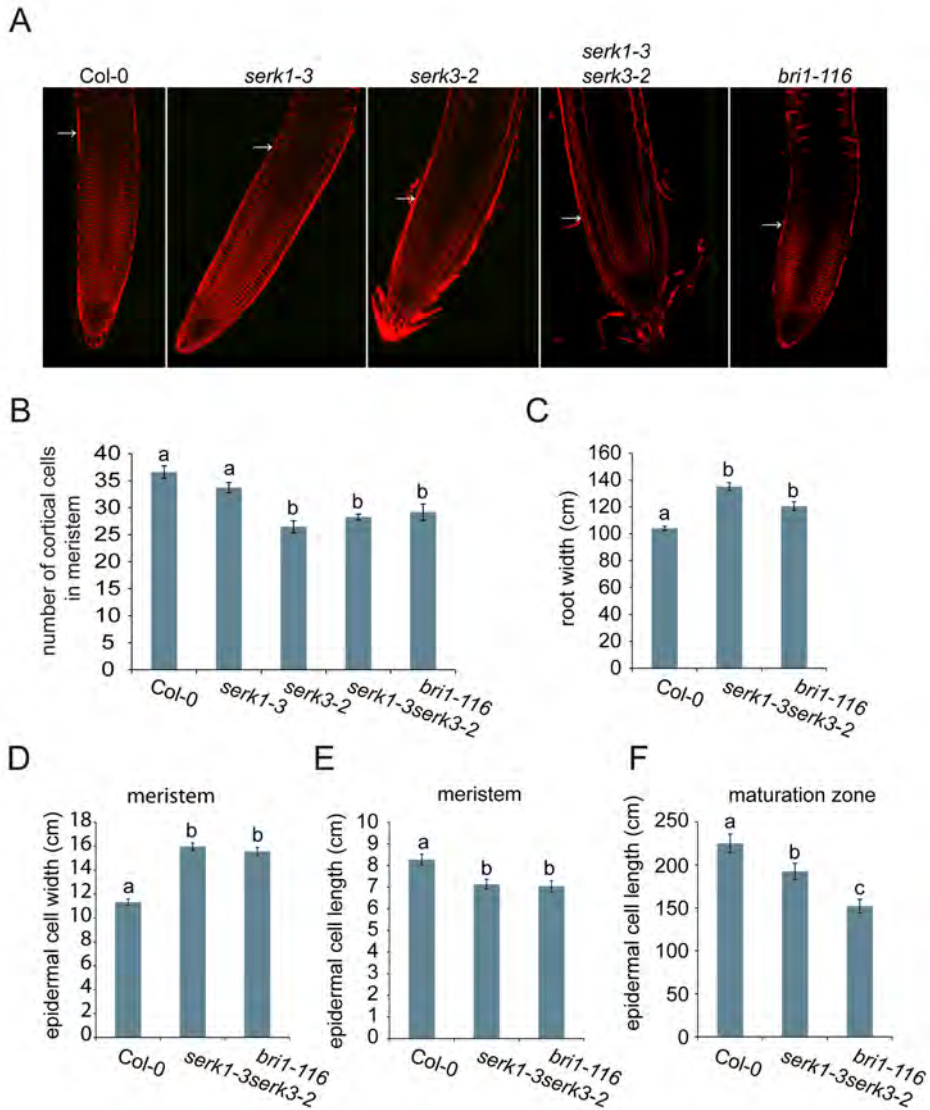


Figure S2. Phenotypical analysis of the *serk1-3serk3-2* double mutant. Data presented in this figure corroborates data previously presented by Du et al. (2012) who showed a similar trend for the *serk1-8bak1-4 (serk1-8serk3-2)* combination. A-B) Meristem size and width of the *serk1-3serk3-2* double mutant compared to wild type *serk1-3* and *serk3-2* single and *bri1-116* mutants. The meristem size and cortical cell number is significantly reduced in the *serk1-3serk3-2* double mutant. Images of the meristem were made using a Confocor-LSM510 microscope after staining of the roots for 5 minutes with FM4-64. The *serk1-3serk3-2* double mutant exhibits a increased root width (C) and epidermal cell width (D) while the epidermal cell length is slightly reduced (E) when compared to the wild type lines. The cell length in the maturation zone of the *serk1-3serk3-2* mutant is reduced when compared to the wild type lines but still longer compared to the *bri1-116* mutant. This may explain why the roots of the *serk1-3serk3-2* double mutants are longer when compared to the *bri1-116* mutant while the meristem size is reduced to the same extend. For all measurements $n \geq 10$ roots measured in two

independent r
ANOVA, usir

one way

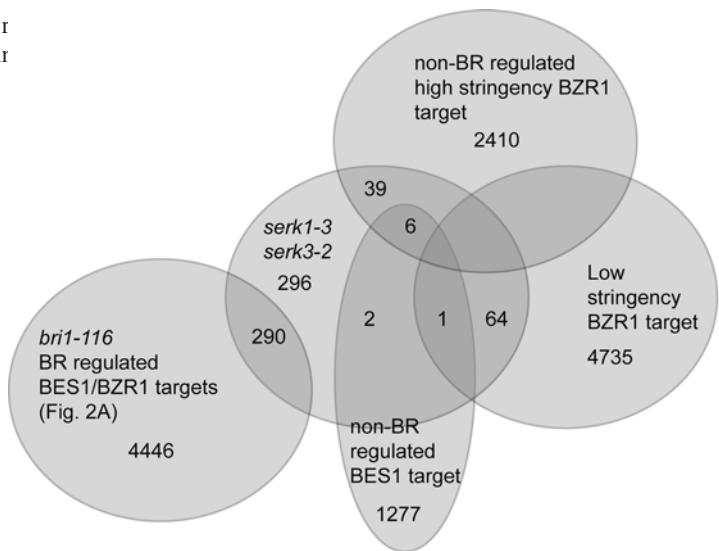


Figure S3. Comparison of genes differentially regulated in *serk1-3serk3-2* and BES1/BZR1 target genes. In total, 290 genes are differentially regulated in the *serk1-3serk3-2* double mutant and known as BR related BES1/BZR1 target genes or differentially regulated in the *bri1-116* mutant. The Venn diagram compares genes differentially regulated in the *serk1-3serk3-2* double mutant with non-BR related BZR1/BES1 target genes and low stringency BZR1 target genes. Overlap between *bri1-116* and non-BR related BZR1/BES1 targets and low stringency BZR1 target genes is not taken into account but can be found in Sun et al. (210) and Yu et al. (2010). Data on BZR1/BES1 target genes and genes differentially regulated in the *bri1-116* mutant is derived from literature (Sun et al., 2010; Yu et al., 2010).

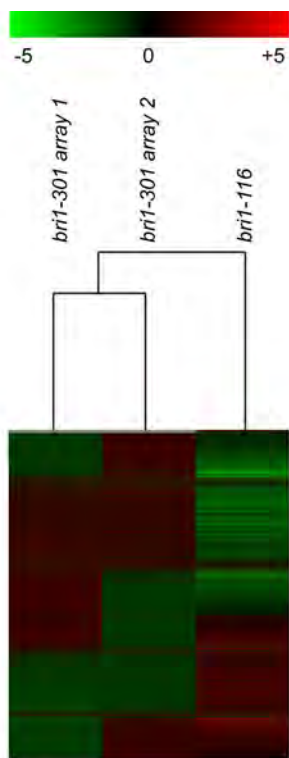


Figure S4. HCL analysis of the *bri1-301* mutant versus the *bri1-116* mutant line. In total, 4 genes are differentially regulated in the *bri1-301* mutant and 3531 in the *bri1-116* mutant. An HCL analysis was performed to assess if genes in the *bri1-301* mutant have the same transcriptional profile when compared to the *bri1-116* mutant. Results show that there is no clear correlation between these lines.

Table S1. Genes differentially regulated in the *serk1-3* mutant analysed using MAPMAN

AGI	Other names	cellular functions/ functions in*		FC
		phosphofructokinase		
AT4G26270	PFK3	glycolysis	(PFK)	2.2
AT1G71840		development	WD-40 repeat family	8.1
AT1G60960	IRT3	transport	metal	10.0
AT4G26190		not assigned	unknown	2.8

AGI = Arabidopsis Genome Initiative gene identification number.
Other name(s) = abbreviated common names for genes
FC = fold change compared to the wild type gene expression
*Cellular functions are derived using MAPMAN

Table S2. Genes differentially regulated in the *serk3-2* mutant analysed using MAPMAN

AGI	Other names	cellular functions/ functions in		FC
AT4G05180	PSBQ, PSBQ-2, PSII-Q	Photosystems	light reaction	3.1
AT1G51400		Photosystems	light reaction	2.1
AT1G03600		Photosystems	light reaction	2.5
AT1G31330	PSAF	Photosystems	light reaction	2.3
AT3G16140	PSAH-1	Photosystems	light reaction	3.6
AT4G12800	PSAL	Photosystems	light reaction	3.3
AT1G68010	HPR	Photosystems	photorespiration	2.9
AT2G24270	ALDH11A3	glycolysis	aldehyde dehydrogenase	2.4
AT5G14740	CA2, CA18	TCA	carbonate dehydratase	4.6
AT4G38770	PRP4, ATPRP4	cell wall	proline rich proteins	3.4
AT2G15880		cell wall	LRR	2.4
AT1G10550	XTH33, XET	cell wall	modification	-2.1
AT4G18550		lipid metabolism	lipid degradation	-3.11
AT1G68010	HPR	amino acid metabolism	degradation, lycerate dehydrogenas	2.9
AT1G74670		hormone metabolism	gibberellin-responsive protein, putative	2.0
AT3G56940	CRD1, CHL27, ACSF	tetrapyrrole synthesis	magnesium-protoporphyrin IX monomethyl ester (oxidative) cyclase	3.1
AT2G21100		biotic stress	pathogen related proteins	-2.3
AT5G38940		abiotic stress	unspecified	9.5
AT4G36430		misc.peroxidases	peroxidase, putative	-3.7
AT3G06210		misc.acid and other phosphatases		-2.6
AT3G52820	ATPAP22, PAP22	misc.acid and other phosphatases	phosphatase	-2.4
AT4G12480	pEARLI 1	misc.protease inhibitor	Lipid transfer protein (LTP) family protein	4.6
AT4G28530	anac074	RNA.regulation of transcription	NAC domain transcription factor family	-3.4
AT1G11190	BFN1, ENDO1	DNA synthesis	endodeoxyribonuclease	-3.0
AT3G45010	scpl48	protein degradation		-2.4
AT4G04460		protein degradation	aspartyl protease family protein	-2.6
AT4G17245		protein degradation	zinc finger (C3HC4-type RING finger) family protein	4.8
AT2G24710	ATGLR2.3, GLR2.3	signalling	in sugar and nutrient physiology	2.8
AT3G18890		signalling	light	2.0
AT4G28530	anac074	development	unspecified	-3.4
AT1G28330	DYL1	development	unspecified	2.1

AGI = Arabidopsis Genome Initiative gene identification number.

Other name(s) = abbreviated common names for genes

FC = fold change compared to the wild type gene expression

Genes marked in grey are identified in multiple cellular functions/functions in according to MAPMAN

*Cellular functions are derived using MAPMAN

Table S2. continued

Other names		cellular functions/ functions in		FC
AT2G03260		transport	phosphate, EXS family protein	2.7
AT1G60960	IRT3	transport	metal	8.2
AT1G53270		ABC transporters and multidrug resistance systems	ABC transporter family protein	-2.7
AT5G19700		ABC transporters and multidrug resistance systems	MATE efflux protein-related	3.0
AT5G65980		transport misc	auxin efflux carrier family protein	3.8
AT2G07600		not assigned no ontology		3.3
AT1G21326		not assigned no ontology		3.1
AT4G01050		not assigned no ontology	hydroxyproline rich proteins	2.0
AT5G04730		not assigned unknown		2.5
AT3G16660		not assigned unknown		3.2
AT4G21250		not assigned unknown		2.2
AT2G20835		not assigned unknown		2.3
AT4G04223		not assigned unknown		2.7

AGI = Arabidopsis Genome Initiative gene identification number.

Other name(s) = abbreviated common names for genes

FC = fold change compared to the wild type gene expression

Genes marked in grey are identified in multiple cellular functions/functions in according to MAPMAN

*Cellular functions are derived using MAPMAN

Table S3. Genes differentially regulated in the *serk1-3serk3-2* double mutant

AGI = Arabidopsis Genome Initiative gene identification number.

FC = fold change compared to the wild type gene expression

down-regulated genes							
AGI	FC	AGI	FC	AGI	FC	AGI	FC
AT2G22510	-10.8	AT4G26790	-4.0	AT4G28940	-2.9	AT4G27850	-2.4
AT5G06200	-7.5	AT1G03700	-3.9	AT5G19600	-2.9	AT2G47200	-2.4
AT2G23540	-7.1	AT1G52580	-3.9	AT1G73290	-2.9	AT2G19050	-2.4
AT1G55990	-7.1	AT1G14550	-3.7	AT3G56730	-2.8	AT2G38760	-2.4
AT3G50400	-7.1	AT5G13580	-3.7	AT1G05100	-2.8	AT5G62480	-2.4
AT3G06390	-6.9	AT2G01530	-3.7	AT3G04370	-2.8	AT1G50590	-2.3
AT2G01520	-6.8	AT1G49430	-3.6	AT1G51260	-2.8	AT4G39770	-2.3
AT5G12420	-6.8	AT2G03200	-3.6	AT2G48130	-2.8	AT3G52790	-2.3
AT5G06090	-6.4	AT2G41170	-3.6	AT5G23190	-2.8	AT4G02830	-2.3
AT5G44550	-6.2	AT4G28530	-3.5	AT2G24430	-2.8	AT3G55230	-2.3
AT4G20390	-6.1	AT4G11320	-3.5	AT3G22060	-2.8	AT3G44540	-2.3
AT1G78990	-5.9	AT2G18370	-3.5	AT1G80180	-2.8	AT1G31935	-2.3
AT5G09520	-5.7	AT5G16770	-3.5	AT2G05440	-2.8	AT3G23090	-2.3
AT2G35380	-5.4	AT1G14730	-3.5	AT5G52790	-2.7	AT1G28815	-2.3
AT4G38080	-5.3	AT2G36295	-3.5	AT1G23330	-2.7	AT4G12545	-2.3
AT5G47635	-5.2	AT3G18400	-3.3	AT2G33205	-2.7	AT1G05660	-2.3
AT4G33610	-5.2	AT5G01600	-3.3	AT1G08430	-2.7	AT3G46700	-2.3
AT1G34670	-5.1	AT1G04220	-3.3	AT2G35980	-2.7	AT5G58910	-2.3
AT5G09530	-5.0	AT5G13900	-3.2	AT2G46680	-2.7	AT3G01190	-2.3
AT1G74460	-5.0	AT1G54540	-3.2	AT4G36430	-2.7	AT1G61130	-2.3
AT5G37690	-4.9	AT4G24130	-3.2	AT4G22090	-2.7	AT2G26290	-2.3
AT5G19410	-4.9	AT2G40250	-3.2	AT5G65800	-2.6	AT1G28400	-2.2
AT5G14130	-4.8	AT2G21100	-3.2	AT3G49330	-2.6	AT3G51890	-2.2
AT3G44550	-4.8	AT2G02820	-3.2	AT2G38110	-2.6	AT4G16750	-2.2
AT1G49960	-4.6	AT2G18150	-3.1	AT1G01610	-2.6	AT1G17180	-2.2
AT5G07130	-4.6	AT3G07970	-3.1	AT5G10430	-2.5	AT3G12720	-2.2
AT5G37990	-4.6	AT3G52920	-3.1	AT2G48140	-2.5	AT5G16570	-2.2
AT1G68850	-4.5	AT1G01600	-3.1	AT4G03540	-2.5	AT1G10140	-2.2
AT1G56320	-4.3	AT5G05390	-3.0	AT1G52342	-2.5	AT1G77590	-2.2
AT4G36610	-4.3	AT3G11430	-3.0	AT3G60840	-2.5	AT5G65230	-2.2
AT5G07475	-4.3	AT4G02090	-3.0	AT3G14225	-2.5	AT5G55970	-2.2
AT1G53270	-4.3	AT4G35420	-3.0	AT1G70210	-2.5	AT1G72230	-2.2
AT2G40370	-4.2	AT2G45970	-3.0	AT1G17300	-2.5	AT3G22620	-2.2
AT2G31540	-4.2	AT5G49350	-3.0	AT3G50640	-2.5	AT5G47530	-2.2
AT5G41570	-4.1	AT4G35160	-3.0	AT3G48940	-2.4	AT4G29340	-2.2
AT5G58860	-4.0	AT1G64000	-2.9	AT3G21680	-2.4	AT5G63590	-2.2
AT5G08250	-4.0	AT1G18870	-2.9	AT4G01890	-2.4	AT1G78390	-2.1
AT5G09480	-4.0	AT4G24140	-2.9	AT2G46130	-2.4	AT4G10500	-2.1
AT5G10230	-4.0	AT4G17215	-2.9	AT5G55590	-2.4	AT5G58780	-2.1
AT4G12550	-4.0	AT1G71740	-2.9	AT3G15450	-2.4	AT5G42250	-2.1

Table S3. continued

down-regulated genes		up-regulated genes					
AGI	FC	AGI	FC	AGI	FC	AGI	FC
AT2G30210	-2.1	AT1G29430	2.0	AT1G60550	2.1	AT3G24615	2.2
AT4G29905	-2.1	AT5G18220	2.0	AT2G41090	2.1	AT1G76450	2.2
AT4G37700	-2.1	AT5G14320	2.0	AT2G21610	2.1	AT1G78370	2.2
AT3G01970	-2.1	AT3G06962	2.0	AT5G39530	2.1	AT1G19150	2.2
AT3G50970	-2.1	AT5G13140	2.0	AT1G16400	2.1	ATMG00920	2.2
AT2G47270	-2.1	AT1G75690	2.0	AT2G29630	2.1	AT1G78970	2.2
AT4G37010	-2.1	AT1G02390	2.0	AT4G32260	2.1	AT2G42600	2.2
AT3G49190	-2.1	AT1G04420	2.0	AT1G19350	2.1	AT1G74470	2.2
AT1G43160	-2.1	AT4G22890	2.0	ATCG00970	2.1	AT5G56860	2.2
AT1G67270	-2.1	AT1G71500	2.0	ATCG01160	2.1	AT4G16890	2.2
AT3G46280	-2.1	AT4G09040	2.0	AT1G18075	2.1	AT3G54600	2.2
AT3G10910	-2.1	AT3G51820	2.0	AT1G26770	2.1	AT4G01310	2.2
AT3G10912	-2.1	AT1G74730	2.0	AT5G51451	2.1	AT3G42628	2.2
AT4G38060	-2.1	AT5G30510	2.0	AT1G79040	2.1	AT5G38410	2.2
AT3G07780	-2.1	AT1G44446	2.0	AT1G34200	2.1	AT4G38840	2.2
AT1G58037	-2.1	AT5G48300	2.0	AT3G27940	2.1	AT3G20470	2.2
AT3G59690	-2.1	AT4G22270	2.0	AT1G22150	2.1	AT5G51010	2.2
AT4G08160	-2.1	AT2G43137	2.0	AT2G03260	2.1	AT4G35200	2.2
AT2G37070	-2.1	AT5G04360	2.0	AT3G16250	2.1	AT4G25010	2.2
AT1G73410	-2.1	AT1G26560	2.0	AT1G73110	2.1	AT4G12470	2.2
AT4G15290	-2.1	AT2G38140	2.0	AT1G32385	2.1	AT5G57500	2.2
AT5G40590	-2.1	AT3G22210	2.0	AT3G63540	2.1	AT4G20360	2.2
AT3G07600	-2.1	AT1G79850	2.0	AT5G05740	2.1	AT4G39366	2.2
AT5G67340	-2.1	AT2G07813	2.0	AT5G49780	2.1	AT2G20570	2.2
AT1G73330	-2.1	ATMG01260	2.0	AT5G13510	2.1	AT5G42070	2.3
AT5G40270	-2.0	AT4G12030	2.1	AT3G27906	2.1	AT1G01170	2.3
AT5G39340	-2.0	AT1G49405	2.1	AT1G23310	2.1	AT2G16660	2.3
AT2G36410	-2.0	AT4G16950	2.1	AT4G33000	2.1	AT5G58140	2.3
AT5G04220	-2.0	AT4G18390	2.1	AT5G45469	2.2	AT2G05540	2.3
AT3G47220	-2.0	AT1G33600	2.1	AT3G62030	2.2	AT1G54780	2.3
AT1G79700	-2.0	AT5G14910	2.1	AT1G52190	2.2	AT1G34418	2.3
AT4G38830	-2.0	AT5G46450	2.1	AT1G21060	2.2	AT3G21090	2.3
AT2G39530	-2.0	AT5G47440	2.1	AT2G26910	2.2	AT3G23110	2.3
AT4G26580	-2.0	AT3G01730	2.1	AT3G61700	2.2	AT5G63180	2.3
AT2G27370	-2.0	AT3G59780	2.1	AT1G29785	2.2	AT1G33790	2.3
AT1G53680	-2.0	AT5G40380	2.1	AT1G73885	2.2	AT4G22880	2.3
AT5G51680	-2.0	AT2G07764	2.1	AT3G14420	2.2	AT4G17695	2.3
AT5G17650	-2.0	ATMG00380	2.1	ATCG00990	2.2	AT4G34190	2.3
		AT1G49380	2.1	ATCG01140	2.2	AT1G73602	2.3
		AT2G28950	2.1	AT1G76100	2.2	AT1G49030	2.3

Table S3. continued

AGI	FC	AGI	FC	AGI	FC	AGI	FC
AT4G21280	2.3	AT5G65330	2.4	AT4G25420	2.5	AT5G48485	2.7
AT1G78630	2.3	AT1G24020	2.4	AT1G31650	2.5	AT5G66190	2.7
AT4G13195	2.3	AT4G10060	2.4	AT2G24090	2.5	AT1G33670	2.7
AT4G34419	2.3	AT4G24510	2.4	AT3G52840	2.5	AT5G58330	2.7
AT4G09650	2.3	AT1G71830	2.4	AT3G22121	2.5	AT1G26945	2.7
AT4G09010	2.3	AT4G34250	2.4	AT3G26932	2.5	AT4G01050	2.7
AT1G15260	2.3	AT5G13630	2.4	AT1G31330	2.6	AT1G77640	2.8
AT3G61310	2.3	AT4G14630	2.4	AT1G29070	2.6	AT4G16980	2.8
AT3G54050	2.3	AT2G29650	2.4	AT1G05835	2.6	AT2G20260	2.8
AT4G27260	2.3	AT2G18300	2.4	AT5G57800	2.6	AT1G27921	2.8
AT2G43141	2.3	AT3G21950	2.4	AT3G44020	2.6	AT4G25960	2.8
AT1G32780	2.3	AT4G18480	2.4	AT5G46240	2.6	AT1G78170	2.8
AT1G69530	2.3	AT1G09390	2.4	AT2G24720	2.6	AT2G05100	2.8
AT1G73600	2.3	AT2G40610	2.4	AT5G07020	2.6	AT2G04039	2.8
AT5G19940	2.3	AT1G60600	2.4	AT1G49100	2.6	AT1G26250	2.8
AT1G35680	2.3	AT5G54600	2.4	AT5G38980	2.6	AT4G21620	2.8
ATCG00580	2.3	AT1G31900	2.4	AT1G78490	2.6	AT5G65870	2.8
AT2G35260	2.3	AT2G32440	2.5	AT3G01480	2.6	AT3G25920	2.8
AT5G64770	2.4	AT2G38230	2.5	AT3G05180	2.6	AT3G63140	2.8
AT2G20180	2.4	AT1G15980	2.5	AT5G13170	2.6	AT1G31800	2.8
AT2G09795	2.4	AT2G39470	2.5	AT3G27830	2.6	AT1G56500	2.9
AT4G23820	2.4	AT5G25980	2.5	AT3G13120	2.6	AT2G39730	2.9
AT3G54210	2.4	AT1G67700	2.5	AT3G09390	2.6	AT1G72970	2.9
AT1G54010	2.4	AT4G16370	2.5	AT3G22120	2.6	AT1G51870	2.9
AT3G47470	2.4	AT1G74890	2.5	AT1G51400	2.6	AT2G05520	2.9
AT2G41312	2.4	AT1G71480	2.5	AT3G02110	2.7	AT1G76620	2.9
AT4G33870	2.4	AT1G66940	2.5	AT3G51600	2.7	AT3G53280	2.9
AT2G43100	2.4	AT4G18970	2.5	AT1G06680	2.7	AT5G26300	2.9
AT1G01320	2.4	AT3G55240	2.5	AT5G27360	2.7	AT2G34930	2.9
AT5G07190	2.4	AT5G19110	2.5	AT3G08940	2.7	AT1G33811	2.9
AT2G07678	2.4	AT1G03630	2.5	AT1G23210	2.7	AT1G47395	2.9
AT1G51805	2.4	AT1G64430	2.5	AT1G02475	2.7	AT4G16860	2.9
AT1G14700	2.4	AT1G52220	2.5	AT4G08040	2.7	AT4G15530	2.9
AT3G44890	2.4	AT1G29440	2.5	AT1G70830	2.7	AT2G04570	2.9
AT4G39364	2.4	AT1G07720	2.5	AT5G67070	2.7	AT2G21330	2.9
AT4G36810	2.4	AT4G30650	2.5	AT2G14960	2.7	AT2G10940	2.9
AT1G14440	2.4	AT2G30010	2.5	AT4G24770	2.7	AT5G64040	2.9
AT1G61520	2.4	AT3G12780	2.5	AT4G36540	2.7	AT5G52780	2.9
AT3G23290	2.4	AT5G57240	2.5	AT2G41100	2.7	AT1G71380	2.9
AT5G04230	2.4	AT2G16230	2.5	AT4G29020	2.7	AT5G08000	2.9

Table S3. continued

AGI	FC	AGI	FC	AGI	FC	AGI	FC
AT1G77490	2.9	AT2G44910	3.2	AT1G27950	3.7	AT3G18890	4.2
AT1G69160	2.9	AT5G49770	3.2	AT1G29450	3.7	AT3G26060	4.2
AT3G51420	3.0	AT5G48490	3.3	AT3G58990	3.7	AT1G55670	4.2
AT1G50732	3.0	AT3G47295	3.3	AT1G20340	3.7	AT4G39330	4.2
AT1G52100	3.0	AT5G39890	3.3	AT5G58250	3.7	AT1G08380	4.3
AT1G53440	3.0	AT3G46780	3.3	AT5G22555	3.7	AT1G74670	4.3
AT1G44830	3.0	AT4G28780	3.3	AT2G36870	3.7	AT1G35290	4.3
AT2G45740	3.0	AT3G50820	3.3	AT4G16410	3.8	AT1G26240	4.3
AT5G66570	3.0	AT4G04890	3.3	AT5G23060	3.8	AT3G51340	4.4
AT3G51510	3.0	AT4G03280	3.3	AT3G16140	3.8	AT4G13770	4.4
AT4G39361	3.0	AT3G14415	3.4	AT3G14210	3.8	AT4G12490	4.4
AT2G34420	3.0	AT5G47610	3.4	AT5G23120	3.8	AT2G05070	4.5
AT1G11120	3.0	AT4G21870	3.4	AT1G73780	3.8	AT1G72645	4.6
AT2G45550	3.0	AT1G67105	3.4	AT3G02020	3.8	AT3G48200	4.6
AT4G00050	3.0	AT1G12900	3.4	AT4G21750	3.9	AT5G38420	4.6
AT1G56680	3.0	AT5G23010	3.5	AT2G26330	3.9	AT2G16630	4.6
AT3G26070	3.0	AT1G45201	3.5	AT1G73610	3.9	AT2G32690	4.6
AT2G37660	3.1	AT1G32080	3.5	AT4G28080	3.9	AT1G15125	4.7
AT4G33220	3.1	AT1G29910	3.5	AT5G01870	3.9	AT3G20820	4.7
AT3G57157	3.1	AT1G05700	3.5	AT1G64510	3.9	AT1G20620	4.8
AT1G62290	3.1	AT1G32900	3.5	AT1G44575	3.9	AT1G29660	4.8
AT1G15820	3.1	AT5G02760	3.5	AT4G08780	3.9	AT5G01530	4.8
AT3G33000	3.1	AT5G13400	3.5	AT1G64670	3.9	AT3G55800	4.8
ATCG00150	3.1	AT1G03680	3.5	AT5G54270	3.9	AT5G19700	4.8
AT2G40802	3.1	AT5G22500	3.5	AT1G67740	4.0	AT4G21250	4.8
AT3G20365	3.1	AT1G74970	3.6	AT2G24710	4.0	AT4G17245	4.9
ATCG00240	3.1	AT1G09340	3.6	AT2G07600	4.0	AT3G47650	4.9
AT2G06520	3.1	AT3G46490	3.6	AT4G10340	4.0	AT3G55330	4.9
AT5G07180	3.2	AT4G38825	3.6	AT2G13360	4.0	AT4G28750	4.9
AT4G18220	3.2	AT2G37640	3.6	AT1G72610	4.0	AT5G44580	5.0
AT5G04140	3.2	AT5G45670	3.6	AT4G12800	4.0	AT3G26650	5.0
AT1G61800	3.2	AT4G27440	3.6	AT1G64710	4.0	AT2G43510	5.0
AT4G36250	3.2	AT1G20020	3.6	AT4G23713	4.1	AT4G05180	5.0
AT3G51410	3.2	AT2G34650	3.6	AT4G38970	4.1	AT1G51500	5.0
AT1G32990	3.2	AT1G70760	3.6	AT1G32060	4.1	AT1G68590	5.1
AT3G10450	3.2	AT3G19710	3.6	AT3G56940	4.1	AT2G42840	5.1
AT1G66970	3.2	AT1G03600	3.6	AT2G42220	4.1	AT1G63570	5.1
AT4G04640	3.2	AT1G68530	3.6	AT5G03120	4.2	AT4G38770	5.1
AT1G49750	3.2	AT5G09660	3.7	AT2G30570	4.2	AT1G56430	5.2
AT2G43010	3.2	AT2G45080	3.7	AT1G49860	4.2	AT1G42970	5.2

Table S3. continued

AGI	FC	AGI	FC
AT1G09310	5.2	AT5G25610	7.9
AT4G08150	5.3	AT5G38940	8.2
AT2G23010	5.3	AT5G20630	8.3
AT1G29510	5.3	AT3G63160	8.3
AT1G52230	5.3	AT1G70260	8.6
AT4G25050	5.4	AT4G37800	8.7
AT5G36910	5.4	AT5G38430	9.3
AT5G46110	5.4	AT3G04290	9.3
AT3G50440	5.5	AT1G17840	9.4
AT3G61470	5.6	AT5G42800	10.1
AT4G32950	5.6	AT5G18080	10.8
AT1G68010	5.6	AT2G24270	11.1
AT5G43370	5.6	AT3G44970	12.4
AT2G46820	5.7	AT2G05380	13.5
AT1G71840	5.7	AT3G21720	13.5
AT5G42530	5.8	AT5G18030	13.7
AT5G67385	5.8	AT4G12480	18.0
AT2G15050	5.8	AT1G31580	23.7
AT1G29930	5.9	AT2G38530	26.6
AT3G59060	6.0	AT4G23560	26.9
AT1G29670	6.0		
AT2G34430	6.2		
AT3G45140	6.2		
AT2G23170	6.4		
AT1G08090	6.4		
AT5G15780	6.5		
AT5G26000	6.6		
AT1G17200	6.6		
AT2G38540	6.7		
AT1G55260	6.9		
AT3G21055	7.0		
AT5G65980	7.0		
AT4G16515	7.1		
AT1G30560	7.2		
AT5G49630	7.2		
AT5G54770	7.4		
AT3G16370	7.5		
AT2G20835	7.5		
AT4G04223	7.7		
AT3G16660	7.9		

Table S4. BR related and non-BR related genes differentially regulated in *serk1-3serk3-2*

Genes differentially regulated in *serk1-3serk3-2*, *bri1-116* and BR regulated BZR1 and BES1 targets genes (1 gene)

AGI	Gene name
AT4G27260	GH3.5, WES1

Genes differentially regulated in *serk1-3serk3-2*, *bri1-116* and BR regulated BZR1 target genes (49 genes)

AGI	Gene name	AGI	Gene name
AT4G28530	anac074	AT2G41100	TCH3, ATCAL4
AT2G46680	ATHB-7, ATHB7	AT5G58330	
AT3G46700		AT1G77640	
AT4G16750		AT1G77490	TAPX
AT1G10140		AT5G66570	PSBO-1, OEE1, OEE33, OE33, PSBO1, MSP-1
			UNE10
AT5G55970		AT4G00050	GPT2
AT3G46280		AT1G61800	ATHB4, ATHB-4
AT1G29430		AT2G44910	
AT1G04420		AT5G47610	
AT1G71500		AT5G02760	
AT5G14910		AT1G09340	CRB, CSP41B
AT1G76100	PETE1	AT1G03600	
AT5G56860	GNC	AT1G68530	CUT1, POP1, CER6, G2, KCS6
AT4G16890	SNC1, BAL	AT1G29450	
AT2G20570	GPR11, GLK1	AT5G01870	
AT1G78630	emb1473	AT1G72610	GLP1, ATGER1, GER1
AT1G69530	ATEXPA1, EXP1, AT-EXP1, ATEXP1, ATHEXP ALPHA 1.2	AT1G64710	
AT2G40610	ATEXPA8, EXP8, ATEXP8, ATHEXP ALPHA 1.11	AT1G29660	
AT4G16370	ATOPT3, OPT3	AT5G01530	
AT1G29440		AT4G17245	
AT4G25420	GA5, GA20OX1, AT2301, ATGA20OX1	AT3G61470	LHCA2
AT5G38980		AT2G46820	PTAC8, TMP14, PSAP, PSI-P
AT3G13120		AT1G29670	
AT3G22120	CWLP	AT5G54770	THI1, TZ, THI4
AT4G08040	ACS11		

Genes differentially regulated in *serk1-3serk3-2*, *bri1-116* and BR regulated BES1 target genes (3 genes)

AGI	Gene name	AGI	Gene name
AT1G07720		AT3G59060	PIL6, PIF5
AT5G13400			

Table S4. continued

Genes differentially regulated in <i>serk1-3serk3-2</i> and <i>bri1-116</i> (214 genes)			
AGI	Gene name	AGI	Gene name
AT5G06200		AT1G23310	GGT1, AOAT1
AT2G01530	MLP329	AT4G33000	CBL10, ATCBL10
AT2G03200		AT3G62030	ROC4
AT4G11320		AT1G21060	
AT1G14730		AT3G14420	
AT1G04220	KCS2	AT1G76450	
AT2G18150		AT1G19150	LHCA6, LHCA2*1
AT3G52920		AT1G78970	LUP1, ATLUP1
AT1G01600	CYP86A4	AT1G74470	
AT4G02090		AT4G01310	
AT4G35160		AT4G38840	
AT1G18870	ICS2	AT5G51010	
AT1G71740		AT4G20360	ATRAB8D, ATRABE1B
AT5G19600	SULTR3;5	AT5G42070	
AT1G08430		AT1G01170	
AT4G36430		AT1G54780	
AT5G65800	ACS5, CIN5, ETO2, ATACS5	AT4G34190	SEP1
AT1G01610	ATGPAT4	AT4G21280	PSBQ, PSBQA, PSBQ-1
AT5G10430	AGP4, ATAGP4	AT4G09650	ATPD
AT1G17300		AT4G09010	APX4
AT3G50640		AT1G15260	
AT2G38760	ANNAT3	AT3G61310	
AT4G39770		AT5G19940	
AT3G23090		AT1G35680	
AT1G28400		AT2G35260	
AT1G72230		AT3G54210	
AT3G22620		AT3G47470	LHCA4, CAB4
AT5G47530		AT3G44890	RPL9
AT5G63590	FLS3	AT1G61520	LHCA3
AT5G42250		AT3G23290	LSH4
AT2G30210	LAC3	AT5G04230	PAL3, ATPAL3
AT2G47270		AT4G10060	
AT4G37010	CEN2	AT5G13630	GUN5, CCH, CHLH, CCH1
AT3G10910		AT2G29650	ANTR1, PHT4;1
AT4G38060		AT2G18300	
AT3G59690	IQD13	AT4G18480	CHLI1, CH42, CH-42, CHL11, CHLI-1
AT1G73330	ATDR4	AT1G60600	ABC4
AT5G39340	AHP3, ATHP2	AT5G54600	
AT2G36410		AT2G32440	KAO2, CYP88A4
AT2G27370		AT2G39470	PPL2
AT5G14320		AT5G25980	TGG2, BGLU37
AT5G13140		AT1G67700	
AT1G75690		AT4G18970	
AT4G22890	PGR5-LIKE A	AT1G52220	
AT3G51820	ATG4, G4, CHLG	AT2G30010	
AT1G74730		AT3G12780	PGK1
AT5G30510	RPS1, ARRPS1	AT2G24090	
AT2G38140	PSRP4	AT1G31330	PSAF
AT3G22210		AT1G29070	
AT1G79850	RPS17, CS17, PRPS17	AT5G57800	FLP1, YRE, CER3, WAX2
AT4G18390		AT3G44020	
AT1G60550	ECHID, DHNS	AT5G07020	
AT4G32260	PDE334	AT3G01480	CYP38
AT1G79040	PSBR	AT3G05180	
AT5G05740	ATEGY2, EGY2	AT3G27830	RPL12-A, RPL12
AT5G13510		AT3G09390	MT2A, ATMT-K, ATMT-1

Table S4. continued

Genes differentially regulated in <i>serk1-3serk3-2</i> and <i>bri1-116</i> (214 genes)(continued)			
AGI	Gene name	AGI	Gene name
AT1G51400		AT1G20340	DRT112, PETE2
AT3G02110	scpl25	AT5G58250	
AT1G06680	PSBP-1, OEE2, PSII-P, OE23	AT4G16410	
AT3G08940	LHCB4.2	AT5G23060	CaS
AT1G02475		AT3G16140	PSAH-1
AT4G24770	RBP31, ATRBP31, CP31, ATRBP33	AT5G23120	HCF136
AT4G36540	BEE2	AT1G64510	
AT4G29020		AT1G64670	BDG1
AT5G48485	DIR1	AT5G54270	LHCB3, LHCB3*1
AT5G66190	ATLFNR1, FNR1	AT1G67740	PSBY, YCF32
AT4G01050	RPL15	AT4G10340	LHCB5
AT2G20260	PSAE-2	AT4G12800	PSAL
AT2G05100	LHCB2.1, LHCB2	AT4G38970	
AT3G25920	RPL15	AT3G56940	CRD1, CHL27, ACSF
AT3G63140	CSP41A	AT2G42220	
AT1G31800	CYP97A3, LUT5	AT2G30570	PSBW
AT1G56500		AT3G26060	ATPRX Q
AT2G39730	RCA	AT1G55670	PSAG
AT2G34930		AT1G08380	PSAO
AT1G33811		AT2G05070	LHCB2.2, LHCB2
AT2G04570		AT3G55800	SBPASE
AT2G21330		AT3G47650	
AT5G64040	PSAN	AT3G55330	PPL1
AT1G71380	ATGH9B3, ATCEL3	AT4G28750	PSAE-1
AT3G51420	SSL4, ATSSL4	AT3G26650	GAPA, GAPA-1
AT1G52100		AT4G05180	PSBQ, PSBQ-2, PSII-Q
AT1G44830		AT1G68590	
AT3G51510		AT2G42840	PDF1
AT2G34420	LHB1B2, LHCB1.5	AT1G42970	GAPB
AT2G37660		AT1G09310	
AT4G33220	PME44, ATPME44	AT4G08150	KNAT1, BP, BP1
AT1G62290		AT2G23010	SCPL9
AT1G15820	LHCB6, CP24	AT1G29510	SAUR68
AT2G06520	PSBX	AT1G52230	PSAH2, PSAH-2, PSI-H
AT5G04140		AT4G25050	ACP4
AT1G32990	PRPL11	AT5G46110	APE2, TPT
AT4G04640	ATPC1	AT1G68010	HPR
AT1G49750		AT1G29930	CAB1, AB140, CAB140, LHCB1.3
AT3G47295		AT2G34430	LHB1B1, LHCB1.4
AT3G50820	PSBO2, PSBO-2, OEC33	AT5G26000	TGG1, BGLU38
AT4G03280	PETC, PGR1	AT2G38540	LTP1
AT3G14415		AT1G55260	
AT1G12900	GAPA-2	AT3G21055	PSBTN
AT1G29910	CAB3, AB180, LHCB1.2	AT4G16515	
AT1G03680	ATHM1, TRX-M1, ATM1	AT5G49630	AAP6
AT1G74970	RPS9, TWN3	AT3G16370	
AT5G45670		AT5G25610	RD22
AT4G27440	PORB	AT5G38940	
AT1G70760	CRR23	AT5G20630	GLP3, GLP3A, GLP3B, ATGER3, GER3
AT5G09660	PMDH2	AT3G63160	
AT1G27950		AT1G17840	WBC11, ABCG11, DSO, COF1, ATWBC11

Table S4. continued

Genes differentially regulated in *serk1-3serk3-2*, BR regulated BZR1 and BES1 targets (1 gene)

AGI	Gene name
AT1G69160	

Genes differentially regulated in *serk1-3serk3-2* and BR regulated BES1 targets (4 genes)

AGI	Gene name	AGI	Gene name
AT1G79700		AT1G74670	
AT1G32900		AT3G04290	ATLTL1, LTL1

Genes differentially regulated in *serk1-3serk3-2* and BR regulated BZR1 targets (18 genes)

AGI	Gene name	AGI	Gene name
AT5G14130		AT1G51805	
AT2G41170		AT4G36810	GGPS1
AT5G01600	ATFER1, FER1	AT2G38230	ATPDX1.1, PDX1.1
AT3G22060		AT3G51600	LTP5
AT1G70210	CYCD1;1	AT2G10940	
AT5G40380		AT4G18220	
AT2G41090		AT3G14210	ESM1
AT5G63180		AT4G37800	
AT5G64770		AT1G31580	ECS1, CXC750

Genes differentially regulated in *serk1-3serk3-2* and non-BR regulated BZR1/ BES1 targets (6 genes)

AGI	Gene name	AT1G05700
AT5G06090	ATGPAT7	AT3G20820
AT1G19350	BES1, BZR2	AT5G18080
AT1G09390		

Genes differentially regulated in *serk1-3serk3-2* and non-BR regulated BZR1 targets (39 genes)

AGI	Gene name	AGI	Gene name
AT2G22510		AT4G34250	KCS16
AT5G08250		AT3G55240	
AT3G11430		AT5G19110	
AT5G49350		AT5G13170	SAG29
AT4G24140		AT5G67070	RALFL34
AT1G80180		AT1G26945	KDR
AT2G38110	ATGPAT6	AT1G76620	
AT4G03540		AT1G53440	
AT2G47200		AT3G51410	
AT5G62480	ATGSTU9, GST14, GST14B	AT2G34650	PID, ABR
AT3G55230		AT2G45080	cycp3;1
AT5G16570	GLN1;4	AT4G28080	
AT4G29905		AT1G15125	
AT1G02390	ATGPAT2	AT5G44580	
AT1G33600		AT4G32950	
AT2G28950	ATEXPA6, ATEXP6, ATHEXP	AT3G45140	LOX2, ATLOX2
	ALPHA 1.8		
AT2G42600	ATPPC2	AT2G23170	GH3.3
AT2G16660		AT2G20835	
AT4G23820		AT1G70260	
AT5G07190	ATS3		

Genes differentially regulated in *serk1-3serk3-2*, non-BR regulated BES1 target genes and low stringency BZR1 target genes (1 gene)

AGI	Gene name
AT1G78170	

Table S4. continued

Genes differentially regulated in *serk1-3serk3-2*, BR regulated BZR1 and BES1 targets (1 gene)

AGI	Gene name
AT1G69160	

Genes differentially regulated in *serk1-3serk3-2* and BR regulated BES1 targets (4 genes)

AGI	Gene name	AGI	Gene name
AT1G79700		AT1G74670	
AT1G32900		AT3G04290	ATLTL1, LTL1

Genes differentially regulated in *serk1-3serk3-2* and BR regulated BZR1 targets (18 genes)

AGI	Gene name	AGI	Gene name
AT5G14130		AT1G51805	
AT2G41170		AT4G36810	GGPS1
AT5G01600	ATFER1, FER1	AT2G38230	ATPDX1.1, PDX1.1
AT3G22060		AT3G51600	LTP5
AT1G70210	CYCD1;1	AT2G10940	
AT5G40380		AT4G18220	
AT2G41090		AT3G14210	ESM1
AT5G63180		AT4G37800	
AT5G64770		AT1G31580	ECS1, CXC750

Genes differentially regulated in *serk1-3serk3-2* and non-BR regulated BZR1/ BES1 targets (6 genes)

AGI	Gene name	AT1G05700
AT5G06090	ATGPAT7	AT3G20820
AT1G19350	BES1, BZR2	AT5G18080
AT1G09390		

Genes differentially regulated in *serk1-3serk3-2* and non-BR regulated BZR1 targets (39 genes)

AGI	Gene name	AGI	Gene name
AT2G22510		AT4G34250	KCS16
AT5G08250		AT3G55240	
AT3G11430		AT5G19110	
AT5G49350		AT5G13170	SAG29
AT4G24140		AT5G67070	RALFL34
AT1G80180		AT1G26945	KDR
AT2G38110	ATGPAT6	AT1G76620	
AT4G03540		AT1G53440	
AT2G47200		AT3G51410	
AT5G62480	ATGSTU9, GST14, GST14B	AT2G34650	PID, ABR
AT3G55230		AT2G45080	cycp3;1
AT5G16570	GLN1;4	AT4G28080	
AT4G29905		AT1G15125	
AT1G02390	ATGPAT2	AT5G44580	
AT1G33600		AT4G32950	
AT2G28950	ATEXPA6, ATEXP6, ATHEXP	AT3G45140	LOX2, ATLOX2
AT2G42600	ALPHA 1.8	AT2G23170	GH3.3
AT2G16660	ATPPC2	AT2G20835	
AT4G23820		AT1G70260	
AT5G07190	ATS3		

Genes differentially regulated in *serk1-3serk3-2*, non-BR regulated BES1 target genes and low stringency BZR1 target genes (1 gene)

AGI	Gene name
AT1G78170	

Table S4. continued

Genes differentially regulated in <i>serk1-3serk3-2</i> and non-BR regulated BES1 targets (2 genes)			
AGI	Gene name	AGI	Gene name
AT3G21090		AT1G72645	
Genes differentially regulated in <i>serk1-3serk3-2</i> low stringency BZR1 target genes (64 genes)			
AGI	Gene name	AGI	Gene name
AT3G50400		AT2G43141	
AT5G09520		AT2G43100	
AT5G47635		AT1G14700	PAP3, ATPAP3
AT5G09530		AT4G24510	CER2
AT5G07475		AT1G66940	
AT5G09480		AT2G16230	
AT1G14550		AT3G52840	BGAL2
AT2G45970	CYP86A8, LCR	AT3G26932	DRB3
AT2G05440		AT4G16980	
AT3G60840	MAP65-4	AT4G25960	PGP2
AT4G27850		AT2G05520	GRP-3, ATGRP-3, GRP3
AT3G52790		AT3G53280	CYP71B5
AT3G51890		AT1G47395	
AT1G17180	ATGSTU25	AT4G16860	RPP4
AT1G78390	NCED9, ATNCED9	AT4G15530	PPDK
AT1G43160	RAP2.6	AT2G45740	PEX11D
AT3G07780	OBE1	AT1G56680	
AT5G67340		AT1G66970	GDPDL1
AT5G40270		AT2G37640	ATEXPA3, ATEXP3, ATHEXP ALPHA 1.9, EXP3
AT5G04220	SYTC, ATSYTC, NTMC2TYPE1.3, NTMC2T1.3	AT2G36870	
AT4G38830		AT5G03120	
AT1G26560	BGLU40	AT1G49860	ATGSTF14
AT1G18075	MIR159B, MIR159	AT4G12490	
AT1G26770	ATEXPA10, AT-EXP10, ATEXP10, ATHEXP ALPHA 1.1, EXP10	AT1G20620	CAT3, SEN2, ATCAT3
AT2G26910	PDR4, ATPDR4	AT4G38770	PRP4, ATPRP4
AT1G73885		AT3G50440	ATMES10, MES10
AT1G78370	ATGSTU20	AT5G42530	
AT4G12470		AT5G15780	
AT3G23110	AtRLP37	AT2G24270	ALDH11A3
AT4G17695	KAN3	AT5G18030	
AT1G49030		AT4G12480	pEARLI 1
AT4G13195	CLE44	AT4G23560	AtGH9B15

Table S4. continued

Genes differentially regulated in the *serk1-3serk3-2* mutant and not differentially regulated in *br1-116* or known as BES1/BZR1 target (296 genes)

AGI	Gene name	AGI	Gene name
AT2G23540		AT1G52190	
AT1G55990		AT3G61700	
AT3G06390		AT1G29785	
AT2G01520	MLP328	ATCG00990	TRNN.1
AT5G12420		ATCG01140	TRNN.2
AT5G44550		AT3G24615	
AT4G20390		ATMG00920	ORF215B
AT1G78990		AT3G54600	
AT2G35380		AT3G42628	
AT4G38080		AT5G38410	
AT4G33610		AT3G20470	GRP-5, ATGRP-5, GRP5, ATGRP5
AT1G34670	AtMYB93	AT4G35200	
AT1G74460		AT4G25010	
AT5G37690		AT5G57500	
AT5G19410		AT4G39366	
AT3G44550		AT5G58140	PHOT2, NPL1
AT1G49960		AT2G05540	
AT5G07130	LAC13	AT1G34418	
AT5G37990		AT1G33790	
AT1G68850		AT4G22880	LDOX, TDS4, TT18, ANS
AT1G56320		AT1G73602	CPuORF32
AT4G36610		AT4G34419	
AT1G53270		AT3G54050	
AT2G40370	LAC5	AT1G32780	
AT2G31540		AT1G73600	
AT5G41570	WRKY24, ATWRKY24	ATCG00580	PSBE
AT5G58860	CYP86A1, CYP86	AT2G20180	PIL5
AT5G10230	ANNAT7, ANN7	AT2G09795	
AT4G12550	AIR1	AT1G54010	
AT4G26790		AT2G41312	
AT1G03700		AT4G33870	
AT1G52580	ATRBL5	AT1G01320	
AT5G13580		AT2G07678	
AT1G49430		AT4G39364	
AT2G18370		AT1G14440	AtHB31
AT5G16770	AtMYB9	AT5G65330	AGL78
AT2G36295		AT1G24020	MLP423
AT3G18400	anac058	AT1G71830	SERK1, ATSERK1
AT5G13900		AT4G14630	GLP9
AT1G54540		AT3G21950	
AT4G24130		AT1G31900	
AT2G40250		AT1G15980	NDF1
AT2G21100		AT1G74890	ARR15
AT2G02820	MYB88	AT1G71480	
AT3G07970	QRT2	AT1G03630	POR C, PORC
AT5G05390	LAC12	AT1G64430	
AT4G35420		AT4G30650	
AT1G64000	WRKY56, ATWRKY56	AT5G57240	ORP4C
AT4G17215		AT1G31650	ATROPGEF14, ROPGEF14
AT4G28940		AT3G22121	
AT1G73290	scpl5	AT1G05835	
AT3G56730		AT5G46240	KAT1
AT1G05100	MAPKKK18	AT2G24720	ATGLR2.2, GLR2.2
AT3G04370	PDLP4	AT1G49100	
AT1G51260	LPAT3	AT1G78490	CYP708A3

Table S4. continued

Genes differentially regulated in the *serk1-3serk3-2* mutant and not differentially regulated in *bri1-116* or known as BES1/BZR1 target (296 genes)(continued)

AGI	Gene name	AGI	Gene name
AT2G48130		AT5G27360	SFP2
AT5G23190	CYP86B1	AT1G23210	AtGH9B6
AT2G24430	ANAC038	AT1G70830	MLP28
AT5G52790		AT2G14960	GH3.1
AT1G23330		AT1G33670	
AT2G33205		AT1G27921	
AT2G35980	YLS9, NHL10, ATNHL10	AT2G04039	
AT4G22090		AT1G26250	
AT3G49330		AT4G21620	
AT2G48140	EDA4	AT5G65870	ATPSK5
AT1G52342		AT1G72970	HTH, EDA17
AT3G14225	GLIP4	AT1G51870	
AT3G48940		AT5G26300	
AT3G21680		AT5G52780	
AT4G01890		AT5G08000	E13L3, PDCB2
AT2G46130	WRKY43, ATWRKY43	AT1G50732	
AT5G55590	QRT1	AT4G39361	
AT3G15450		AT1G11120	
AT2G19050		AT2G45550	CYP76C4
AT1G50590		AT3G26070	
AT4G02830		AT3G57157	
AT3G44540	FAR4	AT3G33000	
AT1G31935		ATCG00150	ATPI
AT1G28815		AT2G40802	
AT4G12545		AT3G20365	
AT1G05660		ATCG00240	TRNY
AT5G58910	LAC16	AT5G07180	ERL2
AT3G01190		AT4G36250	ALDH3F1
AT1G61130	SCPL32	AT3G10450	SCPL7
AT2G26290	ARSK1	AT2G43010	PIF4, SRL2
AT3G12720	ATY53, ATMYB67	AT5G49770	
AT1G77590	LACS9	AT5G48490	
AT5G65230	AtMYB53	AT5G39890	
AT4G29340	PRF4	AT3G46780	PTAC16
AT4G10500		AT4G28780	
AT5G58780		AT4G04890	PDF2
AT4G37700		AT4G21870	
AT3G01970	WRKY45, ATWRKY45	AT1G67105	
AT3G50970	LTI30, XERO2	AT5G23010	MAM1, IMS3
AT3G49190		AT1G45201	TLL1
AT1G67270		AT1G32080	
AT3G10912	CPuORF63	AT5G22500	FAR1
AT1G58037		AT3G46490	
AT4G08160		AT4G38825	
AT2G37070		AT1G20020	ATLFNR2, FNR2
AT1G73410	ATMYB54, MYB54	AT3G19710	BCAT4
AT4G15290	ATCSLB05, CSLB05, ATCSLB5	AT3G58990	
AT5G40590		AT5G22555	
AT3G07600		AT1G73780	
AT3G47220	ATPLC9, PLC9	AT3G02020	AK3
AT2G39530		AT4G21750	ATML1
AT4G26580		AT2G26330	ER, QRP1
AT1G53680	ATGSTU28	AT1G73610	
AT5G51680		AT1G44575	NPQ4, PSBS
AT5G17650		AT4G08780	

Table S4. continued

Genes differentially regulated in the *serk1-3serk3-2* mutant and not differentially regulated in *bri1-116* or known as BES1/BZR1 target (296 genes)(continued)

AGI	Gene name	AGI	Gene name
AT5G18220		AT2G24710	ATGLR2.3, GLR2.3
AT3G06962		AT2G07600	
AT4G09040		AT2G13360	AGT, AGT1
AT1G44446	CH1, ATCAO, CAO	AT4G23713	MIR319A, MIR319
AT5G48300	ADG1, APS1	AT1G32060	PRK
AT4G22270		AT3G18890	
AT2G43137		AT4G39330	ATCAD9, CAD9
AT5G04360	ATPU1, ATLDA, PU1	AT1G35290	
AT2G07813		AT1G26240	
ATMG01260	ORF205	AT3G51340	
AT4G12030		AT4G13770	CYP83A1, REF2
AT1G49405		AT3G48200	
AT4G16950	RPP5	AT5G38420	
AT5G46450		AT2G16630	
AT5G47440		AT2G32690	ATGRP23, GRP23
AT3G01730		AT5G19700	
AT3G59780		AT4G21250	
AT2G07764		AT2G43510	ATTI1
ATMG00380	TRNN	AT1G51500	CER5, D3, ABCG12, WBC12, ATWBC12
AT1G49380		AT1G63570	
AT2G21610	PE11, ATPE11	AT1G56430	ATNAS4, NAS4
AT5G39530		AT5G36910	THI2.2
AT1G16400	CYP79F2	AT5G43370	APT1, PHT2, PHT1;2
AT2G29630	THIC	AT1G71840	
ATCG00970	RRN5S	AT5G67385	
ATCG01160	RRN5S	AT2G15050	LTP7
AT5G51451		AT1G08090	ATNRT2
AT1G34200		AT1G17200	
AT3G27940	LBD26	AT5G65980	
AT1G22150	SULTR1;3	AT1G30560	
AT2G03260		AT4G04223	
AT3G16250	NDF4	AT3G16660	
AT1G73110		AT5G38430	
AT1G32385		AT5G42800	DFR, TT3, M318
AT3G63540		AT3G44970	
AT5G49780		AT2G05380	GRP3S
AT3G27906		AT3G21720	ICL
AT5G45469		AT2G38530	LTP2

Table S5. Over representation analysis of genes differentially regulate in the *serk1-3serk3-2* double mutant**There are four groups defined for genes differentially regulated in the *serk1-3serk3-2* double mutant****Group 1** BR regulated BZR1/BES1 targets and differentially regulated in the *bri1-116* mutant**Group 2** non-BR related BES1/BSR1 targets**Group 3** low stringency BZR1 targets**Group 4** not differentially regulated in the *bri1-116* mutant or BZR1/BES1 target* Metabolic related genes marked with an asterisk (*) in the remarks column are photosynthesis related and differentially regulated in the *bri1-116* mutant

IDENTIFIER	Common name	<i>serk1-3</i>	<i>serk3-2</i>	<i>serk1-3serk3-2</i>	Group	Remarks
		FC	FC	FC		
glycerolipid metabolism / glycerophospholipid metabolism						
AT5G06090	GPAT7	-1.5	-2.0	-6.4	2	Suberin biosynthesis
AT3G11430	GPAT5	-1.1	-1.4	-3.0	2	
AT1G51260	LPAT3	-1.4	-1.7	-2.8	4	
AT2G38110	GPAT6	1.3	-1.4	-2.6	2	Cutin biosynthesis
AT1G01610	GPAT4	-1.2	-1.6	-2.6	1	Cutin biosynthesis
phenylalanine metabolism						
AT5G14130	AT5G14130	-1.1	-1.3	-4.8	1	down-regulated in the <i>bri1-116</i> mutant
AT1G68850	AT1G68850	-1.2	-2.0	-4.5	4	
AT1G14550	AT1G14550	1.2	-1.4	-3.7	3	
AT2G18150	AT2G18150	1.1	-1.9	-3.1	1	
AT4G36430	AT4G36430	-1.4	-3.7	-2.7	1	
AT3G01190	AT3G01190	1.1	-1.0	-2.3	4	down-regulated in the <i>bri1-116</i> mutant
biosynthesis of secondary metabolites						
AT5G14130	AT5G14130	-1.1	-1.3	-4.8	1	down-regulated in the <i>bri1-116</i> mutant
AT1G68850	AT1G68850	-1.2	-2.0	-4.5	4	
AT5G58860	CYP86A1	1.1	-2.3	-4.0	4	
AT1G14550	AT1G14550	1.2	-1.4	-3.7	3	
AT2G18150	AT2G18150	1.1	-1.9	-3.1	1	
AT1G01600	CYP86A4	-1.1	-2.7	-3.1	1	down-regulated in the <i>bri1-116</i> mutant
AT1G18870	ICS2	-1.5	-1.7	-2.9	1	down-regulated in the <i>bri1-116</i> mutant
AT5G23190	CYP86B1	-1.3	-1.4	-2.8	4	
AT4G36430	AT4G36430	-1.4	-3.7	-2.7	1	
AT5G65800	ACS5	-1.3	-1.6	-2.6	1	
AT3G01190	AT3G01190	1.1	-1.0	-2.3	4	
AT5G63590	FLS3	-1.1	-1.3	-2.2	1	down-regulated in the <i>bri1-116</i> mutant
AT1G78390	NCED9	-1.1	-1.2	-2.1	3	down-regulated in the <i>bri1-116</i> mutant
AT5G58780	AT5G58780	-1.4	-2.6	-2.1	4	
AT5G42250	AT5G42250	1.2	1.3	-2.1	1	
phenylpropanoid biosynthesis						
AT5G14130	AT5G14130	-1.1	-1.3	-4.8	1	down-regulated in the <i>bri1-116</i> mutant
AT1G68850	AT1G68850	-1.2	-2.0	-4.5	4	
AT1G14550	AT1G14550	1.2	-1.4	-3.7	3	
AT2G18150	AT2G18150	1.1	-1.9	-3.1	1	
AT4G36430	AT4G36430	-1.4	-3.7	-2.7	1	
AT3G01190	AT3G01190	1.1	-1.0	-2.3	4	down-regulated in the <i>bri1-116</i> mutant
fatty acid metabolism						
AT1G49430	LACS2	1.0	-3.0	-3.6	4	Cutin biosynthesis
AT1G77590	LACS9	-1.1	-1.4	-2.2	4	down-regulated in the <i>bri1-116</i> mutant
AT5G42250	AT5G42250	1.2	1.3	-2.1	1	

Table S5. continued

IDENTIFIER	Common name	<i>serk1-3</i> FC	<i>serk3-2</i> FC	<i>serk1-3serk3-2</i> FC	Group	Remarks
metabolic pathways						
AT5G06090	GPAT7	-1.5	-2.0	-6.4	2	
AT5G14130	AT5G14130	-1.1	-1.3	-4.8	1	
AT1G68850	AT1G68850	-1.2	-2.0	-4.5	4	
AT1G14550	AT1G14550	1.2	-1.4	-3.7	3	
AT1G49430	LACS2	1.0	-3.0	-3.6	4	
AT2G18150	AT2G18150	1.1	-1.9	-3.1	1	down-regulated in the <i>br1-116</i> mutant
AT3G11430	GPAT5	-1.1	-1.4	-3.0	2	
AT1G18870	ICS2	-1.5	-1.7	-2.9	1	
AT1G51260	LPAT3	-1.4	-1.7	-2.8	4	
AT4G36430	AT4G36430	-1.4	-3.7	-2.7	1	down-regulated in the <i>br1-116</i> mutant
AT2G38110	GPAT6	1.3	-1.4	-2.6	2	
AT1G01610	GPAT4	-1.2	-1.6	-2.6	1	
AT3G01190	AT3G01190	1.1	-1.0	-2.3	4	
AT5G16570	GLN1;4	-1.1	-1.2	-2.2	2	
AT1G77590	LACS9	-1.1	-1.4	-2.2	4	
AT5G63590	FLS3	-1.1	-1.3	-2.2	1	down-regulated in the <i>br1-116</i> mutant
AT1G78390	NCED9	-1.1	-1.2	-2.1	3	
AT5G42250	AT5G42250	1.2	1.3	-2.1	1	down-regulated in the <i>br1-116</i> mutant
stilbenoid, diarylheptanoid and gingerol biosynthesis / limonene and pinene degradation						
AT5G58860	CYP86A1	1.1	-2.3	-4.0	4	Suberin biosynthesis
AT1G01600	CYP86A4	-1.1	-2.7	-3.1	1	down-regulated in the <i>br1-116</i> mutant
AT5G23190	CYP86B1	-1.3	-1.4	-2.8	4	Suberin biosynthesis
photosynthesis						
AT4G32260	AT4G32260	1.0	1.6	2.1	1	up-regulated in the <i>br1-116</i> mutant
AT1G79040	PSBR	-1.2	1.5	2.1	1	up-regulated in the <i>br1-116</i> mutant
AT1G76100	PETE1	-1.1	1.5	2.2	1	up-regulated in the <i>br1-116</i> mutant
AT4G09650	ATPD	1.1	1.5	2.3	1	up-regulated in the <i>br1-116</i> mutant
AT1G31330	PSAF	1.1	2.3	2.6	1	up-regulated in the <i>br1-116</i> mutant
AT1G06680	PSBP-1	-1.3	1.9	2.7	1	
AT5G66190	FNR1	-1.3	1.5	2.7	1	up-regulated in the <i>br1-116</i> mutant
AT2G20260	PSAE-2	1.0	1.5	2.8	1	up-regulated in the <i>br1-116</i> mutant
AT5G64040	PSAN	-1.4	1.7	2.9	1	up-regulated in the <i>br1-116</i> mutant
AT5G66570	PSBO1	-1.1	2.2	3.0	1	up-regulated in the <i>br1-116</i> mutant
AT4G04640	ATPC1	1.1	1.6	3.2	1	up-regulated in the <i>br1-116</i> mutant
AT3G50820	PSBO2	1.0	2.1	3.3	1	up-regulated in the <i>br1-116</i> mutant
AT4G03280	PETC	-1.1	1.6	3.3	1	up-regulated in the <i>br1-116</i> mutant
AT1G20020	FNR2	-1.1	1.4	3.6	4	
AT1G03600	AT1G03600	-1.0	2.5	3.6	1	up-regulated in the <i>br1-116</i> mutant
AT1G20340	DRT112	-1.2	2.3	3.7	1	up-regulated in the <i>br1-116</i> mutant
AT3G16140	PSAH-1	-1.1	3.6	3.8	1	up-regulated in the <i>br1-116</i> mutant
AT1G44575	NPQ4	-1.2	1.6	3.9	4	
AT1G67740	PSBY	-1.1	1.6	4.0	1	up-regulated in the <i>br1-116</i> mutant
AT4G12800	PSAL	-1.1	3.1	4.0	1	up-regulated in the <i>br1-116</i> mutant
AT2G30570	PSBW	-1.2	2.7	4.2	1	up-regulated in the <i>br1-116</i> mutant
AT1G55670	PSAG	-1.3	2.6	4.2	1	up-regulated in the <i>br1-116</i> mutant
AT3G55330	PPL1	-1.1	1.5	4.9	1	up-regulated in the <i>br1-116</i> mutant
AT4G28750	PSAE-1	-1.2	2.8	4.9	1	up-regulated in the <i>br1-116</i> mutant
AT4G05180	PSBQ-2	1.0	3.1	5.0	1	up-regulated in the <i>br1-116</i> mutant
AT1G52230	PSAH2	-1.0	3.1	5.3	1	up-regulated in the <i>br1-116</i> mutant

Table S5. continued

IDENTIFIER	Common name	<i>serk1-3</i> FC	<i>serk3-2</i> FC	<i>serk1-3serk3-2</i> FC	Group	Remarks
photosynthesis – antenna proteins						
AT1G19150	LHCA6	-1.0	1.1	2.2	1	up-regulated in the <i>br1-116</i> mutant
AT3G47470	LHCA4	-1.2	2.2	2.4	1	up-regulated in the <i>br1-116</i> mutant
AT1G61520	LHCA3	-1.0	1.8	2.4	1	up-regulated in the <i>br1-116</i> mutant
AT3G08940	LHCB4.2	-1.1	1.6	2.7	1	up-regulated in the <i>br1-116</i> mutant
AT2G05100	LHCB2.1	-1.1	1.5	2.8	1	up-regulated in the <i>br1-116</i> mutant
AT2G34420	LHB1B2	-1.0	2.0	3.0	1	up-regulated in the <i>br1-116</i> mutant
AT1G15820	LHCB6	-1.1	1.9	3.1	1	up-regulated in the <i>br1-116</i> mutant
AT5G54270	LHCB3	-1.4	3.8	3.9	1	up-regulated in the <i>br1-116</i> mutant
AT4G10340	LHCB5	-1.4	3.8	4.0	1	up-regulated in the <i>br1-116</i> mutant
AT2G05070	LHCB2.2	-1.1	3.4	4.5	1	up-regulated in the <i>br1-116</i> mutant
AT5G01530	AT5G01530	-1.1	2.1	4.8	1	up-regulated in the <i>br1-116</i> mutant
AT3G61470	LHCA2	1.1	2.9	5.6	1	up-regulated in the <i>br1-116</i> mutant
AT1G29930	CAB1	-1.2	3.0	5.9	1	up-regulated in the <i>br1-116</i> mutant
AT2G34430	LHB1B1	1.0	2.8	6.2	1	up-regulated in the <i>br1-116</i> mutant
carbon fixation in photosynthetic organisms						
AT1G23310	GGT1	1.1	1.7	2.1	1	up-regulated in the <i>br1-116</i> mutant
AT2G42600	ATPPC2	-1.1	1.2	2.2	2	
AT5G38410	AT5G38410	-1.0	1.3	2.2	4	
AT3G54050	AT3G54050	1.1	1.3	2.3	4	
AT3G12780	PGK1	-1.2	1.2	2.5	1	up-regulated in the <i>br1-116</i> mutant
AT4G15530	PPDK	-1.1	1.1	2.9	3	
AT2G21330	AT2G21330	-1.3	1.5	2.9	1	up-regulated in the <i>br1-116</i> mutant
AT1G12900	GAPA-2	-1.2	1.5	3.4	1	up-regulated in the <i>br1-116</i> mutant
AT5G09660	PMDH2	-1.2	2.1	3.7	1	
AT4G38970	AT4G38970	-1.6	3.6	4.1	1	up-regulated in the <i>br1-116</i> mutant
AT1G32060	PRK	1.0	2.5	4.1	4	
AT5G38420	AT5G38420	-1.1	2.1	4.6	4	
AT3G55800	SBPASE	-1.1	2.5	4.8	1	
AT3G26650	GAPA	1.0	1.8	5.0	1	up-regulated in the <i>br1-116</i> mutant
AT1G42970	GAPB	-1.3	3.2	5.2	1	up-regulated in the <i>br1-116</i> mutant
AT5G38430	AT5G38430	-1.0	2.1	9.3	4	
metabolic pathways						
AT1G02390	GPAT2	-1.2	1.0	2.0	2	
AT3G51820	G4	-1.0	1.3	2.0	1	up-regulated in the <i>br1-116</i> mutant
AT1G44446	CH1	1.0	1.2	2.0	4	
AT5G48300	ADG1	-1.0	-1.0	2.0	4	
AT1G60550	ECHID	-1.2	-1.0	2.1	1	up-regulated in the <i>br1-116</i> mutant
AT2G29630	THIC	1.1	1.2	2.1	4	
AT4G32260	AT4G32260	1.0	1.6	2.1	1	up-regulated in the <i>br1-116</i> mutant*
AT1G79040	PSBR	-1.2	1.5	2.1	1	up-regulated in the <i>br1-116</i> mutant*
AT1G23310	GGT1	1.1	1.7	2.1	1	up-regulated in the <i>br1-116</i> mutant
AT2G42600	ATPPC2	-1.1	1.2	2.2	2	
AT1G74470	AT1G74470	-1.0	1.5	2.2	1	up-regulated in the <i>br1-116</i> mutant
AT5G38410	AT5G38410	-1.0	1.3	2.2	4	
AT4G22880	LDOX	1.0	-1.1	2.3	4	
AT4G09650	ATPD	1.1	1.5	2.3	1	up-regulated in the <i>br1-116</i> mutant*
AT3G54050	AT3G54050	1.1	1.3	2.3	4	
AT1G32780	AT1G32780	1.1	1.2	2.3	4	
AT4G36810	GGPS1	-1.1	1.3	2.4	1	
AT5G04230	PAL3	-1.0	-1.1	2.4	1	up-regulated in the <i>br1-116</i> mutant
AT5G13630	GUN5	-1.0	1.7	2.4	1	up-regulated in the <i>br1-116</i> mutant
AT4G18480	CHL1	1.1	1.6	2.4	1	up-regulated in the <i>br1-116</i> mutant
AT1G60600	ABC4	-1.1	1.1	2.4	1	up-regulated in the <i>br1-116</i> mutant
AT2G32440	KAO2	1.2	1.6	2.5	1	up-regulated in the <i>br1-116</i> mutant

Table S5. continued

IDENTIFIER	Common name	<i>serk1-3</i> FC	<i>serk3-2</i> FC	<i>serk1-3serk3-2</i> FC	Group	Remarks
metabolic pathways (continued)						
AT1G03630	PORC	-1.0	1.1	2.5	4	
AT3G12780	PGK1	-1.2	1.2	2.5	1	up-regulated in the <i>br1-116</i> mutant
AT4G25420	GA20OX1	-1.1	-1.0	2.5	1	down-regulated in the <i>br1-116</i> mutant
AT3G52840	BGAL2	-1.2	1.9	2.5	3	
AT1G31330	PSAF	1.1	2.3	2.6	1	up-regulated in the <i>br1-116</i> mutant*
AT1G06680	PSBP-1	-1.3	1.9	2.7	1	
AT3G08940	LHCB4.2	-1.1	1.6	2.7	1	up-regulated in the <i>br1-116</i> mutant*
AT5G66190	FNR1	-1.3	1.5	2.7	1	up-regulated in the <i>br1-116</i> mutant*
AT2G20260	PSAE-2	1.0	1.5	2.8	1	up-regulated in the <i>br1-116</i> mutant*
AT2G05100	LHCB2.1	-1.1	1.5	2.8	1	up-regulated in the <i>br1-116</i> mutant*
AT4G15530	PPDK	-1.1	1.1	2.9	3	
AT2G21330	AT2G21330	-1.3	1.5	2.9	1	up-regulated in the <i>br1-116</i> mutant
AT5G64040	PSAN	-1.4	1.7	2.9	1	up-regulated in the <i>br1-116</i> mutant*
AT5G66570	PSBO1	-1.1	2.2	3.0	1	up-regulated in the <i>br1-116</i> mutant*
AT2G34420	LHB1B2	-1.0	2.0	3.0	1	up-regulated in the <i>br1-116</i> mutant*
AT1G15820	LHCB6	-1.1	1.9	3.1	1	up-regulated in the <i>br1-116</i> mutant*
AT4G04640	ATPC1	1.1	1.6	3.2	1	up-regulated in the <i>br1-116</i> mutant*
AT3G50820	PSBO2	1.0	2.1	3.3	1	up-regulated in the <i>br1-116</i> mutant*
AT4G03280	PETC	-1.1	1.6	3.3	1	up-regulated in the <i>br1-116</i> mutant*
AT3G14415	AT3G14415	1.2	2.6	3.4	1	
AT1G12900	GAPA-2	-1.2	1.5	3.4	1	up-regulated in the <i>br1-116</i> mutant
AT5G23010	MAM1	-1.1	1.1	3.5	4	
AT4G27440	PORB	1.1	1.3	3.6	1	photosynthesis related
AT1G20020	FNR2	-1.1	1.4	3.6	4	up-regulated in the <i>br1-116</i> mutant*
AT3G19710	BCAT4	-1.3	1.2	3.6	4	
AT1G03600	AT1G03600	-1.0	2.5	3.6	1	up-regulated in the <i>br1-116</i> mutant*
AT5G09660	PMDH2	-1.2	2.1	3.7	1	
AT3G16140	PSAH-1	-1.1	3.6	3.8	1	up-regulated in the <i>br1-116</i> mutant*
AT3G02020	AK3	-1.4	-1.3	3.8	4	
AT1G44575	NPQ4	-1.2	1.6	3.9	4	
AT4G08780	AT4G08780	-1.2	-1.2	3.9	4	
AT5G54270	LHCB3	-1.4	3.8	3.9	1	up-regulated in the <i>br1-116</i> mutant*
AT1G67740	PSBY	-1.1	1.6	4.0	1	up-regulated in the <i>br1-116</i> mutant*
AT4G10340	LHCB5	-1.4	3.8	4.0	1	up-regulated in the <i>br1-116</i> mutant*
AT2G13360	AGT	-1.2	2.3	4.0	4	
AT4G12800	PSAL	-1.1	3.1	4.0	1	up-regulated in the <i>br1-116</i> mutant*
AT4G38970	AT4G38970	-1.6	3.6	4.1	1	up-regulated in the <i>br1-116</i> mutant
AT1G32060	PRK	1.0	2.5	4.1	4	
AT3G56940	CRD1	-1.1	3.1	4.1	1	up-regulated in the <i>br1-116</i> mutant
AT2G30570	PSBW	-1.2	2.7	4.2	1	up-regulated in the <i>br1-116</i> mutant*
AT1G55670	PSAG	-1.3	2.6	4.2	1	up-regulated in the <i>br1-116</i> mutant*
AT2G05070	LHCB2.2	-1.1	3.4	4.5	1	up-regulated in the <i>br1-116</i> mutant*
AT5G38420	AT5G38420	-1.1	2.1	4.6	4	
AT1G20620	CAT3	-1.1	1.2	4.8	3	
AT5G01530	AT5G01530	-1.1	2.1	4.8	1	up-regulated in the <i>br1-116</i> mutant*
AT3G55800	SBPASE	-1.1	2.5	4.8	1	
AT3G55330	PPL1	-1.1	1.5	4.9	1	up-regulated in the <i>br1-116</i> mutant*
AT4G28750	PSAE-1	-1.2	2.8	4.9	1	up-regulated in the <i>br1-116</i> mutant*
AT3G26650	GAPA	1.0	1.8	5.0	1	up-regulated in the <i>br1-116</i> mutant
AT4G05180	PSBQ-2	1.0	3.1	5.0	1	up-regulated in the <i>br1-116</i> mutant*
AT1G42970	GAPB	-1.3	3.2	5.2	1	up-regulated in the <i>br1-116</i> mutant
AT1G52230	PSAH2	-1.0	3.1	5.3	1	up-regulated in the <i>br1-116</i> mutant*
AT1G29930	CAB1	-1.2	3.0	5.9	1	up-regulated in the <i>br1-116</i> mutant*
AT2G34430	LHB1B1	1.0	2.8	6.2	1	up-regulated in the <i>br1-116</i> mutant*
AT3G45140	LOX2	-1.0	1.2	6.2	2	
AT5G38430	AT5G38430	-1.0	2.1	9.3	4	
AT3G21720	ICL	1.5	1.5	13.5	4	

Table S5. continued

IDENTIFIER	Common name	<i>serk1-3</i> FC	<i>serk3-2</i> FC	<i>serk1-3serk3-2</i> FC	Group	Remarks
porphyrin and chlorophyll metabolism						
AT3G51820	G4	-1.0	1.3	2.0	1	up-regulated in the <i>bri1-116</i> mutant
AT1G44446	CH1	1.0	1.2	2.0	4	
AT1G74470	AT1G74470	-1.0	1.5	2.2	1	up-regulated in the <i>bri1-116</i> mutant
AT5G13630	GUN5	-1.0	1.7	2.4	1	up-regulated in the <i>bri1-116</i> mutant
AT4G18480	CHL1	1.1	1.6	2.4	1	up-regulated in the <i>bri1-116</i> mutant
AT1G03630	PORC	-1.0	1.1	2.5	4	
AT4G27440	PORB	1.1	1.3	3.6	1	
AT3G56940	CRD1	-1.1	3.1	4.1	1	up-regulated in the <i>bri1-116</i> mutant
glyoxylate and dicarboxy-late metabolism						
AT5G38410	AT5G38410	-1.0	1.3	2.2	4	
AT3G14415	AT3G14415	1.2	2.6	3.4	1	
AT5G09660	PMDH2	-1.2	2.1	3.7	1	
AT5G38420	AT5G38420	-1.1	2.1	4.6	4	
AT5G38430	AT5G38430	-1.0	2.1	9.3	4	
AT3G21720	ICL	1.5	1.5	13.5	4	
glucosinolate biosynthesis						
AT1G16400	CYP79F2	-1.3	-1.2	2.1	4	
AT5G23010	MAM1	-1.1	1.1	3.5	4	
AT3G19710	BCAT4	-1.3	1.2	3.6	4	
AT4G13770	CYP83A1	-1.2	1.5	4.4	4	

Table S6. Genes differentially regulated in the *bri1-301* mutant

AGI	Other name (s)	cellular functions/ functions in*		FC**	FC**
				Array	Array
				1	2
AT1G09000	ANP1, MAPKKK1	Protein modification	Post-translational modification	2.2	1.8
AT5G01600	ATFER1, FER1	metal handling	binding, chelation and storage	-2.3	1.1
AT1G60960	IRT3	transport	metal	9.4	1.9
AT3G01345		not assigned	unknown	103.9	39.4

AGI = Arabidopsis Genome Initiative gene identification number.

Other name(s) = abbreviated common names for genes

FC = fold change compared to the wild type gene expression

*Cellular functions are derived using MAPMAN

**FDR 1 %, 1.5 fold change.

Table S7. Cutin and suberin biosynthesis genes differentially regulated in *serk1-3*, *serk3-2* and *bri1-116* mutants

AGI	Common name	<i>serk1-3</i>		<i>serk3-2</i>		<i>serk1-3serk3-2</i>		<i>bri1-116</i> *	
		FC	FDR	FC	FDR	FC	FDR	<i>bri1-116</i> /Col-0 ratio	Geo2R FC
Cutin biosynthesis									
At4g00360	ATT1, CYP86A2	-1.0	0.9	-2.2	0.1	-1.3	0.4	0.15	-2.44
At2g45970	CYP86A8, LCR	-1.1	0.8	-1.4	0.3	-3.0	0.0		
At1g01600	CYP86A4	-1.1	0.9	-2.7	0.1	-3.1	0.0	0.13	-2.12
At3g10570	CYP77A6	-1.1	0.8	-1.2	0.3	1.0	0.6		
At2g47240	CER8, LACS1,								
	CER8, LACS1	1.2	0.7	1.2	0.4	-1.2	0.3		
At1g49430	LACS2, LRD2	1.0	0.9	-3.0	0.0	-3.6	0.0		
At1g01610	ATGPAT4, GPAT4	-1.2	0.8	-1.6	0.2	-2.6	0.0	0.64	-0.57
At2g38110	ATGPAT6, GPAT6	1.3	0.8	-1.4	0.5	-2.6	0.0		
At4g00400	AtGPAT8, GPAT8	-1.1	0.8	-1.4	0.2	1.6	0.1	0.22	-1.27
At3g48720	DCF	-1.2	0.5	-1.1	0.4	1.1	0.4		
At5g23940	DCR, EMB3009,								
	PEL3	1.1	0.9	-1.0	0.7	-1.3	0.2	2.54	1.30
At1g72970	EDA17, HTH	-1.3	0.7	-1.1	0.6	2.9	0.0		
At1g64670	BDG1, CED1	1.1	0.8	1.2	0.4	3.9	0.0	0.36	-1.37
	ABCG11,								
	ATWBC11,								
AT1G17840	AtABCG11, COF1,								
	DSO, WBC11	-1.0	0.9	1.5	0.3	9.4	0.0	0.53	-0.91
At1g51460	ABCG13	1.1	0.9	-1.1	0.5	-1.0	0.6		
	ABCG32, ATPDR4,								
	PDR4, PEC1	-1.2	0.8	1.0	0.8	2.2	0.0		
At1g15360	SHN1, WIN1	-1.0	0.9	-1.0	0.8	-1.2	0.2		
At5g11190	SHN2	-1.0	0.9	1.1	0.6	-1.2	0.4		
At5g25390	SHN3	1.1	0.8	1.0	0.8	-1.2	0.3		
At2g33510	NA	-1.0	0.9	1.0	0.7	-1.1	0.5		
Suberin biosynthesis									
AT5G58860	CYP86, CYP86A1	1.1	0.9	-2.3	0.1	-4.0	0.0		
AT5G23190	CYP86B1	-1.3	0.7	-1.4	0.3	-2.8	0.0		
AT1G04220	KCS2	-1.1	0.9	-1.5	0.1	-3.3	0.0	0.29	-2.05
AT5G43760	KCS20	-1.1	0.9	-1.2	0.4	-1.8	0.0	0.27	-1.71
AT3G11430	ATGPAT5, GPAT5	-1.1	0.9	-1.4	0.4	-3.0	0.0		
AT5G41040	NA	-1.0	0.9	-1.2	0.4	-1.9	0.0	0.52	-0.77
AT5G22500	FAR1	1.3	0.8	1.4	0.5	3.5	0.0		
AT3G44540	FAR4, FAR4	1.2	0.8	-1.4	0.4	-2.3	0.0		
AT3G44550	FAR5	1.1	0.9	-1.7	0.2	-4.8	0.0		
AT2G28670	ESB1	-1.2	0.6	-1.2	0.3	-1.7	0.0	0.44	-0.85
	ABCG11,								
	ATWBC11,								
	AtABCG11, COF1,								
AT1G17840	DSO, WBC11	-1.0	0.9	1.5	0.3	9.4	0.0	0.53	-0.91

**bri1-116*/Col-o ratio derived from Sun et al. (2010) FC valued downloaded from the GEO2R data base

Chapter 7

General discussion



Parts of this discussion have been published as:

Computational modelling of the BRI1-receptor system

G. Wilma van Esse, Klaus Harter and Sacco C. de Vries

Plant, Cell and Environment (2013)

Cells respond to the external environment via a limited set of signalling pathways using plasma membrane (PM) localised receptors as antennas for ligand perception and signal transduction. In general, the response of a cell to an external stimulus depends on the ligand as well as the receptor availability. The resulting signal transduction cascade is often complicated, including various proteins and activated targets. Some ligand perceiving receptors are capable of regulating different biological processes, depending on the ligand and its concentration (Krall et al., 2011). Moreover, distinct activation profiles of the same set of signalling proteins can result in activation of different target genes while the specificity of the signal transduction can be determined by the spatial and temporal dynamics of downstream targets of the main ligand perceiving receptor (Kholodenko, 2006). Different approaches can be employed in modelling, depending on the purpose of the model. For example, the use of Boolean logics that are based on the principle of bivalence i.e. any statement is either true or false. In case of network models each component is represented by a node. Different nodes are connected through a direct relationship attributed by a binary value of 1 (activating) or 0 (inhibitory). This approach gives a qualitative view on the network and does not allow intermediate situations. Hence, no information about the quantitative contribution of different nodes or detailed spatial and temporal dynamics is obtained. Another is to use phenomenological considerations combined with temporal dynamics described using chemical kinetics (also referred to as Ordinary Differential Equations; ODEs). The computation of pathway intermediates is of interest as the output of the signal transduction cascade is dependent on the amount and sub-cellular localization of proteins activated rather than an on/ off state.

To illustrate the importance of a combination of modelling and experimental approaches, we first present an example of animal signalling. In Epidermal Growth Factor Receptor (EGFR) mediated signalling, computational modelling was employed to elucidate the crosstalk between EGF and insulin pathways. EGFR and insulin receptor (IR) activate the Extracellular signal-Regulated Kinase (ERK) and phosphatidylinositol 3-kinase (PI3K/ AKT) pathways through different signalling cascades. At low EGF level insulin amplifies ERK activation thereby affecting mitogenic signalling. The crosstalk nodes of EGFR and IR signalling cascades were studied using a model that comprises all pathway components including the positive and negative feedback loops. The temporal dynamics were described using ODEs. The model uses dynamic data such as EGFR or insulin induced Ras-GTP, ERK, AKT and Grb2-associated binder 1 (GAB1) phosphorylation status as training (or calibration) data for model validation and *in silico* prediction of the unknown parameters. From this it was predicted, and subsequently verified experimentally that the crosstalk between EGF and insulin signalling is regulated at the level of protein adaptors such as GAB1, insulin receptor substrate (IRS) and

the small membrane anchored GTPase, Ras (Borisov et al., 2009). Other EGFR modelling studies addressed receptor (hetero)-oligomerisation and activation (Klein et al., 2004), non-linear signal amplification (Schoeberl et al., 2002) and endosomal or PM localization of the EGFR (Resat et al., 2003). Therefore, it is of interest to see whether such a combined approach of modelling and experiments when applied to plant signalling would also result in the prediction of key components of receptor trafficking or crosstalk.

In plants, the use of mathematical models has steadily increased over the past few years. For example, modelling studies have been used to address plant architecture in terms of auxin signalling and transport (Grieneisen et al., 2007; Laskowski et al., 2008; Vernoux et al., 2011), crosstalk (Ibañes et al., 2009; Liu et al., 2010; Sankar et al., 2011) and vascular trafficking (Kato et al., 2010). However, mechanistic models of signal transduction cascades using actual protein concentration and activity of the different components are to date rarely used in plant systems biology. The construction of mechanistic and kinetic models is not only essential to address protein dynamics but can also provide insight into how signalling is regulated by a few core regulators while some of their interacting proteins are shared between different signalling cascades. Biochemical kinetics is based on mass action laws, hence the affinity between the different components in a pathway as well as their concentration is important for the reaction rate and thus the signalling output. To this end, quantification of the pathway components and their effect on the output of the signalling cascade is necessary. Often, accurate data sets for model calibration and validation are unavailable, and can be extremely challenging to obtain (Kholodenko, 2006). The relationship between different signalling components and the control of gene expression can be studied by techniques such as microarray analysis and deep sequencing (Ruffel et al., 2010). The control of signalling at the protein level can be evaluated by the use of protein arrays (Popescu et al., 2007; Popescu et al., 2007) and LC-MS/MS based methodologies (Petricka et al., 2012). These approaches enable protein detection and quantification in specific cell types but do not provide the cellular resolution that is obtained by fluorescence based microscopy methods (Verveer and Bastiaens, 2008; Harter et al., 2012).

After identification and quantification of various components in a signal transduction cascade a kinetic model that gives insight into the protein activities and signalling output can be constructed. After that, the challenge is to couple the output of the kinetic model to physiological readouts such as plant growth and developmental processes as cell division, elongation and organ architecture but also to immunity and stress responses. This thesis described SERK mediated BRI1 signalling using such a mathematical model approach. For this, the modulatory effect of SERK co-receptors on BR signalling was incorporated in a mathematical

model that describes root growth and hypocotyl elongation based on BRI1 receptor activity. In this chapter the results obtained by this more quantitative analysis of BR signalling will be discussed.

***In vivo* quantification of proteins using fluorescence microscopy**

To obtain more knowledge about the quantitative contribution of protein in a signal transduction cascade a good insight in to the amount and sub-cellular localization is essential. Microscopy techniques such as Fluorescence Correlation Spectroscopy (FCS), Fluorescence Recovery After Photobleaching (FRAP) and Fluorescence Lifetime Imaging Microscopy (FLIM) to detect Förster Resonance Energy Transfer (FRET) are suitable for quantitative studies of protein dynamics and interactions *in vivo* (Ries et al., 2009; van Royen et al., 2009; Bucherl et al., 2010).

Confocal imaging provides a high cellular resolution, which enables detection of fluorescently tagged proteins in the plant membrane, nucleolus and cytosol (Mathur, 2007; Berg and Beachy, 2008). When applying imaging for quantitation purposes, a number of problems associated with the technique need to be considered. Auto fluorescence of the cell wall and chloroplast, the properties of the fluorophore such as the extinction coefficient, quantum yield, photo bleaching rate, applied level of laser power and pH sensitivity of the fluorophore can influence the outcome of the experiments (reviewed in North, 2006). Quantification of proteins using confocal microscopy is used in animal systems (Sugiyama et al., 2005) and more recently also *in planta* (Van Esse et al., 2011). In principle, the method can be applied on any confocal microscope taking into account the linearity, gain and offset of the detector. It was found to be essential to establish calibration curves using a standard solution of GFP. The laser intensity might fluctuate during the day or between days, and require that the calibration curves are taken along with each measurement. To obtain spatial resolution, one can record z-stack images using Nyquist sampling. However, this approach results in severe loss of fluorescence intensity due to photo bleaching rendering it largely unsuitable for quantification purposes. An alternative approach was applied by Van Esse et al. (2011). In that work, two-dimensional confocal images of BRI1-GFP in roots were obtained in a single scan to minimise photo bleaching. Next, a number of calculation steps (Fig. 1) were made to obtain a parameter described as the BRI1 receptor density (i.e. number of BRI1-GFP molecules per μm^2 of PM) from which the number of BRI1 receptors per cell could be derived using an averaged cell dimension model. The fluorescence intensity at the PM was then compared with the fluorescence intensity of the calibration curve to obtain the concentration of BRI1. Since this value is derived from a two-dimensional image, it is referred to as the apparent concentration (C_{app}). Next, the volume of 1 μm^2 of PM (referred to as apparent

volume; V_{app}) was calculated by multiplying the surface area of the region of interest (ROI) by the slice thickness (z). The resolution of the confocal microscope does not allow visualization of one single PM. Therefore, for PM-located proteins, the calculation needs to take into account that, except for the externally facing membrane of epidermal cells, the imaged area around the PM contains two adjacent membranes and vesicles in close proximity of the PM. All calculations were done assuming an equal distribution of BRI1 between the two PM. Using the BRI1 receptor density at the PM and in the cytoplasm and the cell size the number of BRI1 receptors per cell can be estimated. With the exception of the quiescent centre (QC), all fluorescence intensity measurements were performed at the anticlinal cell wall. However, when there appears to be a large difference in fluorescence intensity between adjacent cells, it is advisable to choose another joined wall or to adjust the calculations.

The number of BRI1 molecules in a root epidermal cell is about 22,000 in the meristem and 80,000 in the maturation zone. Taking into account the size difference between cells, the receptor density remains more or less constant throughout the root meristem and becomes reduced in the maturation zone. This raised the question whether the total number of BRI1 receptors per cell or the receptor density determines the sensitivity for BRs. It is of this interest to note that the root meristem cells are most active in BR signalling (González-García et al., 2011; Hacham et al., 2011) suggesting that receptor density is important for BRI1 mediated BR signalling. However, it is not easy to design an experiment to test this directly in plant cells.

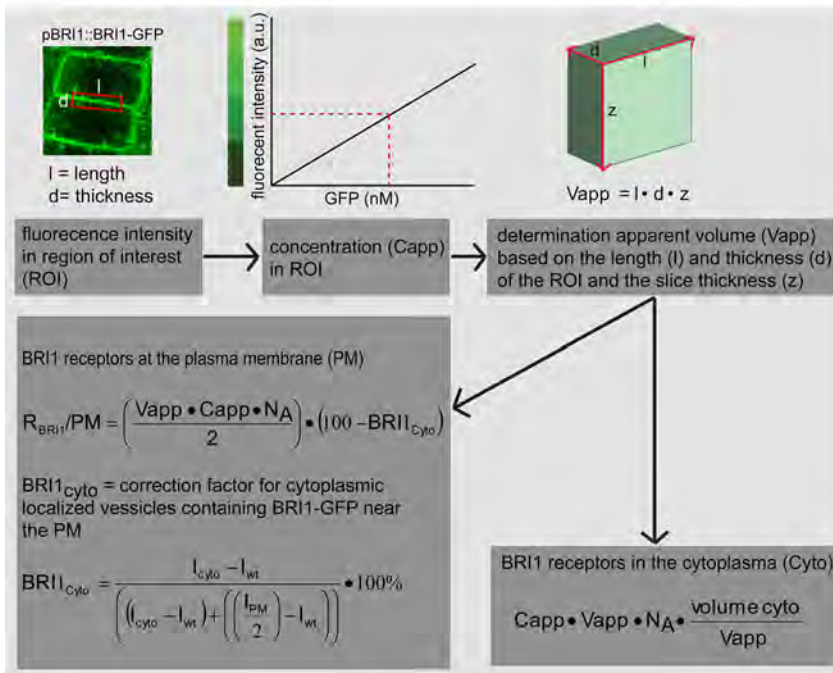


Figure 1. Quantification of the BRI1 receptor *in planta* using confocal microscopy. The fluorescence intensity is measured at the plasma membrane (PM) and cytoplasm (Cyto) separately. Next the apparent concentration (C_{app}) of GFP in the selected region of interest (ROI) is determined using a calibration curve consisting of GFP in solution. The volume of the ROI is defined by the length (l), thickness (d) and slice thickness (z) of the imaged area. The receptor density at the PM ($R_{BRI1/PM}$) can be calculated by multiplying the apparent volume (V_{app}) with C_{app} and Avogadro's constant (N_A). The calculated number of BRI1 receptors is divided by two to correct for the fact that the imaged area consist of two PM and multiplied by the fraction of BRI1 that is estimated to reside on the PM in the selected ROI ($100 - BRI1_{Cyto}$). The latter is approximated by ratio imaging where the fluorescence intensity (I) in the cytoplasm (I_{Cyto}) is compared to the intensity at the PM (I_{PM}) after subtraction of the auto fluorescence (I_{wt}). The number BRI1 receptors in the cytoplasm is calculated by multiplying the amount of BRI1-GFP molecules in the ROI ($C_{app} \cdot V_{app} \cdot N_A$) by the number of ROIs in the cytoplasm ($\text{volume cyto} / V_{app}$).

Modelling BRI1 mediated signalling using BL as the starting point

BRI1 mediated signalling is one of the few systems in plant biology where the ligand and receptor concentrations can be used as a starting point for modelling (van Esse et al., 2012). The model consists of two parts, a biochemical and a phenomenological model (Fig. 2). The biochemical model is based on mass action laws and employs BRI1 receptor and BL ligand concentration as input to calculate the BRI1 receptor occupancy. The biochemical pathway that is activated by the BRI1 signal is considered as a "black box" and not explicitly modelled. The phenomenological model is used to couple the estimated concentration of activated BRI1 molecules (i.e. BRI1 receptor occupancy) to a physiological readout such

as root growth or hypocotyl elongation. At present there is no technique available to reliably determine BRI1 receptor occupancy at physiological level during active signalling. Therefore, BRI1 occupancy was estimated by describing the steady state equilibrium between free BRI1 and free BL (Van Esse et al., 2012) using several assumptions such as ambient endogenous BL level and the dissociation constant (K_d) between BRI1 and BL (Wang et al., 2001; Caño-Delgado et al., 2004). The number of BRI1 receptors occupied by BL ([BRI1 BL]) determined in the biochemical model was used as input for the phenomenological model. Model parameters such as the length in absence of BR signalling $RL(0,0,t)$, the maximum growth in absence of inhibition $E_{max}(t)$ at discrete time points, the half maximum response values (k values) were calibrated with the actual measured root lengths in wild type plants in response to increasing amounts of BL. Since the exact structure of the phenomenological model is unknown, different model structures had to be tested and compared based on the Akaike (AIC) and Bayesian (BIC) error criterion. The model with the best fit to wild type root growth and the best predictive power was selected. Experimental verification was done by comparing the model predictions with actual measurements of root length of *bri1* mutant lines. The model shows that, similar to animal systems, about 1% of the total number of BRI1 receptors is occupied by ligand at BR concentrations that are stimulatory to root growth. The emerging picture from that work is that ligand availability rather than BRI1 receptor density is an important parameter for sensitivity essential for proper signal transduction. In BRI1 mediated signalling, it is unknown if the unoccupied receptors contribute to the signal by e.g. lateral signal propagation. This concept stems from EGFR signalling experiments where it was observed that receptor activation was possible in the absence of directly activating ligand (Verveer et al., 2000). Another possible explanation for these “spare receptors” is that there is one common downstream target which “guards” the signalling output. Whenever a single or a limited number of the receptors is activated, the downstream target will also be activated. This would result in a sensitive and centralised signal transduction cascade. The concept of “spare receptors” has been proposed previously for the elongation factor Tu (EF-TU) receptor in *Arabidopsis* (Albert et al., 2010).

Interestingly, the switch between activation and reduction of root growth depends on the BRI1 occupancy levels. When the BRI1 receptor level is reduced *in silico*, the root continues to grow until the maximum occupancy level is reached, while inhibition of root growth is completely absent. In other words, the signal of the BRI1 receptor never reaches the level that is necessary to induce the switch from ligand dependent stimulation to inhibition of root growth. In reality, such behaviour is observed for weak *bri1* mutant alleles. The recessive nature of *bri1* null mutants indicates that high BRI1 receptor density does provide a certain level of

robustness. This enables the plant to still respond to high and low ligand stimulus even under extreme conditions. Altogether, BRI1 may be, similar to EGFR, a core regulator capable of inducing different signals based on its occupancy level and/or complex composition.

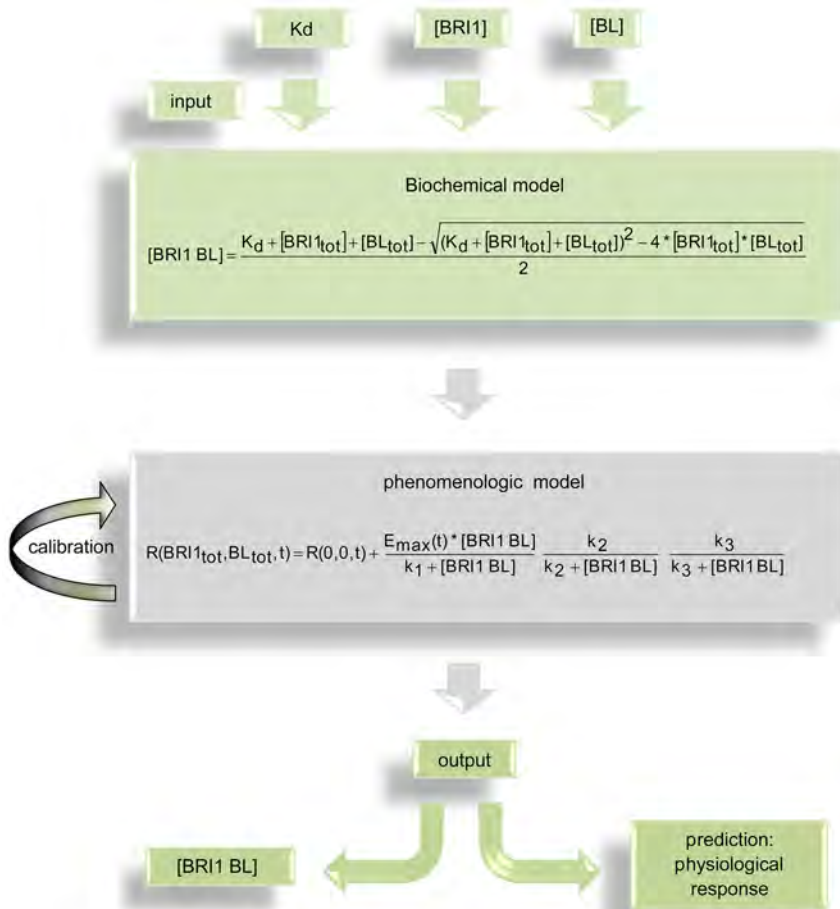


Figure 2. Schematic overview of combining a biochemical and phenomenological model. For the biochemical model, the BRI1 receptor and BL ligand concentrations as well as the dissociation constant (K_d) between BRI1 and BL is used. The amount of BRI1 in complex with BL $[BRI1 BL]$ can be calculated. The phenomenological model couples the amount of BRI1 occupied with BL to a physiological readout such as root growth. The half maximum response values (k_1 , k_2 and k_3), the maximum root growth ($E_{max(0)}$) and the root growth in absence of BR signalling ($R_{0,0,t}$) are unknown parameters which are estimated by calibrating the model to root growth of wild type lines. The model predicts the effect of an altered BRI1 receptor concentration at different ligand concentration. In addition, the BRI1 occupancy levels at different BL concentrations are calculated.

Modelling of SERK mediated BRI1 signalling

Using mathematical modelling, the effect of SERK1 and SERK3 on the signal transduced by ligand occupied BRI1 receptor was simulated. Growth assays of *serk1*, *serk3* and *serk1serk3* mutants were used to train the model on the modulating effects of SERK1 and SERK3 on BRI1 mediated signalling. A leave-one-out cross-validation was done to authenticate the model. Interestingly, when calibrated on the wild type, *serk1*, and *serk3* single mutants the model predicts that roots of the *serk1serk3* double will be completely insensitivity towards BL while the hypocotyl remains BR responsive. Experimental root growth and hypocotyl elongation measurements corroborate these model predictions and point towards a role for BRI1 alone or a difference in co-receptor usage between root and shoot. In this respect, different co-receptor usage may be a mechanism by which the sensitivity of a cell for BR is regulated. The model also shows that SERKs mainly affect the magnitude of the signal transduced by BRI1. This is in line with previous reports by Wang et al. (2008) which showed that activation of SERK3 by BRI1 upon BL application results in the reciprocal transphosphorylation of BRI1, thereby enhancing the signalling output. One question arising from this observation is how SERKs mechanistically enhances the BRI1 output. One possibility is that they transiently stabilise actively signalling BRI1 receptor complexes. This concept stems from the animal field where EGFR mediated signalling is prolonged in presence of its non-ligand binding co-receptor ERBB2. EGFR signalling is attenuated by ubiquitination and degradation of the activated EGFR complex. ERBB2 prevents this by altering the phosphorylation pattern on the EGFR kinase domain thereby regulating the ubiquitin ligases resulting in a stabilization of the EGFR-ERBB2 heterodimer (Hartman et al., 2012). In this context it is of interest to note that attenuation of BRI1 mediated signalling is regulated via phosphorylation of specific residues (Oh et al., 2012). However, whether or not SERK co-receptors stabilise active BRI1 receptor complexes remains to be elucidated.

Crosstalk between BR signalling and other signalling pathways

Similar to animal systems, plant RLK mediated signalling pathways influence other pathways. BRI1 mediated signalling has been reported to modulate several hormonal pathways mediated by for example auxin (Hardtke, 2007), gibberellins (Wang et al., 2009; Jaillais and Vert, 2012) and ethylene (De Grauwe et al., 2005; Nemhauser et al., 2006; Santner et al., 2009). Different signalling pathways can have an indirect effect on each other or directly by sharing the same components (Vert and Chory, 2011). The BR-regulated BIN2 kinase, for example, phosphorylates the transcriptional repressor auxin response factor 2 (ARF2), resulting a loss of ARF2 DNA binding (Nemhauser and Chory, 2004; Nemhauser et al., 2004; Vert et al., 2008). A more indirect form of crosstalk is represented by the BR transcriptional regulators BES1 and BZR1 which are capable of binding to promoters of genes involved in light perception, abscisic acid (ABA), cytokinin, gibberellins, jasmonic acid and defence signalling (Sun et al., 2010; Yu et al., 2011). Because SERK3 is a co-receptor that is both involved in development in association with BRI1 and in defence with Flagellin Sensitive 2 (FLS2), it has been implicated as a potential crosstalk point between the BRI1 and FLS2 mediated signalling pathways (Chinchilla et al., 2007; Chinchilla et al., 2009; Vert and Chory, 2011). However, the restriction of FLS2-mediated signalling by BR appears unidirectional and independent of SERK3 activation (Albrecht et al., 2012). In a different study, it was concluded that BR signalling affects defence both in a SERK3 dependent as well as in an independent fashion (Belkhadir et al., 2012). Simulations show that BRI1 signalling is able to operate while the majority of the SERK co-receptors are used by other signalling pathways thereby favouring a model where there is no limited SERK3 availability. This points towards a mechanism where different pathways are separated i.e. there are different pools of SERK co-receptors assigned to a main ligand perceiving receptor which are not freely interchangeable (Albrecht et al., 2012; Fig. 3).

Modelling helps to elucidate how BRI1 mediated signalling modulates other pathways. For example, the gene *Brevis Radix X* (BRX) has been identified as crosstalk point between auxin and BR signalling pathways using microarray analysis (Mouchel et al., 2006). *brx* mutants have a severe reduction in root length due to a reduced meristem and cell size (Mouchel et al., 2004). Expression of BRX is induced by high auxin levels and reduced at high BR levels while presence of BRX itself is essential for proper CPD expression (Mouchel et al., 2006). This led to the conclusion that BRX connects a feedback loop between auxin and BR signalling. Boolean logics were used to elucidate where the gene BRX should be placed in the BR and auxin signalling cascades and how BRX contributes to establishment of different cell fates (Sankar et al., 2011). To overcome the

limitations associated with a shortage in quantitative data, a combination of Boolean (discrete) and ODE based modelling was used by applying a Standardized Qualitative Dynamical Systems methodology (Mendoza and Xenarios, 2006; Di Cara et al., 2007). The resulting hybrid model converts networks of auxin and BR signalling into a continual system where the activity of pathway components in time is represented by arbitrary values. For the ODEs, default kinetic parameters were used that can be replaced when the actual values become available. The auxin and BR pathways were connected via BRX, ARF2 and NGATHA (NGA1, a transcription factor downstream of BRX). Different models were constructed in which it was tested whether BRX activates or inhibits NGA1. Some of the model variants assumed a direct influence of BRX on auxin responsive gene expression. For validation, the genetic interaction between ARF2 and BRX was studied using *arf2brx* double mutant lines by measuring root length and/or cell elongation. The model validation does not include time dependent activation status of the pathway components by e.g. measuring the phosphorylation at different time points. Instead, validation relies on the correlation between the model predictions represented in arbitrary units and the observed phenotype.

Phenomenological considerations have demonstrated that polar auxin transport and BR signalling control radial patterning of vascular bundles in Arabidopsis (Ibañes et al., 2009). In that study, slices of the vascular bundle were imaged using light microscopy. The model uses the stem diameter, the number of cells and intervacular bundles as quantitative parameters together with the appearance of DR5-GUS expression as readout for auxin maxima. The resulting mathematical model incorporates the auxin flux across the vascular ring of proliferating cells, polar auxin transport between cells and the apoplast and passive diffusion across the apoplast. As model validation auxin maxima were predicted in wild type but also in various mutant lines with defective auxin transport or auxin overproducing mutants. The potential of combining modelling and experimental data was nicely demonstrated when the same model was employed to compute the phenotypical behaviour of mutants defective in BR signalling which also show an altered number of vascular bundles. From this work the authors concluded that the coordinated action of BRs and auxin is essential in establishing the periodic arrangement of vascular bundles in the shoot (Ibañes et al., 2009). Simulations were done by using as initial condition an almost homogenous distribution of auxin across a ring consisting of vascular cells. The model is neither dependent on the initial auxin concentration nor on the mechanistics of the signal transduction pathway, thereby differing from the models for BRI1 mediated signalling established in this thesis. Interestingly, in both cases, model predictions were based on phenomenological considerations.

Current models for BR mediated signalling propose a ligand induced recruitment of SERK co-receptors towards BRI1 (Li et al., 2002; Wang et al., 2005). However, such a mechanism is not in line with the low mobility of BRI1 in the PM of root meristem epidermal cells and points to a mechanism where BRI1-SERK hetero-oligomers exist as PM located preformed complexes. Mixed populations of monomers and dimers formed via a dynamic equilibrium between transiently dimerising monomers has been observed for several receptors in mammalian systems such as the G coupled protein receptor (GPCR) and the EGFR (Chung et al., 2010; Lemmon and Schlessinger, 2010; Calebiro et al., 2013). Clearly, additional experimental verification using single molecule imaging techniques will be essential to determine if such a mechanism also applies to BRI1-SERK oligomerisation.

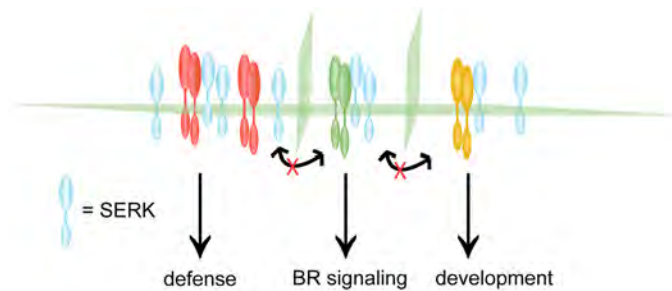


Figure 3. Limited movement of PM localised receptors. The cartoon illustrates how compartmentalization of SERK related processes can help to prevent crosstalk of the signals at the receptor level. PM localised receptors cannot freely diffuse; instead movement is restricted which results in different pools of SERK that are not freely interchangeable. A possible mechanism to active this is by preformation of the hetero-oligomers.

FUTURE CHALLENGES

Until now, current models for BRI1 mediated signalling have helped explaining complex physiological responses. Imaging has been a useful tool in these studies to quantify the amount of receptors or the number of cells in the vasculature tissue, but has not been used directly as data to be included directly in the models. The challenge will be to extend the modelling and imaging tools towards the cellular level to describe local protein interactions, protein quantity, and activity in terms of read-out of signalling activity. The mathematical modelling approach presented in **this thesis** provides a starting point to extend the genetic model based on Boolean logics with downstream components of the BRI1 signal transduction cascade in a more quantitative matter. Quantitative imaging data such as FRET-FLIM analysis can be employed to improve the modelling parameters and verify predictions of activity and interaction status.

One example, where to go, is the recent study describing a fast BRI1-dependent BR response pathway in the plasma membrane of *Arabidopsis thaliana* (Elgass et al., 2009; Elgass et al., 2010; Caesar et al., 2011; Witthoft et al., 2011). The authors used a combination of quantitative wavelength-specific fluorescence imaging, one-chromophore fluorescence lifetime microscopy (ocFLM), fluorescence intensity decay shape analysis microscopy (FIDSAM) (Schleifenbaum et al., 2010) combined with FRET (FRET-FIDSAM) and FRET-FLIM to characterise initial subcellular events of BRI1-GFP function at the cytoplasm-plasma membrane-apoplast interface (Fig. 4). The quantitative physiological readouts in this study were the dynamic change in the plasma membrane potential determined by ocFLS of BRI1-GFP and in the dimension of the cell wall as indicator for insetting cell elongation. By this approach not only the kinetics of BRI1(-GFP) action could be followed *in vivo* at high spatio-temporal resolution but also the competence of specific *Arabidopsis* cells to respond to BR could be determined (Elgass et al., 2010). In addition, the physical interaction of BRI1-GFP with the P-type ATPase was found and a dynamic alteration of both proteins within the membrane complex in response to BR observed by FRET-FIDSAM. In combination with the quantification of ligand-bound BRI1, possible other components of the BRI1-P-ATPase complex, these quantitative data of a relative simple BR response pathway offer the possibility of future computational modelling.

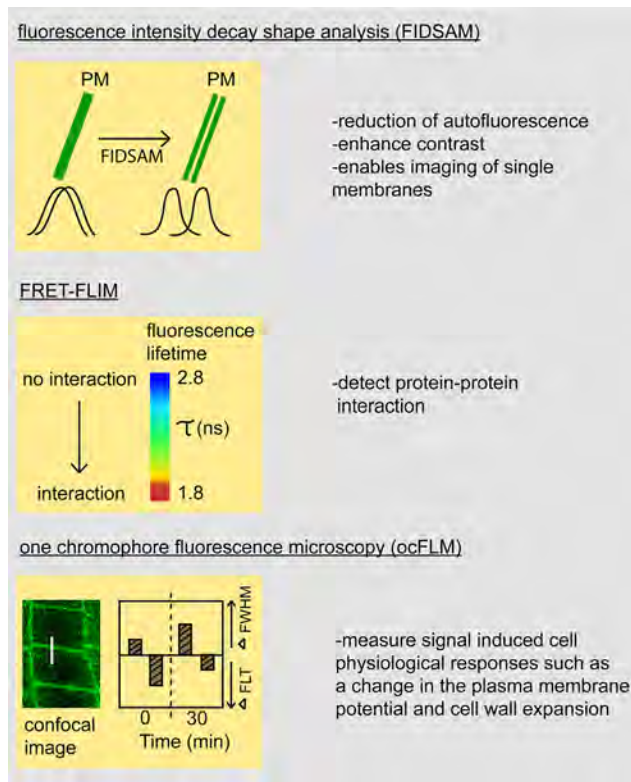


Figure 4. Combining fluorescence microscopy techniques. Combining FIDSAM (top panel) with FLIM (FLIM-FIDSAM), FRET-FLIM (middle panel) and ocFLM (bottom panel) can provide a more complete view of intracellular dynamics, cell specific physiological responses and interactions. Top panel: FIDSAM enables imaging of two single isolated plasma membranes (PMs), which normally would appear as one. The Gaussian curves indicate the distribution of fluorescence intensity before and after FIDSAM. FIDSAM is based on the difference in fluorescence intensity decay patterns between the autofluorescence background and fluorophore. Middle panel: Fluorescence Lifetime Imaging Microscopy (FLIM) to detect Förster Resonance Energy Transfer (FRET) is used to measure protein-protein interaction. The decrease in fluorescence lifetime is used as measure for interaction between the fluorophores. Bottom panel: One-Chromophore Fluorescence Lifetime Microscopy (ocFLM). The white bar in the confocal image provides an example of the area where the full width half maximum (FWHM) of the Gaussian curve over the PM and fluorescent lifetime (FLT) is measured. The graph illustrates the readout e.g. the FWHM and FLT after application of BL at time points 0 and 30 minutes. With ocFLM signal induced physiological responses such as change in the plasma membrane potential and cell wall expansion is determined by measuring respectively the FLT and FWHM.

In general, these kinds of experiments need to be designed in a way that data can be incorporated directly into the modelling cycle by e.g. determination of the maximum and minimum values of the tested model parameters. For example, at this moment it is unknown how many downstream targets of BRI1 are activated by BR at physiological ligand concentrations. It is likely that a rather limited set of targets is active in any given cell type and perhaps only at precise moments during the cell cycle. So far, imaging of the BRI1 receptors is not capable of resolving the ligand-occupied ones. Inclusion of probes or methods to do this would directly enable verification of model predictions by quantitative image analysis (Fig. 5). Modelling can also be helpful to explain imaging data, especially for events that take place in small numbers in precise locations. Finally, the combination of quantitative imaging and modelling may elucidate how receptors can be shared by different pathways within the same cell without affecting other pathways.

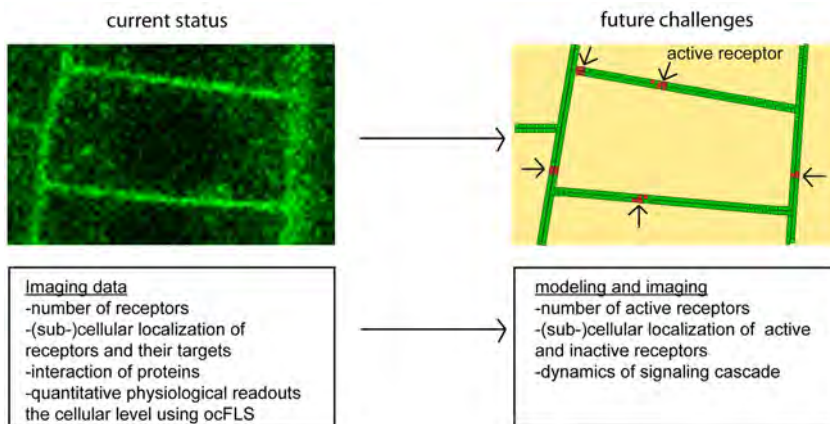


Figure 5. Future challenges in combining imaging data with mathematical models. The left image is a real confocal image of the BRI1-GFP protein, clearly showing localization at the PM and in intracellular membrane compartments. This represents the current status of imaging applications. On the right a fictional picture of BRI1 is shown describing the number of active receptors as predicted by the model. PM localised receptors not active in signalling are presented as green dots, active ones as red dots. Ideally this would be coupled to activation of downstream targets and transcriptional regulators in order to model the dynamics of the signalling cascade. At the moment the transport and routing of active BRI1 and its downstream targets is unknown and not indicated in the figure. Abbreviations: ocFLM stands for one-chromophore fluorescence lifetime microscopy

REFERENCES

- Aker J, de Vries SC** (2008) Plasma Membrane Receptor Complexes. *Plant Physiology* **147**: 1560-1564
- Akman OE, Watterson S, Parton A, Binns N, Millar AJ, Ghazal P** (2012) Digital clocks: simple Boolean models can quantitatively describe circadian systems. *Journal of the Royal Society Interface* **9**: 2365-2382
- Akutsu T, Miyano S, Kuhara S** (1999) Identification of genetic networks from a small number of gene expression patterns under the Boolean network model. *Pacific Symposium on Biocomputing*: 17-28
- Albert M, Jehle AK, Mueller K, Eisele C, Lipschis M, Felix G** (2010) Arabidopsis thaliana pattern recognition receptors for bacterial elongation factor Tu and flagellin can be combined to form functional chimeric receptors. *The Journal of Biological Chemistry* **285**: 19035-19042
- Albrecht C, Boutrot F, Segonzac C, Schwessinger B, Gimenez-Ibanez S, Chinchilla D, Rathjen JP, De Vries SC, Zipfel C** (2012) Brassinosteroids inhibit pathogen-associated molecular pattern-triggered immune signaling independent of the receptor kinase BAK1. *Proceedings of the National Academy of Sciences of the United States of America* **109**: 303-308
- Albrecht C, Russinova E, Hecht V, Baaijens E, De Vries S** (2005) The Arabidopsis thaliana SOMATIC EMBRYOGENESIS RECEPTOR-LIKE KINASES1 and 2 control male sporogenesis. *Plant Cell* **17**: 3337-3349
- Albrecht C, Russinova E, Kemmerling B, Kwaaitaal M, De Vries SC** (2008) Arabidopsis Somatic Embryogenesis Receptor Kinase proteins serve brassinosteroid-dependent and -independent signaling pathways. *Plant Physiology* **148**: 611-619
- Alonso JM, Stepanova AN, Leisse TJ, Kim CJ, Chen H, Shinn P, Stevenson DK, Zimmerman J, Barajas P, Cheuk R, Gadrinab C, Heller C, Jeske A, Koesema E, Meyers CC, Parker H, Prednis L, Ansari Y, Choy N, Deen H, Geralt M, Hazari N, Hom E, Karnes M, Mulholland C, Ndubaku R, Schmidt I, Guzman P, Aguilar-Henonin L, Schmid M, Weigel D, Carter DE, Marchand T, Risseuw E, Brogden D, Zeko A, Crosby WL, Berry CC, Ecker JR** (2003) Genome-wide insertional mutagenesis of *Arabidopsis thaliana*. *Science* **301**: 653-657
- Alvarado D, Klein DE, Lemmon MA** (2010) Structural Basis for negative cooperativity in growth factor binding to an EGF receptor. *Cell* **142**: 568-579
- Asami T, Min YK, Nagata N, Yamagishi K, Takatsuto S, Fujioka S, Murofushi N, Yamaguchi I, Yoshida S** (2000) Characterization of Brassinazole, a Triazole-Type Brassinosteroid Biosynthesis Inhibitor. *Plant Physiology* **123**: 93-100
- Bacia K, Kim SA, Schwillle P** (2006) Fluorescence cross-correlation spectroscopy in living cells. *Nature Methods* **3**: 83-89
- Backes C, Keller A, Kuentzer J, Kneissl B, Comtesse N, Elnakady YA, Müller R, Meese E, Lenhof HP** (2007) GeneTrail-advanced gene set enrichment analysis. *Nucleic Acids Res* **35**: W186-W192
- Bajguz A, Tretyn A** (2003) The chemical characteristic and distribution of brassinosteroids in plants. *Phytochemistry* **62**: 1027-1046
- Bak S, Feyereisen R** (2001) The involvement of two p450 enzymes, CYP83B1 and CYP83A1, in auxin homeostasis and glucosinolate biosynthesis. *Plant Physiology* **127**: 108-118
- Bak S, Tax FE, Feldmann KA, Galbraith DW, Feyereisen R** (2001) CYP83B1, a cytochrome P450 at the metabolic branch point in auxin and indole glucosinolate biosynthesis in Arabidopsis. *Plant Cell* **13**: 101-111
- Bancos S, Nomura T, Sato T, Molnar G, Bishop GJ, Koncz C, Yokota T, Nagy F,**

- Szekeres M** (2002) Regulation of transcript levels of the Arabidopsis cytochrome p450 genes involved in brassinosteroid biosynthesis. *Plant Physiology* **130**: 504-513
- Band LR, Fozard JA, Godin C, Jensen OE, Pridmore T, Bennett MJ, King JR** (2012) Multiscale systems analysis of root growth and development: modeling beyond the network and cellular scales. *Plant Cell* **24**: 3892-3906
- Barnidge DR, Dratz EA, Martin T, Bonilla LE, Moran LB, Lindall A** (2003) Absolute Quantification of the G Protein-Coupled Receptor Rhodopsin by LC/MS/MS Using Proteolysis Product Peptides and Synthetic Peptide Standards. *Analytical Chemistry* **75**: 445-451
- Baxter I, Hosmani PS, Rus A, Lahner B, Borevitz JO, Muthukumar B, Mickelbart MV, Schreiber L, Franke RB, Salt DE** (2009) Root suberin forms an extracellular barrier that affects water relations and mineral nutrition in Arabidopsis. *PLoS Genetic* **5**: e1000492
- Beck M, Zhou J, Faulkner C, MacLean D, Robatzek S** (2012) Spatio-temporal cellular dynamics of the Arabidopsis flagellin receptor reveal activation status-dependent endosomal sorting. *Plant Cell* **24**: 4205-4219
- Beisson F, Li-Beisson Y, Pollard M** (2012) Solving the puzzles of cutin and suberin polymer biosynthesis. *Current Opinions in Plant Cell Biology* **15**: 329-337
- Beisson F, Li Y, Bonaventure G, Pollard M, Ohlrogge JB** (2007) The acyltransferase GPAT5 is required for the synthesis of suberin in seed coat and root of Arabidopsis. *Plant Cell* **19**: 351-368
- Belkhadir Y, Jaillais Y, Epple P, Balsemao-Pires E, Dangi JL, Chory J** (2012) Brassinosteroids modulate the efficiency of plant immune responses to microbe-associated molecular patterns. *Proceedings of the National Academy of Sciences of the United States of America* **109**: 297-302
- Benjamini Y, Hochberg Y** (1995) Controlling the False Discovery Rate: A Practical and Powerful Approach to Multiple Testing. *Journal of the Royal Statistical Society. Series B (Methodological)* **57**: 289-300
- Berg H, Sewell A** (2011) Dynamic Tuning of T Cell Receptor Specificity by Co-Receptors and Costimulation. *In* C Molina-Paris, G Lythe, eds, *Mathematical Models and Immune Cell Biology*. Springer New York, pp 47-73
- Berg RH, Beachy RN, Kevin FS** (2008) Fluorescent Protein Applications in Plants. *In* *Methods in Cell Biology*, **85**:153-177
- Berkers JA, van Bergen en Henegouwen PM, Boonstra J** (1991) Three classes of epidermal growth factor receptors on HeLa cells. *The Journal of Biological Chemistry* **266**: 922-927
- Besschetnova TY, Montefusco DJ, Asinas AE, Shrout AL, Antommattei FM, Weis RM** (2008) Receptor density balances signal stimulation and attenuation in membrane-assembled complexes of bacterial chemotaxis signaling proteins. *Proceedings of the National Academy of Sciences of the United States of America* **105**: 12289-12294
- Birnbaum K, Shasha DE, Wang JY, Jung JW, Lambert GM, Galbraith DW, Benfey PN** (2003) A gene expression map of the Arabidopsis root. *Science* **302**: 1956-1960
- Birtwistle MR, Kholodenko BN** (2009) Endocytosis and signalling: a meeting with mathematics. *Molecular Oncology* **3**: 308-320
- Borisov N, Aksamitiene E, Kiyatkin A, Legewie S, Berkhout J, Maiwald T, Kaimachnikov NP, Timmer J, Hoek JB, Kholodenko BN** (2009) Systems-level interactions between insulin-EGF networks amplify mitogenic signaling. *Molecular Systems Biology* **5**: 256

- Boudsocq M, Willmann MR, McCormack M, Lee H, Shan L, He P, Bush J, Cheng SH, Sheen J** (2010) Differential innate immune signalling via Ca(2+) sensor protein kinases. *Nature* **464**: 418-422
- Bouquin T, Meier C, Foster R, Nielsen ME, Mundy J** (2001) Control of specific gene expression by gibberellin and brassinosteroid. *Plant Physiology* **127**: 450-458
- Boutte Y, Frescatada-Rosa M, Men S, Chow CM, Ebine K, Gustavsson A, Johansson L, Ueda T, Moore I, Jurgens G, Grebe M** (2010) Endocytosis restricts Arabidopsis KNOLLE syntaxin to the cell division plane during late cytokinesis. *EMBO Journal* **29**: 546-558
- Bowling SA, Clarke JD, Liu Y, Klessig DF, Dong X** (1997) The cpr5 mutant of Arabidopsis expresses both NPR1-dependent and NPR1-independent resistance. *Plant Cell* **9**: 1573-1584
- Brandman O, Meyer T** (2008) Feedback loops shape cellular signals in space and time. *Science* **322**: 390-395
- Brenner WG, Romanov GA, Kollmer I, Burkle L, Schmulting T** (2005) Immediate-early and delayed cytokinin response genes of Arabidopsis thaliana identified by genome-wide expression profiling reveal novel cytokinin-sensitive processes and suggest cytokinin action through transcriptional cascades. *Plant Journal* **44**: 314-333
- Brent R** (2009) Cell signaling: what is the signal and what information does it carry? *FEBS Letters* **583**: 4019-4024
- Bücherl C, Aker J, de Vries S, Borst JW** (2010) Probing protein-protein Interactions with FRET-FLIM. *Methods in Molecular Biology* **655**: 389-399
- Caesar K, Elgass K, Chen Z, Huppenberger P, Witthoft J, Schleifenbaum F, Blatt MR, Oecking C, Harter K** (2011) A fast brassinolide-regulated response pathway in the plasma membrane of Arabidopsis thaliana. *Plant Journal* **66**: 528-540
- Calderon Villalobos LI, Lee S, De Oliveira C, Ivetac A, Brandt W, Armitage L, Sheard LB, Tan X, Parry G, Mao H, Zheng N, Napier R, Kepinski S, Estelle M** (2012) A combinatorial TIR1/AFB-Aux/IAA co-receptor system for differential sensing of auxin. *Nature Chemical Biology* **8**: 477-485
- Calebiro D, Rieken F, Wagner J, Sungkaworn T, Zabel U, Borzi A, Cocucci E, Zurn A, Lohse MJ** (2013) Single-molecule analysis of fluorescently labeled G-protein-coupled receptors reveals complexes with distinct dynamics and organization. *Proceedings of the National Academy of Sciences of the United States of America* **110**: 743-748
- Caño-Delgado A, Yin Y, Yu C, Vafeados D, Mora-Garcia S, Cheng JC, Nam KH, Li J, Chory J** (2004) BRL1 and BRL3 are novel brassinosteroid receptors that function in vascular differentiation in Arabidopsis. *Development* **131**: 5341-5351
- Charette SJ, Lambert H, Nadeau PJ, Landry J** (2010) Protein quantification by chemiluminescent Western blotting: Elimination of the antibody factor by dilution series and calibration curve. *Journal of Immunological Methods* **353**: 148-150
- Chen Y, Wei LN, Muller JD** (2003) Probing protein oligomerization in living cells with fluorescence fluctuation spectroscopy. *Proceedings of the National Academy of Sciences of the United States of America* **100**: 15492-15497
- Chen YZ, Pang QY, He Y, Zhu N, Branstrom I, Yan XF, Chen S** (2012) Proteomics and metabolomics of Arabidopsis responses to perturbation of glucosinolate biosynthesis. *Molecular Plant* **5**: 1138-1150
- Chinchilla D, Shan L, He P, de Vries S, Kemmerling B** (2009) One for all: the receptor-associated kinase BAK1. *Trends in Plant Science* **14**: 535-541

- Chinchilla D, Zipfel C, Robatzek S, Kemmerling B, Nurnberger T, Jones JD, Felix G, Boller T** (2007) A flagellin-induced complex of the receptor FLS2 and BAK1 initiates plant defence. *Nature* **448**: 497-500
- Cho SK, Larue CT, Chevalier D, Wang H, Jinn TL, Zhang S, Walker JC** (2008) Regulation of floral organ abscission in *Arabidopsis thaliana*. *Proceedings of the National Academy of Sciences of the United States of America* **105**: 15629-15634
- Chory J, Nagpal P, Peto CA** (1991) Phenotypic and Genetic Analysis of *det2*, a New Mutant That Affects Light-Regulated Seedling Development in *Arabidopsis*. *Plant Cell* **3**: 445-459
- Chory J, Reinecke D, Sim S, Washburn T, Brenner M** (1994) A Role for Cytokinins in De-Etiolation in *Arabidopsis* (*det* Mutants Have an Altered Response to Cytokinins). *Plant Physiology* **104**: 339-347
- Chung I, Akita R, Vandlen R, Toomre D, Schlessinger J, Mellman I** (2010) Spatial control of EGF receptor activation by reversible dimerization on living cells. *Nature* **464**: 783-787
- Citri A, Yarden Y** (2006) EGF-ERBB signalling: towards the systems level. *Nature Reviews Molecular Cell Biology* **7**: 505-516
- Clark SE, Running MP, Meyerowitz EM** (1993) CLAVATA1, a regulator of meristem and flower development in *Arabidopsis*. *Development* **119**: 397-418
- Clark SE, Williams RW, Meyerowitz EM** (1997) The CLAVATA1 Gene Encodes a Putative Receptor Kinase That Controls Shoot and Floral Meristem Size in *Arabidopsis*. *Cell* **89**: 575-585
- Clouse SD** (1996) Molecular genetic studies confirm the role of brassinosteroids in plant growth and development. *Plant Journal* **10**: 1-8
- Clouse SD, Langford M, McMorris TC** (1996) A brassinosteroid-insensitive mutant in *Arabidopsis thaliana* exhibits multiple defects in growth and development. *Plant Physiology* **111**: 671-678
- Clouse SD, Sasse JM** (1998) BRASSINOSTEROIDS: Essential Regulators of Plant Growth and Development. *Annual Review of Plant Physiology and Plant Molecular Biology* **49**: 427-451
- Colcombet J, Boisson-Dernier A, Ros-Palau R, Vera CE, Schroeder JI** (2005) *Arabidopsis* SOMATIC EMBRYOGENESIS RECEPTOR KINASES1 and 2 are essential for tapetum development and microspore maturation. *Plant Cell* **17**: 3350-3361
- Cowley GP, Smith JA, Gusterson BA** (1986) Increased EGF receptors on human squamous carcinoma cell lines. *British Journal of Cancer* **53**: 223-229
- De Grauwe L, Vandenbussche F, Tietz O, Palme K, Van Der Straeten D** (2005) Auxin, ethylene and brassinosteroids: tripartite control of growth in the *Arabidopsis* hypocotyl. *Plant and Cell Physiology* **46**: 827-836
- Deng Z, Zhang X, Tang W, Oses-Prieto JA, Suzuki N, Gendron JM, Chen H, Guan S, Chalkley RJ, Peterman TK, Burlingame AL, Wang ZY** (2007) A proteomics study of brassinosteroid response in *Arabidopsis*. *Molecular & Cellular Proteomics* **6**: 2058-2071
- Denoux C, Galletti R, Mammarella N, Gopalan S, Werck D, De Lorenzo G, Ferrari S, Ausubel FM, Dewdney J** (2008) Activation of defense response pathways by OGs and Flg22 elicitors in *Arabidopsis* seedlings. *Molecular Plant* **1**: 423-445
- DeWitt AE, Dong JY, Wiley HS, Lauffenburger DA** (2001) Quantitative analysis of the EGF receptor autocrine system reveals cryptic regulation of cell response by ligand capture. In *Journal of Cell Science* **114**: 2301-2313
- Di Cara A, Garg A, De Micheli G, Xenarios I, Mendoza L** (2007) Dynamic simulation of regulatory networks using SQUAD. *BMC Bioinformatics* **8**: 462

- Di Rubbo S, Irani NG, Russinova E** (2011) PP2A phosphatases: the “on-off” regulatory switches of brassinosteroid signaling. *Science Signalling* **4**: pe25
- Doerner P** (1993) Patterning the Arabidopsis root. *Current Biology* **3**: 867-869
- Domergue F, Vishwanath SJ, Joubes J, Ono J, Lee JA, Bourdon M, Alhattab R, Lowe C, Pascal S, Lessire R, Rowland O** (2010) Three Arabidopsis fatty acyl-coenzyme A reductases, FAR1, FAR4, and FAR5, generate primary fatty alcohols associated with suberin deposition. *Plant Physiology* **153**: 1539-1554
- Du J, Yin H, Zhang S, Wei Z, Zhao B, Zhang J, Gou X, Lin H, Li J** (2012) Somatic Embryogenesis Receptor Kinases Control Root Development Mainly via Brassinosteroid-Independent Actions in Arabidopsis thaliana. *Journal of Integrative Plant Biology* **54**: 388-399
- Dubrovsky JG, Soukup A, Napsucialy-Mendivil S, Jeknic Z, Ivanchenko MG** (2009) The lateral root initiation index: an integrative measure of primordium formation. *Annals of Botany* **103**: 807-817
- Edgar R, Domrachev M, Lash AE** (2002) Gene Expression Omnibus: NCBI gene expression and hybridization array data repository. *Nucleic Acids Research* **30**: 207-210
- Eisen MB, Spellman PT, Brown PO, Botstein D** (1998) Cluster analysis and display of genome-wide expression patterns. *Proceedings of the National Academy of Sciences of the United States of America* **95**: 14863-14868
- Elgass K, Caesar K, Schleifenbaum F, Stierhof YD, Meixner AJ, Harter K** (2009) Novel application of fluorescence lifetime and fluorescence microscopy enables quantitative access to subcellular dynamics in plant cells. *PLoS One* **4**: e5716
- Elgass K, Caesar K, Wanke D, Harter K, Meixner AJ, Schleifenbaum F** (2010) Application of FLIM-FIDSAM for the in vivo analysis of hormone competence of different cell types. *Analytical and Bioanalytical Chemistry* **398**: 1919-1925
- Espinosa-Soto C, Padilla-Longoria P, Alvarez-Buylla ER** (2004) A gene regulatory network model for cell-fate determination during Arabidopsis thaliana flower development that is robust and recovers experimental gene expression profiles. *Plant Cell* **16**: 2923-2939
- Fabregas N, Ibañes M, Caño-Delgado AI** (2010) A systems biology approach to dissect the contribution of brassinosteroid and auxin hormones to vascular patterning in the shoot of Arabidopsis thaliana. *Plant Signal Behavior* **5**: 903-906
- Ferrell JE, Jr.** (2002) Self-perpetuating states in signal transduction: positive feedback, double-negative feedback and bistability. *Current Opinion in Cell Biology* **14**: 140-148
- Freeman M** (2000) Feedback control of intercellular signalling in development. *Nature* **408**: 313-319
- Fricker M, Runions J, Moore I** (2006) Quantitative fluorescence microscopy: from art to science. *Annual Review of Plant Biology* **57**: 79-107
- Friedrichsen DM, Joazeiro CA, Li J, Hunter T, Chory J** (2000) Brassinosteroid-insensitive-1 is a ubiquitously expressed leucine-rich repeat receptor serine/threonine kinase. *Plant Physiology* **123**: 1247-1256
- Fujioka S, Li J, Choi YH, Seto H, Takatsuto S, Noguchi T, Watanabe T, Kuriyama H, Yokota T, Chory J, Sakurai A** (1997) The Arabidopsis deetiolated2 mutant is blocked early in brassinosteroid biosynthesis. *Plant Cell* **9**: 1951-1962
- Fujita H, Toyokura K, Okada K, Kawaguchi M** (2011) Reaction-diffusion pattern in shoot apical meristem of plants. *PLoS One* **6**: e18243

- Gadella TW, Jr., Jovin TM** (1995) Oligomerization of epidermal growth factor receptors on A431 cells studied by time-resolved fluorescence imaging microscopy. A stereochemical model for tyrosine kinase receptor activation. *The Journal of Cell Biology* **129**: 1543-1558
- Gakamsky DM, Luescher IF, Pramanik A, Kopito RB, Lemonnier F, Vogel H, Rigler R, Pecht I** (2005) CD8 kinetically promotes ligand binding to the T-cell antigen receptor. *Biophysical Journal* **89**: 2121-2133
- Gao G, Zhang S, Wang C, Yang X, Wang Y, Su X, Du J, Yang C** (2011) Arabidopsis CPR5 independently regulates seed germination and postgermination arrest of development through LOX pathway and ABA signaling. *PLoS One* **6**: e19406
- Gao GF, Rao Z, Bell JI** (2002) Molecular coordination of alphabeta T-cell receptors and coreceptors CD8 and CD4 in their recognition of peptide-MHC ligands. *Trends Immunology* **23**: 408-413
- Geldner N, Hyman DL, Wang X, Schumacher K, Chory J** (2007) Endosomal signaling of plant steroid receptor kinase BRI1. *Genes and Development* **21**: 1598-15602
- Geldner N, Robatzek S** (2008) Plant receptors go endosomal: A moving view on signal transduction. *Plant Physiology* **147**: 1565-1574
- Gendreau E, Traas J, Desnos T, Grandjean O, Caboche M, Hofte H** (1997) Cellular basis of hypocotyl growth in *Arabidopsis thaliana*. *Plant Physiology* **114**: 295-305
- Genoud T, Trevino Santa Cruz MB, Metraux JP** (2001) Numeric simulation of plant signaling networks. *Plant Physiology* **126**: 1430-1437
- Gentleman RC, Carey VJ, Bates DM, Bolstad B, Dettling M, Dudoit S, Ellis B, Gautier L, Ge Y, Gentry J, Hornik K, Hothorn T, Huber W, Iacus S, Irizarry R, Leisch F, Li C, Maechler M, Rossini AJ, Sawitzki G, Smith C, Smyth G, Tierney L, Yang JY, Zhang J** (2004) Bioconductor: open software development for computational biology and bioinformatics. *Genome Biology* **5**: R80
- Goldsbury C, Thies E, Konzack S, Mandelkow E-M** (2007) Quantification of Amyloid Precursor Protein and Tau for the Study of Axonal Traffic Pathways. *The Journal of Neuroscience* **27**: 3357-3363
- Gomez-Gomez L, Boller T** (2000) FLS2: an LRR receptor-like kinase involved in the perception of the bacterial elicitor flagellin in *Arabidopsis*. *Molecular Cell* **5**: 1003-1011
- Gonzalez-Carranza ZH, Shahid AA, Zhang L, Liu Y, Ninsuwan U, Roberts JA** (2012) A novel approach to dissect the abscission process in *Arabidopsis*. *Plant Physiology* **160**: 1342-1356
- González-García MP, Vilarrasa-Blasi J, Zhiponova M, Divol F, Mora-García S, Russinova E, Caño-Delgado AI** (2011) Brassinosteroids control meristem size by promoting cell cycle progression in *Arabidopsis* roots. *Development* **138**: 849-859
- Gou X, Yin H, He K, Du J, Yi J, Xu S, Lin H, Clouse SD, Li J** (2012) Genetic evidence for an indispensable role of somatic embryogenesis receptor kinases in brassinosteroid signaling. *PLoS Genetics* **8**: e1002452
- Grieneisen VA, Xu J, Maree AFM, Hogeweg P, Scheres B** (2007) Auxin transport is sufficient to generate a maximum and gradient guiding root growth. *Nature* **449**: 1008-1013
- Guo R, Qian H, Shen W, Liu L, Zhang M, Cai C, Zhao Y, Qiao J, Wang Q** (2013) BZR1 and BES1 participate in regulation of glucosinolate biosynthesis by brassinosteroids in *Arabidopsis*. *Journal of Experimental Botany* doi:10.1093/jxb/ert094
- Hacham Y, Holland N, Butterfield C, Ubada-Tomas S, Bennett MJ, Chory J, Savaldi-Goldstein S** (2011) Brassinosteroid perception in the epidermis controls root meristem size. *Development* **138**: 839-848

- Halfhill MD, Millwood RJ, Stewart CN, Jr.** (2005) Green fluorescent protein quantification in whole plants. *Methods in Molecular Biology* **286**: 215-226
- Hardtke CS** (2007) Transcriptional auxin-brassinosteroid crosstalk: who's talking? *Bioessays* **29**: 1115-1123
- Harter K, Meixner AJ, Schleifenbaum F** (2012) Spectro-microscopy of living plant cells. *Molecular Plant* **5**: 14-26
- Hartman Z, Zhao H, Agazie YM** (2012) HER2 stabilizes EGFR and itself by altering autophosphorylation patterns in a manner that overcomes regulatory mechanisms and promotes proliferative and transformation signaling. *Oncogene* doi:10.1038/onc.2012.418
- He K, Gou X, Yuan T, Lin H, Asami T, Yoshida S, Russell SD, Li J** (2007) BAK1 and BKK1 Regulate Brassinosteroid-Dependent Growth and Brassinosteroid-Independent Cell-Death Pathways. *Current Biology* **17**: 1109-1115
- He Z, Wang Z-Y, Li J, Zhu Q, Lamb C, Ronald P, Chory J** (2000) Perception of Brassinosteroids by the Extracellular Domain of the Receptor Kinase BRI1. *Science* **288**: 2360-2363
- Hecht V, Vielle-Calzada JP, Hartog MV, Schmidt ED, Boutilier K, Grossniklaus U, de Vries SC** (2001) The Arabidopsis SOMATIC EMBRYOGENESIS RECEPTOR KINASE 1 gene is expressed in developing ovules and embryos and enhances embryogenic competence in culture. *Plant Physiology* **127**: 803-816
- Heese A, Hann DR, Gimenez-Ibañez S, Jones AME, He K, Li J, Schroeder JI, Peck SC, Rathjen JP** (2007) The receptor-like kinase SERK3/BAK1 is a central regulator of innate immunity in plants. *Proceedings of the National Academy of Sciences of the United States of America* **104**: 12217-12222
- Heidebrecht F, Heidebrecht A, Schulz I, Behrens SE, Bader A** (2009) Improved semiquantitative Western blot technique with increased quantification range. *Journal of Immunological Methods* **345**: 40-48
- Hennig L, Menges M, Murray JA, Grissem W** (2003) Arabidopsis transcript profiling on Affymetrix GeneChip arrays. *Plant Molecular Biology* **53**: 457-465
- Herbst JJ, Opreko LK, Walsh BJ, Lauffenburger DA, Wiley HS** (1994) Regulation of postendocytic trafficking of the epidermal growth factor receptor through endosomal retention. *Journal Biological Chemistry* **269**: 12865-12873
- Hofer R, Briesen I, Beck M, Pinot F, Schreiber L, Franke R** (2008) The Arabidopsis cytochrome P450 CYP86A1 encodes a fatty acid omega-hydroxylase involved in suberin monomer biosynthesis. *Journal Experimental Botany* **59**: 2347-2360
- Hothorn M, Belkhadir Y, Dreux M, Dabi T, Noel JP, Wilson IA, Chory J** (2011) Structural basis of steroid hormone perception by the receptor kinase BRI1. *Nature* **474**: 467-471
- Hsieh M-y, Yang S, Raymond-Stinz M, Edwards J, Wilson B** (2010) Spatio-temporal modeling of signaling protein recruitment to EGFR. *BMC Systems Biology* **4**: 57
- Hubbard SR, Miller WT** (2007) Receptor tyrosine kinases: mechanisms of activation and signaling. *Current opinion in Cell Biology* **19**: 117-123
- Ibañez M, Fàbregas N, Chory J, Caño-Delgado AI** (2009) Brassinosteroid signaling and auxin transport are required to establish the periodic pattern of Arabidopsis shoot vascular bundles. *Proceedings of the National Academy of Sciences of the United States of America* **106**: 13630-13635
- Irani NG, Di Rubbo S, Mylle E, Van den Begin J, Schneider-Pizon J, Hnilikova J, Sisa M, Buyst D, Vilarrasa-Blasi J, Szatmari AM, Van Damme D, Mishev K, Codreanu MC, Kohout L, Strnad M, Caño-Delgado AI, Friml J, Madder A, Russinova E** (2012) Fluorescent castasterone reveals BRI1 signaling from the plasma membrane. *Nature Chemical Biology* **8**: 583-589

- Jaillais Y, Belkhadir Y, Balsemao-Pires E, Dangl JL, Chory J** (2011) Extracellular leucine-rich repeats as a platform for receptor/coreceptor complex formation. *Proceedings of the National Academy of Sciences of the United States of America* **108**: 8503-8507
- Jaillais Y, Hothorn M, Belkhadir Y, Dabi T, Nimchuk ZL, Meyerowitz EM, Chory J** (2011) Tyrosine phosphorylation controls brassinosteroid receptor activation by triggering membrane release of its kinase inhibitor. *Genes & Development* **25**: 232-237
- Jaillais Y, Vert G** (2012) Brassinosteroids, gibberellins and light-mediated signalling are the three-way controls of plant sprouting. *Nature Cell Biology* **14**: 788-790
- Jeong YJ, Shang Y, Kim BH, Kim SY, Song JH, Lee JS, Lee MM, Li J, Nam KH** (2010) BAK7 displays unequal genetic redundancy with BAK1 in brassinosteroid signaling and early senescence in Arabidopsis. *Molecules and Cells* **29**: 259-266
- Jinn TL, Stone JM, Walker JC** (2000) HAESA, an Arabidopsis leucine-rich repeat receptor kinase, controls floral organ abscission. *Genes and Development* **14**: 108-117
- Kang B, Wang H, Nam KH, Li J** (2010) Activation-tagged suppressors of a weak brassinosteroid receptor mutant. *Molecular Plant* **3**: 260-268
- Karlova R, Boeren S, Russinova E, Aker J, Vervoort J, De Vries S** (2006) The Arabidopsis SOMATIC EMBRYOGENESIS RECEPTOR-LIKE KINASE1 protein complex includes BRASSINOSTEROID-INSENSITIVE1. *Plant Cell* **18**: 626-638
- Kato N, He H, Steger AP** (2010) A systems model of vesicle trafficking in Arabidopsis pollen tubes. *Plant Physiology* **152**: 590-601
- Keller A, Backes C, Al-Awadhi M, Gerasch A, Kuntzer J, Kohlbacher O, Kaufmann M, Lenhof HP** (2008) GeneTrailExpress: a web-based pipeline for the statistical evaluation of microarray experiments. *BMC Bioinformatics* **9**: 552
- Kemmerling B, Schwedt A, Rodriguez P, Mazzotta S, Frank M, Qamar SA, Mengiste T, Betsuyaku S, Parker JE, Mussig C, Thomma BP, Albrecht C, de Vries SC, Hirt H, Nurnberger T** (2007) The BRI1-associated kinase 1, BAK1, has a brassinolide-independent role in plant cell-death control. *Current Biology* **17**: 1116-22
- Kholodenko BN** (2006) Cell-signalling dynamics in time and space. *Nature Reviews Molecular Cell Biology* **7**: 165-176
- Kim BH, Kim SY, Nam KH** (2013) Assessing the diverse functions of BAK1 and its homologs in arabidopsis, beyond BR signaling and PTI responses. *Molecules and Cells* **35**: 7-16
- Kim TW, Guan S, Burlingame A, Wang ZY** (2011) The CDG1 Kinase Mediates Brassinosteroid Signal Transduction from BRI1 Receptor Kinase to BSU1 Phosphatase and GSK3-like Kinase BIN2. *Molecular Cell* **43**: 561-571
- Kim TW, Guan S, Sun Y, Deng Z, Tang W, Shang JX, Sun Y, Burlingame AL, Wang ZY** (2009) Brassinosteroid signal transduction from cell-surface receptor kinases to nuclear transcription factors. *Nature Cell Biology* **11**: 1254-1260
- Kino T, Su YA, Chrousos GP** (2009) Human glucocorticoid receptor isoform beta: recent understanding of its potential implications in physiology and pathophysiology. *Cellular and Molecular Life Sciences* **66**: 3435-3448
- Kinoshita T, Caño-Delgado A, Seto H, Hiranuma S, Fujioka S, Yoshida S, Chory J** (2005) Binding of brassinosteroids to the extracellular domain of plant receptor kinase BRI1. *Nature* **433**: 167-171
- Kirik V, Bouyer D, Schobinger U, Bechtold N, Herzog M, Bonneville JM, Hulskamp M** (2001) CPR5 is involved in cell proliferation and cell death control and encodes a novel transmembrane protein. *Current Biology* **11**: 1891-1895
- Kito K, Ito T** (2008) Mass spectrometry-based approaches toward absolute quantitative proteomics. *Current Genomics* **9**: 263-274

- Klein P, Mattoon D, Lemmon MA, Schlessinger J** (2004) A structure-based model for ligand binding and dimerization of EGF receptors. *Proceedings of the National Academy of Sciences of the United States of America* **101**: 929-934
- Klipp E, Liebermeister W** (2006) Mathematical modeling of intracellular signaling pathways. *BMC Neuroscience* doi:10.1186/1471-2202-7-S1-S10
- Klipp E, Liebermeister W, Wierling C, Kowald A, Lehrach H, Herwig H** (2009). *Systems Biology: A Textbook*. ISBN:978-3-527-31874-2, Wiley-Blackwell, Weinheim. **1**: 181-184.
- Kobayashi K, Baba S, Obayashi T, Sato M, Toyooka K, Keranen M, Aro EM, Fukaki H, Ohta H, Sugimoto K, Masuda T** (2012) Regulation of root greening by light and auxin/cytokinin signaling in Arabidopsis. *Plant Cell* **24**: 1081-1095
- Kondo S, Iwashita M, Yamaguchi M** (2009) How animals get their skin patterns: fish pigment pattern as a live Turing wave. *The International Journal of Developmental Biology* **53**: 851-856
- Kondo S, Miura T** (2010) Reaction-diffusion model as a framework for understanding biological pattern formation. *Science* **329**: 1616-1620
- Krall JA, Beyer EM, MacBeath G** (2011) High- and low-affinity epidermal growth factor receptor-ligand interactions activate distinct signaling pathways. *PLoS One* **6**: e15945
- Kuszynski CA, Miller KA, Rizzino A** (1993) Influence of cell density and receptor number on the binding and distribution of cell surface epidermal growth factor receptors. In *Vitro Cellular and Developmental Biology - Animal* **29A**: 708-713
- Kwaaitaal M, Schor M, Hink MA, Visser AJ, de Vries SC** (2011) Fluorescence Correlation Spectroscopy and Fluorescence Recovery After Photobleaching to study receptor kinase mobility in planta. *Methods in Molecular Biology* **779**: 225-242
- Kwaaitaal MACJ, de Vries SC** (2007) The SERK1 gene is expressed in procambium and immature vascular cells. *Journal of Experimental Botany* **58**: 2887-2896
- Lamesch P, Berardini TZ, Li D, Swarbreck D, Wilks C, Sasidharan R, Muller R, Dreher K, Alexander DL, Garcia-Hernandez M, Karthikeyan AS, Lee CH, Nelson WD, Ploetz L, Singh S, Wensel A, Huala E** (2012) The Arabidopsis Information Resource (TAIR): improved gene annotation and new tools. *Nucleic Acids Research* **40**: D1202-1210
- Laskowski M, Grieneisen VA, Hofhuis H, Hove CA, Hogeweg P, Marée AF, Scheres B** (2008) Root system architecture from coupling cell shape to auxin transport. *PLoS Biology* **6**
- Lemmon MA, Schlessinger J** (2010) Cell signaling by receptor tyrosine kinases. *Cell* **141**: 1117-1134
- Lewis MW, Leslie ME, Fulcher EH, Darnielle L, Healy PN, Youn JY, Liljegren SJ** (2010) The SERK1 receptor-like kinase regulates organ separation in Arabidopsis flowers. *Plant Journal* **62**: 817-828
- Li E, Placone J, Merzlyakov M, Hristova K** (2008) Quantitative measurements of protein interactions in a crowded cellular environment. *Analytical Chemistry* **80**: 5976-5985
- Li J** (2010) Multi-tasking of somatic embryogenesis receptor-like protein kinases. *Current Opinion in Plant Biology* **13**: 509-514
- Li J, Chory J** (1997) A Putative Leucine-Rich Repeat Receptor Kinase Involved in Brassinosteroid Signal Transduction. *Cell* **90**: 929-938
- Li J, Nagpal P, Vitart V, McMorris TC, Chory J** (1996) A role for brassinosteroids in light-dependent development of Arabidopsis. *Science* **272**: 398-401
- Li J, Nam KH** (2002) Regulation of brassinosteroid signaling by a GSK3/SHAGGY-like kinase. *Science* **295**: 1299-1301

- Li J, Wen J, Lease KA, Doke JT, Tax FE, Walker JC** (2002) BAK1, an Arabidopsis LRR Receptor-like Protein Kinase, Interacts with BRI1 and Modulates Brassinosteroid Signaling. *Cell* **110**: 213-222
- Li Y, Beisson F, Koo AJ, Molina I, Pollard M, Ohlrogge J** (2007) Identification of acyltransferases required for cutin biosynthesis and production of cutin with suberin-like monomers. *Proceedings of the National Academy of Sciences of the United States of America* **104**: 18339-18344
- Lin K, Kools H, de Groot PJ, Gavai AK, Basnet RK, Cheng F, Wu J, Wang X, Lommen A, Hooiveld GJ, Bonnema G, Visser RG, Muller MR, Leunissen JA** (2011) MADMAX - Management and analysis database for multiple -omics experiments. *J Integr Bioinform* **8**: 160
- Lingwood D, Kaiser HJ, Levental I, Simons K** (2009) Lipid rafts as functional heterogeneity in cell membranes. *Biochemical Society Transactions* **37**: 955-960
- Liu J, Mehdi S, Topping J, Tarkowski P, Lindsey K** (2010) Modelling and experimental analysis of hormonal crosstalk in Arabidopsis. *Molecular Systems Biology* **6**: 373
- Lu D, Wu S, Gao X, Zhang Y, Shan L, He P** (2010) A receptor-like cytoplasmic kinase, BIK1, associates with a flagellin receptor complex to initiate plant innate immunity. *Proceedings of the National Academy of Sciences of the United States of America* **107**: 496-501
- Lu P, Vogel C, Wang R, Yao X, Marcotte EM** (2007) Absolute protein expression profiling estimates the relative contributions of transcriptional and translational regulation. *Nature Biotechnology* **25**: 117-124
- Luo XM, Lin WH, Zhu S, Zhu JY, Sun Y, Fan XY, Cheng M, Hao Y, Oh E, Tian M, Liu L, Zhang M, Xie Q, Chong K, Wang ZY** (2010) Integration of Light- and Brassinosteroid-Signaling Pathways by a GATA Transcription Factor in Arabidopsis. *Developmental Cell* **19**: 872-883
- Macdonald JL, Pike LJ** (2008) Heterogeneity in EGF-binding affinities arises from negative cooperativity in an aggregating system. *Proceedings of the National Academy of Sciences of the United States of America* **105**: 112-117
- Malamy JE, Benfey PN** (1997) Organization and cell differentiation in lateral roots of Arabidopsis thaliana. *Development* **124**: 33-44
- Marmor MD, Yarden Y** (2004) Role of protein ubiquitylation in regulating endocytosis of receptor tyrosine kinases. *Oncogene* **23**: 2057-2070
- Martinière A, Lavagi I, Nageswaran G, Rolfe DJ, Maneta-Peyret L, Luu DT, Botchway SW, Webb SE, Mongrand S, Maurel C, Martin-Fernandez ML, Kleine-Vehn J, Friml J, Moreau P, Runions J** (2012) Cell wall constrains lateral diffusion of plant plasma-membrane proteins. *Proceedings of the National Academy of Sciences of the United States of America* **109**: 12805-12810
- Masubelele NH, Dewitte W, Menges M, Maughan S, Collins C, Huntley R, Nieuwland J, Scofield S, Murray JA** (2005) D-type cyclins activate division in the root apex to promote seed germination in Arabidopsis. *Proceedings of the National Academy of Sciences of the United States of America* **102**: 15694-15699
- Mathur J** (2007) The illuminated plant cell. *Trends in Plant Science* **12**: 506-513
- Meinhardt H** (2008) Models of biological pattern formation: from elementary steps to the organization of embryonic axes. *Current Topics in Developmental Biology* **81**: 1-63
- Meissner O, Haberlein H** (2003) Lateral mobility and specific binding to GABA(A) receptors on hippocampal neurons monitored by fluorescence correlation spectroscopy. *Biochemistry* **42**: 1667-1672
- Mendoza L, Xenarios I** (2006) A method for the generation of standardized qualitative dynamical systems of regulatory networks. *Theoretical Biology and Medical Modelling* **3**: 13

- Michaelis L, Menten ML** (1913) Die Kinetik der Invertinwirkung. *Biochem. Z.* **49**: 333-369
- Middleton AM, Ubeda-Tomas S, Griffiths J, Holman T, Hedden P, Thomas SG, Phillips AL, Holdsworth MJ, Bennett MJ, King JR, Owen MR** (2012) Mathematical modeling elucidates the role of transcriptional feedback in gibberellin signaling. *Proceedings of the National Academy of Sciences of the United States of America* **109**: 7571-7576
- Molfetta R, Gasparrini F, Santoni A, Paolini R** (2010) Ubiquitination and endocytosis of the high affinity receptor for IgE. *Molecular Immunology* **47**: 2427-2434
- Mora-García S, Vert G, Yin Y, Caño-Delgado A, Cheong H, Chory J** (2004) Nuclear protein phosphatases with Kelch-repeat domains modulate the response to brassinosteroids in *Arabidopsis*. *Genes and Development* **18**: 448-460
- Moseyko N, Feldman LJ** (2001) Expression of pH-sensitive green fluorescent protein in *Arabidopsis thaliana*. *Plant, Cell & Environment* **24**: 557-563
- Mouchel CF, Briggs GC, Hardtke CS** (2004) Natural genetic variation in *Arabidopsis* identifies BREVIS RADIX, a novel regulator of cell proliferation and elongation in the root. *Genes & Development* **18**: 700-714
- Mouchel CF, Osmont KS, Hardtke CS** (2006) BRX mediates feedback between brassinosteroid levels and auxin signalling in root growth. *Nature* **443**: 458-461
- Muraro D, Byrne H, King J, Bennett M** (2013) The role of auxin and cytokinin signalling in specifying the root architecture of *Arabidopsis thaliana*. *Journal of Theoretical Biology* **317**: 71-86
- Muraro D, Byrne H, King J, Voss U, Kieber J, Bennett M** (2011) The influence of cytokinin-auxin cross-regulation on cell-fate determination in *Arabidopsis thaliana* root development. *Journal of Theoretical Biology* **283**: 152-167
- Müssig C, Shin GH, Altmann T** (2003) Brassinosteroids Promote Root Growth in *Arabidopsis*. *Plant Physiology* **133**: 1261-1271
- Nagata N, Min YK, Nakano T, Asami T, Yoshida S** (2000) Treatment of dark-grown *Arabidopsis thaliana* with a brassinosteroid-biosynthesis inhibitor, brassinazole, induces some characteristics of light-grown plants. *Planta* **211**: 781-790
- Nam KH, Li J** (2002) BRI1/BAK1, a Receptor Kinase Pair Mediating Brassinosteroid Signaling. *Cell* **110**: 203-212
- Nawy T, Lee J-Y, Colinas J, Wang JY, Thongrod SC, Malamy JE, Birnbaum K, Benfey PN** (2005) Transcriptional Profile of the *Arabidopsis* Root Quiescent Center. *The Plant Cell* **17**: 1908-1925
- Nemhauser JL, Chory J** (2004) BRing it on: new insights into the mechanism of brassinosteroid action. *Journal of Experimental Botany* **55**: 265-270
- Nemhauser JL, Hong F, Chory J** (2006) Different Plant Hormones Regulate Similar Processes through Largely Nonoverlapping Transcriptional Responses. *Cell* **126**: 467-475
- Nemhauser JL, Mockler TC, Chory J** (2004) Interdependency of brassinosteroid and auxin signaling in *Arabidopsis*. *PLoS Biology* **2**: E258
- Neves SR, Iyengar R** (2002) Modeling of signaling networks. *BioEssays* **24**: 1110-1117
- Niederhuth CE, Patharkar OR, Walker JC** (2013) Transcriptional profiling of the *Arabidopsis* abscission mutant *hae hsl2* by RNA-Seq. *BMC Genomics* **14**: 37
- Noguchi T, Fujioka S, Choe S, Takatsuto S, Yoshida S, Yuan H, Feldmann KA, Tax FE** (1999) Brassinosteroid-insensitive dwarf mutants of *Arabidopsis* accumulate brassinosteroids. *Plant Physiology* **121**: 743-752
- North AJ** (2006) Seeing is believing? A beginners' guide to practical pitfalls in image acquisition. *Journal of Cell Biology* **172**: 9-18
- Ntoukakis V, Schwessinger B, Segonzac C, Zipfel C** (2011) Cautionary notes on the use of C-terminal BAK1 fusion proteins for functional studies. *Plant Cell* **23**: 3871-3878

- Oh E, Zhu JY, Wang ZY** (2012) Interaction between BZR1 and PIF4 integrates brassinosteroid and environmental responses. *Nature Cell Biology* **14**: 802-809
- Oh MH, Wang X, Clouse SD, Huber SC** (2012) Deactivation of the Arabidopsis BRASSINOSTEROID INSENSITIVE 1 (BRI1) receptor kinase by autophosphorylation within the glycine-rich loop. *Proceedings of the National Academy of Sciences of the United States of America* **109**: 327-332
- Owen DM, Williamson DJ, Magenau A, Gaus K** (2012) Sub-resolution lipid domains exist in the plasma membrane and regulate protein diffusion and distribution. *Nature Communications* **3**: 1256
- Patterson SE** (2001) Cutting loose. Abscission and dehiscence in Arabidopsis. *Plant Physiology* **126**: 494-500
- Petricka JJ, Schauer MA, Megraw M, Breakfield NW, Thompson JW, Georgiev S, Soderblom EJ, Ohler U, Moseley MA, Grossniklaus U, Benfey PN** (2012) The protein expression landscape of the Arabidopsis root. *Proceedings of the National Academy of Sciences of the United States of America* **109**: 6811-6818
- Popescu SC, Popescu GV, Bachan S, Zhang Z, Seay M, Gerstein M, Snyder M, Dinesh-Kumar SP** (2007) Differential binding of calmodulin-related proteins to their targets revealed through high-density Arabidopsis protein microarrays. *Proceedings of the National Academy of Sciences of the United States of America* **104**: 4730-4735
- Popescu SC, Snyder M, Dinesh-Kumar S** (2007) Arabidopsis protein microarrays for the high-throughput identification of protein-protein interactions. *Plant Signal Behavior* **2**: 416-420
- Postel S, Kufner I, Beuter C, Mazzotta S, Schwedt A, Borlotti A, Halter T, Kemmerling B, Nurnberger T** (2010) The multifunctional leucine-rich repeat receptor kinase BAK1 is implicated in Arabidopsis development and immunity. *European Journal Cell Biology* **89**: 169-174
- Resat H, Ewald JA, Dixon DA, Wiley HS** (2003) An integrated model of epidermal growth factor receptor trafficking and signal transduction. *Biophysical Journal* **85**: 730-743
- Richards HA, Halfhill MD, Millwood RJ, Stewart CN, Jr.** (2003) Quantitative GFP fluorescence as an indicator of recombinant protein synthesis in transgenic plants. *Plant Cell Reports* **22**: 117-121
- Ries J, Yu SR, Burkhardt M, Brand M, Schwille P** (2009) Modular scanning FCS quantifies receptor-ligand interactions in living multicellular organisms. *Nature Methods* **6**: 643-645
- Ritchie K, Shan XY, Kondo J, Iwasawa K, Fujiwara T, Kusumi A** (2005) Detection of non-Brownian diffusion in the cell membrane in single molecule tracking. *Biophysical Journal* **88**: 2266-2277
- Roberts JA, Whitelaw CA, Gonzalez-Carranza ZH, McManus MT** (2000) Cell Separation Processes in Plants—Models, Mechanisms and Manipulation. *Annals of Botany* **86**: 223-235
- Roux M, Schwessinger B, Albrecht C, Chinchilla D, Jones A, Holton N, Malinovskiy FG, Tör M, de Vries S, Zipfel C** (2011) The Arabidopsis leucine-rich repeat receptor-like kinases BAK1/SERK3 and BKK1/SERK4 are required for innate immunity to hemibiotrophic and biotrophic pathogens. *Plant Cell* **23**: 2440-2455
- Ruffel S, Krouk G, Coruzzi GM** (2010) A systems view of responses to nutritional cues in Arabidopsis: toward a paradigm shift for predictive network modeling. *Plant Physiology* **152**: 445-452
- Russinova E, Borst JW, Kwaaitaal M, Caño-Delgado A, Yin Y, Chory J, de Vries SC** (2004) Heterodimerization and endocytosis of Arabidopsis brassinosteroid receptors BRI1 and AtSERK3 (BAK1). *Plant Cell* **16**: 3216-3229

- Ryu H, Cho H, Kim K, Hwang I** (2010) Phosphorylation dependent nucleocytoplasmic shuttling of BES1 is a key regulatory event in brassinosteroid signaling. *Molecular Cells* **29**: 283-290
- Ryu H, Kim K, Cho H, Park J, Choe S, Hwang I** (2007) Nucleocytoplasmic Shuttling of BZR1 Mediated by Phosphorylation Is Essential in Arabidopsis Brassinosteroid Signaling. *The Plant Cell* **19**: 2749-2762
- Sankar M, Osmont KS, Rolcik J, Gujas B, Tarkowska D, Strnad M, Xenarios I, Hardtke CS** (2011) A qualitative continuous model of cellular auxin and brassinosteroid signaling and their crosstalk. *Bioinformatics* **27**: 1404-1412
- Santner A, Calderon-Villalobos LI, Estelle M** (2009) Plant hormones are versatile chemical regulators of plant growth. *Nature Chemical Biology* **5**: 301-307
- Savaldi-Goldstein S, Peto C, Chory J** (2007) The epidermis both drives and restricts plant shoot growth. *Nature* **446**: 199-202
- Sawano A, Takayama S, Matsuda M, Miyawaki A** (2002) Lateral Propagation of EGF Signaling after Local Stimulation Is Dependent on Receptor Density. *Developmental Cell* **3**: 245-257
- Schleifenbaum F, Elgass K, Sackrow M, Caesar K, Berendzen K, Meixner AJ, Harter K** (2010) Fluorescence intensity decay shape analysis microscopy (FIDSAM) for quantitative and sensitive live-cell imaging: a novel technique for fluorescence microscopy of endogenously expressed fusion-proteins. *Molecular Plant* **3**: 555-562
- Schmid J, A., Neumeier H** (2005) Evolutions in Science Triggered by Green Fluorescent Protein (GFP). *ChemBioChem* **6**: 1149-1156
- Schoeberl B, Eichler-Jonsson C, Gilles ED, Muller G** (2002) Computational modeling of the dynamics of the MAP kinase cascade activated by surface and internalized EGF receptors. *Nature Biotechnology* **20**: 370-375
- Schulze B, Mentzel T, Jehle AK, Mueller K, Beeler S, Boller T, Felix G, Chinchilla D** (2010) Rapid heteromerization and phosphorylation of ligand-activated plant transmembrane receptors and their associated kinase BAK1. *Journal of Biological Chemistry* **285**: 9444-9451
- Schwessinger B, Roux M, Kadota Y, Ntoukakis V, Sklenar J, Jones A, Zipfel C** (2011) Phosphorylation-Dependent Differential Regulation of Plant Growth, Cell Death, and Innate Immunity by the Regulatory Receptor-Like Kinase BAK1. *PLoS Genetics* **7(4)**: e1002046.
- Seguí-Simarro J, Staehelin L** (2006) Cell cycle-dependent changes in Golgi stacks, vacuoles, clathrin-coated vesicles and multivesicular bodies in meristematic cells of *Arabidopsis thaliana*: A quantitative and spatial analysis. *Planta* **223**: 223-236
- Shankaran H, Resat H, Wiley HS** (2007) Cell surface receptors for signal transduction and ligand transport: a design principles study. *PLoS Computational Biology* **3**: e101
- Shankaran H, Wiley HS, Resat H** (2006) Modeling the effects of HER/ErbB1-3 coexpression on receptor dimerization and biological response. *Biophysical Journal* **90**: 3993-4009
- She J, Han Z, Kim TW, Wang J, Cheng W, Chang J, Shi S, Yang M, Wang ZY, Chai J** (2011) Structural insight into brassinosteroid perception by BRI1. *Nature* **474**: 472-476
- Shimada Y, Goda H, Nakamura A, Takatsuto S, Fujioka S, Yoshida S** (2003) Organ-specific expression of brassinosteroid-biosynthetic genes and distribution of endogenous brassinosteroids in Arabidopsis. *Plant Physiology* **131**: 287-297
- Shiu SH, Bleecker AB** (2001) Receptor-like kinases from Arabidopsis form a monophyletic gene family related to animal receptor kinases. *Proceedings of the National Academy of Sciences of the United States of America* **98**: 10763-10768

- Shiu SH, Karlowski WM, Pan R, Tzeng YH, Mayer KFX, Li WH** (2004) Comparative analysis of the receptor-like kinase family in Arabidopsis and rice. *Plant Cell* **16**: 1220-1234
- Smolen G, Bender J** (2002) Arabidopsis cytochrome P450 cyp83B1 mutations activate the tryptophan biosynthetic pathway. *Genetics* **160**: 323-332
- Smyth GK** (2004) Linear models and empirical bayes methods for assessing differential expression in microarray experiments. *Stat Appl Genetica and Molecular Biology* **3**: Article3
- Song L, Zhou XY, Li L, Xue LJ, Yang X, Xue HW** (2009) Genome-wide analysis revealed the complex regulatory network of brassinosteroid effects in photomorphogenesis. *Molecular Plant* **2**: 755-772
- Sorkin A, von Zastrow M** (2002) Signal transduction and endocytosis: close encounters of many kinds. *Nature Reviews Molecular Cell Biology* **3**: 600-614
- Stenvik GE, Tandstad NM, Guo Y, Shi CL, Kristiansen W, Holmgren A, Clark SE, Aalen RB, Butenko MA** (2008) The EPIP peptide of INFLORESCENCE DEFICIENT IN ABSCISSION is sufficient to induce abscission in arabidopsis through the receptor-like kinases HAESA and HAESA-LIKE2. *Plant Cell* **20**: 1805-1817
- Sugiyama Y, Kawabata I, Sobue K, Okabe S** (2005) Determination of absolute protein numbers in single synapses by a GFP-based calibration technique. *Nature Methods* **2**: 677-684
- Sun L, van Nocker S** (2010) Analysis of promoter activity of members of the PECTATE LYASE-LIKE (PLL) gene family in cell separation in Arabidopsis. *BMC Plant Biol* **10**: 152
- Sun Y, Fan XY, Cao DM, Tang W, He K, Zhu JY, He JX, Bai MY, Zhu S, Oh E, Patil S, Kim TW, Ji H, Wong WH, Rhee SY, Wang ZY** (2010) Integration of Brassinosteroid Signal Transduction with the Transcription Network for Plant Growth Regulation in Arabidopsis. *Developmental Cell* **19**: 765-777
- Szekeres M, Németh K, Koncz-Kálmán Z, Mathur J, Kauschmann A, Altmann T, Rédei GP, Nagy F, Schell J, Koncz C** (1996) Brassinosteroids rescue the deficiency of CYP90, a cytochrome P450, controlling cell elongation and de-etiolation in Arabidopsis. *Cell* **85**: 171-182
- Takano J, Miwa K, Yuan L, von Wiren N, Fujiwara T** (2005) Endocytosis and degradation of BOR1, a boron transporter of Arabidopsis thaliana, regulated by boron availability. *Proceedings of the National Academy of Sciences of the United States of America* **102**: 12276-12281
- Tang W, Kim TW, Osés-Prieto JA, Sun Y, Deng Z, Zhu S, Wang R, Burlingame AL, Wang ZY** (2008) BSKs mediate signal transduction from the receptor kinase BRI1 in Arabidopsis. *Science* **321**: 557-560
- Tang W, Yuan M, Wang R, Yang Y, Wang C, Osés-Prieto JA, Kim TW, Zhou HW, Deng Z, Gampala SS, Gendron JM, Jonassen EM, Lillo C, DeLong A, Burlingame AL, Sun Y, Wang ZY** (2011) PP2A activates brassinosteroid-responsive gene expression and plant growth by dephosphorylating BZR1. *Nature Cell Biology* **13**: 124-131
- Tantikanjana T, Mikkelsen MD, Hussain M, Halkier BA, Sundaresan V** (2004) Functional analysis of the tandem-duplicated P450 genes SPS/BUS/CYP79F1 and CYP79F2 in glucosinolate biosynthesis and plant development by Ds transposition-generated double mutants. *Plant Physiology* **135**: 840-848
- Teramura Y, Ichinose J, Takagi H, Nishida K, Yanagida T, Sako Y** (2006) Single-molecule analysis of epidermal growth factor binding on the surface of living cells. *EMBO Journal* **25**: 4215-4222

- Thimm O, Blasing O, Gibon Y, Nagel A, Meyer S, Kruger P, Selbig J, Muller LA, Rhee SY, Stitt M** (2004) MAPMAN: a user-driven tool to display genomics data sets onto diagrams of metabolic pathways and other biological processes. *Plant Journal* **37**: 914-939
- Torii KU, Mitsukawa N, Oosumi T, Matsuura Y, Yokoyama R, Whittier RF, Komeda Y** (1996) The Arabidopsis ERECTA gene encodes a putative receptor protein kinase with extracellular leucine-rich repeats. *Plant Cell* **8**: 735-746
- Tranchant T, Durand G, Gauthier C, Crepieux P, Ulloa-Aguirre A, Royere D, Reiter E** (2010) Preferential beta-arrestin signalling at low receptor density revealed by functional characterization of the human FSH receptor A189 V mutation. *Molecular Cell Endocrinology* **331**: 109-118
- Turing AM** (1952) The chemical basis of morphogenesis. *Phil. Trans. R. Soc. Lond.* **237**: 37-72
- Uyemura T, Takagi H, Yanagida T, Sako Y** (2005) Single-molecule analysis of epidermal growth factor signaling that leads to ultrasensitive calcium response. *Biophysical Journal* **88**: 3720-3730
- van de Mortel JE, de Vos RC, Dekkers E, Pineda A, Guillod L, Bouwmeester K, van Loon JJ, Dicke M, Raaijmakers JM** (2012) Metabolic and transcriptomic changes induced in Arabidopsis by the rhizobacterium *Pseudomonas fluorescens* SS101. *Plant Physiology* **160**: 2173-2188
- van Esse GW, Harter K, S.C. DV** (2013) Computational modelling of the BRI1 receptor system. *Plant Cell and Environment* doi: 10.1111/pce.12077
- van Esse GW, van Mourik S, Stigter H, Ten Hove CA, Molenaar J, de Vries SC** (2012) A Mathematical Model for BRASSINOSTEROID INSENSITIVE1-Mediated Signaling in Root Growth and Hypocotyl Elongation. *Plant Physiology* **160**: 523-532
- van Esse WG, Westphal AH, Surendran RP, Albrecht C, van Veen B, Borst JW, de Vries SC** (2011) Quantification of the brassinosteroid insensitive1 receptor in *Planta*. *Plant Physiology* **156**: 1691-1700
- van Mourik S, Kaufmann K, van Dijk AD, Angenent GC, Merks RM, Molenaar J** (2012) Simulation of organ patterning on the floral meristem using a polar auxin transport model. *PLoS One* **7**: e28762
- van Mourik S, van Dijk AD, de Gee M, Immink RG, Kaufmann K, Angenent GC, van Ham RC, Molenaar J** (2010) Continuous-time modeling of cell fate determination in Arabidopsis flowers. *BMC Systems Biology* **4**: 101
- Vandepoele K, Raes J, De Veylder L, Rouze P, Rombauts S, Inze D.** (2002) Genome-wide analysis of core cell cycle genes in Arabidopsis. *Plant Cell* **4**: 903-916
- van Royen ME, Farla P, Mattern KA, Geverts B, Trapman J, Houtsmuller AB** (2009) Fluorescence recovery after photobleaching (FRAP) to study nuclear protein dynamics in living cells. *Methods in Molecular Biology* **464**: 363-385
- Verbelen JP, De Cnodder T, Le J, Vissenberg K, Baluska F** (2006) The Root Apex of Arabidopsis thaliana Consists of Four Distinct Zones of Growth Activities: Meristematic Zone, Transition Zone, Fast Elongation Zone and Growth Terminating Zone. *Plant Signal Behavior* **1**: 296-304
- Vernoux T, Brunoud G, Farcot E, Morin V, Van Den Daele H, Legrand J, Oliva M, Das P, Larrieu A, Wells D, Guédon Y, Armitage L, Picard F, Guyomarc'H S, Cellier C, Parry G, Koumproglou R, Doonan JH, Estelle M, Godin C, Kepinski S, Bennett M, De Veylder L, Traas J** (2011) The auxin signalling network translates dynamic input into robust patterning at the shoot apex. *Molecular Systems Biology* **7**: 508
- Vert G, Chory J** (2011) Crosstalk in Cellular Signaling: Background Noise or the Real Thing? *Developmental Cell* **21**: 985-991

- Vert G, Walcher CL, Chory J, Nemhauser JL** (2008) Integration of auxin and brassinosteroid pathways by Auxin Response Factor 2. *Proceedings of the National Academy of Sciences of the United States of America* **105**: 9829-9834
- Verveer PJ, Bastiaens PI** (2008) Quantitative microscopy and systems biology: seeing the whole picture. *Histochemistry and Cell Biology* **130**: 833-843
- Verveer PJ, Wouters FS, Reynolds AR, Bastiaens PIH** (2000) Quantitative imaging of lateral ErbB1 receptor signal propagation in the plasma membrane. *Science* **290**: 1567-1570
- Viotti C, Bubeck J, Stierhof Y-D, Krebs M, Langhans M, van den Berg W, van Dongen W, Richter S, Geldner N, Takano J, Jurgens G, de Vries SC, Robinson DG, Schumacher K** (2010) Endocytic and Secretory Traffic in Arabidopsis Merge in the Trans-Golgi Network/Early Endosome, an Independent and Highly Dynamic Organelle. *The Plant Cell* **22**: 1344-1357
- Wang L, Wang Z, Xu Y, Joo SH, Kim SK, Xue Z, Xu Z, Chong K** (2009) OsGSR1 is involved in crosstalk between gibberellins and brassinosteroids in rice. *Plant Journal* **57**: 498-510
- Wang X, Chory J** (2006) Brassinosteroids regulate dissociation of BKI1, a negative regulator of BRI1 signaling, from the plasma membrane. *Science* **313**: 1118-1122
- Wang X, Goshe MB, Soderblom EJ, Phinney BS, Kuchar JA, Li J, Asami T, Yoshida S, Huber SC, Clouse SD** (2005) Identification and Functional Analysis of in Vivo Phosphorylation Sites of the Arabidopsis BRASSINOSTEROID-INSENSITIVE1 Receptor Kinase. *The Plant Cell*, **17**: 1685-1703
- Wang X, Kota U, He K, Blackburn K, Li J, Goshe MB, Huber SC, Clouse SD** (2008) Sequential transphosphorylation of the BRI1/BAK1 receptor kinase complex impacts early events in brassinosteroid signaling. *Developmental Cell* **15**: 220-235
- Wang Z-Y, Nakano T, Gendron J, He J, Chen M, Vafeados D, Yang Y, Fujioka S, Yoshida S, Asami T, Chory J** (2002) Nuclear-Localized BZR1 Mediates Brassinosteroid-Induced Growth and Feedback Suppression of Brassinosteroid Biosynthesis. *Developmental Cell* **2**: 505-513
- Wang Z-Y, Seto H, Fujioka S, Yoshida S, Chory J** (2001) BRI1 is a critical component of a plasma-membrane receptor for plant steroids. *Nature* **410**: 380-383
- Wang ZY, Bai MY, Oh E, Zhu JY** (2012) Brassinosteroid signaling network and regulation of photomorphogenesis. *Annual Review of Genetics* **46**: 701-724
- Wang ZY, Wang Q, Chong K, Wang F, Wang L, Bai M, Jia C** (2006) The brassinosteroid signal transduction pathway. *Cell Research* **16**: 427-434
- Warren CM, Landgraf R** (2006) Signaling through ERBB receptors: Multiple layers of diversity and control. *Cellular Signalling* **18**: 923-933
- Wiley HS** (2003) Trafficking of the ErbB receptors and its influence on signaling. *Experimental Cell Research* **284**: 78-88
- Wiley HS, Walsh BJ, Lund KA** (1989) Global modulation of the epidermal growth factor receptor is triggered by occupancy of only a few receptors. Evidence for a binary regulatory system in normal human fibroblasts. *Journal of Biological Chemistry* **264**: 18912-18920
- Willemse J, Kulikova O, de Jong H, Bisseling T** (2008) A new whole-mount DNA quantification method and the analysis of nuclear DNA content in the stem-cell niche of Arabidopsis roots. *Plant Journal* **55**: 886-894
- Witthoft J, Caesar K, Elgass K, Huppenberger P, Kilian J, Schleifenbaum F, Oecking C, Harter K** (2011) The activation of the Arabidopsis P-ATPase 1 by the brassinosteroid receptor BRI1 is independent of threonine 948 phosphorylation. *Plant Signal Behavior* **6**: 1063-1066

- Wolf S, Mravec J, Greiner S, Mouille G, Hofte H** (2012) Plant cell wall homeostasis is mediated by brassinosteroid feedback signaling. *Current Biology* **22**: 1732-1737
- Wu G, Wang X, Li X, Kamiya Y, Otegui MS, Chory J** (2011) Methylation of a phosphatase specifies dephosphorylation and degradation of activated brassinosteroid receptors. *Science Signaling* **4**
- Wu J-Q, Pollard TD** (2005) Counting Cytokinesis Proteins Globally and Locally in Fission Yeast. *Science* **310**: 310-314
- Wu JQ, McCormick CD, Pollard TD** (2008) Counting Proteins in Living Cells by Quantitative Fluorescence Microscopy with Internal Standards. *In* JJ Correia, IHW Detrich, eds, *Methods in Cell Biology* **89**: 253-273
- Wu Z, Irizarry RA, Gentleman R, Martinez-Murillo F, Spencer F** (2004) A Model-Based Background Adjustment for Oligonucleotide Expression Arrays. *Journal of the American Statistical Association* **99**: 909-917
- Xu W, Huang J, Li B, Li J, Wang Y** (2008) Is kinase activity essential for biological functions of BRI1? *Cell Research* **18**: 472-478
- Ye H, Li L, Yin Y** (2011) Recent advances in the regulation of brassinosteroid signaling and biosynthesis pathways. *Journal of Integrative Plant Biology* **53**: 455-468
- Yin Y, Wang ZY, Mora-Garcia S, Li J, Yoshida S, Asami T, Chory J** (2002) BES1 accumulates in the nucleus in response to brassinosteroids to regulate gene expression and promote stem elongation. *Cell* **109**: 181-191
- Yu X, Li L, Zola J, Aluru M, Ye H, Foudree A, Guo H, Anderson S, Aluru S, Liu P, Rodermeel S, Yin Y** (2011) A brassinosteroid transcriptional network revealed by genome-wide identification of BES1 target genes in *Arabidopsis thaliana*. *Plant Journal* **65**: 634-646
- Yu X, Li L, Zola J, Aluru M, Ye H, Foudree A, Guo H, Anderson S, Aluru S, Liu P, Rodermeel S, Yin Y** (2011) A brassinosteroid transcriptional network revealed by genome-wide identification of BES1 target genes in *Arabidopsis thaliana*. *Plant Journal* **65**: 634-646
- Zipfel C, Kunze G, Chinchilla D, Caniard A, Jones JD, Boller T, Felix G** (2006) Perception of the bacterial PAMP EF-Tu by the receptor EFR restricts Agrobacterium-mediated transformation. *Cell* **125**: 749-760
- Zipfel C, Robatzek S, Navarro L, Oakeley EJ, Jones JD, Felix G, Boller T** (2004) Bacterial disease resistance in *Arabidopsis* through flagellin perception. *Nature* **428**: 764-767

SUMMARY

Being sessile by nature plants are continuously challenged by biotic and abiotic stress factors. At the cellular level, different stimuli are perceived and translated to the desired response. In order to achieve this, signal transduction cascades have to be interlinked. Complex networks of downstream targets as well as positive and negative regulatory elements are essential for proper signal transduction. This often complicates analysis of signal transduction cascades via genetic approaches as a mutation in one gene results in a pleiotropic phenotype. Pathway components can be placed in the signal transduction cascade based on genetics as well as biochemical interactions between proteins. This results in a signal transduction network which is based on Boolean logics; either the gene is there and is functional (on) or it's mutated and not functional (off). In such a genetic scheme, intermediate conditions and the effect of concentration on pathway components is not taken into account. Also, the effect of intermediate or transient activation states on signal transduction pathways is rarely included. In principle all proteins in a signal transduction network obey mass action laws suggesting that reaction rate and as a consequence the output of the signal depends on the concentration of the reactants. In addition, signals can be subjected to negative feedback thereby resulting in a signal that attenuates itself to maintain cellular homeostasis, or only responds to a stimulus temporarily and only when required. At the cellular level, the cell has to decipher all stimuli to enable the desired integrated cellular response. In this respect, concentration or amplitudes matter very much as the plant must not respond to background noise. Hence a cellular response will only be induced when a signal is above a certain threshold resulting in "switch like" behaviour of the system. Mathematical modelling can help to visualise and explain the temporal and concentration effects of pathway components on the output of signal transduction cascades. In order to do so, the signal transduction cascade needs to be well described with a clear and measurable response. Obviously, to know how receptor concentration affects the signalling output one has to know its numbers, and this was the starting point of the work described in this thesis. The final challenge was to describe the modulatory effect of SERK co-receptors on BR signalling. For this, SERK mediated BRI1 signalling was incorporated in a mathematical model that describes root growth and hypocotyl elongation based on the BRI1 receptor activity.

In **Chapter 1** the brassinosteroid signalling pathway as well as the role of SERK co-receptors on BRI1 mediated signalling is described. BRs are perceived by the plasma membrane localised Brassinosteroid insensitive 1 (BRI1) receptor. For its signalling, BRI1 completely depends on the presence of non-ligand binding co-receptors of the somatic embryogenesis receptor like kinase (SERK) co-receptor family. An added complexity is that SERK co-receptors associate with different main ligand perceiving receptors thereby affecting multiple signalling pathways simultaneously. Therefore, it is important to know how SERK co-receptors modulate the output of the main ligand perceiving receptor and how SERK co-receptors are distributed between the signal transduction cascades. The BRI1 signal transduction pathway is one of the best understood signal transduction cascades in Arabidopsis with clearly described ligands and associated phenotypes. For this reason, the focus of this study was on how SERK co-receptors affect BRI1 mediated signalling quantitatively using a mathematical modelling approach. This requires knowledge on the concentration of the main ligand perceiving receptor, SERK co-receptor and ligand levels. Since the BRI1 and SERK co-receptor concentration was unknown we set out to quantify the number of receptors in a cell. In **Chapter 2** a confocal microscopy based method is described that enables quantification of BRI1, SERK1 and SERK3 *in planta*. The number of BRI1 receptor molecules in root epidermal cells ranges from 22,000 in the meristem to 80,000 in the maturation zone. However, when taking into account differences in cell size, the root meristem cells have the same receptor density which reduces significantly in the maturation zone. The root meristem cells are thought to be most active in BR signalling, suggesting that receptor density rather than total number of BRI1 receptors affects the sensitivity of a cell for BRs.

The next question is, how the physiological response of the cell depends on both ligand stimulation of the receptor and on ligand concentration. To address this, a mathematical modelling approach was employed where the receptor - ligand concentrations were coupled to root growth and hypocotyl elongation as a downstream physiological readout for BR signalling (**Chapter 3**). Based on the BRI1 receptor activity the model faithfully predicts root growth as observed in *bri1* loss-of-function mutants. The model also predicts that a rather low number of receptor molecules are needed to initiate a physiological response. Interestingly, the “switch” between activation and inhibition of root growth depends on the BRI1 occupancy level. This suggests that BRI1 may be a core regulator based on activating different targets based on its occupancy level. Root growth is robust against reduction in the BRI1 receptor level but not to variation in the BR concentration. This indicates that BR signalling is mainly regulated via ligand availability and biochemical activity. Since BRI1 signalling is highly dependent on the presence of SERK co-receptors, it is important to determine how these co-

receptors affect the signalling output. Therefore, in **Chapter 4**, the BRI1 receptor model was extended with two co-receptors, SERK1 and SERK3. The model also takes into account BRI1 signalling independent of SERK1 and SERK3. This may occur due the activity of BRI1 alone, or due to interaction of BRI1 with another co-receptor, for example SERK4. It appears that roots of the *serk1serk3* double mutant are almost completely irresponsive for BRs while the hypocotyl is not, suggesting either a difference in co-receptor usage or a higher activity of BRI1 alone in the hypocotyl. The usage of different co-receptors may reflect a mechanism by which the sensitivity of a cell for BRs is regulated. It appears that co-receptors mainly act by increasing the magnitude of the response. In addition, *in silico* simulations confirm that BRI1 signalling is not impaired when the majority of SERK co-receptors operate in other signalling pathways. The presented model provides a starting point to incorporate the effect of other modulators of the BRI1 signal transduction cascade on a complex physiological response.

Current models for BRI1 mediated signalling postulate that SERK3 is recruited upon ligand binding. However, Fluorescence Recovery After Photo bleaching (FRAP) measurements described in **Chapter 5**, indicate that BRI1 receptors located in root meristem cells have a relatively low mobility. This suggests that BRI1 and SERK already form complexes in the absence of ligand.

It has been repeatedly reported that SERK co-receptors are involved in various biological processes and signal transduction networks. In **Chapter 6**, the changes in gene expression in absence of functional SERK1 and SERK3 are studied using transcriptional analysis. Microarrays were performed on RNA isolated from roots of 4-day-old seedlings of *serk1*, *serk3* and *serk1serk3* mutants.

Hierarchical cluster analysis indicated that *serk3* mutant roots have the same transcriptional pattern when compared to roots of the *serk1serk3* double mutant but to a lower magnitude. More than half of the genes differentially regulated in the *serk1serk3* double mutant relate to BRI1 mediated signalling. In addition, a number of BR dependent and independent metabolic processes are affected in absence of SERK3 indicating that this co-receptor may have an additional function in metabolic control. Performing microarray analysis on receptor mutants is complicated as effects on gene transcripts may be indirect and due to differential regulation of downstream transcriptional regulators. This complexity is further enhanced in the SERK co-receptor mutants as multiple signalling pathways are affected. This raises the question if it is truly possible to correlate alterations in gene expression due to the absence of functional SERK co-receptors to one particular signal transduction pathway. In **Chapter 7**, the general discussion, it is described how modelling of BRI1 signalling in this thesis has contributed to new insights into the brassinosteroid signalling. Microscopy has been an important tool to quantify the number of receptors in a cell or the number of cells in a tissue. What is still

needed is a clear link between a signalling activity, and, therefore, the physiological response of the cell, to local and intracellular protein-protein interactions and protein concentrations. Further expanding the available microscopic techniques and mathematical models to the cellular level is one of the next challenges. The research described in this thesis is a starting point for such an approach to study signal transduction in Arabidopsis.

SAMENVATTING

Planten leven op een vaste plaats en moeten zich daarom voortdurend aanpassen aan biotische en abiotische omgevingsfactoren. Dankzij dit aanpassingsvermogen is een plant goed in staat te groeien en te overleven. Op cellulair niveau worden de verschillende externe stimuli waargenomen door receptoren, die door middel van interactie met andere eiwitten de gewenste reactie coördineren. Maar hoe weet een cel nu wanneer de verdediging aan moet of wanneer te delen en te groeien? Daarvoor moeten de binnenkomende signalen onderling en de bijbehorende reactiepatronen goed op elkaar afgestemd worden. De interactie tussen de verschillende signaaltransductie netwerken is een complexe vraagstelling. Karakterisering van mutanten waarin een bepaald gen is uitgeschakeld levert niet altijd een duidelijk antwoord op aangezien het fenotype veroorzaakt kan zijn door verstoring van meerdere signaaltransductie routes tegelijk. Een genetisch netwerk heeft vaak een structuur die gebaseerd is op simpele schakelingen: het gen functioneert (aan) of functioneert niet (uit). In werkelijkheid, is signaaltransductie veel complexer en zijn de aanwezige hoeveelheden van actieve receptoren en de hoeveelheid liganden erg belangrijk. Om dit beter te kunnen bestuderen zijn kwantitatieve biologische waarnemingen, ondersteund door wiskundige modellen, een belangrijk hulpmiddel.

Een van de best bestudeerde signaal transductie routes in de model plant *Arabidopsis thaliana* is de brassinosterïode signalering. Dit groeihormoon is erg belangrijk voor de ontwikkeling van planten. Brassinosterïoden zijn liganden die binden aan de “Brassinosteriod Insensitive 1” (BRI1) receptor, die een signaal doorgeeft aan andere eiwitten door middel van fosforylering. Dit resulteert uiteindelijk in transcriptionele regulatie van genen die een bepaalde cellulaire reactie coördineren. Uit eerder onderzoek is al gebleken dat BRI1 voor deze signaaltransductie gebruik maakt van niet ligand bindende co-receptoren. De co-receptoren, genaamd “Somatic Embryogenesis Receptor-like Kinases” (SERKs), beïnvloeden dus het signaal dat vanaf BRI1 doorgegeven wordt aan het intracellulaire signaaltransductie netwerk. In totaal zijn er 5 SERK genen bekend, die allen gedeeltelijk redundant functioneren in verschillende signalerings-routes. SERK1, bijvoorbeeld heeft een rol in abscissie, maar is ook gedeeltelijk redundant met SERK3 in de brassinosterïode signalering. SERK3 en SERK4 spelen beiden een belangrijke rol in de afweer tegen pathogenen. Afwijkende fenotypes worden meestal pas waargenomen in lijnen waarin tenminste twee SERK genen zijn uitgeschakeld. Dit bemoeilijkt de fenotypische analyse aangezien er meerdere signalerings-routes verstoord worden.

Om beter te begrijpen hoe een enkele SERK co-receptor tegelijkertijd functioneert in verschillende signalerings-routes is een kwantitatief inzicht in de verdeling van

deze eiwitten erg belangrijk. Daarvoor is het essentieel te weten hoeveel co-receptoren en receptoren er in een cel aanwezig zijn. Daarnaast is het de vraag hoe sterk de signaaltransductie beïnvloed wordt door de aan- of afwezigheid van SERK co-receptoren. **Dit proefschrift** beschrijft hoe brassinosteroïde signalering beïnvloed wordt door ligand, receptor en co-receptor concentraties. Hiervoor is gebruik gemaakt van zowel biochemische, moleculair biologische en genetische benaderingen, in combinatie met wiskundige modellen.

In **Hoofdstuk 1** wordt een uitgebreid overzicht gegeven van brassinosteroïde signaaltransductie-route en de rol van SERK co-receptoren in verschillende biologische processen. Tevens wordt beschreven hoe wiskundige modellen kunnen helpen bij het beschrijven van complexe biologische vraagstellingen. Voor het opstellen van een wiskundig model waarin de hoeveelheid beschikbaar ligand, receptor en co-receptor als startpunt wordt gebruikt is het belangrijk om het aantal receptoren en co-receptoren in een cel te weten. In **Hoofdstuk 2** wordt beschreven hoe confocale microscopie gebruikt kan worden om de hoeveelheid BRI1, SERK1 en SERK3 *in planta* te bepalen. Het aantal BRI1 receptor moleculen in een epidermale wortelcel varieert van 22,000 in het meristeem tot 80,000 in de gestrekte cellen van de maturatie zone. Wanneer echter het verschil in celgrootte in acht wordt genomen blijkt dat de receptordichtheid in alle cellen van het wortelmeristeem gelijk is, maar beduidend lager in de maturatie zone. Dit is een interessante waarneming aangezien cellen in het wortelmeristeem het meest betrokken zijn bij brassinosteroïde signalering. Dit betekent dus dat de receptor-dichtheid en niet het totaal aantal receptoren per cel bepalend is voor de gevoeligheid van een cel voor brassinosteroïden. De vervolgvraag is nu, hoe de fysiologische reactie van de cel na ligand stimulatie afhangt van de concentratie receptor en ligand. Om dit te beantwoorden is, zoals in **Hoofdstuk 3** staat beschreven, gebruik gemaakt van een wiskundig model dat de hoeveelheid ligand gebonden aan de BRI1 receptor koppelt aan wortelgroei en hypocotyl elongatie. Het model is in staat de wortelgroei en hypocotyl elongatie van *bri1* mutanten te voorspellen bij verschillende ligand concentraties. Tevens voorspelt het model ook dat de meerderheid van de beschikbare BRI1 receptoren niet bezet is met ligand. Dat roept de vraag op waarom er dan zo veel “reserve receptoren” zijn. Mogelijk zijn deze receptoren wel betrokken bij de signaal transductie door laterale signaal verspreiding, of is de hoeveelheid van een eiwit dat later in de signaal transductie geactiveerd wordt de beperkende stap.

De activatie en inhibitie van wortelgroei is afhankelijk van de brassinosteroïde concentratie. Bij lage hoeveelheden brassinosteroïde wordt wortelgroei gestimuleerd terwijl die bij hoge concentraties wordt geremd.

Nu blijkt dat de “switch” tussen activatie en remming van wortelgroei gerelateerd is aan de hoeveelheid brassinosteroïde die is gebonden aan BRI1. Wanneer de BRI1 concentratie in het model verlaagd wordt, neemt de wortellengte na toevoeging van ligand toe tot de maximale bezettingsgraad van BRI1, terwijl bij hogere ligand concentraties geen remming van wortelgroei meer wordt waargenomen. In andere woorden, het signaal vanaf BRI1 is niet hoog genoeg om de “switch” tussen stimulering en remming van wortel groei te induceren. Dit typische patroon wordt in werkelijkheid waargenomen bij zwakke *bri1* mutanten die nog een lage signaleringsactiviteit behouden hebben. Sterke *bri1* mutanten waarbij in het geheel geen reactie meer is op exogeen toegevoegde brassinosteroïde zijn recessief. Dit houdt in dat alleen homozygote lijnen een fenotype hebben, wat aangeeft dat het systeem robuust is tegen veranderingen in de BRI1 receptor concentratie. In tegenstelling tot de ongevoeligheid van het systeem voor veranderingen in receptor concentraties, blijkt dat de signalering juist erg gevoelig is voor veranderende ligand concentraties. Dit suggereert dat BRI1 signalering voornamelijk beïnvloed wordt door de beschikbaarheid van het ligand (brassinosteroïde) en de biochemische activiteit van de receptor.

Aangezien BRI1 signalering sterk afhankelijk is van de aanwezigheid van SERK co-receptoren, is het belangrijk om te bepalen hoe deze co-receptoren van invloed zijn op de signaleringsoutput. Daarom wordt in **Hoofdstuk 4** het wiskundige model voor BRI1 signalering uitgebreid met twee co-receptoren, SERK1 en SERK3. Het model houdt ook rekening met BRI1 signalering onafhankelijk van SERK1 en SERK3. Dit is mogelijk door activiteit van BRI1 alleen, of wanneer deze interacteert met een andere co-receptor, zoals SERK4. Wanneer het model gecalibreerd wordt op zowel wild type planten en *serk1* en *serk3* mutanten voorspelt het model dat er nauwelijks een reactie is op brassinosteroïde in de wortel, maar wel in de hypocotyl. Metingen verricht aan de hypocotyl en wortel bevestigen deze voorspelling van het model. Dit wijst erop dat er ten opzichte van de wortel in de hypocotyl een andere co-receptor gebruikt wordt of dat er meer signaleringsactiviteit is van BRI1 alleen. Mogelijk is het gebruik van verschillende co-receptoren een mechanisme om de gevoeligheid van een cel of weefsel voor brassinosteroïde af te stellen.

Het model geeft ook aan dat SERK co-receptoren voornamelijk de sterkte van het signaal beïnvloeden. Een vraag die hieruit voortkomt is hoe dit bewerkstelligd wordt. Een mogelijk biochemisch mechanisme is, in analogie met dierlijke systemen, een stabilisatie van het geactiveerde en ligand gebonden BRI1 receptor complex door de co-receptoren.

Uit de simulatie studies blijkt ook dat brassinosteroïde signalering door de BRI1 receptor niet beïnvloed wordt wanneer de meerderheid van de co-receptoren niet beschikbaar zijn. Dit is een belangrijke waarneming wanneer in gedachten gehouden wordt dat SERK1 en SERK3 in wild type planten in meerdere biologische processen functioneren. Dit geeft aan de SERK co-receptoren niet limiterend zijn in brassinosteroïde signalering.

Huidige modellen voor BRI1 signalering stellen dat SERK co-receptoren, met name SERK3, aangetrokken worden door een met ligand gebonden BRI1 receptor. Echter, uit “Fluorescence Recovery After Photobleaching” (FRAP) metingen, die beschreven worden in **Hoofdstuk 5**, blijkt dat in cellen van het wortelmeristeem zowel BRI1 als SERK3 relatief immobiel zijn. Dit suggereert dat BRI1 en SERK3 al een complex vormen voordat er ligand aanwezig is.

Nu is er herhaaldelijk beschreven dat de SERK co-receptoren betrokken zijn bij verschillende biologische processen en signaaltransductie-netwerken. In **Hoofdstuk 6** wordt de verandering in gen-expressie door afwezigheid van functioneel SERK1 en SERK3 bestudeerd door middel van transcriptionele analyse. De microarrays zijn uitgevoerd met RNA geïsoleerd uit wortels van 4 dagen oude zaailingen van *serk1*, *serk3* en *serk1serk3* mutanten. De *serk3* en *serk1serk3* mutanten vertonen dezelfde trend in termen van differentieel gereguleerde genen, terwijl er geen duidelijke correlatie met *serk1* lijkt te zijn. Meer dan de helft van de genen die transcriptionele veranderingen vertonen in afwezigheid van SERK1 en SERK3 zijn gerelateerd aan brassinosteroïde signalering. Daarnaast blijkt dat er een aantal aan secundair metabolisme gerelateerde processen zijn verstoord. Slechts een deel van deze processen is direct gerelateerd aan de brassinosteroïde signalering. Transcriptionele studies van veranderde gen-expressie door de afwezigheid van een receptor moet tot stand komen via een reactie op het nivo van de transcriptiefactoren. De waargenomen differentieële regulatie van genen kan bijvoorbeeld veroorzaakt worden door transcriptie factoren die niet aangezet worden in afwezigheid van BRI1 signalering of juist wel. In het geval van de SERK co-receptoren kunnen verschillende signaaltransductieroutes betrokken zijn, zodat het niet altijd eenvoudig zal zijn om een verandering in gen-expressie door de afwezigheid van SERK co-receptoren te koppelen aan een specifieke signaleringsroute.

In **Hoofdstuk 7**, de algemene discussie, wordt er beschreven hoe modellering van BRI1 signalering in dit proefschrift heeft bijgedragen aan het verkrijgen van nieuwe inzichten in de brassinosteroïde signalering en een van de gecontroleerde fysiologische processen. Microscopie is hierbij een belangrijk middel geweest voor het bepalen van hoeveelheid beschikbare receptoren en het aantal cellen in een bepaald weefsel. Wat nog ontbreekt is een duidelijke koppeling van signaleringsactiviteit, en dus ook de fysiologische reactie van de cel, aan lokale

en intracellulaire eiwit-eiwit interacties en aan eiwit concentraties. Het verder uitbreiden van de beschikbare microscopische technieken en wiskundige modellen naar het cellulaire niveau behoort tot een van de volgende uitdagingen. Het onderzoek dat in **Dit proefschrift** beschreven wordt is een startpunt om met een dergelijke aanpak signaaltransductie in Arabidopsis te bestuderen.

DANKWOORD

Voor mijn gevoel ben ik pas net begonnen maar de vier (stiekem vijf) jaar zijn toch echt om, alleen het dankwoord schrijven rest nog, voordat ik de deuren van het Transitorium achter me sluit. Sacco, tijdens het schrijven van mijn proefschrift hebben we een goede communicatie opgebouwd met soms felle en hardnekkige discussies waar ik veel van geleerd hebt. Ook tijdens onze wekelijkse werkdinmiddagen op maandagochtend hebben we heel wat besproken. Was het niet over de experimenten dan was het wel over de weekendbezigheden, vliegen, wandelen, mountainbiken, noem maar op. Tja, ik zou er nog zoveel over kunnen schrijven maar het eindresultaat is al te lezen in de rest van dit boekje. Dus voor mij rest alleen nog je te bedanken voor alle hulp steun, adviezen en inspiratie die jij als promotor me in de afgelopen vijf jaar gegeven hebt.

Naast mijn eigen promotor heb ik ook nog erg veel geluk gehad met mijn externe begeleider. Jaap ook jij heel erg bedankt voor alles, wanneer nodig was je er altijd voor me met een luisterend oor en het juiste advies. Tijdens mijn promotieonderzoek heb ik me altijd welkom gevoeld bij Biometris en daar dan ook een erg leuke tijd gehad. Ik wil dan ook graag iedereen op Biometris bedanken hiervoor. In het bijzonder Simon, mijn co-promotor, heel erg bedankt voor je wetenschappelijke bijdrage aan dit proefschrift omtrent de wiskundige modellen. Ook de vele discussies, soms tot 's avonds laat over de telefoon heb ik erg gewaardeerd. Naast je wetenschappelijke bijdrage ben je ook zeker goed gezelschap tijdens congressen, borrels en feestjes dus ook hiervoor bedankt. Dit brengt mij naar de volgende persoon om te bedanken, mijn andere co-promotor. Jan Willem, op microscopie gebied ben je werkelijk waar een expert. Maar zelfs toen mijn project een andere wending nam richting het modelleer werk heb je me daar zo goed mogelijk in gesteund en begeleid. Wanneer nodig ben je er altijd, bedankt hiervoor! Cathy, from start to the end, you always seemed to be there. Whether it was for a scientific discussion at work, or a good glass of wine (Patrick also thanks for your company there!) it was always fun. It has been a great pleasure to have you as a colleague, thank you for all the help and advice. Ook bedankt aan alle ingezetenen van kamer 2064 van het Transitorium. Anna, thank you for all the support during the beginning of my PhD, I really missed our nice discussions when you went back to Australia. Marije, gelukkig kwam jij al snel daarna als vrolijke noot in de groep en hebben we veel leuke (wetenschappelijk) discussies gehad samen. Colette, ook jij erg bedankt niet alleen voor je gezelschap en advies maar ook voor je bijdrage aan dit proefschrift, ik heb veel van je geleerd. Verder kan ik natuurlijk "lotgenoten" Danny, Christoph en Lisette niet vergeten voor de vele discussies en gezellige tijd. Walter, als tegenover buurman in het grote lab was je altijd een goede "vraagbaak", ook jij bedankt voor alle leuke gesprekken. Tijdens mijn AIO-schap heb ik veel hulp gehad van een aantal zeer getalenteerde

studenten. Preethi, thank you for the contribution to the work presented in Chapter 2, you were very enthusiastic and determined. Antsje, samen met jou heb ik gewerkt aan het “FRAP hoofdstuk”. Je was een erg leuke en gezellige maar vooral ook goede student. Ik ben dan ook best een beetje trots dat je als AIO bij biochemie bent gebleven. Ongetwijfeld ga je ook dit onderzoek met zeer veel succes afronden. Jelle, jij ging samen met mij de uitdaging aan om de effecten van *serk1* en *serk3* op wortel en hypocotyl groei te meten. Je bijdrage staat vermeld in hoofdstuk 4, ook jij heel erg bedankt voor je enthousiasme en de vele uren op het lab waarin je aan mijn onderzoek meewerkte. Thanks to everyone who is or was in Sacco's and JW's group in the past years for all the nice discussions we had.

Graag wil ik alle AIO's, post-docs en analisten en vaste staf van Biochemie bedanken voor hun gezelligheid en hulp in de afgelopen jaren. Met name Adrie en Boudewijn erg bedankt voor de hulp bij de microscopie, Willy altijd het goede advies omtrent lab-werk. Sjef, onmisbaar bij het uitvoeren van de ms/ms experimenten en bij de thee pauze. Jaques, bedankt voor de vele leuke gesprekken die we (ook in het weekend) gehad hebben. Dolf, heel erg bedankt voor al je goede adviezen en suggesties. Willem en Huub, jullie bedankt voor de leuke tijd bij het “practicum biologische chemie”. Laura, ook jij heel erg bedankt voor alle ondersteuning en gezellige gesprekken de afgelopen vijf jaar.

Also thanks to Pierre, Jenny, Tila, Martine, Juliane, Anitha, Padraic and all the other members of the EPS PhD council for all the fun we had and the nice party's, PhD days and symposia we organized.

Dan zijn er nog veel vrienden die ervoor gezorgd hebben dat de afgelopen paar jaar in Wageningen supersnel voorbij zijn gevlogen zijn. Bert en Karen, Annemarie en Mark, Peter v B, Rob, Joseline en Pascal, bedankt de vele filmavondjes, BBQ's en etentjes die we gehad hebben en zeker nog komen gaan. Bert, als collega op biochemie stond jij altijd klaar met goed advies, een gezellig gesprek bij de lunch, en zo nu en dan een Belgisch bierfestijn. Ik vind het dan ook heel erg leuk dat je mijn paranimf bent! Corine en Ruben, het spreekwoord: “Beter een goede buur dan een verre vriend” is zeker van toepassing op jullie, bedankt voor alle gezellige avondjes thee drinken. Hopelijk zien we jullie ook nog regelmatig op Nijverheidstraat 6! Also thanks to Nicolas and Krissana for the nice time at Lombardi! Kirsten and Adam, always nice to hear from you, hopefully we'll meet again soon. Ook de rest van onze vrienden natuurlijk, allemaal heel erg bedankt voor de gezelligheid nu en in de toekomst.

Dan als laatste maar zeker niet in het minst belangrijk mijn familie. Pa en Ma heel erg bedankt voor jullie steun tijdens mijn opleiding. Ik heb een lang traject

doorlopen wat ik zeker nooit gehaald zou hebben zonder jullie hulp en wijze raad. Dan Peter, ja ik heb aardig door moeten pipetteren, maar ik wou niet hebben dat je ongelijk zou krijgen. In jouw dankwoord, schreef je dat het je wel eens moeite zou kunnen kosten me voor te blijven qua publicaties. Momenteel is het 16-8 voor jou, dus ik ben al op de helft. Peter, ook jij bedankt voor je hulp en adviezen als “grote broer” maar ook als paranimf. Deze hulp is niet alleen op het persoonlijke vlak, want je bijdrage is ook te lezen in hoofdstuk 6 van dit proefschrift.

Pieter, nu bijna 8 jaar geleden stelde Peter me voor aan zijn “gemoedelijk Brabantse collega” en fytopatholoog. Al snel leerde ik dat *Phytophthora Infestans* toch echt geen schimmel was maar een oömyceet. Sinds onze eerste ontmoeting tijd ben je mijn beste vriend, en hebben we naast de wetenschap veel gedeelde hobby's en interesses. Heel erg bedankt, voor je hulp bij het schrijven en vormgeven, voor het meegaan naar het lab in het weekend en je begrip als ik in de late uren weer eens aan het werk was. Maar boven al voor de leuke tijd die wij samen hebben en nog tegemoet gaan.

Met deze woorden rond ik het laatste schrijfwerk aan mijn proefschrift af, best een lekker gevoel eigenlijk. Nogmaals bedankt allemaal!

CURRICULUM VITAE

Gijsberta Wilhelmina (Wilma) van Esse is geboren te Rhenen op 27 april 1982 en behaalde in 1998 haar mavo diploma aan het Ichtus College te Veenendaal. In datzelfde jaar begon ze aan de opleiding analytische chemie aan Rijn-IJssel college te Arnhem. In 2002 behaalde ze daar haar diploma en begon aan de studie Chemie aan de Hogeschool van Utrecht. Tijdens haar stage bij de groep Medicinal Chemistry & Chemical Biology van de Universiteit van Utrecht heeft ze onder begeleiding van Dr. Ir. Dirk Rijkers en Prof. Dr. Rob Liskamp met behulp van click chemie gewerkt aan het synthetiseren van dendrimeren gekoppeld aan actieve peptiden. In 2005 rondde Wilma haar studie af en behaalde haar BSc diploma. In datzelfde jaar begon ze aan de Master studie Biotechnologie aan de Wageningen Universiteit. Haar eerste afstudeervak was onder begeleiding van Dr. Ir. Erik Limpens en Prof. Dr. Ton Bisseling bij het laboratorium voor Moleculaire Biologie. Bij deze groep bestudeerde ze endosomaal transport in wortelknolletjes gevormd door *rhizobia* bacteriën in *Medicago truncatula*. Het tweede afstudeervak was bij het *laboratorium voor Biochemie* waar zij onder begeleiding van Dr. David van der Meer, Prof. Dr. Ir. Sander Kersten en Prof. Dr. Sacco de Vries werkte aan de isolatie van het PPAR α complex uit HepG2 cellijnen met behulp van immunoprecipitatie. In 2007 behaalde ze haar MSc diploma en in mei 2008 begon ze haar promotie onderzoek bij het Laboratorium voor Biochemie. Onder begeleiding van Dr. Ing. Jan Willem Borst, Dr. Ir. Simon van Mourik en Prof. Dr. Sacco de Vries werkte ze binnen het “systems biology research program (IP/OP)” aan het project “Modeling receptor recruitment into different signaling pathways”. De resultaten van dit onderzoek zijn beschreven in dit proefschrift. Sinds juli 2013 werkt ze als postdoctoraal onderzoeker bij het Max Planck Instituut in Keulen aan axillaire meristeem ontwikkeling in gerst.

LIST OF PUBLICATIONS

Van Esse GW, Harter K, De Vries SC (2013) Computational modeling of the BRI1 receptor system. *Plant Cell and Environment*, DOI: 10.1111/pce.12077

Van Esse GW*, Van Mourik S*, Stigter H, Ten Hove CA, Molenaar J, De Vries SC (2012) A mathematical model for BRI1 mediated signaling in root growth and hypocotyl elongation. *Plant Physiology* (160), pp. 523-32

Van Esse GW, Westphal AH, Surendran RP, Albrecht C, Van Veen B, Borst JW, De Vries SC (2011) Quantification of the brassinosteroid insensitive1 receptor *in planta*. *Plant Physiology* (156), pp. 691-700

Bücherl CA, **Van Esse GW**, Kruis A, Luchtenberg J, Westphal AH, Aker J, Van Hoek A, Albrecht C, Borst JW, De Vries SC (2013) Visualization of BRI1 and BAK1(SERK3) membrane receptor hetero-oligomers during brassinosteroid signalling. . *Plant Physiology* (162), pp. 1911-25

Limpens E, Ivanov S, **Van Esse GW**, Voets G, Fedorova E, Bisseling T (2009) *Medicago* N₂-Fixing symbiosomes acquire the endocytic identity marker Rab7 but delay the acquisition of vacuolar identity. *Plant Cell* 21 (9), pp. 2811-2828

Dijkgraaf I Rijnders AY Soede A, Dechesne AC, **Van Esse GW**, Brouwer AJ, Corstens FHM, Liskamp RMJ (2007) Synthesis of DOTA-conjugated multivalent cyclic-RGD peptide dendrimers via 1,3-dipolar cycloaddition and their biological evaluation: Implications for tumor targeting and tumor imaging purposes. *Organic and Biomolecular Chemistry* 5 (6), pp. 935-944

Rijkers DTS, **Van Esse GW**, Merks R, Brouwer AJ, Jacobs HJF, Pieters RJ, Liskamp RMJ (2005) Efficient microwave-assisted synthesis of multivalent dendrimeric peptides using cycloaddition reaction (click) chemistry. *Chemical Communications* (36), pp. 4581-4583

Joosten JAF, Tholen NTH, Ait El Maate F, Brouwer AJ, **Van Esse GW**, Rijkers DTS, Liskamp RMJ, Pieters RJ (2005) High-yielding microwave-assisted synthesis of triazole-linked glycodendrimers by copper-catalyzed [3+2] cycloaddition. *European Journal of Organic Chemistry* (15), pp.3182-3185

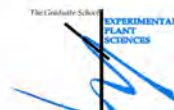
Manuscripts in preparation

Van Esse GW*, Van Mourik S*, Albrecht C, Van Leeuwen J, De Vries SC. A mathematical model for the co-receptors SERK1 and SERK3 in BRI1 mediated signalling. (*Submitted*)

Van Esse GW, Ten Hove CA, Van Esse HP, Boekschoten M, De Vries SC. Transcriptional analysis of *serk1* and *serk3* mutants. (*In preparation*)

*These authors contributed equally

Education Statement of the Graduate School Experimental Plant Sciences



Issued to: **G.W. (Wilma) van Esse**
Date: **18 September 2013**
Group: **Biochemistry, Wageningen University & Research Centre**

1) Start-up phase	date
► First presentation of your project Modelling receptor recruitment into different signalling pathways	Dec 18, 2008
► Writing or rewriting a project proposal	
► Writing a review or book chapter VAN ESSE, G. W., HARTER, K. and DE VRIES, S. C. (2013), Computational modelling of the BRI1 receptor system: Plant, Cell & Environment, doi: 10.1111/pce.12077	Aug 2012
► MSc courses	
► Laboratory use of isotopes	

Subtotal Start-up Phase 4.5 credits*

2) Scientific Exposure	date
► EPS PhD Student Days EPS PhD Student Day, Leiden University EPS PhD Student Day, Utrecht University EPS PhD Student Day, Wageningen University	Feb 26, 2009 Jun 01, 2010 May 20, 2011
► EPS Theme Symposia EPS Theme Symposium 'Developmental Biology of Plants', Leiden University EPS Theme Symposium 'Developmental Biology of Plants', Wageningen University	Jan 30, 2009 Jan 28, 2010
► NWO Lunteren days and other National Platforms Microspectroscopy in Biology, Wageningen ALW/EPW Annual meeting, Lunteren Systems Biology Day ALW/EPW Annual meeting, Lunteren Spring symposium: In singulo biochemistry: biology one molecule at a time, Groningen ALW/EPW Annual meeting, Lunteren	Sep 24, 2008 Apr 06-07, 2009 Jun 10, 2009 Apr 18-20, 2010 Jun 16, 2010 Apr 04-05, 2011 May 27, 2011 Apr 02-03, 2012
► Seminars (series), workshops and symposia Invited Seminars Biochemistry: Delphine Chinchilla (Basel, Switzerland), Niko Geldner (Lausanne, Switzerland), Jan Lohmann (Tubingen, Germany), Enrico Scarpella (Edmonton Canada), Thorsten Nünberger and Anna Koltunow (CSIRO, Australia) EPS Flying Seminar: Simon Gilroy (Wisconsin-Madison, USA) EPS Flying Seminar: Zhenbiao Yang (Riverside, USA) Invited Seminars Biochemistry: Ana Cano Delgado (Barcelona, Spain), Sabrina Sabatini (Rome, Italy), Dorus Gadella (Amsterdam, NL), Bruno Mueller (Zurich, Switzerland) and Klaus Harter (Tubingen, Germany) Jorifi Meeting Groups Sacco de Vries and Cyril Ziegler Invited Seminars Biochemistry: Roeland de Boer (Barcelona, Spain), Teva Vernoux (Lyon, France) and Richard Smith (Bern, Switzerland) The Beauty of Asymmetry in living organisms: Menno Schilthuis (Groningen, NL) Invited Seminars Biochemistry: Wolfgang Lukowitz and Keiko Torii EPS seminar: Veronica Grieneisen Baulcombe	Apr-Dec, 2008 May 19, 2008 Jun 23, 2008 Feb 26, 2009 Feb 05, 2009 Apr-Dec, 2010 Dec 12, 2011 Dec 2011 Dec 17, 2011 Mar-Oct 29, 2012
► Seminar plus	
► International symposia and congresses 20th International Conference on Arabidopsis Research (Edinburg, UK) IPSGA (Tarragona, Spain) 1st International Brassinoesteroid Conference (Barcelona, Spain)	Jun 30- Jul 04, 2009 Jun 28- Jul 02, 2010 Jun 27-29, 2012
► Presentations Oral presentation: PhD retreat Laboratory of Biochemistry (Barcelona, Spain) Oral presentation: Systems Biology Day Oral presentation: ALW/EPW Annual meeting, Lunteren Oral presentation: Systems Biology Day Oral presentation: IPSGA (Tarragona, Spain) Oral presentation: Dep. of Computational & Systems Biology (John Innes Centre, Norwich, UK) Poster presentation: ALW/EPW Annual meeting, Lunteren Poster presentation: 20th International Conference on Arabidopsis Research (Edinburg, UK) Poster presentation: ALW/EPW Annual meeting, Lunteren Poster presentation: 1st International Brassinoesteroid Conference (Barcelona, Spain)	Apr 21, 2009 Jun 10, 2009 Apr 19-20, 2010 Jun 16, 2010 Jun 30, 2010 Mach 20, 2012 Apr 06-07, 2009 Jun 30- Jul 04, 2009 Apr 04-05, 2011 Jun 27-29, 2012 Feb 17, 2011
► IAB interview	Feb 17, 2011
► Excursions PhD retreat Laboratory of Biochemistry to CSIC-IRTA in Barcelona (Spain) Monsanto, Wageningen KeyGene, Wageningen	Apr 21-25, 2009 Jan 27, 2011 Jan 26, 2011

Subtotal Scientific Exposure 24.4 credits*

3) In-Depth Studies	date
► EPS courses or other PhD courses Summer school mathematics and biology-Paris Plant Systems Biology FEBS Advanced Course: "Microspectroscopy: Monitoring Molecular Interactions in Living Cells"	Jul 02-16, 2008 Sep 01-05, 2008 Sep 21-26, 2008
► Journal club Journal club signal transduction group, Laboratory of biochemistry	2008-2012
► Individual research training	

Subtotal In-Depth Studies 13.0 credits*

4) Personal development	date
► Skill training courses PhD Competence assessment Presentation skills EPS Expectations Day 2010 EPS Expectations Day 2011	2009 May 12- 26, 2010 Nov 19, 2010 Nov 18, 2011
► Organisation of PhD students day, course or conference PhD retreat Laboratory of Biochemistry to CSIC-IRTA in Barcelona (Spain) Labouring Laboratory of Biochemistry EPS Expectations Day 2010 EPS PhD student Day 2011 Excursion to Monsanto, Wageningen EPS Expectations Day 2011	Apr 21-25, 2009 Sep 16, 2009 Nov 19, 2010 May 20, 2011 Jan 27, 2011 Nov 18, 2011
► Membership of Board, Committee or PhD council EPS Council EPS Educational committee	2009-2011 2011

Subtotal Personal Development 6.4 credits*

TOTAL NUMBER OF CREDIT POINTS* 48.3

Herewith the Graduate School declares that the PhD candidate has complied with the educational requirements set by the Educational Committee of EPS which comprises of a minimum total of 30 ECTS credits

* A credit represents a normative study load of 28 hours of study.

Cover design: Wilma van Esse

Printed at Wöhrmann Print Service Zutphen, The Netherlands